Investigation of Co-Gasification Characteristics of Biomass and Coal in Fluidized Bed Gasifiers

A thesis submitted in partial fulfillment

of the requirements for the

Degree of Doctor of Philosophy

in

Chemical and Process Engineering

of the University of Canterbury

by

Qixiang Xu

May 2013

Summary

This thesis presents research on the co-gasification characteristic of biomass and coal, and mathematical modelling of the co-gasification process. The whole project contains two major parts: i) experimental investigation and mathematical modelling of reaction kinetics of steam gasification of single char particles of pure coal, pure biomass, and blended coal and biomass; and ii) Experimental investigation and mathematical modelling of gasification characteristics of biomass, coal and their blends in pilot scale gasifiers.

In this research, an extensive literature review was first conducted. Following the literature review, background information and current progress were analysed on physical and chemical processes involved in gasification of biomass and coal and relevant feedstock properties related to gasification. Different types of gasifiers and corresponding gasification mathematical models were examined. In the literature, extensive experimental studies and mathematical modelling on gasification of pure biomass and pure coal have been found. However, there is an apparent knowledge gap in understanding the co-gasification process of biomass and coal, especially for the reaction kinetics of co-pyrolysis char gasification, which is the rate-controlling step within the entire gasification process. In addition, there is no comprehensive mathematical model available in the literature on co-gasification. Therefore the author's main contribution in this research will be gaining a fundamental understanding and developing mathematical models on steam co-gasification processes for single char particles and for blended biomass and coal in fluidized bed gasifiers.

In the first part of the present study, steam gasification experiments were performed to observe the reactivity of char particles of pelletized biomass and coal blends. Eucalyptus nitens and lignite were used as test materials and five different mass blending ratios were tested in a bench gasifier at three different temperatures. From the experimental observation, the gasification characteristics between biomass and coal were distinctly different, and the blended chars had gasification characteristics closer to those of coal char. The overall reactivity of the blended char decreases with the incremental fraction of the coal in the blend, and the effect tends to be reduced at higher temperatures. From the SEM analysis and gasification kinetic tests on pulverized char particles, the distinct gasification characteristics of coal char, biomass char and

blended coal-biomass char can be attributed to the difference in the char microstructure and char yield from the original feedstock. The biomass char is more structurally amorphous, hence internal resistance to the vapour diffusion is significant and the intrinsic reaction is fast due to larger exposed surface area, thus the reaction rate is more inhomogeneous through the whole char volume. On the other hand, coal char that has a denser structure and larger effective pore size causes a more homogeneous overall reaction rate through the whole char volume.

A dynamic mathematical model was developed to simulate the steam gasification process of biomass char, coal char and blend char. The char gasification model developed in the present study considers reactions of steam-gasification, water-gas shift and Bouduard reaction, and mass transport including convective bulk flow, bulk gas as well as Knudsen diffusion of the reactant gases. In addition, char structure evolution has also been quantified in the model. The mathematical model equations were solved to predict the overall gas production rate, producer gas composition profile and carbon consumption rate. The model has been validated by comparison with the experimental data of steam gasification of chars in which close agreement was found. The simulation results have confirmed that the char structure properties including specific reaction surface area and micro-pore size have significant impacts on both the intrinsic reaction rate and the intra particle mass transportation, while the magnitude of these two competing processes determines the overall gasification process. The gasification kinetic parameters of single char derived from the model simulation were then implemented on the co-gasification model of biomass and coal at large scale gasifiers in subsequent studies.

In the second part of the present study, a one-dimensional mathematical model was developed to simulate bubbling fluidized bed (BFB) gasification of coal and biomass blend pellets. The model was based on two phase theory which divides the bed into emulsion phase and bubbling phase. In the gasifier scale model, the heat and mass transfer process as well as reactions in the gasification process are considered while the hydrodynamics of the fluid flow are mathematically quantified by adopting correlations reported in literature. The internal diffusion of gaseous species in char particle has been described by the effectiveness factor for spherical geometry, in which the parameter was derived from the previous single char particle model results. The model has been solved in MATLAB software using a numerical technique to predict the gas composition profile and temperature profile in the gasifier. The model simulation results have

been validated by a set of co-gasification experiments performed on a 50 kW air-steam bubbling fluidized bed gasifier at CRL Energy Ltd., Wellington, New Zealand. In the experiments, lignite and sub-bituminous coal were used as coal feedstocks while pine and eucalypts were used as biomass feedstocks. The gasification tests were operated at 850 - 950°C.

After validation, the gasifier scale model was employed for sensitivity studies from which it was found that producer gas composition is strongly dependent on the char yield and the devolatilization gas distribution in the initial pyrolysis stage in the gasification process. The char reactivity had the least influence on producer gas composition; however, it had significant impact on the dynamic behaviour of the gasification process. On the effect of blending ratio of biomass and coal, it was found that adding biomass into coal had a negative influence on producer gas quality in terms of H_2 and CO content. The effect was more significant for lignite than subbituminous coal. The effect of the biomass type was not significant between eucalypts and pine, since these two types of biomass had similar chemical composition and physical properties.

The gasifier scale model has been further modified for simulation of steam gasification in a bubbling fluidizedbed gasifier. In order to validate the modified model, a series of gasification runs was performed on a 100 kW dual fluidized beds (DFB) gasifier in the Department of Chemical and Process Engineering, University of Canterbury. In the experiments, lignite and pine and their blended pellets were used as feedstocks and the gasification operation temperatures were 780-800°C. The experimental results were then used to validate the mathematical model and then the modified model was employed on parameter sensitivity analysis including the effects of mass blending ratio of biomass in the feedstocks, steam to solid fuel ratio and gasification temperature. The simulation results show that the producer gas composition from gasification of blended pellets was similar to the producer gas composition from gasification of pure lignite when the biomass blending ratio is from 0% to 40%. With an increase in the steam to solid fuel ratio, H_2 and CO_2 contents in the producer gas increased while CO content decreased. H_2 content increased while CO and CO_2 contents decreased with elevated temperature. A Parameter study on the effect of char reactivity shows that the char reactivity has a significant impact on producer gas composition.

In this research, the reaction kinetics of gasification was the main focus in the mathematical model. Further improvement on the model with more comprehensive calculations in fluidisation aspects would be desirable.

Acknowledgments

It is my pleasure and honor to express heartfelt thanks to those people who provided me support during my study, and I presume this thesis would have been impossible without their generous help.

In the very first place I would like to give my sincere gratitude to my supervisor Professor & Dr. Shusheng Pang for his supervision and guidance through the entire period of study. As he is a highly reputed scholar in the area, it seems redundant to say anything further about his academic level, so I just would like to express my true opinions toward him. In Chinese, we have a saying that I could not understand before: *He who teaches me for one day is my father for life*, but now such a sentence is not exaggerated to describe how I consider him. During the early period of my study, I was at the intersection of my life, inclined to sink deeper into melancholia and indeed thought about to quit. But he never abandoned me even I when intended to give up myself; his profound advice ignited my hope, his sincere encouragement helped me to expel my fear, his meticulous care warmed my heart, his patient guidance gave me momentum and his passions in science showed me a positive attitude in overcoming difficulty. Honestly for me, doing a PhD has been the process of maturing in mind rather than gaining knowledge, so in teaching me techniques of how to do a PhD he taught me more how to be a real person. Indeed, his importance for me has been an example of living to learn rather than just being my supervisor. How many decades can a person have? As he has been my teacher for nearly ten years from undergraduate study, Professor Pang is one of the most important people in my entire life's journey.

I also would like to give sincere thanks to my co-supervisor Dr. Chris Williamson, and all the academic staff of the Department of Chemical and Process Engineering (CAPE), for offering me selfless help in solving the academic issues of my project. I have special appreciation for the help of Dr. Woei-Saw who provided much information on the gasifer and the generous sharing of his knowledge. Without him, I could not imagine how to do the CAPE gasification part of this thesis.

I am greatly thankful for the financial, facility and technical support from CRL, Wellington. Also I would like to recognise my co-supervisor Dr. Tana Levi and all the CRL staff for their unreserved efforts in helping and looking after me during the time I was there. This thesis is also

a memorial to Dr. Tony Clemens for his contribution in the coal gasification area and establishment of the CRL part of this project.

I would like to thank all the departmental lab technicians, administration staff and post-grad mates for their help and support, and for making me feeling at home. I would like to give thanks to my good friend Mr. Ziyin Zhang; thanks for his help in my project and continuous companionship from under-grad study.

Last but not least, I would like to give my special thanks to my parents, who are the back yard garden of my mind. In countless times when I was feeling stressed, it was they who listened to my troubles, understood and encouraged me, and gradually helped me to establish my positive way of thinking. It is not possible to express in words my gratitude for what they have done for me in my life.

Table of Contents

List of Figures

As the gasification proceeded, the excess oxygen was consumed by char at the lower region of the bed (Figure 5.9). Due to the char accumulation in the bed more solid fuel was fed (Figure 5.10), and therefore the combustible gas species in the producer gas in the upper layer of the bed could be conserved. In Figure 5.8, it can be seen that at the steady state of the operation, the model predicted gas composition is in close agreement with the measured results.

List of Tables

Nomenclature

A_{bed}	cross sectional area of bed (m^2)
a_B	average interphase area (m^2/m^3)
B_0	gas permeability in the porous media (m^2)
C_i	molar concentration of i^{th} component
c_i	Sutherland's constant of i^{th} gas component(K)
C_{TS}	total number of moles of reaction sites per unit volume of char
$C_{p,i}$	molar heat capacity of the i^{th} gas species (J/mol·K)
d_b	bubble diameter (m)
D_{eff}	effective gas diffusivity (m^2/s)
D_{ij}	binary gas diffusivity (m^2/s)
D_{iK}	Knudsen diffusivity (m^2/s)
D_m	gas mixture diffusivity (m^2/s)
D_p	diameter (m)
d_p	micro-pore diameter (m)
dr	infinitesimal length in radius (m)
E	Eucalypt nitens (biomass type)
$E_{A,j}$	activation energy of j^{th} reaction
F	net gas flow term from emulsion gas to bubble ($mol/m^3/s$)
ΔG_i	standard Gibbs free energy of i^{th} reaction (kJ/mol)
H	specific enthalpy (J/m^3)
ΔH_R	heat of reaction (kJ/mol)
h_b	fluidized bed height (m)

$\boldsymbol{J}$	diffusion flux vector of gas components (mol/m^2/s)
K_{BE}	interphase mass transfer coefficient (m/s)
K_i	equilibrium constant
$k_{0,j}$	pre-exponential factor of j^{th} reaction (1/s)
k_j	Arrhennius rate constants of j^{th} reaction (1/s)
k_c	convective mass transfer coefficient (m/s)
k_m	heat conductivity of the gas mixture (J/m·K)
L	Lignite (coal type)
m	mass (kg)
M_C	total solid fuel mass in bed (kg)
M_S	total char mass in bed (kg)
M_{Sand}	total sand mass in bed (kg)
N_i	net mass flux of i^{th} component
P	*Pinus Radiata* pine (biomass type)
P	pressure (Pa)
$\boldsymbol{R}$	universal gas constant (8.314 J/mol/K)
Re	Reynolds number
R_j	intrinsic reaction rate of the j^{th} reaction
$\boldsymbol{r}$	apparent gasification reactivity (1/s)
r	radius (m)
S	Subbituminous (coal type)
S	specific reactive surface area (m^2/m^3)
s	dimensional space variable (-)
Sc	Schmidt number
Sh	Sherwood number

T	temperature (K)
t	time (s)
u	velocity (m/s)
u_0	superficial velocity (m/s)
u_b	bubble velocity (m/s)
u_{mf}	emulsion gas velocity (m/s)
V	volume (m^3)
$v_{i\,j}$	stoichiometric coefficient of i^{th} component in j^{th} reaction
wt %	weight percentage
X	conversion (-)
Y	solution vector
y_C	mass fraction of pyrolysis char yield
y_i	molar fraction of i^{th} component
z	bed height (m)

Greek letters

α	transportation selectivity factor
ε_b	bubble phase volume fraction
ε_{mf}	minimum fluidisation void fraction
η	effective rate factor of volumetric reaction
θ_i	coverage fraction of i^{th} gas component on the exposed surface.
μ	gas viscosity (kg/m/s)
ρ	density (kg/m^3)
τ	pores tortuosity (-) or time constant (s)
Φ	char structure porosity

ϕ	Thiele modulus
φ	parameter of CO/CO_2
ψ	Pore structure parameter of char

Abbreviations

AAEM	alkali and alkaline earth metal
A/F	air to fuel ratio
ANN	artificial neural network
BFB	bubbling fluidized bed
CFB	circulating fluidized bed
CFD	computational fluid dynamics
DAE	differential algebraic equation
daf	dry and ash free
DAEM	distributed activation energy model
DFB	dual fluidized bed
ER	equivalence ratio
MW	molecular weight (g)
ODE	ordinary differential equation
PDE	partial differential equation
RPM	random pore model
S/F	steam to fuel ratio
SEM	scanning electronic microscopy

Chapter 1 Introduction

In this chapter, the potential of biomass and coal as substitutes of crude oil is briefly introduced. The advantages of producing liquid fuel through gasification from New Zealand biomass and coal resources are then presented. Following this, the objectives of this research are introduced. Finally the summary of each chapter is outlined.

1.1 Global energy issue

Worldwide energy consumption has been greatly increased over the last several decades, due to the global growth in industrialization, economy and population. As a result, the global energy demand increases exponentially and the increasing rate will become more rapid in the future. It has been recognized world-wide that heavy exploitation and use of fossil fuels are leading to foreseeable depletion within several decades (Campbell 1996; Korpela 2006). Despite continuous development of the exploitation technology and frequent reports on the discovery of new reserves of oil and gas, the increased production cannot meet the world's energy demand and thus a gap exists between the demand and the supply of these two fuel resources (Lee et al. 2007). More importantly, extensive use of fossil fuels has contributed to climate change due to Green House Gas emissions. The energy shortage and the negative impact on the environment have created an opportunity for developing alternative, renewable energy resources as substitutes for the oil and the natural gas. In recent years, numerous R&D projects and commercialization of new technologies have been reported on alternative energy that is sustainable and more environmentally friendly.

1.2 Potential of combined usage of biomass and coal

Biomass, including all land and water based vegetation, is produced by green plants and all organic wastes and is widely considered as a renewable energy resource (McKendry 2002).

However, it has not been fully utilized due to the high costs of collection and transportation. Currently, biomass has been used either for direct combustion or through a gasification process to produce producer gas (Goyal et al. 2008; Hotchkiss 2003). The latter case (gasification) is a promising technology for biomass-derived energy due to the specific properties of biomass and its availability(Kotowicz et al. 2013). In gasification, a gas mixture is produced consisting mainly of H_2, CO, CO_2 and CH_4 which is termed as producer gas and could be used as feedstock for manufacturing of hydrogen fuel (by separation from producer gas) (Badwal et al. 2007; Lv et al. 2004; Stiegel and Ramezan 2006), as substituent of some crude oil product such as methanol (Demirbas 2007; Tijmensen et al. 2002), or to generate heat and electricity.

Zerta *et al.* (2008) reported the world energy consumption trend and projection over the next 80 years as shown in Figure 1.1. The percentages of each energy form are presented in Figure 1.2 (Khatib, 2012). From these figures, it can be seen that currently 14% of the worldwide energy consumption is supplied from biomass energy and liquid biofuels. The key reasons for the growing interest in using biomass energy and liquid biofuels are: (1) political benefits such as reduction of dependency on imported oil; (2) creation of employment; (3) environmental friendliness such as in the reduction of emissions of greenhouse gas and other pollutant substances.

At present, biomass is mainly used for electricity and heat through direct combustion. Making liquid fuel through biomass gasification has several potential advantages; however it is not economically viable using the current technologies due to the high costs of processing the low energy density biomass feedstock.

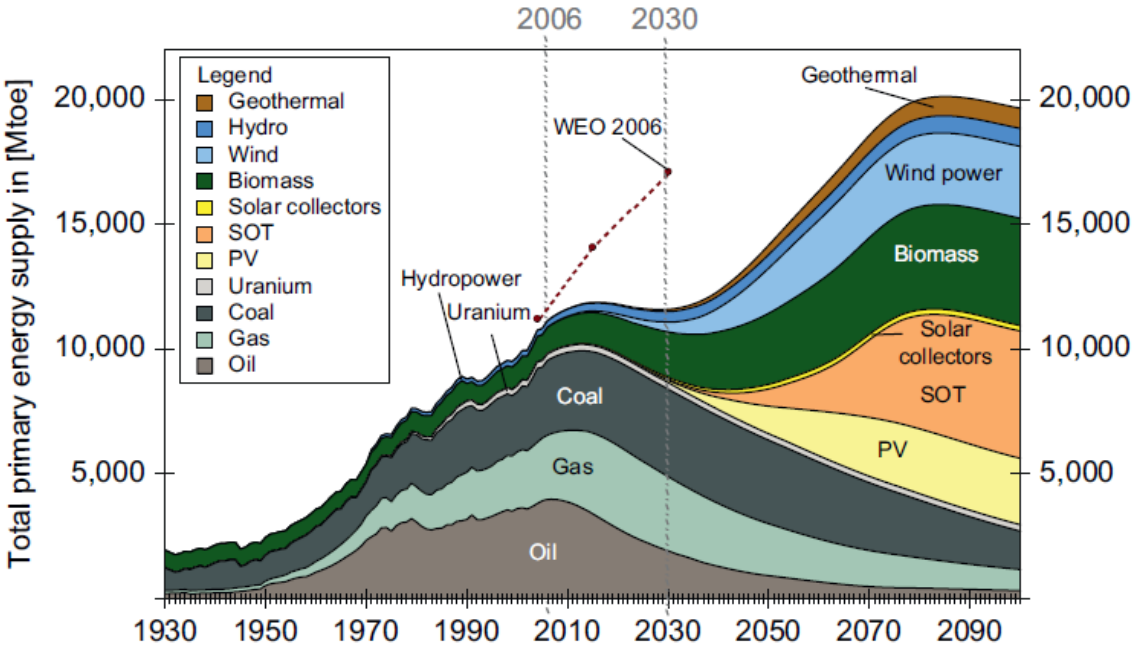

Figure 1.1: Worldwide energy consumption of fuel types from 1930-2090 (Zerta et al. 2008)

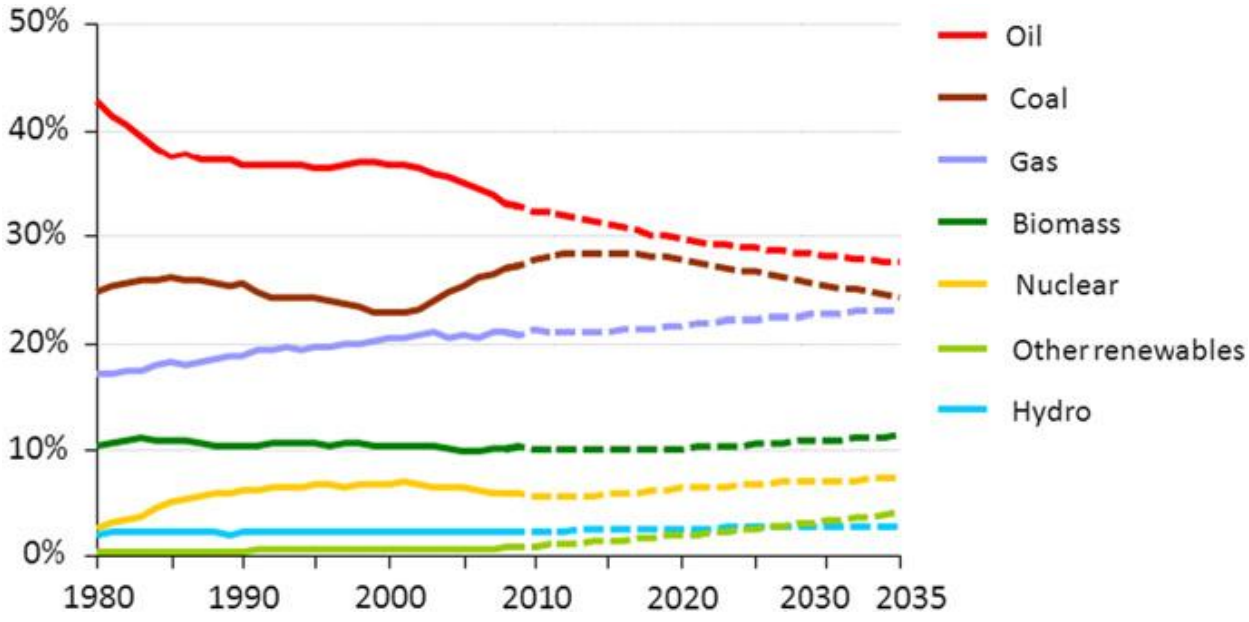

Figure 1.2: Percentage of main energy sources from 1980-2035(Khatib 2012)

Coal is an important conventional fossil fuel with abundant reserve estimated to be around 1000 billion tons in the world, which could be sufficient to last approximately 180 years based on the

current consumption rate (Lee et al. 2007). The common usage of coal is mainly through direct combustion for electricity generation, or as a feedstock for the production of coke and coal gas. Coal could also be converted into substances that could be alternatives of petroleum or natural gas through gasification and subsequent liquefaction. In 1932, the Fischer-Tropsch (F-T) synthesis method that makes liquid fuel from CO and H_2 was invented by the Germans, and the feedstock gas was the gasification producer gas of coal. In 1938, the annual production using F-T liquid fuel reached 590,000 tonnes in Germany. However, with rapid exploitation of crude oil and natural gas in 1940s and 1950s, the mass production of liquid fuel from coal was terminated, and the proportion of coal in worldwide energy consumption dropped from 65% to 27% in that period.

In recent years, due to the continuing increase in oil prices, production of liquid fuel from coal has already shown the potential of economical competitive advantage. This is especially true for the low rank coal which is not suitable for direct combustion and coking; producing liquid fuel from these types of coals could be a more viable option. However, the utilization of coal creates an environmental issue because of its generation of CO_2 and emission of pollutant substances such as SO_x.

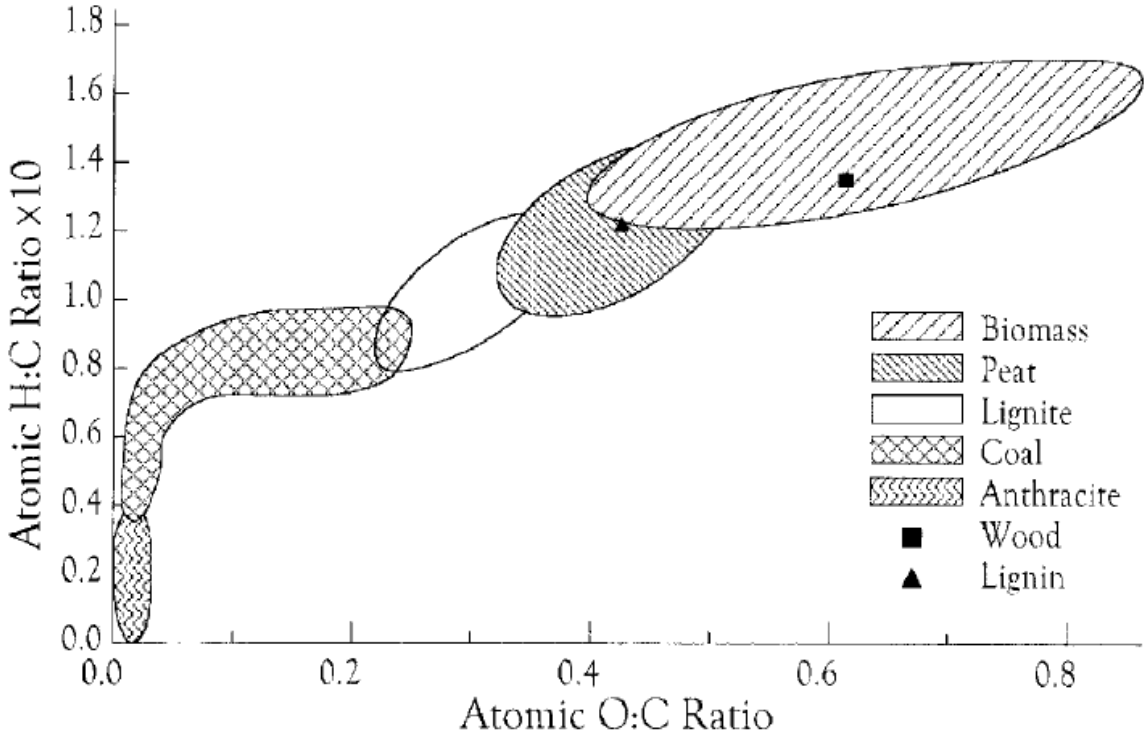

Figure 1.3: Van Krevelen diagram for various solid fuels (McKendry 2002)

With the continuous increase in the crude oil price, production of liquid fuel from coal and biomass is believed to be economically competitive with the crude oil derived liquid fuels in the future. Both biomass and coal are carbonaceous materials originating from plants and have the same basic elemental constituents. The compositions of various solid fuels including coal and biomass are shown in Figure 1.3 (McKendry 2002). Co-utilization of biomass with coal can be achieved by either direct co-combustion or co-gasification. In the latter case, the producer gas can be used for F-T synthesis of liquid fuel which provides a great opportunity for subsiding crude oil derived liquid fuels. Combined use of coal and biomass has great potential and benefits as listed below since they can overcome the disadvantages of each other (Kumabe et al. 2007):

- Economically, the utilization of the blended coal and biomass can achieve more flexible and reliable operation for a large scale energy plant. For instance, the biomass energy plant which is built near a forestry or wood processing industrial area can use the supplemental low-cost coal when the biomass feedstock is in shortage, avoiding the high delivery cost of transporting biomass from long distances. On the other hand, for the coal-fired energy plant,

operating costs can be reduced if low cost biomass from a nearby source can be blended into the feedstock.

- Densification of energy content for the feedstock. Biomass, in general, has a lower carbon fraction hence lower energy content, so adding coal to the biomass can increase the specific energy content of the product or reduce the auxiliary energy inputs.
- The co-gasification of the blended coal and biomass can be enhanced due to the high content metal elements in the biomass which have a catalytic effect on the reactivity of coal gasification. Therefore, the carbon conversion rate to gaseous phase can be enhanced and the yield of tar and residual char decreased (Brown et al. 2000).
- The composition of gasification producer gas could be altered by adjusting the blending ratio of the biomass with coal (Pinto et al. 2003).
- Environmentally, biomass is sustainable and largely carbon neutral as the plants absorb CO_2 during their growth, and thus using biomass for energy reduces the negative impact on the environment compared to using pure coal (Collot et al. 1999). Additionally, the pollutant substances content in biomass is significantly lower than coal. Therefore combined usage of biomass in an energy plant can reduce the emission of net CO_2 and other toxins and meet the requirements of government regulations.

1.3 New Zealand's energy resource potential

New Zealand's energy demand follows the worldwide trend of the majority of energy coming from fossil fuel resources. However, most of its crude oil and oil products are imported. Since the government-approved Kyoto protocol in 2002, the proportion of renewable energy utilization has been encouraged. The biomass is rich in New Zealand from the forestry and wood processing industry with more than 5 million m^3 annual production of wood residues, equivalent to 50 PJ annual energy generation (Penniall and Williamson 2009). Gasification based combined heat and power generation technology is an appropriate fit with the energy strategy of this country. New Zealand also has abundant coal reserves (estimated at 8.6 billion tonnes), of which about 75% is lignite, the lowest ranked coal. It is not energy efficient to transport lignite over long distances (Clemens et al. 2006). The New Zealand lignite has promoted char gasification reactivity

(Clemens et al. 1998), therefore, it would be desirable to utilize both of these two energy fuels in the future to reduce the dependence on imports and reduce the net carbon emission.

1.4 Objective of research

Biomass and coal have quite different physical and chemical properties thus the gasification characteristics of each fuel are expected to be different (Navarro et al. 2007; Prins et al. 2007). Although biomass is a renewable and ideal resource for energy and liquid fuel, its scatting feature and low energy density pose limitations on the commercial scale. The gasification process is the essential step in the production of alternative liquid fuel using thermo-chemical technologies and thus the composition of the producer gas has a significant impact on the down-stream processing. Therefore, in-depth understanding and optimisation of the coal-biomass co-gasification process is important in the design and operation of the future industrial production. Although gasification of each individual fuel has been extensively studied, there is still an apparent knowledge gap in the co-gasification process of coal and biomass and process optimization. The synergetic effect of the coal and the biomass on the co-gasification process can be significant; however, the literature reports are inconclusive and confusing.

The objectives of this project are to investigate the processes of co-gasification of coal and biomass through mathematical modelling and to optimize the operational conditions for production of a syngas with high hydrogen content and low tar concentration. New Zealand lignite and woody biomass available from the forest industry are used in this study to reveal the advantage of co-gasification of coal and biomass in New Zealand.

At the start of this study, an extensive literature review was first conducted on the co-gasification of coal and biomass. From this review it was found that the co-gasification process was dominated by reaction rates of the blended char. Therefore in order to understand the whole process, the properties and reactivity of the coal char, the biomass char and the blended char were investigated both experimentally and theoretically. Co-gasification of blended fuel of biomass and coal was then performed on two pilot scale gasifiers; a 200 kW bubbling fluidized bed gasifier at CRL Energy Ltd., and a 100 kW dual fluidized bed steam gasifier at the University of Canterbury. Mathematical models were developed for simulation of char

gasification and blended fuel co-gasification in the two pilot scale gasifiers. This study is presented in six chapters as outlined below.

1.5 Thesis outline

Chapter 2 presents the literature on the fuel properties and gasification process related to co-gasification of biomass and coal. The literature review shows that the gasification and co-gasification process can be divided into four stages: drying, pyrolysis (devolatilization), char gasification and gas phase reaction. Different types of gasifiers are introduced and compared. Following this, published mathematical models on gasification are analysed, and strengths and weaknesses of the existing models identified. The work plan is proposed and the most suitable model type chosen. Finally the reported studies on co-gasification of biomass and coal are reviewed and summarized.

Chapter 3 describes how steam gasification of biomass char, coal char and blended biomass and coal char was performed. The char reactivity at different blending ratios and different temperatures was experimentally investigated on a bench scale gasification system. The effect of blending ratios was then determined. The gasification reaction mechanism of biomass char, coal char and blended biomass and coal char is proposed.

In Chapter 4, a mathematical model for steam gasification of a single char particle is developed and validated by the experimental results obtained from Chapter 3. The intrinsic reaction rate and gas molecule diffusion are identified as the main affecting factors for the gasification rate and producer gas composition. From the model simulation, the effects of factors that influence the overall char reactivity are analysed.

Chapter 5 first presents the experimental runs for co-gasification of coal and biomass in a bubbling fluidized bed with air and steam being used as the gasification agent. Two types of biomass and two types of coals were used as the raw fuels and pelletized with different blending ratios. A kinetic mathematical model is developed to predict the producer gas composition at different operation conditions. After validation of the experimental results, the model is

employed to examine the effects of fuel properties and operating conditions on producer gas composition.

In Chapter 6, experimental work on steam co-gasification of coal and biomass pellets on a dual fluidized bed gasification system is described. The kinetic mathematical model presented in Chapter 5 is modified and validated for steam co-gasification. The model is then used for sensitivity analysis to quantify the effects of blending ratio, char reactivity and operating conditions on the producer gas composition.

Finally a conclusion and recommendations based on this study are given.

References

Badwal, S., Giddey, S., Ciacchi, F., Clarke, R., and Kao, P. (2007). "Research and developments in hydrogen technologies." *Advances in Applied Ceramics*, 106(1-2), 40-44.

Brown, R. C., Liu, Q., and Norton, G. (2000). "Catalytic effects observed during the co-gasification of coal and switchgrass." *Biomass and Bioenergy*, 18(6), 499-506.

Campbell, C. J. (1996). "Oil shock." *Energy World*(240), 7-12.

Clemens, A. H., Damiano, L. F., and Matheson, T. W. (1998). "The effect of calcium on the rate and products of steam gasification of char from low rank coal." *Fuel*, 77(9–10), 1017-1020.

Clemens, T., Gong, D., and Pearce, S. (2006). "Study on the suitability of New Zealand coals for hydrogen production." *International Journal of Coal Geology*, 65(3-4), 235-242.

Collot, A. G., Zhuo, Y., Dugwell, D. R., and Kandiyoti, R. (1999). "Co-pyrolysis and co-gasification of coal and biomass in bench-scale fixed-bed and fluidized bed reactors." *Fuel*, 78(6), 667-679.

Demirbas, A. (2007). "Progress and recent trends in biofuels." *Progress in Energy and Combustion Science*, 33(1), 1-18.

Goyal, H. B., Seal, D., and Saxena, R. C. (2008). "Bio-fuels from thermochemical conversion of renewable resources: A review." *Renewable and Sustainable Energy Reviews*, 12(2), 504-517.

Hotchkiss, R. (2003). "Coal gasification technologies." *Proceedings of the Institution of Mechanical Engineers, Part A: Journal of Power and Energy*, 217(1), 27-34.

Khatib, H. (2012). "IEA World Energy Outlook 2011—A comment." *Energy Policy*, 48(0), 737-743.

Korpela, S. A. (2006). "Oil depletion in the world." *Current Science*, 91(9), 1148-1152.

Kotowicz, J., Sobolewski, A., and Iluk, T. (2013). "Energetic analysis of a system integrated with biomass gasification." *Energy*, 52(0), 265-278.

Kumabe, K., Hanaoka, T., Fujimoto, S., Minowa, T., and Sakanishi, K. (2007). "Co-gasification of woody biomass and coal with air and steam." *Fuel*, 86(5–6), 684-689.

Lee, S., Speight, J. G., and Loyalka, S. K. (2007). *Handbook of alternative fuel technologies*, Boca Raton : CRC Press, c2007.

Lv, P., Chang, J., Wang, T., Fu, Y., Chen, Y., and Zhu, J. (2004). "Hydrogen-rich gas production from biomass catalytic gasification." *Energy and Fuels*, 18(1), 228-233.

McKendry, P. (2002). "Energy production from biomass (part 1): overview of biomass." *Bioresource Technology*, 83(1), 37-46.

Navarro, R. M., Pena, M. A., and Fierro, J. L. G. (2007). "Hydrogen production reactions from carbon feedstocks: Fossil fuels and biomass." *Chemical Reviews*, 107(10), 3952-3991.

Penniall, C. L., and Williamson, C. J. (2009). "Feasibility study into the potential for gasification plant in the New Zealand wood processing industry." *Energy Policy*, 37(9), 3377-3386.

Pinto, F., Franco, C., Andre, R. N., Tavares, C., Dias, M., Gulyurtlu, I., and Cabrita, I. (2003). "Effect of experimental conditions on co-gasification of coal, biomass and plastics wastes with air/steam mixtures in a fluidized bed system." *Fuel*, 82(15-17), 1967-1976.

Prins, M. J., Ptasinski, K. J., and Janssen, F. J. J. G. (2007). "From coal to biomass gasification: Comparison of thermodynamic efficiency." *Energy*, 32(7), 1248-1259.

Stiegel, G. J., and Ramezan, M. (2006). "Hydrogen from coal gasification: An economical pathway to a sustainable energy future." *International Journal of Coal Geology*, 65(3-4), 173-190.

Tijmensen, M. J. A., Faaij, A. P. C., Hamelinck, C. N., and Van Hardeveld, M. R. M. (2002). "Exploration of the possibilities for production of Fischer Tropsch liquids and power via biomass gasification." *Biomass and Bioenergy*, 23(2), 129-152.

Zerta, M., Schmidt, P. R., Stiller, C., and Landinger, H. (2008). "Alternative World Energy Outlook (AWEO) and the role of hydrogen in a changing energy landscape." *International Journal of Hydrogen Energy*, 33(12), 3021-3025.

Chapter 2 Literature Review

In this chapter, an extensive literature review was conducted on published studies related to gasification of coal and biomass, and co-gasification of their blends. The properties of biomass and coal related to gasification, processes and reactions involved in the gasification are presented in this chapter. Conversion technologies and different types of gasifiers are compared, with a focus on fluidized bed gasification of coal and biomass. Different mathematical models of the gasification process are examined and their strengths and weaknesses compared.

2.1 Biomass and Coal as Alternative Energy Resources

Biomass and coal can be utilized as energy feedstocks through thermochemical or biological conversion pathways to generate various energy products such as heat, electricity, liquid fuels, hydrogen and synthetic gases. Coal is the most broadly used fossil fuel for energy in the world with a large proportion being used for coke production for the iron industry and being used in combustion boilers for industrial and civil heat supply. Low quality coals such as lignite, which is not suitable for direct combustion or coke production, can be processed for the production of liquid fuels or chemicals. Biomass is defined as materials of recent biological origin from plants such as trees, grasses and agricultural crops, as well as animal manures and sewage bio-solids.

2.2 Biomass and Coal Properties

The properties of biomass and coal related to the gasification process are useful for understanding and predicting the gasification process. In this section, the relevant coal and biomass properties are presented and discussed.

2.2.1 Proximate and Ultimate Analysis

Proximate and ultimate analyses are normally the first steps in evaluating the feedstock solid fuels. Proximate analysis gives the fuel characteristics in terms of mass percentage of moisture, volatile matters, fixed carbon and ash content in the solid fuel. It is performed by heating the raw material to a set temperature, and in the case of coal or biomass, the solid fuel decomposition takes place at this temperature to generate volatile gas substances. The moisture content is the water molecules that physio-chemically bond to the solid fuel material; however, for coal or biomass, the moisture content can be removed by heating without any chemical reactions occurring. The volatile matters that are released from coal or biomass decomposition reactions contain a series of gaseous molecules of hydrogen, carbon monoxide, carbon dioxide and other hydrocarbons. The decomposition rate and released gas composition are affected by temperature and heating rate. The decomposition reactions are also termed as pyrolysis or devolatilization. The remaining solid from devolatilization of the solid fuel (biomass or coal) is called char, which consists of fixed carbon and ash. The ash content is defined as the mass percentage (or weight percentage, wt %) of the remaining solid to the chars after char complete combustion. The proximate analysis results for selected biomass and coals are listed in the table below:

Table 2.1: typical proximate analysis data of selected biomass and coals (wet base).

Fuel type	Moisture (wt %)	Volatile matter (wt %)	Fixed carbon (wt %)	Ash (wt %)
Pine (dried)(1)	12	71.5	16	0.5
Eucalyptus (dried)(2)	10.6	74.8	13.9	0.7
Lignite(3)	31.03	34.82	11.86	22.28
Sub-bituminous coal(4)	29.2	30.8	34.4	5.5

(1) & (2) (Franco et al. 2003b) (3) (Haykiri-Acma and Yaman 2007) (4) (Gordillo et al. 2009)

From Table 2.1, it can be seen that in general biomass contains more volatile matters while coals contain more fixed carbon and more ash; therefore, the char yield from the biomass is much lower than that of coals. The moisture content in the biomass is lower because the coal moisture

content is measured as that received whereas the biomass is air-dried from an initial moisture content normally above 100%.

Ultimate analysis gives the elemental constitution of a particular fuel in mass fraction or weight percentage (wt %) in a dry ash-free basis (daf). Ultimate analysis is performed by complete combustion of the fuel normally on the oven-dried material. Composition of the combustion final products are analysed and the main elements of the solid fuel are determined. Ultimate analysis results of the selected biomass and coals are listed in Table 2.2 below.

Table 2.2: Ultimate analysis data of selected biomass and coals (dry ash free basis, daf).

Fuel type	C (wt%)	H (wt%)	O (wt%)	N (wt%)	S (wt%)	H/C	O/C
Pine (1)	51.6	4.9	42.6	0.9	(-)	0.095	0.826
Eucalyptus (2)	52.8	6.4	40.4	0.4	(-)	0.121	0.765
Lignite (3)	56.6	5.6	35.1	1.5	1.2	0.129	0.424
Sub-bituminous(4)	81.2	5.7	8.8	1.0	3.3	0.072	0.239

(1)&(2) (Franco et al. 2003b); (3) (de Souza-Santos 2004); (4) (Skodras and Sakellaropoulos 2002)

From Table 2.2, it can be seen that the biomass contains more oxygen and less carbon compared with the coal. The high oxygen content in the biomass is due to the acid alcoholic groups in the cellulose, hemicelluloses and lignin. However, the coals contain higher contents of sulphur and nitrogen as well as other metal elements. The metal elements are not given in the ultimate analysis but can be determined from ash analysis. It is also observed in Table 2.2 that the ratio of O/C for the biomass is much higher than that of coals while the H/C ratios for the two types of solid fuels (biomass and coal) are similar.

2.2.2 Microstructure and chemical composition

In order to better understand and describe the co-gasification process of biomass and coal, examination and analysis of the microstructure and chemical composition of each fuel as well as their blend is necessary. The chemical composition of the coal and biomass is highly dependent

on the material species and origin. Coal is a combustible, brown to black sedimentary rocky fossil fuel degraded from slow carbonization or a deterioration process of ancient forest body and other plants, which has lain under the earth's surface layer for millions of years. It consists principally of organic substances, namely vitrinite, liptinite, intertinite maceral groups, inorganic minerals, and moisture (Kural 1994). Elementally, coal is composed of mainly carbon and a small proportion of hydrogen and oxygen, and its structure is highly complicated and random; there is no exact structural formula for coal. The chemical formula of coal is generally expressed in the empirical form of CH_xO_y, based on the molar fraction of each element of the coal being analysed. Based on the formation age of the carbonization process, the coal can be classified into different types (de Souza-Santos 2004). In general, the carbon content in the coal increases with the age of carbonization, thus coal with a high carbon fraction is classified as high quality coal that has a higher heating value, such as anthracite and bitumen. On the other hand, coal with a higher oxygen fraction is classified as low quality coal that has a lower heating value, such as lignite.

Oven-dry woody biomass contains three main components: cellulose, hemicellulose and lignin (McKendry 2002). Cellulose and hemicellulose are polysaccharides, which have chemical formulae of $(C_6H_{10}O_5)_m$ and $(C_5H_8O_4)_n$ with the degree of polymerization *m* and *n* being less than 10000 and 50-300 respectively. Lignin consists of aromatic, phenolic and various hydro-carbon groups, and the structure has a high degree of randomness. The fraction of these three main components of biomass varies among the species and origin (Couhert et al. 2009), therefore, biomass composition is normally expressed in empirical form CH_xO_y based on the molar fraction of the elements.

2.3 Thermochemical Conversion of Solid Fuel to Energy

Thermochemical conversion technologies are promising technologies for both current commercial operations and for future energy production. There are three main pathways of the thermochemical conversion process: pyrolysis (liquefaction is classified as a special pyrolysis process), gasification and combustion. The difference between these three routines is the different equivalence ratio (ER) value, which is defined as the ratio of the actual feeding rate of

the oxidization agent i.e. O_2 to the theoretically stoichiometric demand for complete combustion of a given solid fuel.

Pyrolysis is the degradation process of carbonaceous substance, when under heating in absence of oxygen (ER = 0) the solid fuel decomposes into solid char, condensable liquids and non-condensable gases. The product distribution is dependent upon the operating conditions such as temperature, pressure, heating rate and residence time. Based on the heating rate, this process can be classified into slow and fast pyrolysis, with the heating rate in order of 10 K/s and 10^3-10^4 K/s respectively. In general, with elevated temperature and a higher heating rate, gaseous product yield increases and mean molecular weights decrease. The pyrolysis liquid products can be up-graded for liquid fuel, and gas products can be used as fuel gas.

Gasification is the process that converts solid fuel into gaseous products at high temperatures with ER = 0.25 ~ 0.5. In this way, partial combustion occurs to provide heat for overall endothermic gasification reactions among solid char and devolatilization gases to produce a gas mixture that contains combustible gases such as H_2, CO and CH_4 as well as other hydrocarbons. This gas mixture is termed as producer gas or product gas. Producer gas can be used as fuel gas or be further processed into more valuable energy products.

Combustion of solid fuel is the thermal chemical process in which sufficient oxidization agent (air or oxygen) is provided (ER $\geq$1), such that complete oxidization reaction between solid fuel and oxygen can be ensured in order to acquire maximum heat. The gas product from solid fuel combustion consists of mainly H_2O, CO_2, excessive O_2 and N_2 (when air is used) and is referred to as flue gas. The heat being generated from this process can be used to generate electricity or provide heat or both. Coal combustion has been used in commercial power plants for more than a century. In recent years, coal-biomass blends have been used in co-combustion (or co-firing) to partially substitute for coal in large scale power generation plants.

Among the different routines of the thermochemical process, gasification has shown several advantages. Firstly, the energy efficiency of gasification is higher compared to combustion and pyrolysis. Furthermore, there is flexibility for the producer gas applications; that is the producer gas can be used for power and heat generation, for liquid fuel synthesis or for hydrogen purification. In addition, the gasification process can be optimised to achieve the required gas

composition based on the target producer gas application by changing operation conditions and controlling feeding streams (fuel and gasification agents).

2.4 Gasification Processes of Biomass and Coal

The gasification process of biomass, coal and other solid fuels is a complicated process involving a series of physical changes and chemical reactions. In a gasifier, four main stages can be identified:

- Firstly, solid fuel once it enters the gasifier starts drying as the particle temperature increases to 100^{o}C. In this stage, moisture migrates from inner particles to the surface and then evaporates to form water vapour.
- After drying, the solid fuel starts to thermally decompose as the temperature increases to above 200^{o}C, with the volatile matters leaving the fuel particles and residue solid, mainly carbon, retained in the fuel to form chars. This stage is called pyrolysis or devolatilization, which can be further divided into primary and secondary pyrolysis. In primary pyrolysis, the large molecules of the coal or biomass decompose into smaller gas molecules, condensable tars and solid char. The tars are then further thermally decomposed into gas and char, and this step is referred to as secondary pyrolysis.
- Thirdly, the carbon atoms in the solid char react with the gaseous molecules of either the volatile gas or gasification agent gas. These reactions are referred to as heterogeneous reactions in which reaction rates become significant at higher temperatures, typically above 700^{o}C.
- Lastly, reactions between the gaseous species take place and this is referred to as homogeneous reactions.

In each stage, heat and mass transfers take place simultaneously between the solid particles and the gases, which also affects the reaction rates. The overall gasification process is illustrated in Figure 2.1 and the details of each step are described in the following sections.

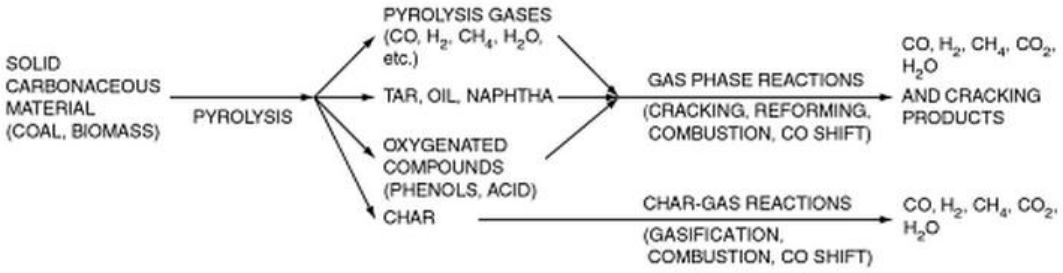

Figure 2.1: Stages of the gasification process of biomass and coal (Higman and Burgt 2003).

2.4.1 Drying

The drying process starts when the solid material is heated, and the drying rate becomes significant when the material is heated to above 100^{o}C. The drying characteristics are related to the type of solid fuel and the level of moisture content. For fresh woody biomass, there are three states of moisture: (1) liquid water in the void space of the wood cell cavities. This state of moisture is also called free water, which is not bonded to the solid constituents of the wood cell wall and therefore is easy to be removed, (2) bound water, which is physic-chemically attached to the hydroxyl groups of the wood solid constituent, and (3) water vapour existing in the void of wood, mainly as water vapour within the vessels and capillaries. The bound water has a maximum moisture content of around 30% above which the additional water exists as free water. The moisture content of the fresh woody biomass varies from up to 200%, e.g. in the outer part of *Pinus radiata* stem (sapwood) to around 40-50% in the core part of the *Pinus radiata* stem (heartwood).

On the other hand, the moisture content in coals varies significantly for different types of coal, for example anthracite coal has a moisture content from 2.8 to 19% (dry base), bituminous coal has a moisture content from 2.2% to 19%, and lignite has a moisture content of 25% to 40%. There are five types of moisture associated with the coal solid constituent (Karthikeyan et al. 2009): (1) interior adsorbed water that exists in pores and micro-capillaries within coal particles, (2) surface adsorbed water that forms a layer of water molecules on the coal surface, (3) capillary water contained in capillaries and small crevices, (4) inter-particle water that is contained in

capillaries or crevices between two or more particles, and (5) adhesion water that forms a film around individual or agglomerated particle surfaces.

Removal of moisture from the solid fuels prior to gasification is important to increase the conversion efficiency and to improve the producer gas quality (Pang and Mujumdar 2010). Since the energy consumption for heating the wet material and evaporating the water is considerably high, it consumes a high quantity of energy in the gasifier. For example, it is reported that about 7~10% of the fuel input is used to evaporate the water in a boiler that burns high moisture coals. Also, the presence of the moisture can affect the pyrolysis product distribution (Demirbas 2008) (Yip et al. 2009) (Min and Zhang 2010). Due to the fast process at high temperature, the drying step is commonly integrated with the pyrolysis stage and water vapour is considered as a gas producer species in the modelling of gasification of solid fuels (Bilbao et al. 1996; de Diego et al. 2002; Massaquoi and Riggs 1983).

2.4.2 Pyrolysis

In the gasification of a solid fuel, pyrolysis occurs after initial drying when the fuel temperature rises over approximately 200^{o}C, in which the solid fuel undergoes a series of complex physical and chemical changes. In the pyrolysis, chemical bonds within large organic molecules and polymers start to break up, thus the sub-groups of hydrocarbons and other simpler molecules are released and evaporate to form volatile matters. The volatile matters can be divided into two main categories: permanent gases and condensable liquids. The gases mainly consist of H_2, CO, CO_2, CH_4, and water vapour, while the condensable gases (tar) are formed mainly by the large hydrocarbon molecules. The condensable gases become liquid when the gas mixture is cooled down to below its boiling point. After the volatile matters escape, the remaining carbon molecules and other minor metal elements are left as solid and are called chars.

The product distribution of pyrolysis (gases, liquid and char) is highly dependent on temperature, heating rate, resident time and pressure. In general, a higher temperature and higher heating rate favours the formation of lighter hydrocarbons and may crack the tar molecules, thus enhancing the yield of permanent gases. On the other hand, a lower temperature and longer residence time favours the formation of char. According to the temperature and the heating rate, the pyrolysis

can be classified as slow or fast pyrolysis. In the gasification process, the temperature is normally above 700°C thus the pyrolysis stage falls into the fast pyrolysis category.

From the above analysis, the actual pyrolysis process of biomass and coal is extremely complicated; therefore, several types of simplified mechanism have been proposed to approximate the pyrolysis of coal, biomass and other solid fuels. These models include:

1. One-component model (Solomon et al. 1988; Thurner and Mann 1981) that considers the solid fuel as single component. Volatile matters, tars and char are generated from a general reaction. The single component model has the semi-global form from which each species in the generated gases, tars and char is regarded as an independent species and determined with its own semi-global kinetics (Shafizadeh and Chin 1977).
2. Multi-component model for biomass that calculates the pyrolysis rates of the main wood constituents (cellulose, hemicellulose and lignin) independently, with different reactions and kinetics (Helsen and Van den Bulck 2000; Orfão et al. 1999).
3. Distributed activation energy model (DAEM) (Navarro et al. 2009; Please et al. 2003; Ulloa et al. 2004) that employs a series of first order reaction kinetics for each element and compound in the generated species. This model assumes that the generating rate of each component is proportional to the original content in the fed solid fuel and the reaction of each component species has corresponding values of activation energy and pre-exponential factors. This model can be employed to calculate the reaction rate of every species generated at a given time.

From the above description, it is apparent that the one component pyrolysis model is the simplest whereas the DAEM is the most complicated. The DAEM has shown satisfactory prediction on the pyrolysis process of coal and biomass at low to medium operating temperatures with a slow heating rate. However, for fast pyrolysis with a high operating temperature and high heating rate in the gasifier, especially coupled with subsequent gasification, the DAEM is too complicated and may not give satisfactory results. In the gasification, the pyrolysis process normally takes a second or a fraction of a second, and thus the whole pyrolysis process can be considered as instantaneous.

The pyrolysis mechanisms and the models described above are illustrated in Figures 2.2 to 2.6. In modelling the fast pyrolysis in gasification, one component model, which predicts the characteristic time of pyrolysis process, is the most commonly used because it is simple and suitable for coupling with subsequent chemical reactions and transport processes (Di Blasi 1998). The one component pyrolysis model can be either simple step or multi-step. For the single step model which is shown in Figure 2.2, the raw solid fuel decomposed into the final products in a lumped overall kinetic. For the multi-step model shown in Figures 2.3,4&6, the solid fuel pyrolysis into the final products via more than one parallel and competing step, the whole pyrolysis reaction network consists of several sub-reactions, each with an individual kinetic.

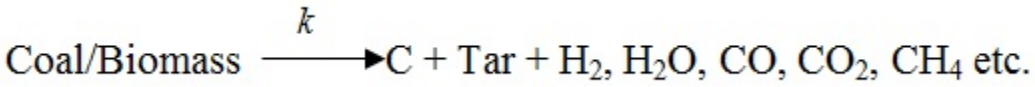

Figure 2.2: Single step mechanism for pyrolysis of coal and biomass.

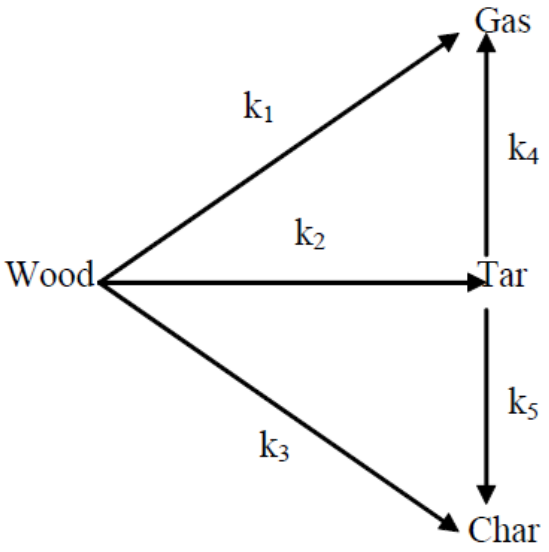

Figure 2.3: Semi global pyrolysis model by Shafizahed and Chin (1977)

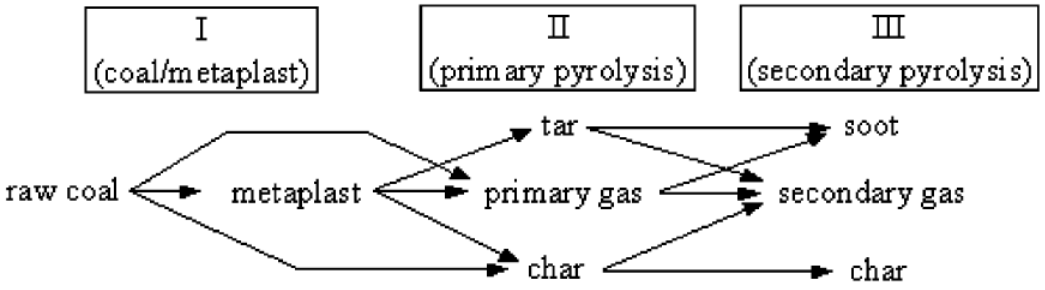

Figure 2.4: Pyrolysis mechanism proposed by Solomon *et al*. (Solomon et al. 1988).

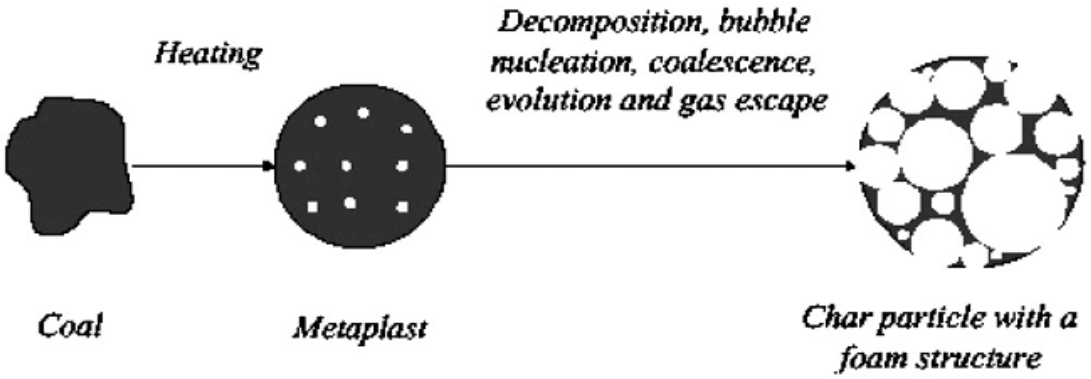

Figure 2.5: Coal structural evolution during pyrolysis (Solomon et al. 1988)

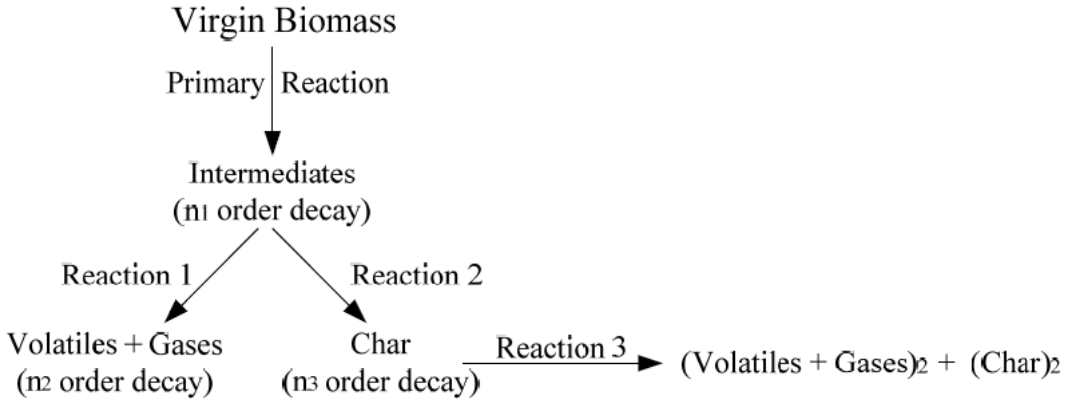

Figure 2.6: Biomass pyrolysis mechanism proposed by (Babu and Chaurasia 2004)

2.4.3 Heterogeneous reactions

In the gasification of coal and biomass, the heterogeneous reactions are those between char and gaseous species, including char combustion, steam gasification reaction, Bouduard reaction and methanation reaction. The heterogeneous reactions are the most important and critical to describe the gasification process since the heterogeneous reaction is slow compared to the pyrolysis and other reactions among gases, therefore, the overall gasification process is dominated by the heterogeneous reactions. This can be demonstrated in Figure 2.7.

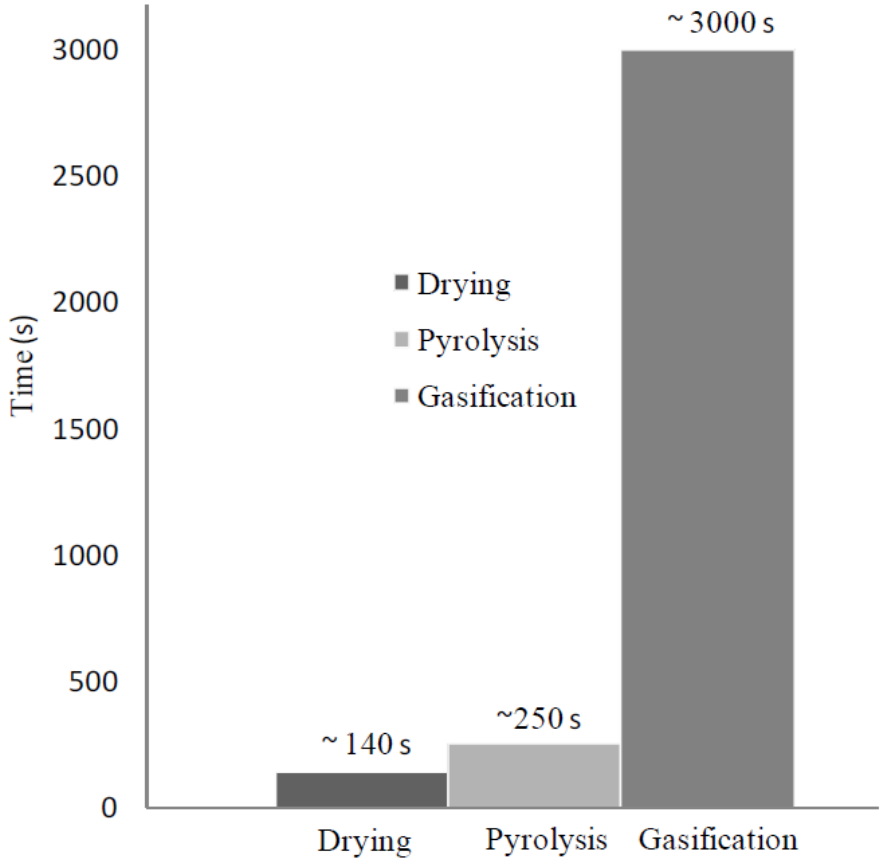

Figure 2.7: Characteristic times of stages in overall gasification process (Basu and Kaushal 2009).

The heterogeneous reactions include the following reactions:

1) Combustion of char including the total and partial oxidization of carbon:

$C + O_2 \rightarrow CO_2 \qquad \Delta H_R = -393.77$ kJ/mol carbon (2.1)

$C + 1/2O_2 \rightarrow CO \qquad \Delta H_R = -110.4$ kJ/mol carbon (2.2)

The ratio between these two carbon oxidization sub-reactions is dependent on temperature and the ER. For excess oxygen where ER>1, the combustion becomes the total oxidization and for ER<1, partial oxidization occurs. CO_2 is the main product at low temperature and formation of CO is favoured at elevated temperature (de Souza-Santos 2004).

2) Steam gasification reaction:

$C + H_2O \rightarrow H_2 + CO \quad \Delta H_R = 138.3$ kJ/mol carbon (2.3)

The steam gasification reaction is the partial oxidization of carbon by steam. Steam gasification can be between char and the supplied steam, or the water vapour generated during the pyrolysis which is called in-situ gasification.

With high steam supply, the other form of steam gasification may occur to form CO_2:

$C + H_2O \rightarrow H_2 + CO_2 \qquad \Delta H_R = 105.44$ kJ/mol carbon (2.4)

3) Boudruad reaction:

$C + CO_2 \rightarrow 2\ CO \quad \Delta H_R = 170.45$ kJ/mol carbon (2.5)

4) Methanation reaction

$C + 2H_2 \rightarrow CH_4 \quad \Delta H_R = -93.8$ kJ/mol carbon (2.6)

Comparing these four heterogeneous reactions, the rate of the combustion reactions (2.1 and 2.2) is the fastest and in an order of magnitude faster than steam gasification reactions (2.3 and 2.4). In turn, the steam gasification reactions are an order of magnitude faster than the Boudruad reaction (2.5), which is faster than the methanation reaction (2.6) (de Souza-Santos 2004).

2.4.4 Homogeneous reactions

The homogeneous reactions are those among gas species; both volatile gases and gasification agent gases, and these reactions include oxidization reactions of combustible gaseous species, water gas shift reaction, and steam methane reforming reaction as described below.

1) Oxidization reactions of combustible gaseous species:

$H_2 + 0.5O_2 \rightarrow H_2O \qquad \Delta H_R = -241.8$ kJ/mol (2.7)

$CO + 0.5O_2 \rightarrow CO_2 \qquad \Delta H_R = -282$ kJ/mol (2.8)

$CH_4 + 2O_2 \rightarrow CO_2 + H_2O \quad \Delta H_R = -802.3$ kJ/mol (2.9)

2) Water gas shift reaction:

$CO + H_2O \leftrightarrow H_2 + CO_2 \quad \Delta H_R = -42$ kJ/mol (2.10)

The forward water gas reaction is promoted at low temperatures whereas the equilibrium shifts to the backward reaction at high temperatures.

3) Steam methane reforming reaction:

$CH_4 + H_2O \leftrightarrow 3H_2 + CO \quad \Delta H_R = 232.8$ kJ/mol (2.11)

The steam methane reforming reaction is the slowest reaction among all homogeneous reactions.

2.5 Char Reactivity

Char reactivity is defined as the char consumption rate per unit mass of remaining char during the gasification and is commonly expressed as a function of char conversion rate, which is defined as the conversion ratio of converted carbon to the initial total carbon mass during the gasification. To understand and model the gasification process, quantification of char reactivity is important since char conversion is very slow and becomes the rate controlling reactions (Everson et al. 2006). Extensive studies on gasification of either pure coal or pure biomass have been found in relevant literature. The char reactivity of a given solid fuel is unique because of its

strong dependence on the structural and chemical properties of the char generated from the given solid fuel.

Substantial differences in the char reactivity have been found between coal char and biomass char, which can be attributed to their structural difference. In general, woody biomass char is more reactive than coal char (Kastanaki and Vamvuka 2006; Smoliński et al. 2011) as biomass char has lower density and is structurally more amorphous (Klose and Wolki 2004). Another reason for the high reactivity of biomass char is the catalytic effect of metal elements in the char (Asadullah et al. 2010). However, for some low rank coals such as lignite, the reactivity is promoted by the catalytic effect of metal elements (Clemens et al. 1998).

Gasification kinetics of blended coal and biomass chars have been experimentally studied in recent years. It has been reported that as the biomass char reactivity is generally higher than that of coal char (Kastanaki and Vamvuka 2005; Mastsumoto et al. 2009), the blended char reactivity can be increased by adding biomass to coals (Zhu et al. 2008). By addition of biomass to the coal, the effective exposed area is increased hence the intrinsic reactivity is enhanced (Lu et al. 2002; Sadhukhan et al. 2009). Also, a synergetic effect has been found that further increases the char reactivity due to the presence of alkali and alkaline earth metal (AAEM) elements. Na and K have the highest enhancement effect on the char reactivity followed by Mg and Ca, while Si and S have a negative effect on the char reactivity. Also, the AAEM can be removed from the solid surface by the volatile phase which may be re-adsorbed by the volatile-char diffusion process (Sonoyama et al. 2006). The presence of AAEM changes the structure of the char surface, and hence enhances the char reactivity (Yu et al. 2002). The volatile-char interaction may be significant enough to influence the char structure hence affect the char reactivity. A series of investigations on the volatilization and catalytic effect indicated that the volatile-AAEM interaction would not only affect the char structure but also affect the volatilization behaviour of the solid fuel. Exact reasons still remain unclear about the AAEM catalytic activity as a function of its concentration (Li et al. 2006; Li and Li 2006; Li et al. 2004; Quyn et al. 2002a; Quyn et al. 2003; Quyn et al. 2002b; Wu et al. 2004; Wu et al. 2002).

The differences in the physical and chemical properties of the biomass chars and the coal chars result in different gasification characteristics (Lu et al. 2002; Sadhukhan et al. 2009). In the

gasification, due to its low density and its amorphous property (Klose and Wolki 2004), the biomass char has shown much higher reactivity than the coal char.

However, the overall gasification reactions of the chars can be influenced by the intrinsic reaction rate and transportation of gases involved (Gupta and Saha 2003). The rate of heterogeneous reactions, which take place on the contact surface of solid char and reactant gas, is dominated by the overall inner surface area of the pores (Bhatia and Perlmutter 1980). The diameter of the pores also influences the transportation of the reactant gases into the solid and the resultant gases out of the solid (Krishna and Wesselingh 1997). Therefore, the gasification rate is dominated by chemical reactions and the rate of mass transfer which is, in turn, affected by the char structure.

In addition to experimental studies, theoretical investigation by mathematical modelling has also been reported in last two decades on the reaction kinetics for char gasification. Biggs and Agarwal (1997) developed a combustion model of a char particle in oxygen, in which reactions and diffusion processes were simulated by solving a one dimensional diffusion equation from which the reaction products were obtained under different operating conditions. Fu Y. Wang and Suresh K. Bhatia (Wang and Bhatia 2001) proposed a similar combustion model to investigate the structural evolution and fragmentation of the char. Yamashita and co-workers (Yamashita et al. 2006) developed a three dimensional model to simulate the structure evolution of the cubic shaped char particle.

2.6 Classification of Gasifiers

The classification of gasifiers has been based on two factors: 1) the way that heat is supplied to the gasifier, and 2) the structural configuration or the means of contact of materials in the gasifier.

For the first approach, gasifiers can be categorized as autothermal or allothermal. An autothermal gasifier provides the necessary heat of reaction by partial oxidation of solid fuel in the reactor with air or pure O_2 being fed into the gasifier as oxidant for a partial combustion reaction. In some cases steam is fed to increase the H_2 content in the producer gas. In an allothermal gasifier, the heat of reaction required is provided from an external source by means of internal circulation

of hot bed material into the gasification zone or by indirect heat supply (a heat exchanger, for example). In this case, pure steam can be fed as a gasification agent hence the hydrogen-rich syngas is produced, which is favourable for synthesis of liquid fuel or hydrogen purification.

Based on the structural configuration of the gasifier or the way of contact of gases and solid fuels in the gasification reactor, the gasifiers can be classified into three types: (1) fixed (moving) bed, (2) fluidized bed, (3) entrained flow.

In a fixed bed gasifier, there is a stationary grate above which the gasification occurs. The solid fuel (biomass, coal or their blends) is fed from the top and the gasification agent can be fed either above or below the grate. The producer gas can also be led out either from the bottom or from the upper part of the gasifier. The gas flow velocity in the fixed bed is very low and in this case the gas just percolates through the bed of solid particles, and the intensity of momentum exchange is not enough to move the particles. Therefore, the solid particle bed remains relatively stationary in a fixed bed gasifier although the feed solid fuel moves downward when the solid volume is reduced during the gasification process.

In a fluidized bed gasifier, the gasification agent is injected from the gasifier bottom and then flows through a bed of solid fuel, chars and inert bed material. The producer gas flows out from the upper part of the gasifier. The gas flow rate in the fluidized bed gasifier is higher than that in a fixed bed gasifier. With the increase in gas velocity, the solid bed will be expanded so that particles detach from neighbouring particles and the bed of particles will behave as fluid. The bed at this point is at the minimum fluidisation condition. Further increase in gas velocity will generate bubbles of excessive gas that bypass the bed and the gasifier operating at this condition is referred to as a bubbling fluidized bed gasifier. Further increase in the gas velocity will short-circuit particles passing through the gas bubbles and eventually lead to their disappearance. At this point the bed is a turbulent fluidized region and the upper bed surface is not clearly recognized.

As gas velocity is further increased to the point that particles start to be entrained upwards, this condition is called terminal velocity. Under this condition, some particles (fine particles of char, ash and inert bed material) will be carried out of the gasifier by the flowing producer gas while the rest of the particles (large particles of solid fuel) fall along the gasifier walls due to loss of

kinetic energy. Gasifiers operating under this condition are called circulating fluidized bed gasifiers.

With further increase in the gas velocity above the fast fluidisation region, a pneumatic transport region is achieved where all particles are completely carried out by the gas stream. Gasifiers operating at this condition are called pneumatic transport gasifiers.

An entrained flow gasifier normally handles liquid feedstock such as biomass pyrolysis slurry or black liquor from a pulp and paper mill, or pulverised fine particles of solid fuel. However, the entrained flow gasifier is beyond the scope of this study, thus it will not be discussed further in this thesis.

At the present, the fixed bed gasifier is the most commonly used gasifier followed by the fluidized bed gasifier. Details of each type of gasifier will be described in the following sections.

2.6.1 Fixed (moving) bed gasifier:

Fixed bed gasifiers can be classified into two types: updraft and downdraft gasifiers depending on the flow direction of gasification agent and producer gas as shown in Figure 2.8(a) for the updraft gasifier and Figure 2.8(b) for the downdraft gasifier. In the downdraft gasifier, carbonaceous solid fuel enters the gasifier from the top, and while moving to the bottom by the effect of gravity it undergoes drying, pyrolysis, combustion and gasification sequentially, and finally the residue ash leaves the gasifier from the bottom. The gasification agent is fed into the reactor at the location above the stationary grate, where combustion takes place, and flows downward through the gasification zone where most H_2 and CO are generated. The producer gas leaves the gasifier from the reactor bottom. On the other hand, for the updraft gasifier, solid fuel enters from the top and undergoes a similar process to that in the down draft gasifier, however the gasification agent is fed from the reactor bottom and the producer gas leaves from the reactor top.

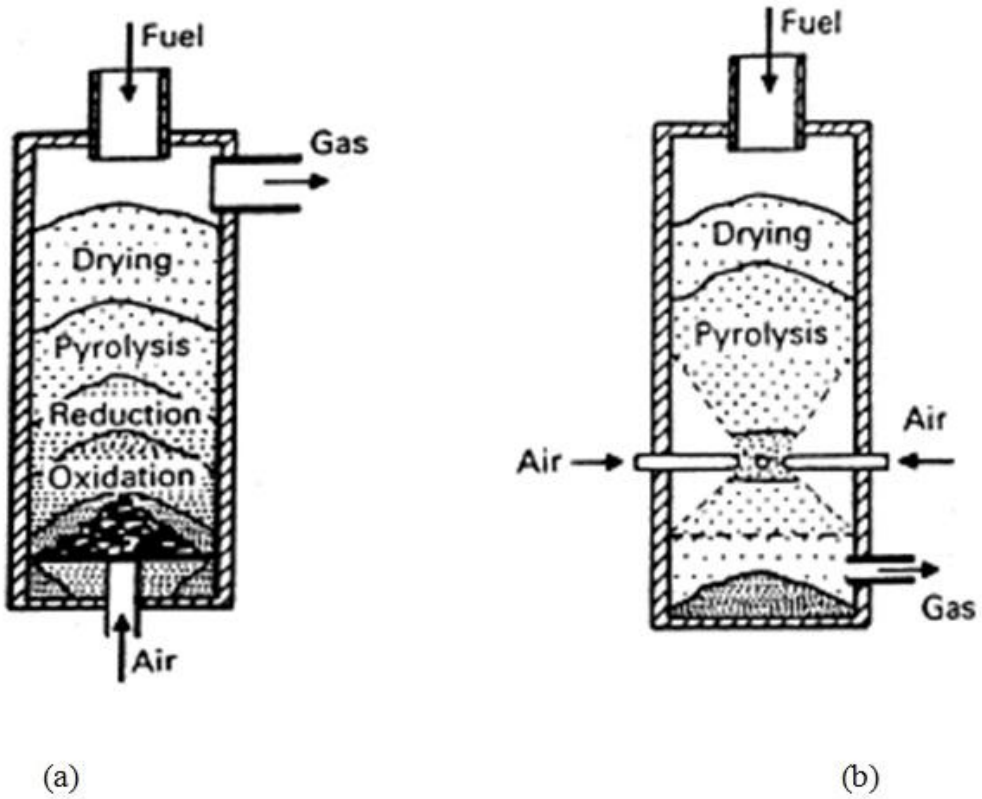

Figure 2.8: Schematic diagram of updraft (a) and downdraft fixed bed gasifier (b) (Warnecke 2000).

Comparing the two types of fixed bed gasifier, the downdraft version has the apparent advantage of low tar content in the producer gas, since the gas product from the pyrolysis goes through the combustion zone where the temperature can be above 1000^{o}C. In this way, the tar and heavy hydrocarbons in the volatile area will be cracked and the producer gas will be clean. In addition, the solid bed of feed fuel and char acts as a filter which removes the fine particulates. The disadvantage of this type of gasifier is the relatively low energy efficiency as the hot producer gas exits at a high temperature. On the other hand, the updraft gasifier has the advantage of high energy efficiency because the inlet solid fuel contacts the hot producer gas; hence the producer gas provides heat for the feed solid fuel for drying and pyrolysis. In this way, the producer gas leaves the reactor at a relatively low temperature. The issue of the updraft gasifier is that the producer gas has a high tar content hence gas cleaning is required to remove these contaminants. For both types of fixed bed gasifiers, the temperature distribution is non-uniform and the gas solid contact is non-homogeneous. Therefore, fixed bed gasifiers are suitable for small-medium scale plants of less than 1 MW for downdraft, and 1-10MW for updraft gasifiers (Basu, 2009).

2.6.2 Fluidized bed gasifier:

A fluidized bed gasifier is operated at the flow regime from the bubbling to circulation fluidized region. Apart from solid fuel, inert particles, normally silica sand and dolomite, are used as bed material as heat carriers or for enhancing heat and mass transfer between the gas and solid phases. The inert bed material is normally 90 wt% to 98 wt% of the total bed inventory (Van Loo and Koppejan 2008). The combustion and gasification reactions are promoted by intensive heat transfer and thorough mixing of solid fuel and gases within the bed. In operating the fluidized bed gasifier, the bed is firstly heated to the desired temperature, then solid fuel is fed into the reactor. The gasification agent (air, pure oxygen, steam or their mixture) is fed from the bottom of the gasifier and evenly injected into the bed by passing through a distributor, which also acts as a fluidisation agent. Based on the flow region and gasifier configuration, fluidized bed gasifiers are normally classified as bubbling fluidized beds (BFB) (Figure 2.9a) or circulating fluidized beds (CFB) (Figure 2.9b). As described earlier, in BFB the gas flow rate is maintained between the minimum fluidisation velocity and terminal velocity. However, in CFB, the gas flow rate is above the terminal velocity with fine particles (ash and un-converted char) and inert bed material being entrained and carried out of the gasifier by the producer gas. Then the particulates are separated from the producer gas in a cyclone where the producer gas leaves from the cyclone top and the inert bed material returns to the gasifier after the ash is removed.

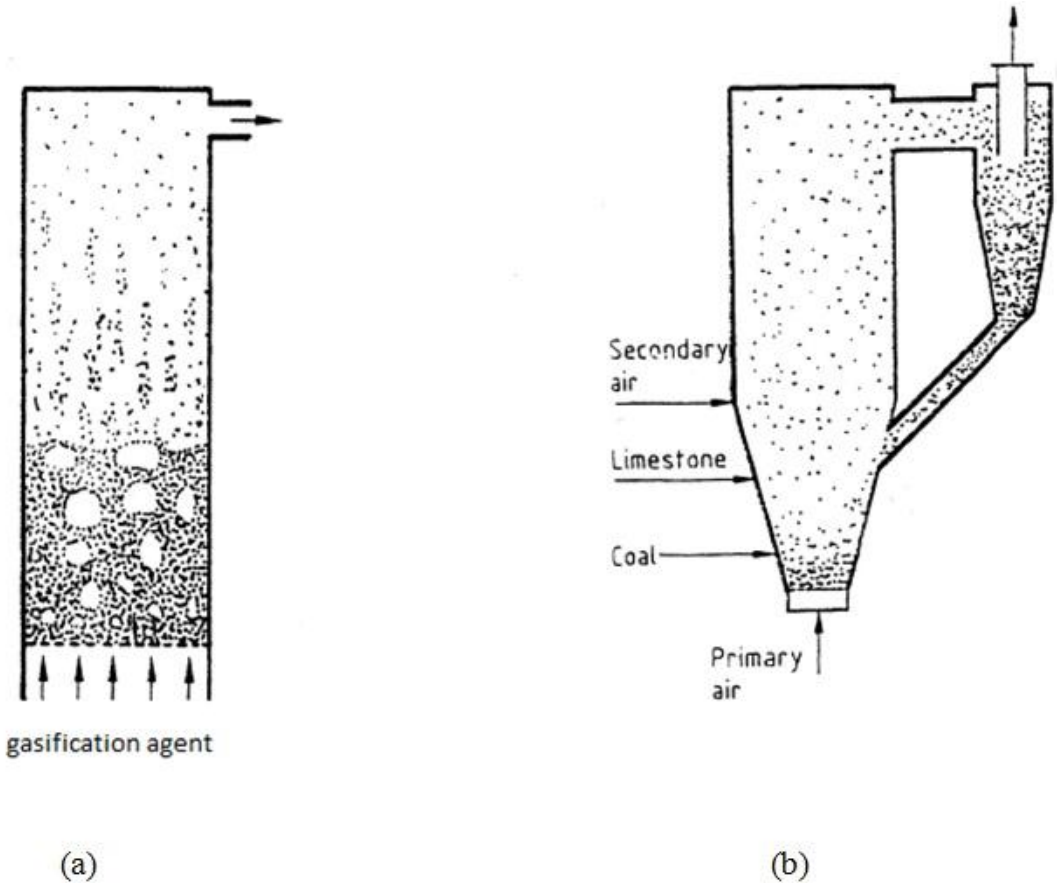

Figure 2.9: Schematic diagram of BFB (a) and CFB (b).

In a fluidized bed gasifier, the drying, pyrolysis (devolatilization) and gasification reactions take place simultaneously and evenly over the whole bed volume. The solid particles in the bed are mixed homogeneously and thus the process can be regarded as isothermal, especially for char particles because mixing is faster than char conversion (Gómez-Barea and Leckner 2010). The enhanced heat and mass transfer in the fluidized bed gasifier enable the solid fuel to be gasified at a relatively low operating temperature (700~900^{o}C) compared to the fixed bed gasifier. The tar content in the producer gas is normally higher than that in the downdraft fixed bed gasifier but is lower than that in the updraft fixed bed gasifier, and thus gas cleaning is required.

The BFB inventory must not be too high otherwise the required gas velocity must be increased for maintaining the fluidisation for the high bed material load. However, if the gas velocity exceeds the terminal velocity the particles will be entrained by the producer gas and leave. Therefore the BFB gasifier chamber is normally designed with a larger diameter so that the

height of the fluidized bed during the operation can be reduced in order to maintain the bubbling fluidisation state. On the other hand, a CFB gasifier can be operated at a higher gas velocity by implementing a cyclone to separate the solid particles and the producer gas. The collected particle is then directed back to the bed therefore the conversion of unreacted char can be further increased.

2.6.3 Entrained flow gasifier

An entrained flow gasifier handles the fine particles of feedstock fuel. The gasification agent velocity is very high so that the solid fuel particles are evenly dispersed and suspended in the stream. Under this flow condition, the gas flow entrains all of the fuel particles and then is injected into the reaction chamber where the fuel is ignited rapidly at a very high temperature, possibly over 2000^{o}C. The heat released by this intensive combustion leads to the instantaneous pyrolysis and simultaneous char gasification of the fuel to produce the producer gas consisting mainly of H_2 and CO. The producer gas of an entrained flow gasifier does not contain tars due to its very high operating temperature, however all ash is entrained by the producer gas thus ash removal is required downstream. Additional energy consumption is required in milling the feedstock into fine particles to a diameter less than 75 μm.

2.7 Modelling of Fluidized Bed Gasification

As the objective of this study was to model and optimize the fluidized bed gasification process, only the mathematical modelling studies related to the fluidized bed gasification process are reviewed and presented in this section. Mathematical modelling of fluidized gasification is important for reactor design and optimization of the gasification operation. Mathematical modelling is a process of using a simplified but representative way to describe and quantify a complicated process by means of equations, based on the fundamental physical, chemical and thermodynamic principles. Once validated, the models can be employed to examine the effect of fed feedstock, operating conditions, gasifier configuration and other factors that cannot be easily

experimentally quantified. In addition, the producer gas composition profile and final producer gas composition from the gasifier, gas yield, temperature profiles in the gasifier can be predicted.

Mathematical modelling of gasification process has been performed for decades, from the initially very simplified equilibrium (or zero dimensional) model based on reaction stoichiometry to the highly sophisticated three dimensional transient model that coupled fluidisation hydrodynamics and reaction kinetics through fundamental mass, momentum and energy balance equations. The gasification modelling approaches can be divided into the following four categories: (1) Equilibrium model, (2) Kinetic model, (3) Computational fluid dynamics gasification model and (4) Neural network model. In the following section, each category is described and discussed.

2.7.1 Equilibrium gasification model

The equilibrium model is also regarded as a zero dimensional model that predicts the producer gas composition from the gasification, based on the assumption of infinite residence time for the reactions to reach an equilibrium state. The result represents the ideal thermodynamically stable composition in corresponding to a given operating temperature and pressure. For simulation of the gasification process using the equilibrium mode, the solid fuel feeding rate and fuel elemental composition, gasification agent flow rate and composition, and operation temperature are required; however, minor elements are commonly ignored. The carbon conversion is assumed to be 100%; oxygen has been completely consumed in combustion with all reactions involved being at equilibrium. The producer gas consists of H_2, CO, CO_2, CH_4, H_2O and N_2 (if air is used as gasification agent). The model can be solved to determine the N-1 unknown variables for the fraction of each species in the producer gas where N is the total number of species in the producer gas.

The element balance for C, H and O are performed assuming that the input moles of each of these elements from the feed stock and the gasification agent are equal to the sum of the same element in the producer gas and ash (if ash is included). The chemical equilibrium constant of j^{th} reaction can be determined from the following equation (de Souza-Santos 2004):

$$K_j = \left(\prod_{i=1}^{n_{CP}} y_i^{\nu_{i,j}} \right) \left(\frac{P}{P_0} \right)^{\sum_{j=1}^{nCP} \nu i,j} = \exp\left(\frac{\Delta G_j}{\boldsymbol{R}T} \right) \tag{2.12}$$

The element balance equation coupled with the reaction equilibrium constants and the overall energy balance equation will form a system of N-1 independent equations with N-1 unknown variables, therefore the producer gas composition can be obtained.

The equilibrium model is simple and can be solved to calculate the theoretical producer gas composition that is most thermodynamically stable. Hence it gives reliable results when the operating temperature is high enough. However in many cases, the operating temperature is in the low to medium range and the carbon conversion is lower than 100%, therefore the equilibrium model is not appropriate in simulation of the gasification process.

2.7.2 Reaction Kinetic gasification model

The reaction kinetic model describes the gasification process with a reaction mechanism and contains a number of reaction kinetics, heat and mass transfer calculations. Therefore, the model consists of a set of high non-linear differential equations. The model needs to be solved using appropriate numerical methods to predict gas composition, gas yield and temperature profile within the gasifier. It needs the information of both reaction kinetics and fluidized bed hydrodynamics, and thus a typical reaction kinetic model contains the two sub-models; one for hydrodynamic and the other for reaction kinetics.

In the earlier kinetics model, the fluidized bed was treated as homogeneous single phase of perfectly mixed gases and solid particles. Either a perfectly-mixed or plug flow approach was used to quantify the flow behaviour based on the configuration of the gasifier. However this earlier kinetics model was not able to reflect the effect of bed hydrodynamics on the gasification process, therefore in the improved kinetics models developed later, the fluidized bed was divided into emulsion and bubble phases as illustrated in Figure 2.10 (Hamel and Krumm 2001). The emulsion phase contains all solids and some gases needed to maintain the bed at the minimum fluidisation state. In the emulsion phase, the gas and solid particles are assumed to be mixed

homogeneously. The bubble phase is formed by the excessive gas and considered as plug flow (Yan et al. 1998). The hydrodynamic model characterizes the gas-solid flow behaviour by using empirical or semi-empirical correlations which quantify key parameters such as bubble diameters, bubble rising velocities, bubble fractions, and emulsion phase voidage. Based on the flow behaviour, mass and heat transfer rates between the gas and emulsion phases can be determined using separate correlations.

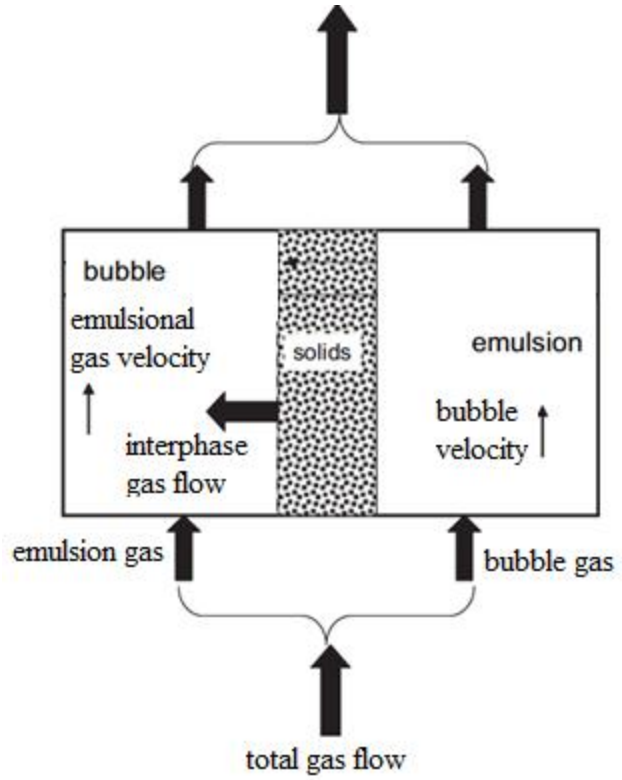

Figure 2.10: Two phase theory of the gas-solid system in a fluidized bed.

In the reaction kinetics model, the homogeneous model may be able to determine the reaction rates for the perfectly mixed single phase from the concentration of gaseous reactants and the reaction rate constants. However, the homogeneous model is not appropriate to describe the heterogeneous reactions between char particles and gases, as it does not include the diffusion mechanism, char structures or total available carbon, all of which will affect the overall gasification reaction rate (Wang and Bhatia 2001). In order to reflect the effects of these factors, several models have been proposed by researchers including: shrinking core model (Kimura 1992), random pore model (Molina and Mondragon 1998), and Johnson's kinetic model (Johnson 1974). The shrinking core model considers the film mass transfer process on the

particle surface, the internal diffusion and the intrinsic reaction rate in a single char particle. The random pore model takes into account the structural evolution of char particles during carbon conversion, which determines the maximum reactive area per unit char volume. Johnson's kinetic model is a semi-empirical model that takes into account the char structure, char type and operating conditions.

The kinetics model with consideration of bed hydrodynamics and reaction kinetics has been widely applied in modelling the fluidized bed gasification of coal and biomass as well as other carbonaceous fuels (Z'Graggen and Steinfeld 2008); (Ross et al. 2005); (Goyal et al. 2010);(Fiaschi and Michelini 2001; Kaushal et al. 2010; Nemtsov and Zabaniotou 2008). This type of kinetics model has recently been extended to include the two phase theory for simulation of solid fuel gasification (Aly 1999; Fuhou 2012). The kinetic model is moderately complex since variables along the gasifier height are considered either as steady state or as transient state depending on the interest of research. The reaction kinetic model is reliable in predicting the gasification process with simple cylindrical geometry since in most cases, the changes of variables in radial direction is negligible.

2.7.3 Computational fluid dynamics gasification model

The computational fluid dynamics (CFD) is a powerful tool in modelling the gas-solid system in the gasifier with complex geometry. The two or three dimensional partial conservation equations of mass, momentum and energy for each species are embedded into the CFD model over the defined domain, which is separated into numerous sub-elements or meshed with finite difference, finite volume or finite element methods. These discrete partial differential equations are solved simultaneously by the solver and results are then displayed. The CFD model has been applied in a fluidized bed gasifier for coal combustion and gasification in BFB, CFB and entrained flow gasifiers, but application in biomass gasification and co-gasification has not been found.

The CFD model for gasification has shown significant advantages over other types of models in modelling the system with intensive gas solid interactions at high gas velocity such as entrained flow combustion and gasification. However, the most significant drawback of the CFD model is that as it is the most sophisticated model, the computational times are significantly longer than

other methods, especially for system with several species being involved. Therefore the reaction kinetic method is still the most common model being used in investigating fluidized beds with slow gas velocity such as BFB.

2.7.4 Artificial neural network (ANN) model

The artificial neural network model is an alternative way of predicting the gasification outcome (producer gas composition, gas yield) without a comprehensive understanding of the details of the process. The principle of ANN is to predict the non-analytical solution corresponding to the system inputs from established input-output relationships. Such relationships were established based on a data pool that contains a large number of combinations of actual observations of inputs and outputs, and algebraic equations in expression of outputs as function of inputs were then built. This process is called training. The algorithm in the system enables the model to possess self-learning ability from new observations by adjusting the weight and threshold values of internal equations; hence the desired output can be given based on the system inputs. The neural network technique has been broadly applied in weather forecasting, signal processing and process simulation. The ANN method has also been applied in modelling gasification (Guo et al. 2001; Puig-Arnavat et al. 2013) (Guo et al. 1997). The main drawback of ANN modelling is the need for an extensive experimental or industrial data pool for training to predict reliable outputs, and inaccurate results can be predicted if the inputs differ from the original data of the neural network that was trained with. In addition, variation of the gasifier configuration and feedstock will also affect prediction accuracy.

In the above sections, four types of main approach in modelling the gasification process have been introduced and briefly discussed. The comparisons are summarized in Table 2.3 (Van Loo and Koppejan 2008).

Table 2.3: Overview of the usefulness of various model types for certain purpose

Application	Type of Model:						
	Thermo dynamic	Empirical		Expert	Physical/Chemical		CFD
		regression	process identification		stationary	dynamic	
System design/ optimization	++			+	++	++	
Apparatus design/ optimization		+		+	++	++	++
Process control design/optimization			++			++	
Selection of fuel for reactor				+	++	++	
Evaluation of opratnl. performance			+			++	

Note: + means the model is suitable for the given application but the accuracy is uncertain. ++ means the model is appropriate.

2.8 Co-gasification of Blended Biomass and Coal

Extensive studies have been found in the literature on gasification of either pure coal or pure biomass. However, there are limited studies reported on the co-gasification of blended biomass and coal, and there is an apparent lack of fundamental understanding of the interactive effects of coal and biomass during the co-gasification. Furthermore, there is no mathematical model on the co-gasification of coal and biomass found in the existing research. Due to the differences in the blending ratio and diversity in fuel (biomass and coal) properties, the mechanism of co-gasification of the blend is complicated and the effects of the blending ratio on the gasification process are still unclear (Franco et al. 2003a; Pan et al. 2000; Pinto et al. 2003; Pinto et al. 2007).

In the reported studies on the co-gasification of biomass and coal, most of the co-gasification tests were performed on a fluidized bed reactor using a gasification agent of air, steam or pure oxygen. From these studies, synergetic effects in the char reactivity have been found which can be attributed to the catalytic effect of AAEM content in the biomass (Andre et al. 2005; Aznar et al. 2006; Chmielniak and Sciazko 2003; de Jong et al. 1999; Gani et al. 2005; McIlveen-Wright et al. 2006; McLendon et al. 2004; Pan et al. 2000). Therefore, with an increase in the biomass blending ratio, the yield of char and tar are decreased and the carbon conversion rate (ratio of carbon elements converted into gas phase to total carbon in feedstock) increases. Cold

gasification efficiency also increases with the biomass blending ratio. However, the specific calorific value of the producer gas from the co-gasification is compromised due to the increase in CO_2 content in the producer gas as a result of biomass decomposition.

However, some studies report that synergetic effects were not found or were insignificant (Aigner et al. 2011; Collot et al. 1999; Kumabe et al. 2007). The possible reason for this is that in these studies, the biomass and coal were fed into the gasifier separately or as a loose mixture, thus the biomass and coal were segregated once entering the gasifier and then gasified separately.

There is no obvious synergetic effect observed in the co-pyrolysis of the biomass and coal mixture, each fuel decomposes independently and the total rate of weight loss equals the sum of weight loss of each fuel (Garcia-Perez et al. 2001; Jones et al. 2005; Meesri and Moghtaderi 2002; Moghtaderi et al. 2004; Pan et al. 1996; Vamvuka et al. 2003a; Vamvuka et al. 2003b; Vamvuka et al. 2003c). However, even in this case, the total volatile generation has shown some synergetic effect (Haykiri-Acma and Yaman 2007), and the initial devolatilization behaviour of the tar and toxic substances might not follow the additive rule. Unfortunately, research on the initial evolving characteristic of other gaseous products has not been found.

In the current practice of co-gasification, coal and biomass are fed into the gasifier after mixing. However, due to the density difference between biomass and coal, the two fuels are segregated in the fluidisation phase and thus the coal and the biomass are pyrolysed and gasified independently. This is undesirable since the difference in mean residence time of the two fuels will limit the robustness of the co-gasification operation. In order to generate co-pyrolysed char, one solution is to pre-mix and press the two fuels into pellets, and in this case, the gasification characteristic will differ from the intrinsic reaction rate because the effect of internal mass transfer resistance will be significant where the particle dimension is greater than a certain value (Paviet et al. 2008).

References

Aigner, I., Pfeifer, C., and Hofbauer, H. (2011). "Co-gasification of coal and wood in a dual fluidized bed gasifier." *Fuel*, 90(7), 2404-2412.

Aly, S. E. (1999). "Three phase model of a batch fluidized bed." *Warme- und Stoffubertragung Zeitschrift*, 34(5), 405-412.

Andre, R. N., Pinto, F., Franco, C., Dias, M., Gulyurtlu, I., Matos, M. A. A., and Cabrita, I. (2005). "Fluidized bed co-gasification of coal and olive oil industry wastes." *Fuel*, 84(12-13), 1635-1644.

Asadullah, M., Zhang, S., Min, Z., Yimsiri, P., and Li, C.-Z. (2010). "Effects of biomass char structure on its gasification reactivity." *Bioresource Technology*, 101(20), 7935-7943.

Aznar, M. P., Caballero, M. A., Sancho, J. A., and Frances, E. (2006). "Plastic waste elimination by co-gasification with coal and biomass in fluidized bed with air in pilot plant." *Fuel Processing Technology*, 87(5), 409-420.

Babu, B. V., and Chaurasia, A. S. (2004). "Pyrolysis of biomass: improved models for simultaneous kinetics and transport of heat, mass and momentum." *Energy Conversion and Management*, 45(9–10), 1297-1327.

Basu, P., and Kaushal, P. (2009). "Modeling of Pyrolysis and Gasification of Biomass in Fluidized Beds: A Review." *Chemical Product and Process Modeling*, 4(1), Art. 21.

Bhatia, S. K., and Perlmutter, D. D. (1980). "A random pore model for fluid-solid reactions: I. Isothermal, kinetic control." *A.I.Ch.E Journal*, 26, 379-386.

Biggs, M. J., and Agarwal, P. K. (1997). "The CO/CO2 product ratio for a porous char particle within an incipiently fluidized bed: a numerical study." *Chemical Engineering Science*, 52(6), 941-952.

Bilbao, R., Mastral, J. F., Ceamanos, J., and Aldea, M. E. (1996). "Modelling of the pyrolysis of wet wood." *Journal of Analytical and Applied Pyrolysis*, 36(1), 81-97.

Chmielniak, T., and Sciazko, M. (2003). "Co-gasification of biomass and coal for methanol synthesis." *Applied Energy*, 74(3-4), 393-403.

Clemens, A. H., Damiano, L. F., and Matheson, T. W. (1998). "The effect of calcium on the rate and products of steam gasification of char from low rank coal." *Fuel*, 77(9–10), 1017-1020.

Collot, A. G., Zhuo, Y., Dugwell, D. R., and Kandiyoti, R. (1999). "Co-pyrolysis and co-gasification of coal and biomass in bench-scale fixed-bed and fluidized bed reactors." *Fuel*, 78(6), 667-679.

Couhert, C., Commandre, J.-M., and Salvador, S. (2009). "Is it possible to predict gas yields of any biomass after rapid pyrolysis at high temperature from its composition in cellulose, hemicellulose and lignin?" *Fuel*, 88(3), 408-417.

de Diego, L. F., García-Labiano, F., Abad, A., Gayán, P., and Adánez, J. (2002). "Modeling of the devolatilization of nonspherical wet pine wood particles in fluidized beds." *Industrial & Engineering Chemistry Research*, 41(15), 3642-3650.

de Jong, W., Andries, J., and Hein, K. R. G. (Year). "Coal/biomass co-gasification in a pressurised fluidized bed reactor." *Renewable Energy. Energy Efficiency, Policy and the Environment. World Renewable Energy Congress V, 20-25 Sept. 1998*, Elsevier, Florence, Italy, 1110-1113.

de Souza-Santos, M. L. (2004). *Solid Fuels Combustion and Gasification,* Marcel Dekker, New York.

Demirbas, A. (2008). "Partial hydrogenation effect of moisture contents on the combustion oils from biomass pyrolysis." *Energy Sources, Part A: Recovery, Utilization, and Environmental Effects*, 30(6), 508-515.

Di Blasi, C. (1998). "Comparison of semi-global mechanisms for primary pyrolysis of lignocellulosic fuels." *Journal of Analytical and Applied Pyrolysis*, 47(1), 43-64.

Everson, R. C., Neomagus, H. W. J. P., Kasaini, H., and Njapha, D. (2006). "Reaction kinetics of pulverized coal-chars derived from inertinite-rich coal discards: Gasification with carbon dioxide and steam." *Fuel*, 85(7-8), 1076-1082.

Fiaschi, D., and Michelini, M. (2001). "A two-phase one-dimensional biomass gasification kinetics model." *Biomass and Bioenergy*, 21(2), 121-132.

Franco, C., Pinto, F., and Gulyurtlu, I. (2003a). "The study of reactions influencing the biomass steam gasification process." *Fuel*, 62(1), 835-842.

Franco, C., Pinto, F., Gulyurtlu, I., and Cabrita, I. (2003b). "The study of reactions influencing the biomass steam gasification process☆." *Fuel*, 82(7), 835-842.

Fuhou, L. (2012). "Operating conditions and kinetics of wastewater treatment in a three-phase biological fluidized bed reactor." *Advances in Chemical Engineering: ICCMME 2011, Vols. 396 - 398*, 396, 1989-1994.

Gani, A., Morishita, K., Nishikawa, K., and Naruse, I. (2005). "Characteristics of co-combustion of low-rank coal with biomass." *Energy and Fuels*, 19(4), 1652-1659.

Garcia-Perez, M., Chaala, A., Yang, J., and Roy, C. (2001). "Co-pyrolysis of sugarcane bagasse with petroleum residue. Part I: Thermogravimetric analysis." *Fuel*, 80(9), 1245-1258.

Gómez-Barea, A., and Leckner, B. (2010). "Modeling of biomass gasification in fluidized bed." *Progress in Energy and Combustion Science*, 36(4), 444-509.

Gordillo, G., Annamalai, K., and Carlin, N. (2009). "Adiabatic fixed-bed gasification of coal, dairy biomass, and feedlot biomass using an air–steam mixture as an oxidizing agent." *Renewable Energy*, 34(12), 2789-2797.

Goyal, A., Pushpavanam, S., and Voolapalli, R. K. (2010). "Modeling and simulation of co-gasification of coal and petcoke in a bubbling fluidized bed coal gasifier." *Fuel Processing Technology*, 91(10), 1296-1307.

Guo, B., Li, D., Cheng, C., Lü, Z.-a., and Shen, Y. (2001). "Simulation of biomass gasification with a hybrid neural network model." *Bioresource Technology*, 76(2), 77-83.

Guo, B., Shen, Y., Li, D., and Zhao, F. (1997). "Modelling coal gasification with a hybrid neural network." *Fuel*, 76(12), 1159-1164.

Gupta, P., and Saha, R. K. (2003). "Analysis of gas-solid noncatalytic reactions in porous particles: finite volume method." *International Journal of Chemical Kinetics*, 36, 1-11.

Hamel, S., and Krumm, W. (2001). "Mathematical modelling and simulation of bubbling fluidized bed gasifiers." *Powder Technology*, 120(1–2), 105-112.

Haykiri-Acma, H., and Yaman, S. (2007). "Synergy in devolatilization characteristics of lignite and hazelnut shell during co-pyrolysis." *Fuel*, 86(3), 373-380.

Helsen, L., and Van den Bulck, E. (2000). "Kinetics of the low-temperature pyrolysis of chromated copper arsenate-treated wood." *Journal of Analytical and Applied Pyrolysis*, 53(1), 51-79.

Higman, C., and Burgt, M. v. d. (2003). *Gasification*, Elsevier.

Johnson, J. L. (1974). "Kinetics of bituminous coal char gasification with gases containing steam and hydrogen." *Advances in Chemistry Series*(13), 145-178.

Jones, J. M., Kubacki, M., Kubica, K., Ross, A. B., and Williams, A. (2005). "Devolatilisation characteristics of coal and biomass blends." *Journal of Analytical and Applied Pyrolysis*, 74(1-2), 502-511.

Karthikeyan, M., Zhonghua, W., and Mujumdar, A. S. (2009). "Low-rank coal drying technologies—current status and new developments." *Drying Technology*, 27(3), 403-415.

Kastanaki, E., and Vamvuka, D. (2005). "A comparative reactivity and kinetic study on the combustion of coal-biomass cha blends." *Fuel*, 85(2006), 1186-1193.

Kastanaki, E., and Vamvuka, D. (2006). "A comparative reactivity and kinetic study on the combustion of coal–biomass char blends." *Fuel*, 85(9), 1186-1193.

Kaushal, P., Abedi, J., and Mahinpey, N. (2010). "A comprehensive mathematical model for biomass gasification in a bubbling fluidized bed reactor." *Fuel*, 89(12), 3650-3661.

Kimura, T. (1992). "Numerical model for reactions in a jetting fluidized bed coal gasifier." *Chemical Engineering Science*, 47(9), 2529-2534.

Klose, W., and Wolki, M. (2004). "On the intrinsic reaction rate of biomass char gasification with carbon dioxide and steam." *Fuel*, 84 885-892.

Krishna, R., and Wesselingh, J. A. (1997). "The Maxwell-Stefan approach to mass transfer." *Chemical Engineering Science*, 52, 861-911.

Kumabe, K., Hanaoka, T., Fujimoto, S., Minowa, T., and Sakanishi, K. (2007). "Co-gasification of woody biomass and coal with air and steam." *Fuel*, 86(5–6), 684-689.

Kural, O. C. (1994). *Coal : resources, properties, utilization, pollution*, Mining Faculty Istanbul Technical University, Istanbul.

Li, X., Hayashi, J.-i., and Li, C.-Z. (2006). "Volatilisation and catalytic effects of alkali and alkaline earth metallic species during the pyrolysis and gasification of Victorian brown coal. Part VII. Raman spectroscopic study on the changes in char structure during the catalytic gasification in air." *Fuel*, 85(10-11), 1509-1517.

Li, X., and Li, C.-Z. (2006). "Volatilisation and catalytic effects of alkali and alkaline earth metallic species during the pyrolysis and gasification of Victorian brown coal. Part VIII. Catalysis and changes in char structure during gasification in steam." *Fuel*, 85(10-11), 1518-1525.

Li, X., Wu, H., Hayashi, J.-I., and Li, C.-Z. (2004). "Volatilisation and catalytic effects of alkali and alkaline earth metallic species during the pyrolysis and gasification of Victorian brown coal. Part VI. Further investigation into the effects of volatile-char interactions." *Fuel*, 83(10), 1273-1279.

Lu, L., Kong, C., Sahajwalla, V., and Harris, D. (2002). "Char structural ordering during pyrolysis and combustion and its influence on char reactivity." *Fuel*, 81 1215-1225.

Massaquoi, J. G. M., and Riggs, J. B. (1983). "Mathematical modeling of combustion and gasification of a wet coal slab—I: Model development and verification." *Chemical Engineering Science*, 38(10), 1747-1756.

Mastsumoto, K., Takeno, K., Ichinose, T., Ogi, T., and Nakanishi, M. (2009). "Gasification reaction kinetics on biomass char obtained as bu-product of gasification in an entrained-flow gasifier with steam and oxygenat 900-1000 ^{o}C." *Fuel*, 88, 519-527.

McIlveen-Wright, D. R., Pinto, F., Armesto, L., Caballero, M. A., Aznar, M. P., Cabanillas, A., Huang, Y., Franco, C., Gulyurtlu, I., and McMullan, J. T. (2006). "A comparison of circulating fluidized bed combustion and gasification power plant technologies for processing mixtures of coal, biomass and plastic waste." *Fuel Processing Technology*, 87(9), 793-801.

McKendry, P. (2002). "Energy production from biomass (part 1): overview of biomass." *Bioresource Technology*, 83(1), 37-46.

McLendon, T. R., Lui, A. P., Pineault, R. L., Beer, S. K., and Richardson, S. W. (2004). "High-pressure co-gasification of coal and biomass in a fluidized bed." *Biomass and Bioenergy*, 26(4), 377-388.

Meesri, C., and Moghtaderi, B. (2002). "Lack of synergetic effects in the pyrolytic characteristics of woody biomass/coal blends under low and high heating rate regimes." *Biomass and Bioenergy*, 23(1), 55-66.

Min, F., and Zhang, M. (2010). "Influence of initial moisture on pyrolysis of fresh biomass." *International Journal of Oil, Gas and Coal Technology*, 3(3), 278.

Moghtaderi, B., Meesri, C., and Wall, T. F. (2004). "Pyrolytic characteristics of blended coal and woody biomass." *Fuel*, 83(6), 745-750.

Molina, A., and Mondragon, F. (1998). "Reactivity of coal gasification with steam and CO_2." *Fuel*, 77, 1831–1839.

Navarro, M. V., Murillo, R., Mastral, A. M., Puy, N., and Bartroli, J. (2009). "Application of the distributed activation energy model to biomass and biomass constituents devolatilization." *AIChE Journal*, 55(10), 2700-2715.

Nemtsov, D. A., and Zabaniotou, A. (2008). "Mathematical modelling and simulation approaches of agricultural residues air gasification in a bubbling fluidized bed reactor." *Chemical Engineering Journal*, 143(1–3), 10-31.

Orfão, J. J. M., Antunes, F. J. A., and Figueiredo, J. L. (1999). "Pyrolysis kinetics of lignocellulosic materials—three independent reactions model." *Fuel*, 78(3), 349-358.

Pan, Y. G., Velo, E., and Puigjaner, L. (1996). "Pyrolysis of blends of biomass with poor coals." *Fuel*, 75(4), 412-418.

Pan, Y. G., Velo, E., Roca, X., Manya, J. J., and Puigjaner, L. (2000). "Fluidized-bed co-gasification of residual biomass/poor coal blends for fuel gas production." *Fuel*, 79(11), 1317-1326.

Pang, S., and Mujumdar, A. S. (2010). "Drying of woody biomass for Bioenergy: Drying technologies and optimization for an integrated Bioenergy plant." *Drying Technology*, 28(5), 690-701.

Paviet, F., Bals, O., and Antonini, G. (2008). "The effects of diffusional resistance on wood char gasification " *Process Safety and Environmental Protection*, 86, 131-140.

Pinto, F., Franco, C., and Andre, R. N. (2003). "Effect of experimental conditions on co-gasification of coal, biomass and plastic wastes with air/steam mixtures in a fluidized bed system." *2003*, 82(15), 1967-1976.

Pinto, F., Lopes, H., and Andre, R. N. (2007). "Effect of catalysts in the quality of syngas and by-products obtained by co-gasification of coal and wastes 1. Tars and nitrogen compounds abatement." *Fuel*, 86(14), 2052-2063.

Please, C. P., McGuinness, M. J., and McElwain, D. L. S. (2003). "Approximations to the distributed activation energy model for the pyrolysis of coal." *Combustion and Flame*, 133(1–2), 107-117.

Puig-Arnavat, M., Hernández, J. A., Bruno, J. C., and Coronas, A. (2013). "Artificial neural network models for biomass gasification in fluidized bed gasifiers." *Biomass and Bioenergy*, 49(0), 279-289.

Quyn, D. M., Wu, H., Bhattacharya, S. P., and Li, C.-Z. (2002a). "Volatilisation and catalytic effects of alkali and alkaline earth metallic species during the pyrolysis and gasification of Victorian brown coal. Part II. Effects of chemical form and valence." *Fuel*, 81(2), 151-158.

Quyn, D. M., Wu, H., Hayashi, J.-I., and Li, C.-Z. (2003). "Volatilisation and catalytic effects of alkali and alkaline earth metallic species during the pyrolysis and gasification of Victorian brown coal. Part IV. Catalytic effects of NaCl and ion-exchangeable Na in coal on char reactivity." *Fuel*, 82(5), 587-593.

Quyn, D. M., Wu, H., and Li, C.-Z. (2002b). "Volatilisation and catalytic effects of alkali and alkaline earth metallic species during the pyrolysis and gasification of Victorian brown coal. Part I. Volatilisation of Na and Cl from a set of NaCl-loaded samples." *Fuel*, 81(2), 143-149.

Ross, D. P., Yan, H.-m., Zhong, Z., and Zhang, D.-k. (2005). "A non-isothermal model of a bubbling fluidized-bed coal gasifier." *Fuel*, 84(12–13), 1469-1481.

Sadhukhan, A. K., Gupta, P., and Saha, R. K. (2009). "Characterization of porous structure of coal from a single devolatilized coal particle: Coal combustion in a fluidized bed." *Fuel Process Technology*, 90, 692-700.

Shafizadeh, F., and Chin, P. P. S. (1977). "Thermal deterioration of wood." In: *ACS Symposium Series 43*, 57–81.

Skodras, G., and Sakellaropoulos, G. P. (2002). "Mineral matter effects in lignite gasification." *Fuel Processing Technology*, 77–78(0), 151-158.

Smoliński, A., Howaniec, N., and Stańczyk, K. (2011). "A comparative experimental study of biomass, lignite and hard coal steam gasification." *Renewable Energy*, 36(6), 1836-1842.

Solomon, P. R., Hamblen, D. G., Carangelo, R. M., Serio, M. A., and Deshpande, G. V. (1988). "General model of coal devolatilization." *Energy & Fuels*, 2(4), 405-422.

Sonoyama, N., Okuno, T., Masek, O., Hosokai, S., Li, C.-Z., and Hayashi, J.-I. (2006). "Interparticle desorption and re-adsorption of alkali and alkaline earth metallic species

within a bed of pyrolyzing char from pulverized woody biomass." *Energy and Fuels*, 20(3), 1294-1297.

Thurner, F., and Mann, U. (1981). "Kinetic invesigation of wood pyrolysis." *Industrial & Engineering Chemistry, Process Design and Development*, 20(3), 482-488.

Ulloa, C., Gordon, A. L., and García, X. (2004). "Distribution of activation energy model applied to the rapid pyrolysis of coal blends." *Journal of Analytical and Applied Pyrolysis*, 71(2), 465-483.

Vamvuka, D., Kakaras, E., Kastanaki, E., and Grammelis, P. (2003a). "Pyrolysis characteristics and kinetics of biomass residuals mixtures with lignite." *Fuel*, 82(15-17), 1949-1960.

Vamvuka, D., Kastanaki, E., and Lasithiotakis, M. (2003b). "Devolatilization and combustion kinetics of low-rank coal blends from dynamic measurements." *Industrial and Engineering Chemistry Research*, 42(20), 4732-4740.

Vamvuka, D., Pasadakis, N., Kastanaki, E., Grammelis, P., and Kakaras, E. (2003c). "Kinetic modeling of coal/agricultural by-product blends." *Energy and Fuels*, 17(3), 549-558.

Van Loo, S., and Koppejan, J. (2008). *The handbook of biomass combustion and co-firing*, Earthscan, London.

Wang, F. Y., and Bhatia, S. K. (2001). "A generalised dynamic model for char particle gasification with structure evolution and peripheral fragmentation." *Chemical Engineering Science*, 56(12), 3683-3697.

Warnecke, R. (2000). "Gasification of biomass: comparison of fixed bed and fluidized bed gasifier." *Biomass and Bioenergy*, 18(6), 489-497.

Wu, H., Hayashi, J.-I., Chiba, T., Takarada, T., and Li, C.-Z. (2004). "Volatilisation and catalytic effects of alkali and alkaline earth metallic species during the pyrolysis and gasification of Victorian brown coal. Part V. Combined effects of Na concentration and char structure on char reactivity." *Fuel*, 83(1), 23-30.

Wu, H., Quyn, D. M., and Li, C.-Z. (2002). "Volatilisation and catalytic effects of alkali and alkaline earth metallic species during the pyrolysis and gasification of Victorian brown

coal. Part III. The importance of the interactions between volatiles and char at high temperature." *Fuel*, 81(8), 1033-1039.

Yamashita, T., Fujii, Y., Morozumi, Y., Aoki, H., and Miura, T. (2006). "Modeling of gasification and fragmentation behavior of char particles having complicated structures." *Combustion and Flame*, 146(1–2), 85-94.

Yan, H.-m., Heidenreich, C., and Zhang, D.-k. (1998). "Mathematical modelling of a bubbling fluidized-bed coal gasifier and the significance of 'net flow'." *Fuel*, 77(9–10), 1067-1079.

Yip, K., Wu, H., and Zhang, D.-k. (2009). "Mathematical modelling of Collie coal pyrolysis considering the effect of steam produced in situ from coal inherent moisture and pyrolytic water." *Proceedings of the Combustion Institute*, 32(2), 2675-2683.

Yu, J. L., Strezov, V., Lucas, J., Liu, G. S., and Wall, T. (Year). "A mechanistic study on char structure evolution during coal devolatilization - Experiments and model predictions." Combustion Institute, Sapporo, Japan, 467-473.

Z'Graggen, A., and Steinfeld, A. (2008). "A two-phase reactor model for the steam-gasification of carbonaceous materials under concentrated thermal radiation." *Chemical Engineering and Processing: Process Intensification*, 47(4), 655-662.

Zhu, W., Song, W., and Lin, W. (2008). "Catalytic gasification of char from co-pyrolysis of coal and biomass." *Fuel Processing Technology*, 89, 890-896.

Chapter 3 Experimental Investigation on Steam Gasification of Biomass and Coal blended Char

In this chapter, experiments were performed in a bench scale gasifier to investigate the effect of coal-to-biomass ratio on the reaction kinetics for steam gasification of the coal-biomass chars. In the experiments, the char particles of coal, biomass and blended coal and biomass were gasified using steam as gasification agent while nitrogen was used as a gas carrier. The gasification temperature was controlled at 850 to 950℃. Gas produced was analysed using a micro-GC to determine gas composition and gas yield from which the carbon conversion rate was also calculated. It was found that the blended coal and biomass chars had very distinct gasification characteristics from those of both the coal char and the biomass char, and the overall reaction rate increased with the increase in the biomass ratio in the blend. The microstructures of the coal char, biomass char and blended char were examined using scanning electronic microscopy (SEM), and it was found that the biomass char was more amorphous whereas the coal char had a larger macro pore size. The former enhanced the intrinsic reaction rate and the latter influenced the intra particle mass transportation in gasification of the blended char. The difference in mass transfer of the gasification agent into the particles between the two fuels was dominant in the char gasification.

3.1 Introduction

The literature review presented in Chapter 2 revealed that the gasification process can be divided into three major stages including drying, initial pyrolysis and subsequent gasification reactions both between char and gases (heterogeneous) and among gases (homogeneous). It was also found that the heterogeneous reactions are dominant in the gasification process as these reactions are slow compared to other reactions involved.

The char of the biomass and coal is an important part of the solid fuel decomposition in the gasifier. The yield and reactivity of the chars are the two most important parameters, since the

yield determines the total available amount of char that can be provided to the gasifier while the reactivity determines the rate of char being converted into gas. According to the results of literature review in Chapter 2, the char yield and reactivity can be influenced by many factors, but a clear trend could not be found. In order to thoroughly understand the co-gasification process of coal and biomass, knowledge of the char yield and reactivity first needs to be obtained. Therefore, the key factors that influence that influence the blending of biomass with coal on the char yield and reactivity were studied.

The objectives of this study were:

- To experimentally investigate the char yield for coal, biomass and blended coal-biomass during the initial pyrolysis;
- To determine the gasification reactivity of coal char, biomass char and blended coal-biomass char;
- To quantify the effects of the coal-biomass ratio on the overall reactivity and gas composition of steam gasification reaction of the coal char, the biomass char and the blended char.

This chapter presents new findings from the experimental work whereas the Chapter 4 will develop and validate a mathematical model to simulate the co-gasification process of the chars of blended biomass and coal. In the experimental work, the gasification characteristics (reaction kinetics and gas composition) were investigated and the microstructure differences between the coal char and the biomass char were examined. The results from this study were used in the mathematical modelling of gasification of coal, biomass, and blended coal and biomass pellets in fluidized bed gasifiers, and are reported in Chapters 5 & 6.

3.2 Experiments

3.2.1 Materials Preparation

In the experiments, t lignite coal and the wood of Eucalyptus nitens were selected as test materials. Lignite is a typical low quality coal that has vast reserves in New Zealand (Clemens et al. 1998) and Eucalyptus nitens is a fast growing plantation hardwood species (Neilsen and

Gerrand 1999). Before the experiments, the coal and the biomass were milled separately and sieved to particle sizes under 450 μm. Then parts of the two fuel particles were thoroughly mixed in a batch blender at the coal to biomass ratio 20:80, 50:50 and 80:20. After this, the fuel mixture of each batch as well as pure coal and pure biomass particles were loaded into a mould as shown in Figure 3.1. The mould consisted of three compartments: one hollow iron cylinder plus two smaller cylinders, as shown in the diagram below.

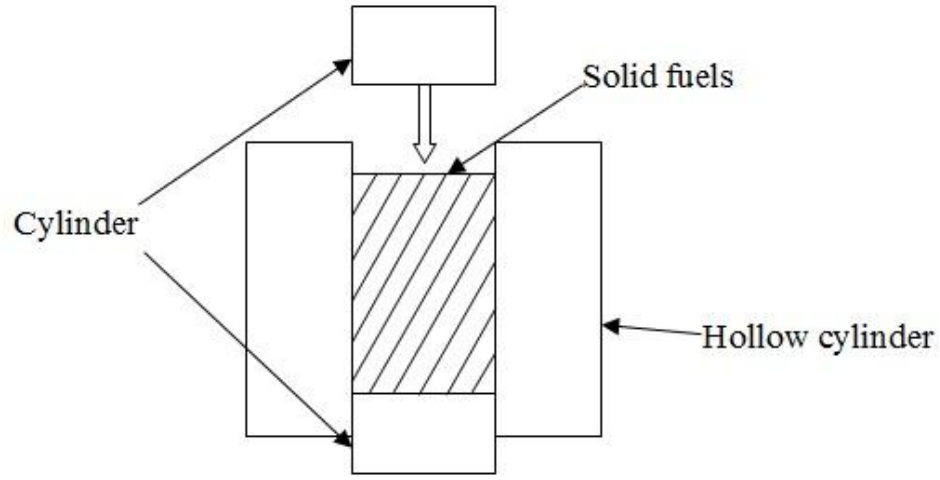

Figure 3.1: Sectional view of mould compartments used for pre-pressing the solid fuel.

A manual presser was firstly used to pre-press the material filled in the mould to make pre-pressed pellets. Then the pre-pressed pellets were compressed under a high pressure of 1.6 MPa by a hydraulic presser to make the final pellets, and in this way would undergo the char generation process (pyrolysis) without fragmentation and segregation of the two fuels. The pressed pellets had a diameter of about 6 mm and length of about 1cm. After this, the pellets of all batches were placed in an oven at 900^{o}C under an air isolated condition for seven minutes to generate solid chars and this pyrolysis process during the oven-heating completely removed the volatile components. The comparison of the pellets made and corresponding chars generated is shown in Figure 3.2 for different ratios of lignite to biomass.

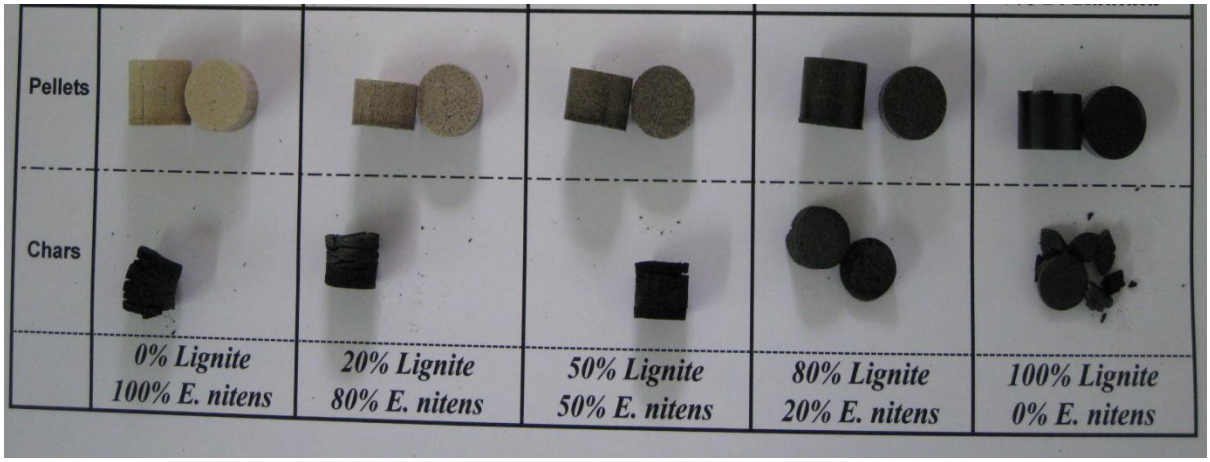

Figure 3.2: coal and biomass pellets and their co-generated chars used for reactivity test.

3.2.2 Apparatus

For the gasification experiments, the char particles were tested in a bench scale gasifier as shown in Figures 3.3 and 3.4, which consists of a nitrogen and water feeding system, a steam generator, a glass tube reactor, a gas cooler and a gas analyzer (Micro-GC). During the gasification experiment, the solid char pellets were held by a porous quartz frits on the bottom of the vertical tube reactor. The tube reactor was submerged into an electrically heated oven, and the temperature in the reaction zone was controlled at 850, 900 and 950°C respectively. Pure nitrogen was fed into the glass tube and residual volatiles were further removed from the char. Once the set temperature was reached, the water pump was started and the steam generator was turned on. Water was formed to steam at a rate of 1.7 mL/min. The gas mixture of nitrogen and generated steam was then fed to the top of the tube reactor in which the steam reacted with the solid char particles. The producer gas generated from the gasification process flew out with the carrier gas (nitrogen) from the outlet at the reactor bottom and then went through a water bath and resin flask to remove water vapour in the gas. Finally the moisture-free producer gas was continuously analysed using the Micro-GC from which the producer gas releasing rate and its composition were obtained and the actual steam gasification reactivity was determined. In each run, 1 g sample chars were loaded in the tube reactor and the nitrogen flow rate was controlled at 600 mL/min.

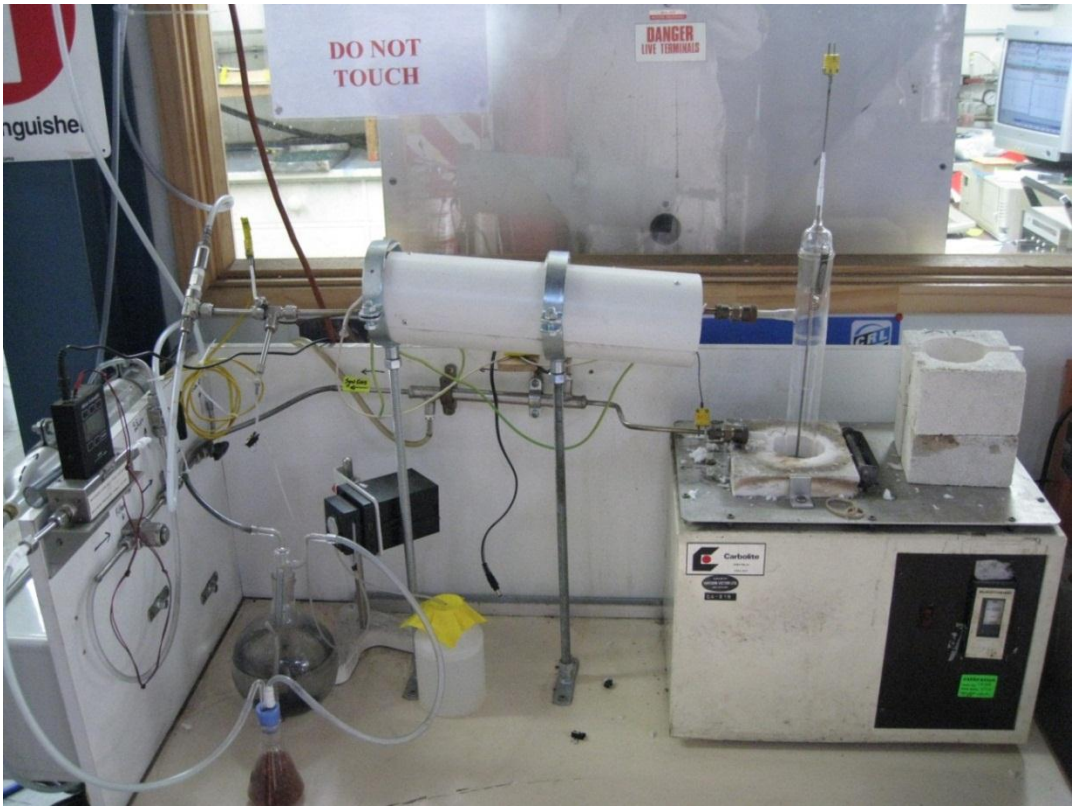

Figure 3.3: Bench scale gasification system of the char reactivity test.

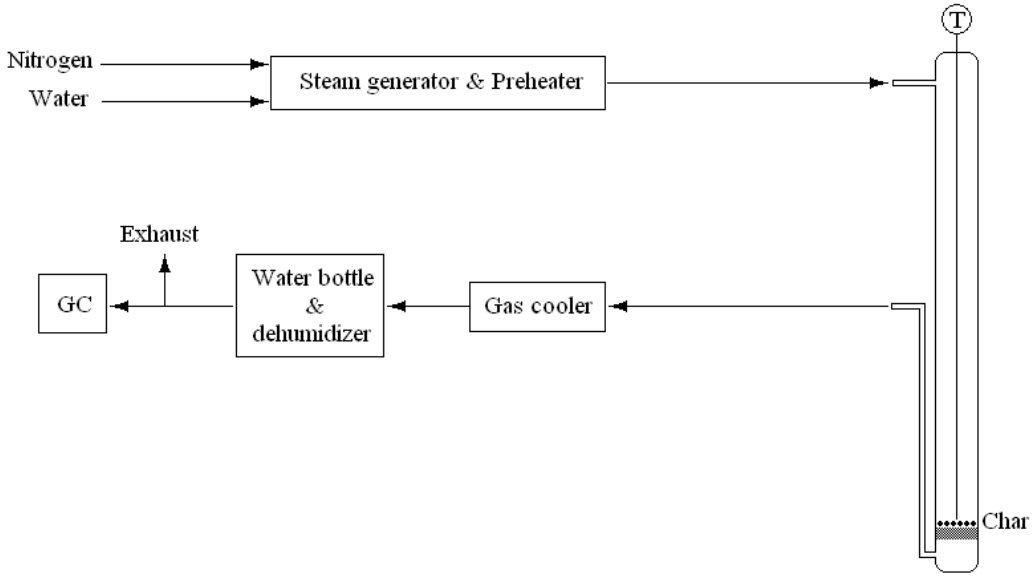

Figure 3.4: Flow Diagram of Experimental setup of the char reactivity test system.

3.2.3 Experiments Performed

(1) Char yield test

In order to understand the effect of the biomass blending ratio on char yield of blended pellets, the char yield test was performed. Pellets were made at coal to biomass blending ratios of 0:100, 20:80, 40:60, 50:50, 60:40, 70:30, 80:20, 90:10, 95:5 and 100:0, then chars of pellets for each blending ratio were generated following the method described in Section 3.2.1. The generated chars were weighed and the char yield was calculated for each blending ratio as the ratio of char mass divided by the initial pellet mass.

(2) Gasification reactivity test

By combining five blending ratio and three operation temperatures, a total of 15 runs of gasification reactivity experiments were carried out using the bench scale gasification system. The three gasification temperatures were 850, 900 & 950^{o}C and the five blending ratios (coal-to-biomass) 0:100 (pure biomass), 20:80, 50:50, 80:20 and 100:0 (pure coal).

(3) Microscopic scanning on char surface

In order to understand the difference in gasification performance between different chars, the microstructure and morphology of chars of coal, biomass and their blend (50:50) were examined using electronic microscopic scanning (SEM). Porosities of the biomass char and the coal chars were determined in terms of the mean pore diameters based on the SEM images.

(4) Tests of milled char reactivity

In order to investigate the effect of the gas diffusion resistance within the char particle, a separate set of experiments was conducted using milled chars of coal and biomass which had much smaller dimensions than the original char particles.

3.3 Results and Discussion

3.3.1 Char Yield of Biomass & Coal blending

The results of the char yield test are shown in the Figure 3.4 in which ratios of the generated char mass to the fresh fuel mass before pyrolysis are displayed as a function of the coal mass blending ratio in the fresh fuel. The results found that the char yield was only 15% for the pure biomass and this increased to 40% for the pure coal. The char yield shows a linear relationship with the coal blending ratio, thus the generated char yield of coal and biomass blend can be calculated once the mass blending ratio is known. This linear trend was similar to the results of other researchers (Sjöström et al. 1999) (Kajitani et al. 2009; Zhu et al. 2008).

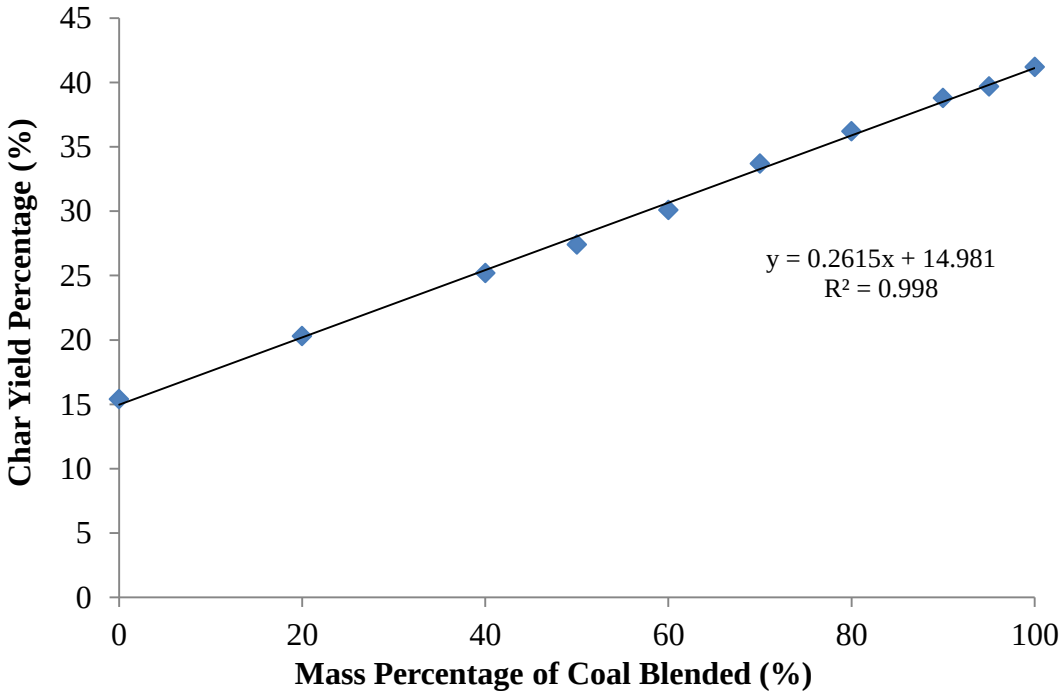

Figure 3.5: The char yield from the pyrolysis of char forming as a function of coal blend ratio.

3.3.2 Characteristics of Char Reactivity in Steam Gasification

From each run of the bench scale gasification experiments, the composition and generation of the producer gas as a function of elapsed time were determined from the continuous Micro-GC

analysis, and the results for an operation temperature of 900°C are shown in Figures 3.6 to 3.10 for coal-to-biomass ratios of 0:100; 20:80; 50:50; 80:20 and 100:0, respectively. In the figures, the nitrogen content is not shown as it only acted as a carrier and was not involved in the gasification reactions. The gas components of the char gasification producer gas were hydrogen (H_2), carbon monoxide (CO) and carbon dioxide (CO_2), which will be used for further analysis.

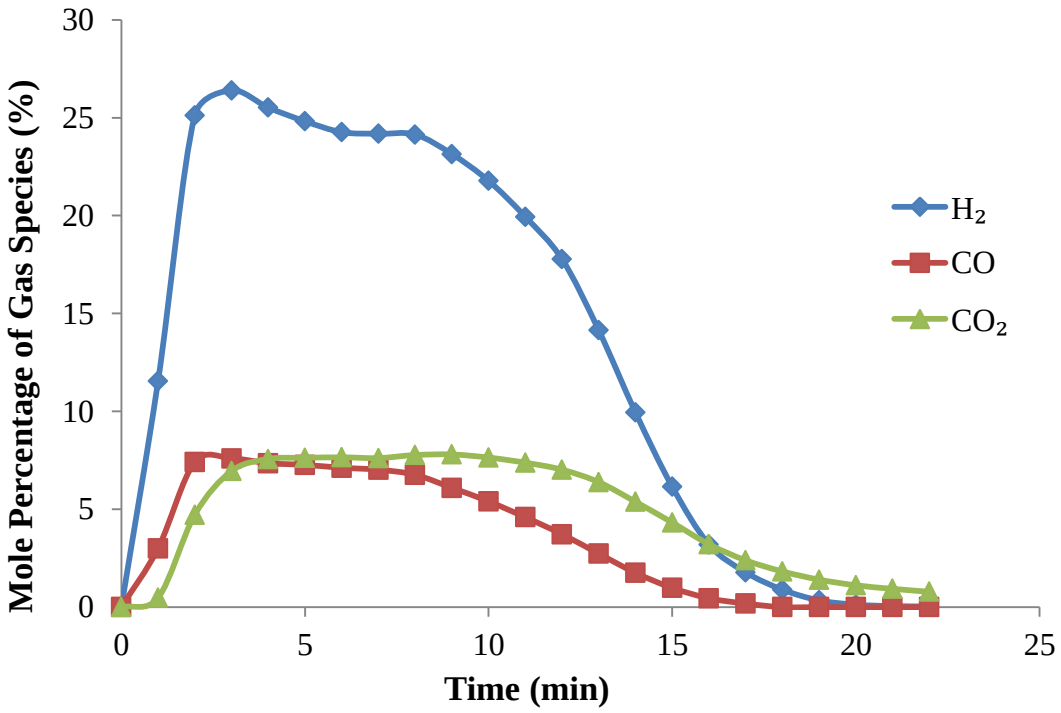

Figure 3.6: Profile of producer gas generation from gasification of biomass chars at 900°C.

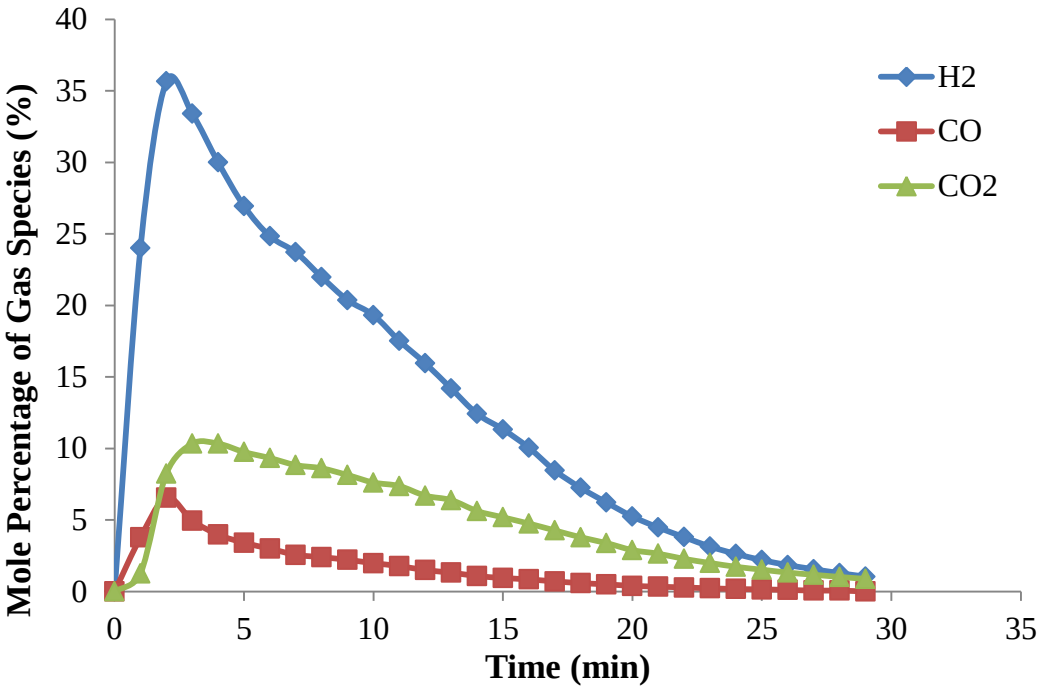

Figure 3.7: Profile of producer gas generation from gasification of chars with coal-to-biomass ratio of 20:80 at 900°C.

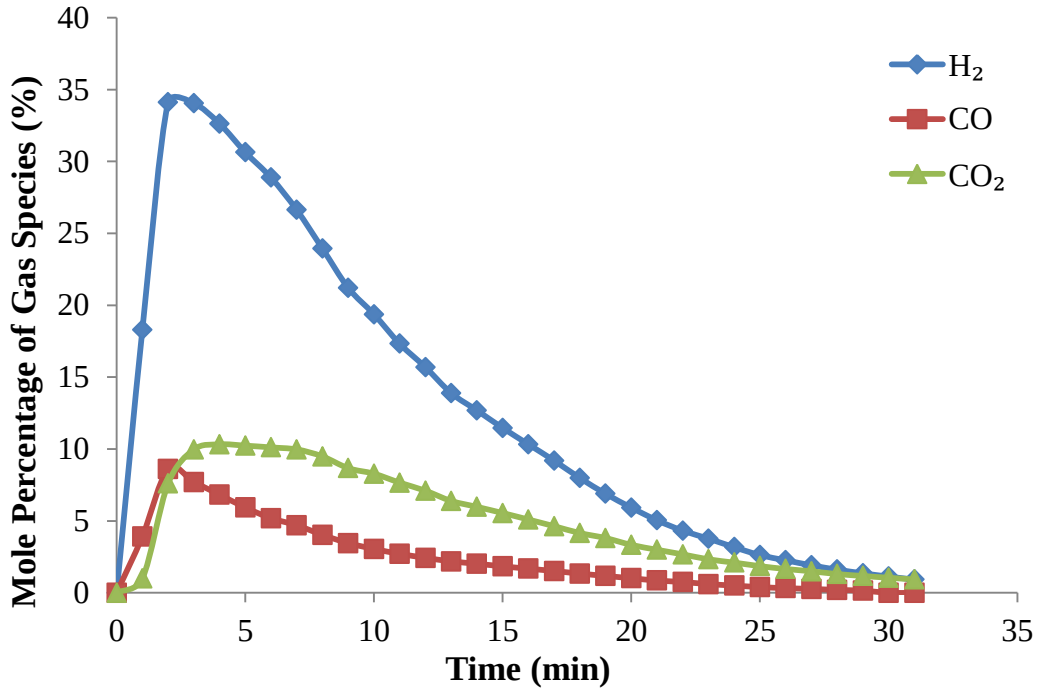

Figure 3.8: Profile of producer gas generation from gasification of chars with coal-to-biomass ratio of 50:50 at 900°C.

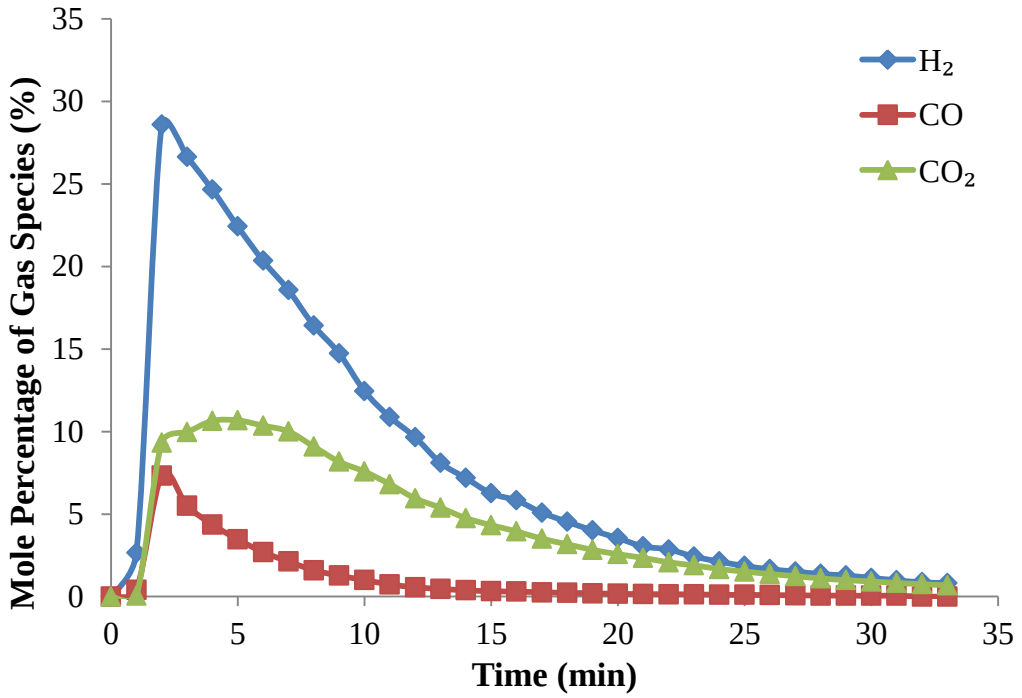

Figure 3.9: Profile of producer gas generation from gasification of chars with coal-to-biomass ratio of 80:20 at 900°C.

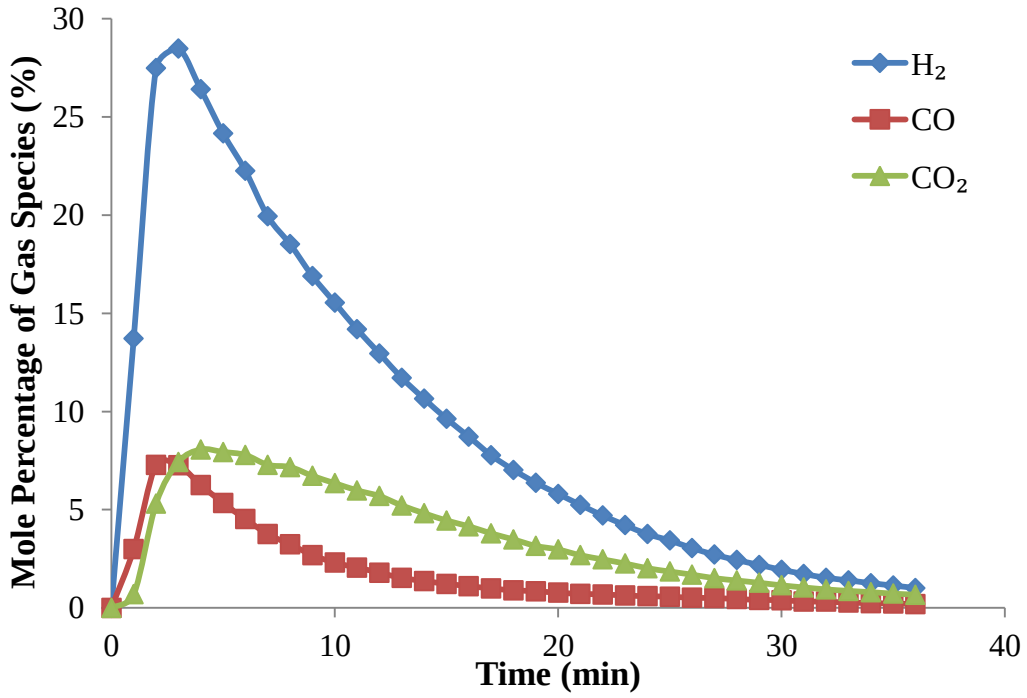

Figure 3.10: Profile of producer gas generation from gasification of coal chars at 900°C.

The results of producer gas composition presented in Figures 3.6 to 3.10 have been used to determine the gas production rate, as the carrier gas (N_2) had a constant volumetric flow rate (600 mL/min). The high concentration of a gas component also means a high production rate of this gas component. From the experimental results of producer gas profiles presented in Figs. 3.6-3.10, it can be seen that the char gasification could be divided into three stages: initial heat-up and slow gas production stage, fast gas production stage and final falling-rate gas production stage. The first stage took about three minutes and the gas production reached the maxima by the end of this stage. In this stage, the maximum values of the gas production rate for different fuels were different. The maximum H_2 compositions (mol/mol) at the end of the first stage of gasification for the five different coal-to-biomass ratio chars were, respectively, 25% (Figure 3.6), 36% (Figure 3.7), 29% (Figure 3.8), 27% (Figure 3.9) and 29% (Figure 3.10). In the second and third stages of the gasification, both the gas production rate and the trends were significantly different for chars with different coal-to-biomass ratios and thus the total gasification time was also different. Therefore, the coal-to-biomass ratio had significant effects on the gas production rate and thus the gasification characteristics, which indicates distinct differences in gasification of coal char and biomass char and reflects the effects of the two-fuel blending.

In Figure 3.6 for the gasification of pure biomass char, the producer gas composition curves were maintained at a relatively constant rate for about 10 minutes in the second stage after reaching the maximum value, and then decreased towards zero in the third stage when the char conversion was completed. A similar trend was found from gasification of the char generated from food waste (Ahmed and Gupta 2010). In contrast, for gasification of pure coal (Figure 3.10), the second and third stages were not distinguishable in that the gasification rate underwent an exponential decay, approaching zero towards the end of the gasification process. It is very interesting to note that once coal was added into the biomass to form a blend, the curves of the gas production rate and composition for blended char were more identical to the pure coal gasification as shown in Figures 3.7 to 3.9. In Figure 3.7, the gas composition profile was significantly changed from the pure biomass (Figure 3.6) when even only 20% coal was added, and the maximum gas compositions for H_2 and CO_2 at the end of the first stage were much higher than those in the gasification of pure coal chars.

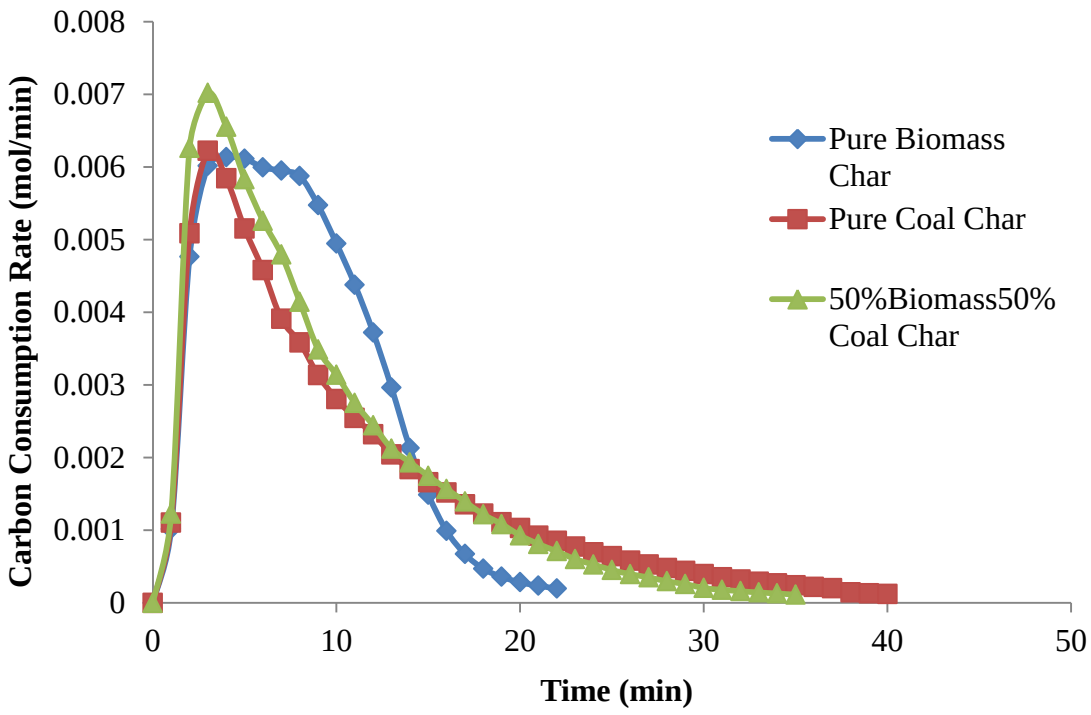

Figure 3.11: Profiles of carbon conversion rates in gasification of different chars at 900^{o}C.

Based on the gas production rate and gas composition from the char gasification, the solid carbon conversion rate can be determined assuming that the solid char is only converted to the three gases (H_2, CO and CO_2). The calculated results of the carbon conversion rate are shown in Figure 3.11 for pure biomass, pure coal and blended coal and biomass at the blending ratio of 50:50. The carbon conversion rate can be used for further investigation into the gasification performance of blended coal and biomass at various blending ratios. From Figure 3.11, it can be seen that the pure biomass char conversion rate was maintained at a relatively constant rate after the initial heating up period followed by a falling rate, while for the pure coal char the carbon conversion rate continued decreasing after reaching the maximum value in the initial heating up period. The carbon conversion rate profile of blended char was similar to that of the pure coal char.

The identical gasification characteristics between blended char and the coal char can be attributed to a number of factors. In the pyrolysis process before gasification, the biomass lost more volatile components than the coal thus the actual char mass formed from the biomass during the pyrolysis stage was less than that from the coal. As shown in Figure 3.5, char yield

was only 15% for the pure biomass and this increased linearly to 40% for the pure coal. It can then be speculated that in the pyrolysis of blended coal and biomass pellets, a higher proportion of the biomass was lost compared to the coal thus leaving more space for the coal char to cover. Figure 3.12 shows the weight of biomass char in the blended biomass and coal chars as a function of biomass ratio. From the figure, a non-linear relationship can be seen between the biomass char proportion and its blending ratio in the fresh fuel, which shows that the properties of blended char are close to the biomass side except for the blend with a high biomass ratio. In addition, the difference in microstructures between the pure biomass and coal are apparent and the coal becomes more influential than the biomass when blended together. This will be discussed later in this chapter.

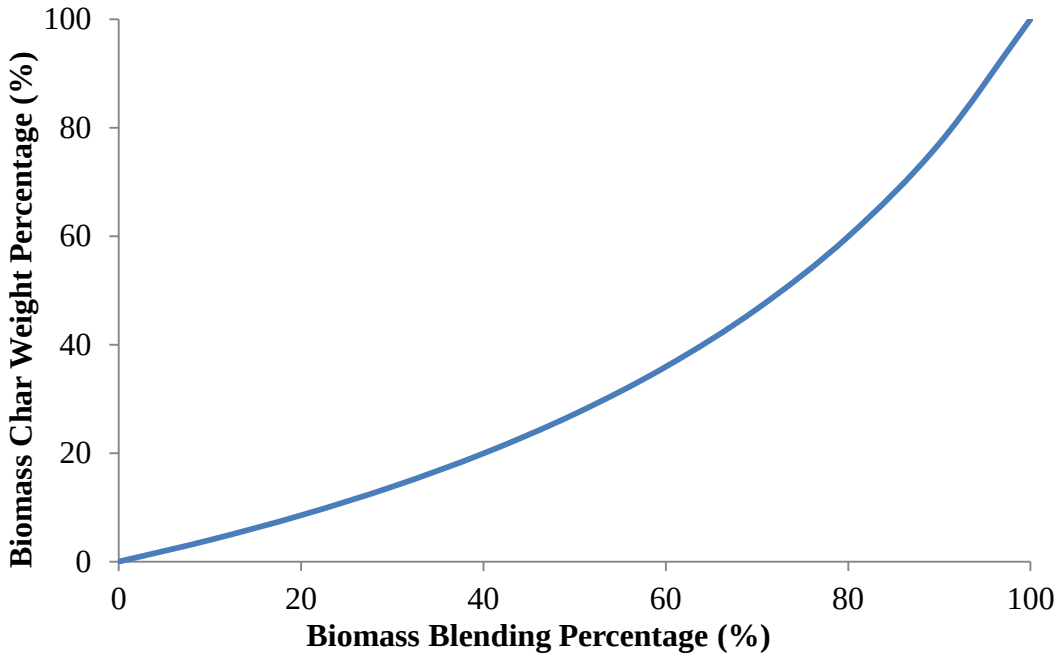

Figure 3.12: Mass proportion of biomass char in generated chars of blended biomass and coal at different blending ratios.

3.3.3Effect of Blending on Apparent Char Reactivity

The apparent gasification reactivity of the char is defined as the char conversion per unit time relative to the remaining carbon mass (*m*), which is calculated by (Keown et al. 2008) as follows:

$$\boldsymbol{r} = \frac{1}{1-X}\frac{dX}{dt} = -\frac{1}{m}\frac{dm}{dt} \quad (3.1)$$

X is the char conversion which shows how much carbon has been converted to gases at the given time (*t*) relative to the total carbon mass (m_o) during the gasification. *X* is determined by (Cetin et al. 2005) thus:

$$X = 1 - \frac{m}{m_0} \quad (3.2)$$

The total carbon mass in the char (m_o) was calculated as the mass difference between the char loaded into the reactor and the ash remaining after the gasification test.

The remaining carbon mass (*m*) at any given time can be determined by:

$$m = m_0 - \int_{t=0}^{t}(-\frac{dC}{dt}MW_c)dt \quad (3.3)$$

In which MW_C is the molar mass of the carbon (12g/mol). $-\frac{dC}{dt}$ is the molar consumption rate of the carbon which can be determined from the GC results.

Since the flow rate and N_2 feed were maintained as constant through the experiment, the molar flow rate of each gaseous species can be obtained from the instantaneous GC data, therefore, the molar consumption rate of solid carbon $-\frac{dC}{dt}$ at any particular time can be calculated as the summation of the molar flow rate of all gaseous species which contain the carbon element (CO and CO_2 in this study):

$$-\frac{dC}{dt} = \frac{CO\% + CO_2\%}{N\%} \times \frac{PV_{N2}}{RT} \quad (3.4)$$

Where *CO%*, CO_2*%* and N_2*%* are the instantaneous volumetric percentage of CO, CO_2 and N_2 in the producer gas mixture; V_{N2} is the volumetric flow rate of nitrogen feed, 600 mL/min in this case. *P* and *T* are the pressure and temperature of nitrogen at feed point.

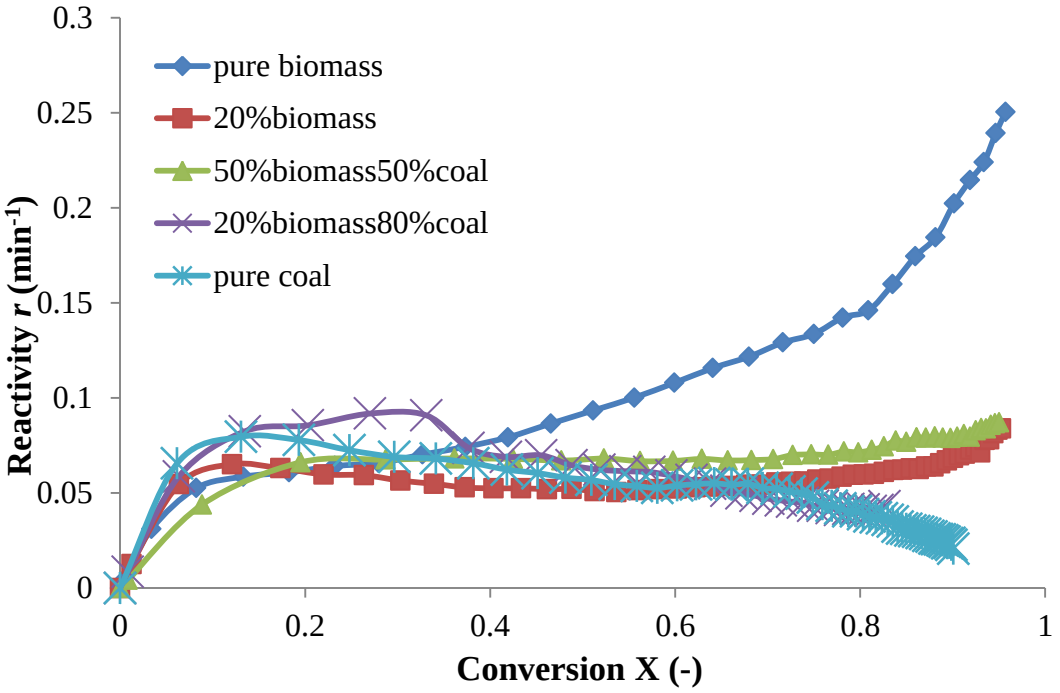

Figure 3.13: Apparent gasification reactivity as a function of char conversion rate at 850°C.

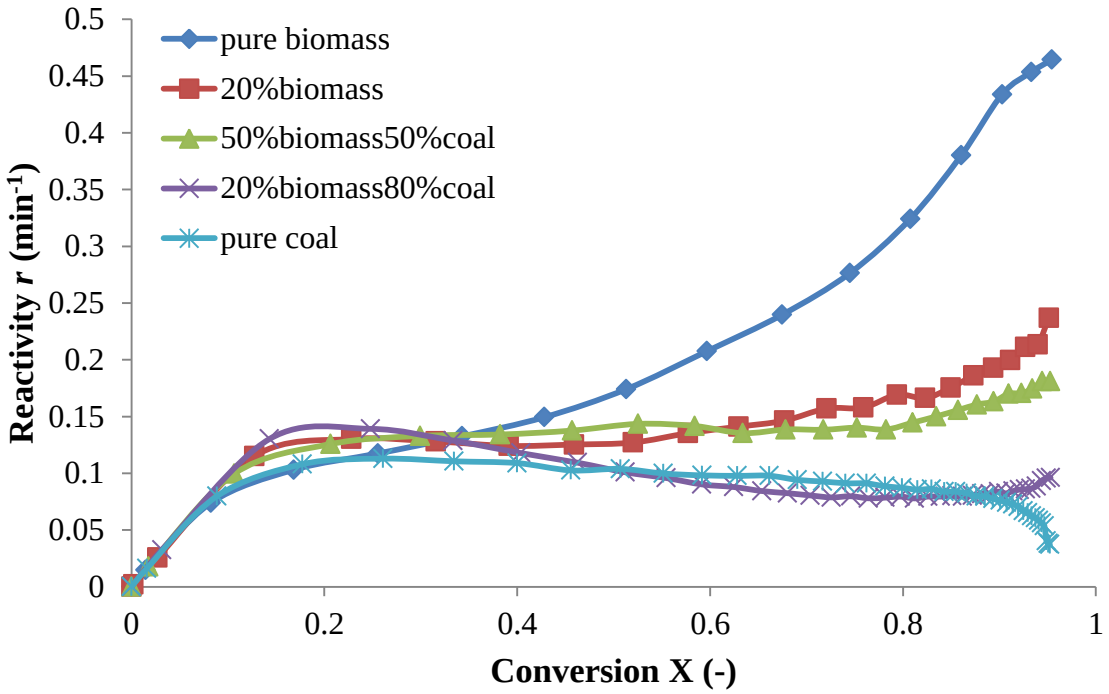

Figure 3.14: Apparent gasification reactivity as a function of char conversion rate at 900°C.

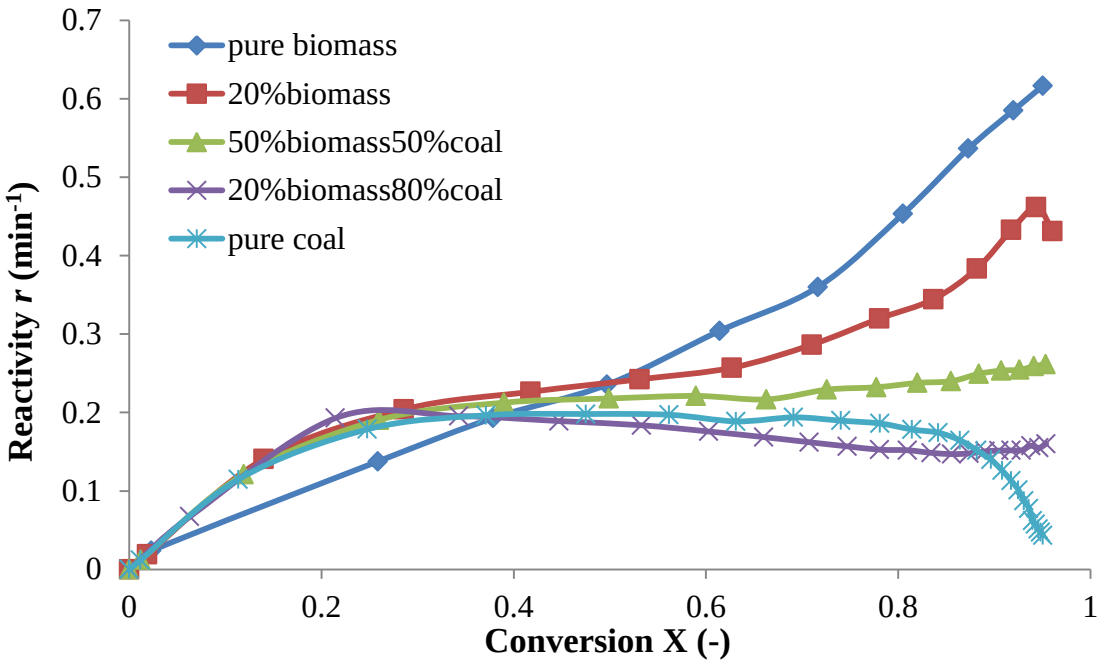

Figure 3.15: Apparent gasification reactivity as a function of char conversion rate at 950°C.

The calculated results of gasification reactivity for chars with various coal-to-biomass ratios are shown in Figures 3.14 to 3.15 for gasification tests at 850, 900 and 950°C, respectively. From these figures, it can be seen that all of the chars had similar reactivity from the start until the char conversion reached 0.4. After this point, the reactivity of pure biomass char increased rapidly and became the highest toward the end of the gasification. In the whole gasification process, the coal char showed the lowest or near lowest gasification reactivity. This is because the reactivity of biomass char is generally higher than the coal char (Smoliński et al. 2011). The reactivity of the blended chars fell between these two extreme cases. A similar trend was found in the char gasification test of coal and biomass by other researchers (Kastanaki and Vamvuka 2006; Zhu et al. 2008). Based on these findings, it is concluded that adding coal to biomass in the blend had a negative effect on the gasification reactivity although the effect was reduced as the gasification temperature increased.

The influence of the gasification temperature can be examined by comparing the elapsed time when the char conversion was completed. The results are shown in Figure 3.16, from which is found that with higher temperatures, the elapsed time for complete conversion of the chars was reduced, showing that the gasification reactivity was increased. The influence of the gasification

temperature can be due to the reduced difference in the apparent activation energy between the biomass and coal chars at higher temperatures. Fig. 3.16 shows that the complete carbon conversion time also increases with the coal proportion in the blended chars, since coal char has higher apparent activation energy than the biomass (Campbell et al. 2002; Gil et al. 2012; Moghtaderi 2007).

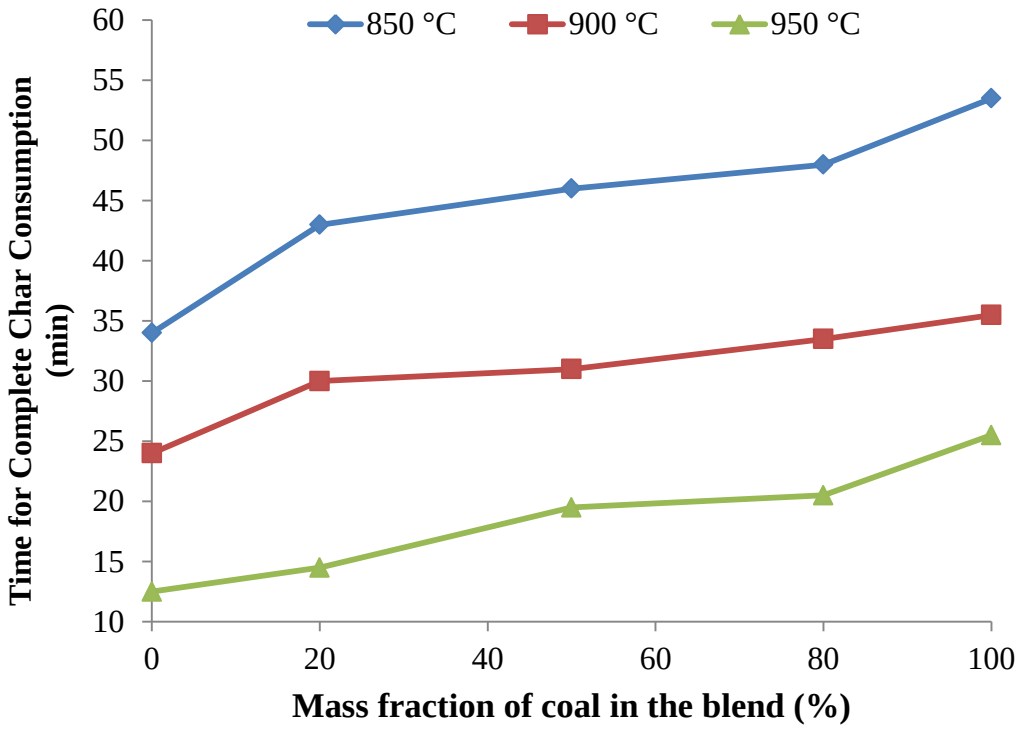

Figure 3.16: Effect of gasification temperature and blending ratio on complete conversion time of the solid chars.

3.3.4 Morphology of the Chars

The SEM images of biomass char, coal char and blended coal-biomass chars are illustrated in Figure 3.17, from which it can be seen that in micrometer order, the biomass char matrix (Figure 3.17a) is significantly more amorphous than the coal char (Figure 3.17c). For the biomass char, there is a large amount of finer voids between the carbonaceous matters forming the structure of thinner clusters, as the result of the internal texture of the fiber bundles becoming sparse during pyrolysis (Okumura et al. 2009). For the coal char, the carbonaceous materials are more likely to

be segregated in the form of more compacted clusters and large cracks. These differences can be used to explain the different gasification characteristics between the biomass char and the coal char (Lu et al. 2002) (Wang et al. 2012) (Alonso et al. 2001). For the biomass char, the fine voids can allow a more uniform gas transfer through the gasification process, thus high gasification reactivity can be maintained throughout the gasification process. However, for the coal char, the large cracks make it possible for fast gas transfer in the early stages of the gasification, although the compacted clusters mean high resistance for the gas transfer from the compacted clusters to the large cracks.

The microstructure of the blended char shows the major characteristics of the coal char where large cracks and compact clusters are observed. Therefore, the gasification characteristics are closer to those of the coal char. The observed differences in the char microstructures are consistent with previous findings of gas production and carbon conversion rates during the gasification process of these chars.

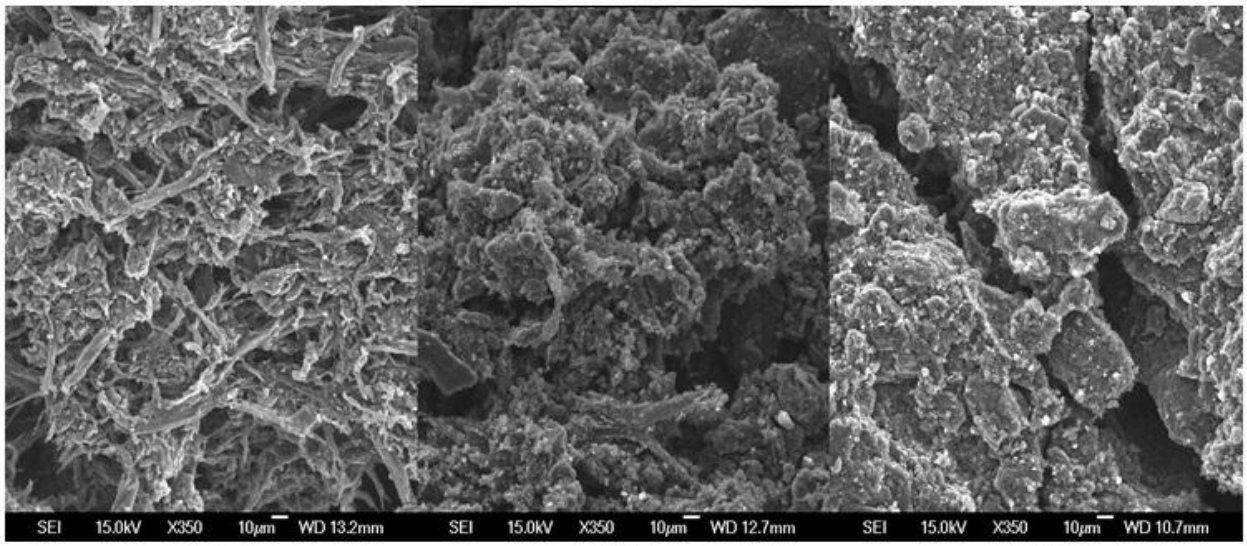

Figure 3.17: The electronic microscopic scanning images of surface of (a) pure biomass char, (b) 50:50 blended char and (c) pure coal char. All images have a magnification of ×350.

3.3.5 Analysis of Char Gasification Mechanism

During char gasification using water vapour as the gasification agent, there are three distinct steps which influence the overall gas production and carbon conversion rates: (1) diffusion of the water vapour molecules into the char particles, (2) heterogeneous reaction on the surface of the char matrix and (3) gaseous products moving out from the char particles by diffusion under a gas concentration gradient within the particle and by the bulk gas flow due to the gradient of partial pressure. In the non-catalytic gas solid reactions between the water vapour and the solid char, if both the vapour diffusion resistance and intrinsic reaction rate are large enough, the vapour molecules will initially react near the particle surface before further diffusing into the centre of the solid particle. On the other hand, if the vapour diffusion rate is significantly faster than the intrinsic reaction rate, the vapour concentration within the article will be uniform and the whole solid volume will have a similar conversion rate. In this case, the overall reaction rate will be similar to the intrinsic reaction (Gupta and Saha 2003). The resistance of inward diffusion of water vapour molecules into the char particles can be significant for the apparent char size of millimeter level (Paviet et al. 2008a). In this study, the pellet size was large enough to generate significant diffusion resistance, which had a competing effect with heterogeneous reactions.

From Figure 3.6, it has been noticed that the overall gasification rate of biomass char stayed relatively constant after the initial heat-up period, which indicates an inhomogeneous reaction rate during the gasification, and that the effective reaction volume of the biomass char can be limited by the vapour diffusion resistance (Paviet et al. 2008b) (Ollero et al. 2002). Therefore reactions occurred at and near the char particle surface while the surface continuously moved inward with the char conversion. However, figure 3.10 shows that the coal char gasification exhibited a typical first order kinetic characteristic from which exponential decay in the reaction rate was observed. This confirms that vapour diffusion resistance within the coal char can be negligible in the gasification compared to the intrinsic reaction rate. Therefore, it can be concluded that the gasification reactions between the water vapour and the solid char occurred within the whole volume of the char particle because the vapour could penetrate into the char particle through the large cracks. However, the resistance to the resultant gas diffusion plays a dominant role.

Figure 3.18 shows the results of the carbon consumption rate and char conversion rate *(X)* from the experiments with different char particle size, from which it is observed that the overall conversion rate of the coal chars was hardly increased after the chars had been milled to finer particles with smaller diameters. The negligible effect of particle size for the coal chars confirms that the vapour can easily diffuse into the coal char particle thus the particle diameter is not a critical factor. However, for the biomass char, the conversion rate of the milled chars was increased significantly compared to the original biomass pellet chars. In the milled biomass char, the particle diameter was significantly reduced thus the surface area to the particle mass was much higher and the carbon conversion rate was significantly increased in the first and second stages of the gasification.

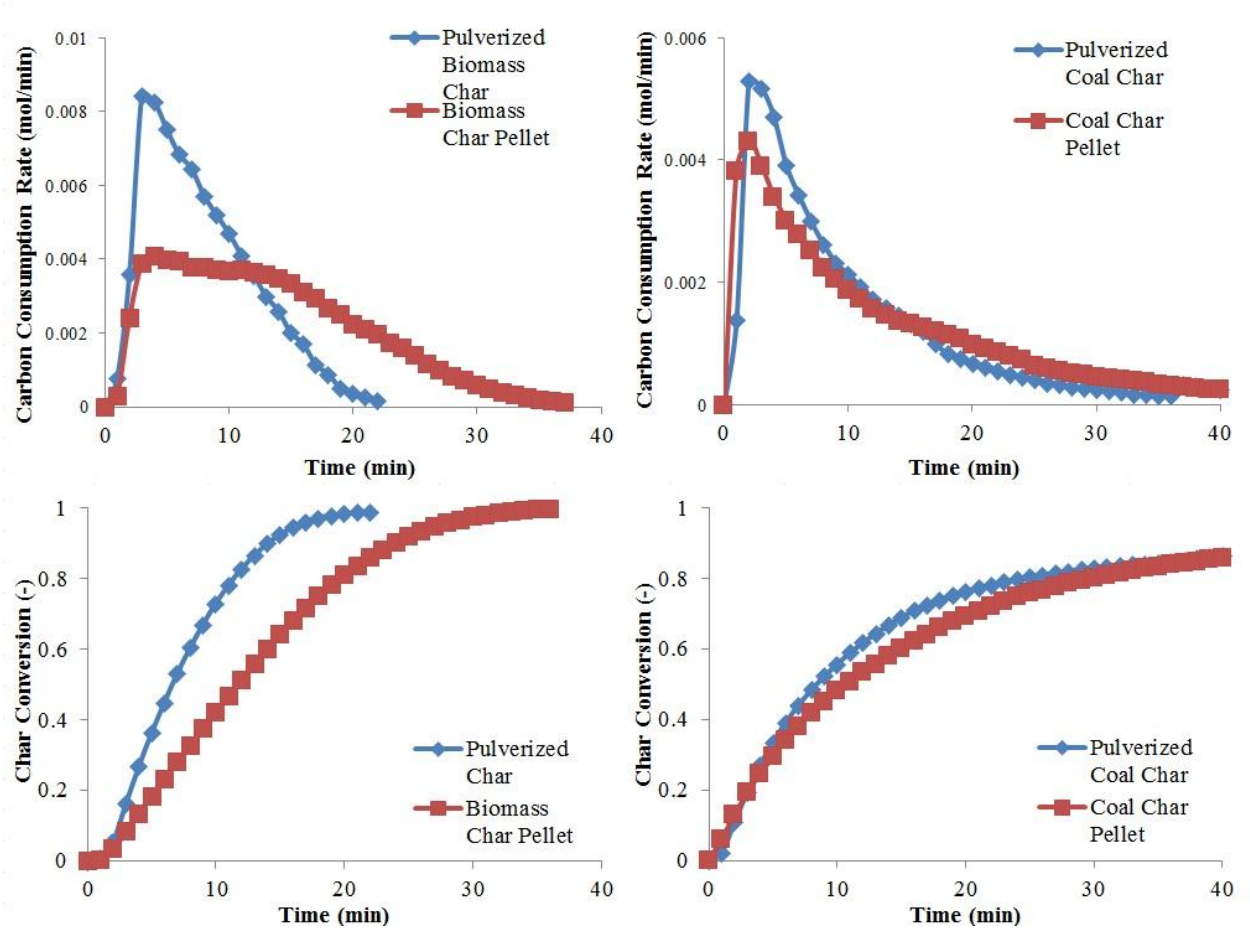

Figure 3.18 : Effect of char particle size (and thus the vapour diffusion resistance) on the gasification of biomass char and coal char.

The difference in the vapour diffusion resistance between the biomass char and the coal char can be attributed to the distinct structural properties of these two solids. From the SEM analysis, it has been found that the biomass char is much more amorphous than the coal char, hence the specific effective surface area is greater and the intrinsic reactivity is enhanced compared to the coal char. On the other hand, the diffusion rate for the small biomass char is relatively slower due to the smaller pore size, which limits the inward Knudsen diffusion of water vapour. However, the coal char shows a denser cluster and large cracks, which results in larger effective pore diameter.

Based on the above mechanisms, a mathematical model has been developed and validated using the experimental results to simulate the gasification process of chars of biomass, coal and blended biomass and coal. This will be presented in the next chapter.

3.4 Conclusion

The gas production rate, carbon conversion rate and reactivity for gasification of biomass char, coal char and blended coal and biomass chars have been experimentally investigated in this part of the research. Sample char particles were produced from pyrolysis of pellets of pure biomass (Eucalyptus nitens), pure coal (lignite) and their blends at three different blending ratios. A series of gasification tests were carried out in a bench scale reactor at three different temperatures. The composition of the producer gas and gas production rate were continuously analysed by using a Micro-GC. Based on the gas analysis results, the carbon conversion rate and gasification reactivity were then determined.

The gasification of biomass chars, coal chars and the chars of blended biomass and coal can be represented by three stages: initial heat-up and slow gasification stage, fast gasification rate stage and falling rate stage. In the initial heat-up stage, the gasification rate increased to the maximum values which vary with the coal-to-biomass ratio. The overall conversion rate of biomass char maintained at a relatively constant rate after the initial heat-up period, followed by a falling rate

towards the end of the process. For gasification of the coal char, the reaction rate decreased continuously after the maximum value was reached.

The reaction rate of the blended coal and biomass chars has gasification characteristics between those of pure biomass char and pure coal char but closer to those of the pure coal char. This is because the biomass loses more mass during the pyrolysis when the char is made. The overall reactivity of the blended coal-biomass char decreases with the incremental fraction of the coal in the blend, and the effect of the coal tends to be reduced at higher gasification temperatures.

The differences in the gasification characteristics between the coal char and the biomass char can be further explained by the SEM image analysis. The biomass char has a more amorphous structure; however, the effective pore size is smaller than that of coal char. The coal char has a more packed cluster structure and large cracks are present. The chars of blended biomass and coal are similar to the coal char. The distinct gasification characteristics of the coal char and the biomass char are due to the differences in vapour diffusion within the char particles. The internal resistance to the vapour diffusion in the biomass char is significant and intrinsic reaction is fast due to its amorphous structure, hence the significant gradient in the vapour concentration along the char radius resulting in an inhomogeneous overall reaction rate through volume. However, in the gasification of the coal char, the denser structure and larger effective pore size cause the homogeneous overall reaction rate and the resultant gas diffusion outside the particle plays an important role.

The experimental results will be used in the development and validation of a mathematical model for char gasification which will be presented in Chapter 4.

References

Ahmed, I. I., and Gupta, A. K. (2010). "Pyrolysis and gasification of food waste: Syngas characteristics and char gasification kinetics." *Applied Energy*, 87(1), 101-108.

Alonso, M. J. G., Borrego, A. G., Alvarez, D., Parra, J. B., and Menéndez, R. (2001). "Influence of pyrolysis temperature on char optical texture and reactivity." *Journal of Analytical and Applied Pyrolysis*, 58–59(0), 887-909.

Campbell, P. A., Mitchell, R. E., and Ma, L. (2002). "Characterization of coal char and biomass char reactivities to oxygen." *Proceedings of the Combustion Institute*, 29(1), 519-526.

Cetin, E., Gupta, R., and Moghtaderi, B. (2005). "Effect of pyrolysis pressure and heating rate on radiata pine char structure and apparent gasification reactivity." *Fuel*, 84(10), 1328-1334.

Clemens, A. H., Damiano, L. F., and Matheson, T. W. (1998). "The effect of calcium on the rate and products of steam gasification of char from low rank coal." *Fuel*, 77(9–10), 1017-1020.

Gil, M. V., Riaza, J., Álvarez, L., Pevida, C., Pis, J. J., and Rubiera, F. (2012). "Kinetic models for the oxy-fuel combustion of coal and coal/biomass blend chars obtained in N2 and CO2 atmospheres." *Energy*, 48(1), 510-518.

Gupta, P., and Saha, R. K. (2003). "Analysis of gas-solid noncatalytic reactions in porous particles: finite volume method." *International Journal of Chemical Kinetics*, 36, 1-11.

Kajitani, S., Zhang, Y., Umemoto, S., Ashizawa, M., and Hara, S. (2009). "Co-gasification Reactivity of Coal and Woody Biomass in High-Temperature Gasification†." *Energy & Fuels*, 24(1), 145-151.

Kastanaki, E., and Vamvuka, D. (2006). "A comparative reactivity and kinetic study on the combustion of coal–biomass char blends." *Fuel*, 85(9), 1186-1193.

Keown, D. M., Hayashi, J.-I., and Li, C.-Z. (2008). "Drastic changes in biomass char structure and reactivity upon contact with steam." *Fuel*, 87(7), 1127-1132.

Lu, L., Kong, C., Sahajwalla, V., and Harris, D. (2002). "Char structural ordering during pyrolysis and combustion and its influence on char reactivity." *Fuel*, 81(9), 1215-1225.

Moghtaderi, B. (2007). "A study on the char burnout characteristics of coal and biomass blends." *Fuel*, 86(15), 2431-2438.

Neilsen, W. A., and Gerrand, A. M. (1999). "Growth and branching habit of Eucalyptus nitens at different spacing and the effect on final crop selection." *Forest Ecology and Management*, 123(2–3), 217-229.

Okumura, Y., Hanaoka, T., and Sakanishi, K. (2009). "Effect of pyrolysis conditions on gasification reactivity of woody biomass-derived char." *Proceedings of the Combustion Institute*, 32(2), 2013-2020.

Ollero, P., Serrera, A., Arjona, R., and Alcantarilla, S. (2002). "Diffusional effects in TGA gasification experiments for kinetic determination." *Fuel*, 81(15), 1989-2000.

Paviet, F., Bals, O., and Antonini, G. (2008a). "The effects of diffusional resistance on wood char gasification " *Process Safety and Environmental Protection*, 86, 131-140.

Paviet, F., Bals, O., and Antonini, G. (2008b). "The effects of diffusional resistance on wood char gasification." *Process Safety and Environmental Protection*, 86(2), 131-140.

Sjöström, K., Chen, G., Yu, Q., Brage, C., and Rosén, C. (1999). "Promoted reactivity of char in co-gasification of biomass and coal: synergies in the thermochemical process." *Fuel*, 78(10), 1189-1194.

Smoliński, A., Howaniec, N., and Stańczyk, K. (2011). "A comparative experimental study of biomass, lignite and hard coal steam gasification." *Renewable Energy*, 36(6), 1836-1842.

Wang, B., Sun, L., Su, S., Xiang, J., Hu, S., and Fei, H. (2012). "Char Structural Evolution during Pyrolysis and Its Influence on Combustion Reactivity in Air and Oxy-Fuel Conditions." *Energy & Fuels*, 26(3), 1565-1574.

Zhu, W., Song, W., and Lin, W. (2008). "Catalytic gasification of char from co-pyrolysis of coal and biomass." *Fuel Processing Technology*, 89(9), 890-896.

Chapter 4 Mathematical Modelling of Reaction Kinetics and Producer Gas Composition of Steam Gasification of Blended Coal and Biomass Chars

In Chapter 3, the differences between gasification of biomass chars, coal char and blended biomass-coal chars were experimentally investigated and the results show that these differences are mainly due to the difference in microstructures of these chars. In this chapter, a mathematical model of char gasification is developed based on reaction kinetics and gas transportation of both the producer gas and the gasification agent (steam). The model also includes mass conservation equations for each of the gas components and solid carbon involved in the gasification process. The model consists of a set of highly-nonlinear differential equations which are solved to predict the gas production rate, gas composition and carbon consumption rate during the gasification. From the modelling, it has been confirmed that the char gasification process is dominated by the characteristics of char matrix including the exposed surface area and the micro-pore size. The former determines the intrinsic reaction rate and the latter influences the intra particle mass transportation. Biomass char has a more amorphous structure, thus the intrinsic reaction rate is enhanced. For coal char, the larger pore size enables the high transport rate of the gasification agent (water vapour) into the char particles but the resultant gases have to overcome higher resistance to transfer through compact clusters. For simulation of the blended biomass and coal, the blend properties are determined based on the blend proportion of each fuel. The developed mathematical model is validated using the experimental results presented in Chapter 3, and close agreement between the simulation results and the experimental data has been observed. The close agreement between the simulation results and experimental data suggests that the approach in this work can adequately quantify the gasification kinetics and the gas composition.

4.1 Introduction

The process of solid fuel gasification within a fluidized bed reactor can be divided into two main steps after a short drying process: 1) initial fast pyrolysis of the raw materials, and 2) subsequent

gasification of resultant chars and gases (Higman and Burgt 2003). The former is a short process generating solid char and volatile gases, while the latter consists of a series of heterogeneous reactions of the chars with a gasification agent (air, oxygen or steam) and homogeneous reactions among reactant and resultant gases. The char gasification process is a much slower conversion process compared to the initial pyrolysis thus it is dominant in the whole gasification process (Everson et al. 2006). Therefore, fundamental understanding and quantifying of the char gasification are crucial for optimization of the whole gasification process and for design of the gasifier.

In the char gasification, char structure is normally porous and gaseous molecules diffuse through the particle hence overall gasification behaviour is governed by the rates of gaseous transport as well as various chemical reaction kinetics (Ballal et al. 1989). Dynamic modelling of gasification of a single char particle is important in understanding the gasification process and reactivity, especially for char with a mean diameter in the order of millimetres, which is large enough to create a concentration gradient within the particle (Ollero et al. 2002; Paviet et al. 2008). However, this mechanism cannot be reflected in the lump model (Wang and Bhatia 2001b). Therefore, a dynamic model is needed for investigation of the char gasification characteristics under different operating conditions. However, existing dynamic models focus on the air or oxygen gasification; a dynamic model that simulates steam gasification of coal and biomass blend char has not been found in the literature. Also, existing models are generally restricted to a narrow range of char characteristics (sole feedstock), hence lack the robustness for solving the co-gasification of different types of chars with various properties. Furthermore, in understanding the co-gasification process of blended coal and biomass, the reactivity of the blend chars has been found to have a synergetic effect and the simple additive rule could not be applied to predict the gasification behaviour. The single particle model based on fundamental physical and chemical phenomena will also be useful to quantify the gasification process.

In Chapter Three, a series of gasification tests was performed in order to experimentally investigate the gasification process and understand the gasification mechanism. From this investigation, it was concluded that biomass char has higher intrinsic reactivity while coal char has better effective gas permeability. The objectives of Chapter Four are to develop a dynamic mathematical mode for the char gasification and to validate the developed model using the

experimental results presented in Chapter Three. In the char gasification, steam is used as the gasification agent and the chars include biomass char, coal char and chars of the blended biomass and coal. From the developed model, the influence of structure difference on the gasification characterises will be examined and reasons for the differences in gasification performance of the different types of chars will be investigated.

4.2 Development of A Mathematical Model for Steam Gasification of Chars

4.2.1 Transfer process for reactant and resultant gases in a solid char

In gasification, although the chemical reactions between the gasification agent (steam) and carbonaceous materials are the same for both the biomass char and the coal char, the physical and the structural properties among these two types of chars are significantly different, which results in very different characteristics exhibited in the gasification process. Char gasification is a complicated process consisting of both physical and chemical processes within a char particle: (1) gasification agent diffusion from bulk gas into the particle through the micro-pores, (2) chemical reactions among gases, and between gas and char matrix, (3) resultant gases moving out from the char particle by diffusion and bulk flow through the micro-pores. The above processes can be illustrated in a schematic diagram as shown in Figure 4.1.

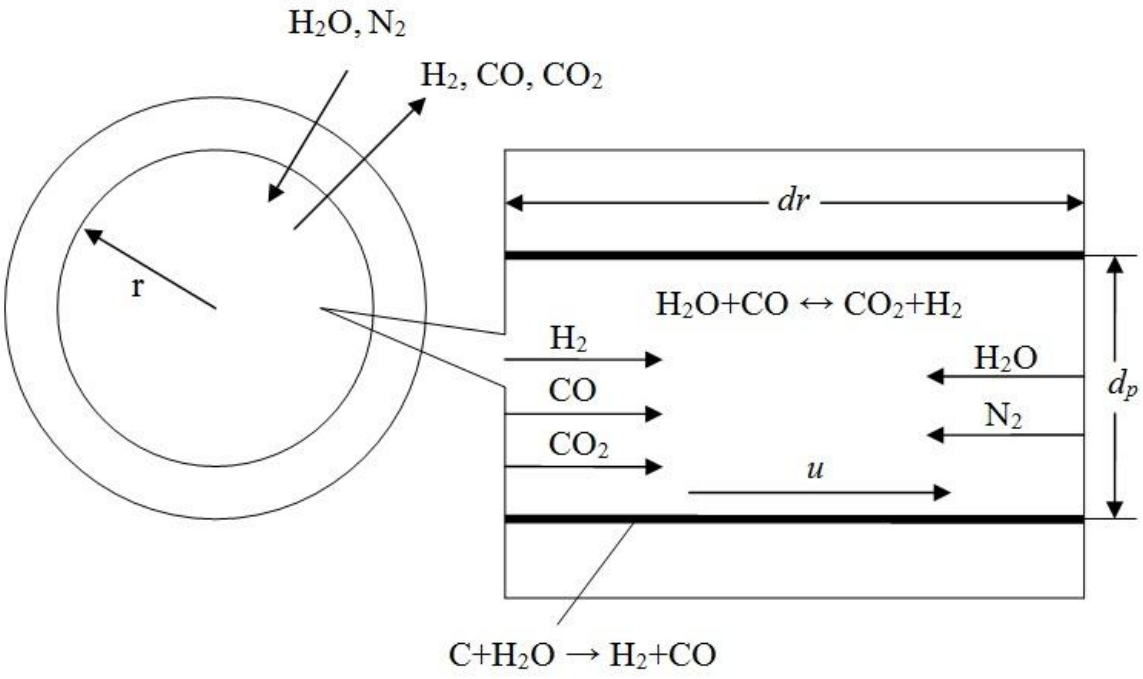

Figure 4.1: Schematic diagram of steam gasification of a single char particle. d_r is the infinitesimal length in radius direction of the char particle, d_p is the diameter of the micro-pore.

4.2.2 Mass conservation in a spherical coordinate

The modelling of steam gasification of a single char particle includes mass balances of all matters involved, transportation of gas phase reactants and products, and reaction kinetics of the gases and the char over an infinitesimal volume over the char diameter increment or the micro-pore length increment, d_r. In the development of the gasification model, it is assumed that all the macro char particles are regular spheres with the same initial size and micro-pore diameter. Other assumptions include:

- For the small and spherical char particles, all deviation variables are only the functions of time (t) and distance in char radius (r). This assumption is tenable for a fluidized bed reactor because the gases flow through the char bed with high velocity and the variation in gas composition and gas film mass transfer coefficient outside the char particles are the minimum.

- Due to the small size of the char particle and the slow char gasification process, it is assumed that the char particle has a uniform temperature distribution.
- Three chemical reactions occurring in the char gasification are considered, these are:

Steam Gasification Reaction: $H_2O + C \rightarrow H_2 + CO$ (4.1)

Water-Gas Shift Reaction: $H_2O + CO \leftrightarrow H_2 + CO_2$ (4.2)

Bouduard Reaction: $CO_2 + C \rightarrow 2CO$ (4.3)

Therefore, the resultant gases from the char gasification are H_2, CO and CO_2.

The above assumptions were justified. The uniform temperature assumption was verified by calculating the dimensionless Biot number of char particles, and in this case the Biot number was very small. Heat transfer between gases within the pores and char matrix could also enhance the thermal diffusion rate. An assumption that only considers the above three predominant reactions was verified by the producer gas composition of bench scale gasifier in Chapter three, in which the extremely low CH_4 content indicates that the methanation reaction rate can be negligible.
In the model, the independent variables involved are: 1) molar concentration of the gaseous species of H_2O (gasification agent), H_2, CO, CO_2 and N_2 (carrier gas), nominated as C_i, i = 1 to 5; and 2) local conversion rate of solid char X_s.

Based on the isothermal assumption, only mass balance calculations are needed in the model which is derived as follows (Biggs and Agarwal 1997):

$$\frac{\partial(\Phi C_i)}{\partial t} + \frac{1}{r^2}\frac{1}{\partial r}\left(r^2 N_i\right) = \sum_{j=1}^{3} v_{ij} R_j \qquad (4.4)$$

Where

Φ is the porosity of the char structure;

N_i is the net mass flux of i^{th} component, i =1, 2 … 5;

v_{ij} is the stoichiometric coefficient of i^{th} component in j^{th} reaction;

R_j is the intrinsic reaction rate of the j^{th} reaction as given in Equations (4.1) to (4.3).

Using the matrix form, the above mass conservation equation of all gas species can be expressed as:

$$\frac{\partial(\Phi \mathbf{C})}{\partial t} + \frac{1}{r^2}\frac{1}{\partial r}\left(r^2 \mathbf{N}\right) = \mathbf{vR} \tag{4.5}$$

In which **C** is the vector of gas component concentration with 5 rows, $\mathbf{C} = \begin{bmatrix} C_1 \\ C_2 \\ C_3 \\ C_4 \\ C_5 \end{bmatrix}$

N is the vector of gas component net fluxes, also of 5 rows.

R is the vector of intrinsic rates of all reactions with 3 columns.

v is the matrix of stoichiometric coefficients with 5×3 elements, $\mathbf{v} = \begin{bmatrix} -1 & -1 & 0 \\ 1 & 1 & 0 \\ 1 & -1 & 2 \\ 0 & 1 & -1 \\ 0 & 0 & 0 \end{bmatrix}$

Initial and boundary conditions for Equation (4.5) are:

$$\begin{aligned} &\frac{\partial \mathbf{C}}{\partial r} = 0 \text{ at } r = 0, \forall t = [0, t_{final}]; \\ &\mathbf{C} = \mathbf{C}_s \text{ at } r = r_a, \forall t = [0, t_{final}]; \\ &\mathbf{C}\big|_{t=0} = \mathbf{C_0}, \forall r = [0, r_a]; \end{aligned} \tag{4.6}$$

$\mathbf{C}_s$ is the concentration vector of a gas species on the apparent surface of the particle and will be introduced in 4.2.6. $\mathbf{C}_0$ is the gas concentration vector of pure N_2 at gasification temperature.

The net flux vector **(N)** is the sum of the diffusion and the convection of the bulk gas in the porous structure within the char particle:

$$\mathbf{N} = \mathbf{J} + u\mathbf{C} = -\frac{\Phi}{\tau}\left(D_{eff}\nabla \mathbf{C} + u\mathbf{C}\right) \tag{4.7}$$

Where **J** is the diffusion flux vector of gas components; u is the linear gas velocity of the bulk gas phase; τ is the tortuosity of the pores which is unity ($\tau = 1$) for cylindrical shaped pores; and D_{eff} is the effective diffusivity of the gas components in the char matrix.

4.2.3 Transportation of gas molecules in the char matrix

For diffusion of gas species in a porous structure, if the length of mean free path of the gas molecules is larger than the micro-pore diameter, the collision between the gas molecules and the pore wall becomes more frequent and the overall diffusivity of the gas in the solid structure is reduced due to the restriction of the molecule transportation by the narrow space within the pore. This phenomenon is well known as Knudsen Diffusion and, in this model, the mean pore diameter is in the order of a micrometer which is significantly less than the mean free path of gas molecules corresponding to the gasification temperatures investigated. Therefore, determination of the diffusivity of gas components in the char needs to take into account the effect of both diffusion and convective bulk flow. The diffusion of i^{th} gas component in the char matrix could be evaluated by the dusty-gas model, which implements the Knudsen diffusivity (second term on RHS of equation 4.8) into the Maxwell-Stephan multi-component diffusion model (first term on RHS of equation 4.8). On the other hand, viscous flow occurs under the pressure gradient within the pores which also contributes to the component overall flux. Under normal pressure conditions the relationship among species flux, species concentration gradient (first term on LHS of equation 4.8) and pressure gradient (second term on LHS of equation 4.8) acting on the i^{th} gas component can be described by the following equation (Krishna and Wesselingh 1997):

$$-\left(\nabla C_i + \frac{B_0}{D_{iK}\mu} C_i \nabla P\right) = \sum_{j=1}^{n} \frac{y_j N_i - y_i N_j}{D_{ij}^e} + \frac{N_i}{D_{iK}^e}; \quad i = 1,2,...,n \tag{4.8}$$

Where D_{ij}^e and D_{iK}^e are, respectively, the effective gas phase diffusivity and Knudsen diffusivity in the porous material:

$$D_{ij}^e = \frac{\Phi}{\tau} D_{ij}; \; D_{iK}^e = \frac{\Phi}{\tau} D_{iK} \tag{4.9}$$

By applying the Ideal Gas Law, the following equations can be derived:

$$\nabla P = \boldsymbol{R}T\nabla C_t \tag{4.10}$$

$$C_t = \sum_{i=1}^{n} C_i \tag{4.11}$$

Equation (4.8) can also be expressed in a matrix form:

$$-\frac{\Phi}{\tau}\left(\nabla \mathbf{C} + \frac{\boldsymbol{R}TB_0}{\mu}\nabla C_t[\mathbf{A}]\mathbf{C}\right) = [\mathbf{B}]\mathbf{N} \tag{4.12}$$

By re-arranging the above equation, the molar flux of gas components (**N**) can be determined by:

$$\mathbf{N} = -\frac{\Phi}{\tau}\left([\mathbf{B}]^{-1}\nabla \mathbf{C} + \frac{\boldsymbol{R}TB_0}{\mu}\nabla C_t[\mathbf{B}]^{-1}[\mathbf{A}]\mathbf{C}\right) \tag{4.13}$$

Substitute Equation (4.13) into Equation (4.5), the mass balance for gas components becomes:

$$\frac{\partial(\Phi\mathbf{C})}{\partial t} = \frac{1}{r^2}\frac{1}{\partial r}\left[r^2\frac{\Phi}{\tau}\left([\mathbf{B}]^{-1}\frac{\partial \mathbf{C}}{\partial r} + \frac{\boldsymbol{R}TB_0}{\mu}\frac{\partial C_t}{\partial r}[\mathbf{B}]^{-1}[\mathbf{A}]\mathbf{C}\right)\right] + \mathbf{vR} \tag{4.14}$$

In the above equation, **[A]** and **[B]** are 5-dimensional square matrices. Their diagonal and off-diagonal elements are calculated by:

$$A_{ii} = \frac{1}{D_{iK}} \tag{4.15}$$

$$A_{ij} = 0 \tag{4.16}$$

$$B_{ii} = \frac{1}{D_{iK}} + \sum_{\substack{j=1 \\ j\neq i}}^{n}\frac{y_j}{D_{ij}} \tag{4.17}$$

$$B_{ij} = -\frac{y_i}{D_{ij}} \qquad i = 1, \ldots, 5 \tag{4.18}$$

The Knudsen Diffusion coefficient of i^{th} component in the pore, D_{iK}, is calculated by (Jackson 1977):

$$D_{iK} = \frac{d_p}{3}\sqrt{\frac{8RT}{\pi MW_i}} \tag{4.19}$$

Where d_p is the mean diameter of pores.

The binary diffusion coefficient of component (D_{ij}) for species i in reaction j is estimated by correlation given by Hirschfelder (Welty et al. 1969):

$$D_{ij} = \frac{0.001858\,T^{3/2}\sqrt{\frac{1}{MW_i}+\frac{1}{MW_j}}}{P\sigma_{ij}^{\,2}\Omega_D} \tag{4.20}$$

In which MW_i and MW_j are the molecular weight of component i and j, respectively.

In Equation (4.14), B_0 is the gas permeability of the porous char particle. With laminar gas flow in a cylindrical pore, B_0 can be evaluated by using the Hagen-Poiseuille equation (Perry et al. 1997):

$$B_0 = \frac{d_p^{\,2}}{32} \tag{4.21}$$

The gas mixture viscosity in Equation (4.14) can be evaluated by Wilke correlation (Welty et al. 1969):

$$\mu = \sum_{i=1}^{n}\frac{y_i\mu_i}{\sum y_i\phi_{ij}} \tag{4.22}$$

$$\phi_{ij} = \frac{1}{\sqrt{8}}\left(1+\frac{M_i}{M_j}\right)^{-1/2}\left[1+\left(\frac{\mu_i}{\mu_j}\right)^{1/2}\left(\frac{MW_j}{MW_i}\right)^{1/4}\right]^2 \tag{4.23}$$

However, for the single gas species, the viscosity of i^{th} component is determined by Sutherland's formula (Arnold 1933):

$$\mu_i = \mu_{0,i}\left(\frac{T_{0,i}+c_i}{T+c_i}\right)\left(\frac{T}{T_{0,i}}\right)^{3/2} \tag{4.24}$$

Where $T_{0,i}$ is the reference temperature, $\mu_{0,i}$ is the reference viscosity at reference temperature, and c_i is the Sutherland's constant.

4.2.4 Gasification reaction kinetics

In this model, the three main reactions considered are expressed in Equations (4.1) to (4.3) and illustrated in Figure 4.1. Among the three reactions, the water gas shift reaction (Equation 4.2) is the gas phase homogeneous reaction within the void space of the char pores for conversion of H_2O (C_1) and CO(C_3) to H_2(C_2) and CO_2 (C_4). The kinetics of this reaction are expressed as (de Souza-Santos 2004):

$$R_2 = k_2\left(C_1C_3 - \frac{C_2C_4}{K_2}\right)\Phi = k_{0,2}e^{-E_{A,2}/RT}\left(C_1C_3 - \frac{C_2C_4}{K_{0,2}e^{-\Delta G_2/\boldsymbol{RT}}}\right)\Phi \tag{4.25}$$

Where k_2 is the reaction kinetic constant, K_2 is the equilibrium constant, and $k_{0,2}$ and $K_{0,2}$ are, respectively, the pre-exponential factors. $E_{A,2}$ is the activation energy and ΔG_2 is the Gibbs free energy of the water gas shift reaction (Equation 4.2).

The intrinsic rates R_i of the other two heterogeneous reactions of the char gasification are dependent on temperature *k(T),* concentration of the gasification agent (steam) *f(C)* and the activated reaction surface area *S(X)* of the solid. In general, kinetic models for the intrinsic rates of heterogeneous reactions can be expressed as the product of three affecting parameters (Fermoso et al. 2008):

$$R_i = k(T)\cdot f(C)\cdot S(X) \tag{4.26}$$

In which *k* is the apparent rate constant which can be considered as a unique function of temperature, *T,* and is usually expressed in the Arrhenius equation:

$$k(T) = k_{0,j}e^{-E_{Aj}/\boldsymbol{RT}},\ j = 1, 2, 3 \tag{4.27}$$

where k_0 and $E_{A,j}$ are the pre-exponential factor and the activation energy, respectively.

The gas component function in Equation (4.26), $f(C)$, represents the effect of the gas concentration on the reaction rate. The reaction between steam and carbonaceous material can be expressed by the Langmuir-Hinshelwood type formulation (Klose and Wölki 2005). However in this model, it will be simplified to $f(C) = C$ since the system was operated at atmospheric pressure, at which the intrinsic rate is linearly related to the concentration of the gasification agent for both steam and CO_2 (Molina and Mondragon 1998).

The specific reactive surface area evolution function in Equation (4.26), $S(X)$, describes the change of the geometrical property of the solid char as the gasification proceeds. In the initial stage of the gasification process, the total surface area increases due to the size increase of the char pores during the initial char consumption period. After the initial stage, the pores contract and apparent char particle size is reduced, which causes the reduction of the total surface area. Therefore, the random pore model(RPM), which contains the competing effect of single pore size increase and destruction of the overlapping region on the total surface area, is implemented to determine the surface area evolution (Bhatia and Perlmutter 1980):

$$S(X) = S_0(1-X_s)\sqrt{1-\psi\ln(1-X_s)} \tag{4.28}$$

RPM assumes that pores of the particles are composed of randomly cylindrical pores of arbitrary size distribution, and the reaction surface is given by the internal surface of the pores exposed to the gas hence the reaction rate is proportional to its associated surface area (Fei et al. 2011). Where S_0 is the specific surface area of char at $X_s = 0$. ψ is the dimensionless parameter indicating the nature of pore structure:

$$\psi = \frac{4\pi L_0(1-\Phi_0)}{S_0^2} \tag{4.29}$$

In the above equation, L_0, S_0 and Φ_0 represent the initial pore surface, pore length and solid porosity respectively(Bhatia 1987). The value of parameter ψ is mainly dependent on the type of the solid fuel and the char formation condition (Matsumoto et al. 2009), (Sadhukhan et al. 2009).

Combining all of three reaction parameters, *k(T)*, *f(C)* and *S(X)*, the complete form of the intrinsic reaction rate vector becomes:

$$\mathbf{R} = \begin{pmatrix} R_1 \\ R_2 \\ R_3 \end{pmatrix} = \begin{pmatrix} k_{0,1} e^{-E_{A,1}/RT} S_0 (1-X_s)\sqrt{1-\psi \ln(1-X_s)}\; C_1 \\ k_{0,2} e^{-E_{A,2}/RT} \left(C_1 C_3 - \dfrac{C_2 C_4}{K_{2,0} e^{-\Delta G_2/RT}} \right) \left[\Phi_0 + (1-\Phi_0) X_s \right] \\ k_{0,3} e^{-E_{A,3}/RT} S_0 (1-X_s)\sqrt{1-\psi \ln(1-X_s)}\; C_4 \end{pmatrix} \tag{4.30}$$

4.2.5 Char structural evolution

The local conversion of char is evaluated from the total carbon consumption rate:

$$\frac{\partial X_s}{\partial t} = -\frac{MW_C}{\rho_C} \mathbf{v_C R} \tag{4.31}$$

in which MW_C and ρ_c are the molecular weight and density of the char respectively. The stoichiometric coefficient vector, $\mathbf{v_C}$ = [-1, 0, -1]. It is assumed that the density of the solid phase remains constant regardless of the char conversion; the porosity is a unique function of conversion:

$$\Phi(X_s) = \Phi_0 + (1-\Phi_0) X_s \tag{4.32}$$

In this model, the pores are assumed to be cylinders with axis direction normal to the particle surface. Since the porosity and specific surface area are the total volume and inner surface area of all pores respectively, the local mean pore diameter can be determined from the surface area and porosity of the char:

$$d_p = \frac{4\Phi(X_s)}{S(X_s)} = \frac{4\left[\Phi_0 + (1-\Phi_0) X_s\right]}{S_0 (1-X_s)\sqrt{1-\psi \ln(1-X_s)}} \tag{4.33}$$

With the gasification proceeding after a certain stage, the char particle shrinks and the apparent radius (r_a) of the char particle starts to reduce. This critical point corresponds to the process when local conversion at the particle outer surface causes fragmentation. In the model, the critical conversion point for the fragmentation (X_{cr}) is introduced in order to determine the

dynamic of r_a. When the local conversion at the surface is below X_{cr} the apparent radius remains unchanged, but beyond X_{cr} further conversion of char at the surface will cause shrinkage in the particle radius. Based on this consideration, the change in char apparent radius with time can mathematically be expressed as:

$$\frac{\partial r_a}{\partial t} = 0 \text{ if } X_s(r_a) < X_{cr}\,; \quad \frac{\partial r_a}{\partial t} = -\frac{\partial X_s(r_a)}{\partial t} \Big/ \frac{\partial X_s(r_a)}{\partial r} \text{ if } X_s(r_a) \geq X_{cr} \tag{4.34}$$

4.2.6 Surface gas concentration

Gas concentration at the outer surface of the char particle is evaluated in order to provide boundary conditions for solving the proposed model. It is assumed that at the char surface the external convective mass transfer rate for the gas components to the surface must be equal to the transportation rate through the char particle surface (no accumulation at the surface), hence:

$$\mathbf{N}(r_a) = -\frac{\Phi}{\tau}\left([\mathbf{B}]^{-1}\frac{\partial \mathbf{C}}{\partial r} + \frac{RTB_0}{\mu}\frac{\partial}{\partial r}\mathbf{C}_t[\mathbf{B}]^{-1}[\mathbf{A}]\mathbf{C} \right)\Bigg|_{r_a} = k_c[C_b - \mathbf{C}(r_a)] \tag{4.35}$$

Where C_b is the component concentration in the bulk gas outside the char particle; k_c is the mass transfer coefficient which is determined from the correlation of forced convection mass transfer of a spherical particle (Baxter and Robinson 2004):

$$k_c = \frac{ShD_m}{2r_a}\,; \; Sh = 2.0 + 0.552\, Re^{0.5} Sc^{1/3} \tag{4.36}$$

4.2.7 Numerical Method for Solving the Developed Model

In the developed model, gas species concentration (**C**) and char conversion rate X_s are the objective variables to be determined. Since porosity is the function of conversion rate, the left hand side of Equation (4.14) can be re-arranged as follows:

$$\frac{\partial \mathbf{C}}{\partial t} = \frac{\dfrac{\partial(\Phi \mathbf{C})}{\partial t} - \mathbf{C}\dfrac{\partial \Phi}{\partial t}}{\Phi} = \frac{\dfrac{\partial(\Phi \mathbf{C})}{\partial t} - \mathbf{C}(1-\Phi_0)\dfrac{\partial X_s}{\partial t}}{\Phi} \tag{4.37}$$

Since char particle apparent radius starts to reduce after the critical carbon conversion rate and will eventually approach zero, the moving boundary method is used in solving the proposed model (Ebahimi et al. 2008).

As the model involves a series of partial differential equations (PDEs), the model can only be solved using an appropriate numerical technique. In solving the model, the solid char particle is divided into *N* discrete nodes from the centre to the outer surface of the particle, and physical properties at each node are evaluated by the central difference method. The radius coordinate, *r,* is replaced by dimensionless spatial variable, *s*, therefore, the domain concerned is converted into an expression of relative coordinate:

$$r = r_a \cdot s\,,\ \forall r \in [0,\ r_a];\ \ \forall s \in [0, 1]$$

Therefore, the derivative of variables represented by **Y** at all nodes is transformed from the original PDEs (Wang and Bhatia 2001b):

$$\left.\frac{\partial \mathbf{Y}}{\partial t}\right|_s = \left.\frac{\partial \mathbf{Y}}{\partial t}\right|_r - \frac{\partial \mathbf{Y}}{\partial s}\frac{\partial s}{\partial r_a}\frac{\partial r_a}{\partial t} \tag{4.38}$$

Where the variable *s* is defined as:

$$\frac{\partial s}{\partial r_a} = -\frac{s}{r_a} \tag{4.39}$$

In order to obtain the numerical solution, the original PDEs were converted into a set of ordinary differential algebraic equations (DAEs), by converting the continuous variables into discrete expression on *N* equal-space segments along the particle radius, thus the original six PDEs can be converted into 6×*N* DAEs. In solving the model, different sizes of discrete nodes and different time steps were tried to obtain converging and stable solutions using Matlab software. It was found that the number of elements should be equal to, or greater than, 50 in order for the model to provide converging solutions at all possible input operating conditions. The numerical result of a convergence of gasification scenario of 50:50 coal-to-biomass ratio blend char at 900^{o}C was selected as an example of the numerical convergence of model results and is illustrated in Figure 4.2. Since the steady state values for all three gas components are zero at $t \to \infty$, the absolute

values of error in gas composition at a fixed time point after gasification started (t=300 seconds) were used to be the convergence criterion and are presented in Figure 4.2. From the graph, a satisfactory convergence of numerical results can be achieved at the number of elements greater than 40.

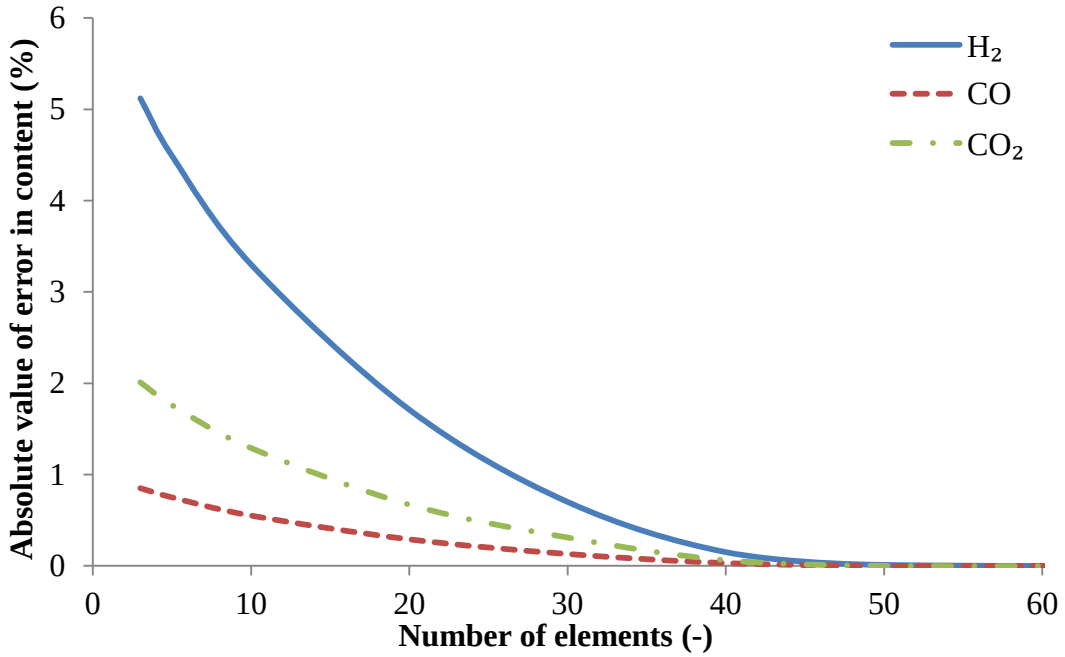

Figure 4.2: Convergence of simulation result of gasification of coal and biomass at 50:50 blending ratio at 900^{o}C.

The initial conditions can be established from the operational condition. At the start of the gasification process (t = 0), gas compositions of the steam (H_2O) and three resultant gas species (H_2, CO and CO_2) are zero within the char particles ($C_1 = C_2 = C_3 = C_4 = 0$). The composition of nitrogen (C_5) corresponding to atmospheric pressure and operating temperature can be calculated using the Ideal Gas Law. The solid char conversion at the start is zero ($X_s = 0$).

The boundary conditions for the gaseous species at the char centre ($r = 0$) and at the char surface ($r = r_a$) have been given in Equation (4.6). Since there is no transportation of solid char occurring, the boundary condition for carbon conversion (X_s) is not needed.

The numerical scheme of solving the developed model can be described in four steps:

- Firstly, the time derivatives of deviation variables at a given radial position, $\left.\frac{\partial \mathbf{Y}}{\partial t}\right|_r$, are evaluated from the differential equations by the central difference method.
- The moving boundary method is then used to transform the time derivatives of the deviation variables into a dimensionless form, $\left.\frac{\partial \mathbf{Y}}{\partial t}\right|_s$.
- PDEs are desecrated into DAEs in order to obtain the numerical solution.
- Finally MATLAB software, which employs the ode15 method, is coded to integrate the DAEs for prediction of required values of gas species concentrations and carbon conversion rate.

The above procedures can be applied to both the gasification of biomass char and the gasification of coal char using corresponding microstructural properties such as area to volume ratio, pore structure parameter and porosity. For simulation of the gasification of blended biomass and coal char, a simple method of interpolating the solid material properties is used to quantify the blend properties.

4.3 Simulation Results and Discussion

4.3.1 Simulation results and comparison with experimental data

The developed model for the steam gasification of solid chars has been solved for operating temperatures of 850, 900 and 950°C as used in the experiments being described in the previous chapter. The input values for the simulations are given in Table 4.1 for biomass char and coal char, respectively. For simulation of blended biomass and coal chars, the properties of the blended chars are determined as a linear relationship with the proportion of biomass char and coal char in the blend char which is, in turn, calculated based on their corresponding fuel proportion in the feedstock as well as the generated char in the devolatilization. The values of pre-exponential factors and activation energy in determination of the reaction kinetics for reactions Equation (4.1) and Equation (4.3) are shown in the table below.

Table 4.1: Input Parameters and Values in the Model Simulation

Symbol	Description	Coal	Biomass
Ψ	Pore structure parameter of char	10	2
S_0	Initial specific area of char	13000 m^2/m^3	200000 m^2/m^3
Φ_0	Initial porosity of char	0.6	0.8
$k_{0,1}$	Pre-exponential factor of reaction 1	29 (s^{-1})	
$k_{0,3}$	Pre-exponential factor of reaction 3	4364 (s^{-1})	
$E_{A,1}$	Activation energy of reaction 1	175.84 kJ/mol (Zhu et al. 2008)	
$E_{A,3}$	Activation energy of reaction 3	248.12 kJ/mol (Wang and Bhatia 2001a)	

By using the input data given in Table 4.1, the developed model has been solved to predict gas production rates, product gas composition, and carbon consumption rate in the steam gasification of pure biomass char, pure coal char and blended biomass and coal char. These are the essential fitting parameters within the reasonable range listed in references. The values without reference indicated were overall the best fitting parameters with experimental data. In the table above, the numerical values of the initial specific area S_0 of biomass and coal differ by an order of magnitude. Such difference indicates that biomass char has a more amorphous structure than the coal char, which is one of the conclusions in the previous chapter. The simulated results for gasification of pure biomass char at 900°C are shown in Figure 4.3 for the gas production rate and gas composition and in Figure 4.4 for the carbon consumption rate. In the simulations, the heat-up stage is not included as the model does not include the heat transfer process. In the practical gasification process, the char derived from the initial pyrolysis has a temperature close to the operation temperature, thus the char heat-up does not exist. Nevertheless, the heat-up stage in the char gasification tests was very short (about 2 minutes) compared to the complete gasification process (22 minutes or longer). The corresponding results for the gasification of coal char are shown in Figures 4.5 and 4.6. In all of the figures, the experimental data are also presented for comparison with the model simulation results.

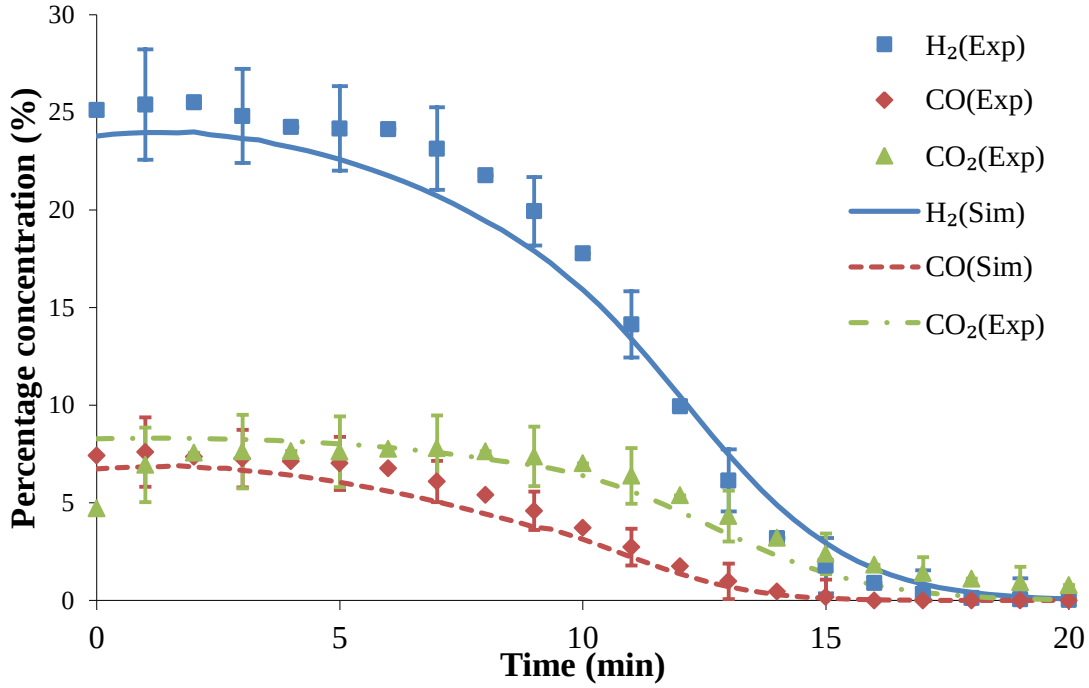

Figure 4.3: Simulated and experimental results of gas production rate and gas composition in steam gasification of pure wood char at 900 ^{o}C.

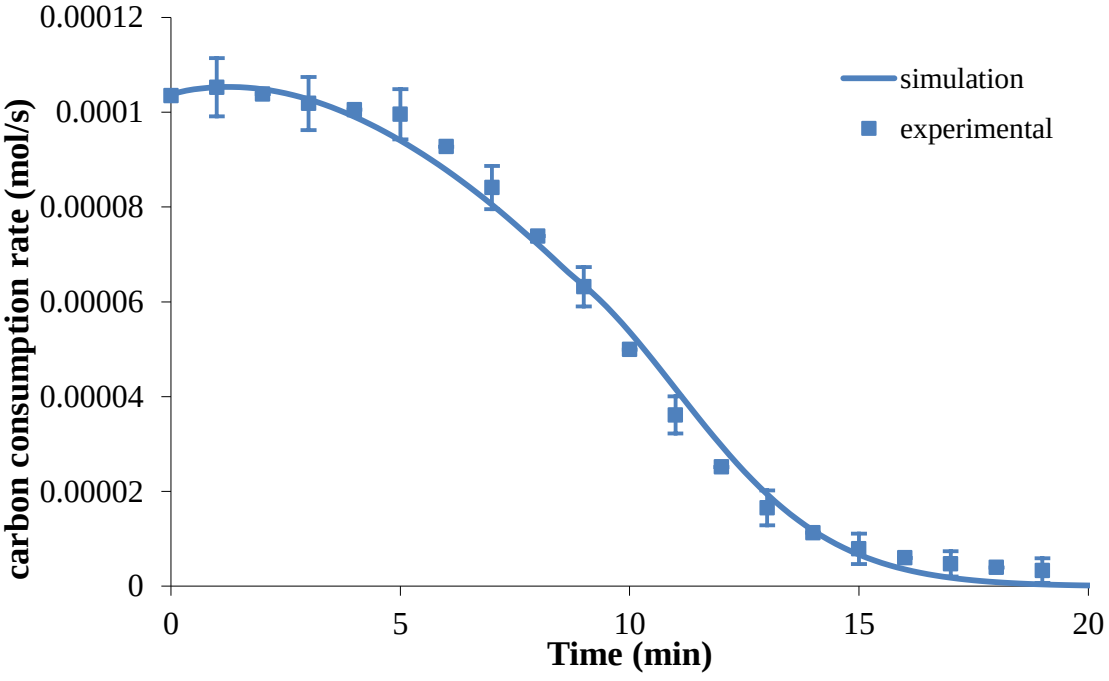

Figure 4.4: Simulated and experimental results of carbon consumption rate for steam gasification of pure wood char at 900 ^{o}C.

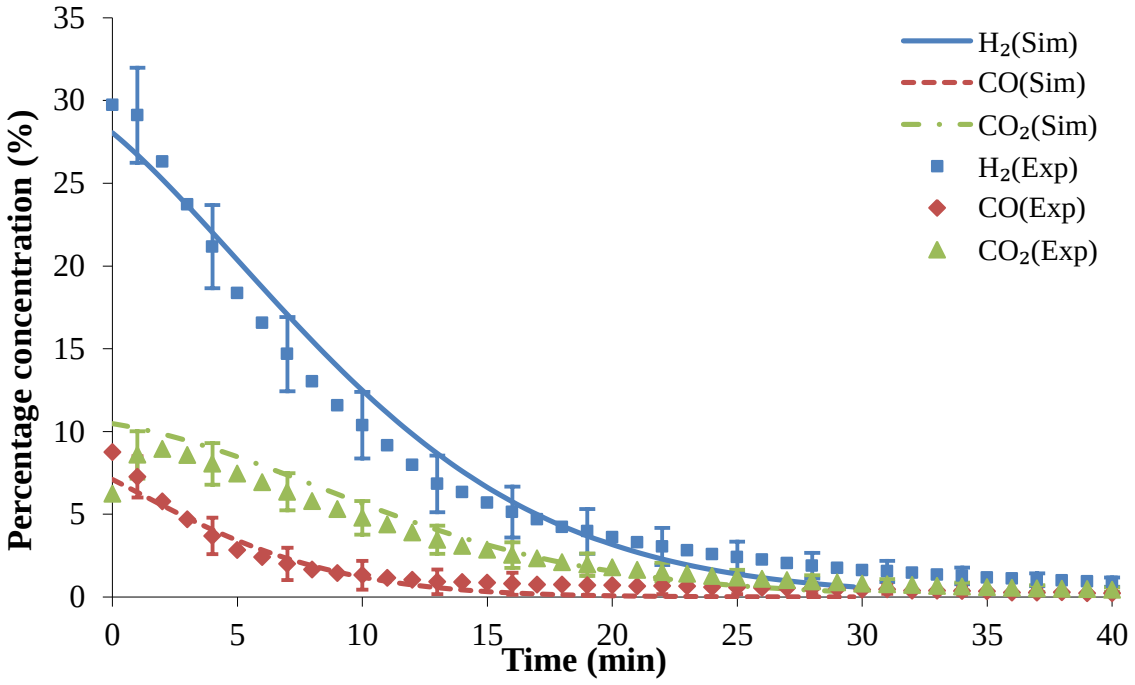

Figure 4.5: Simulated and experimental results of gas production rate and gas composition in steam gasification of pure coal char at 900°C.

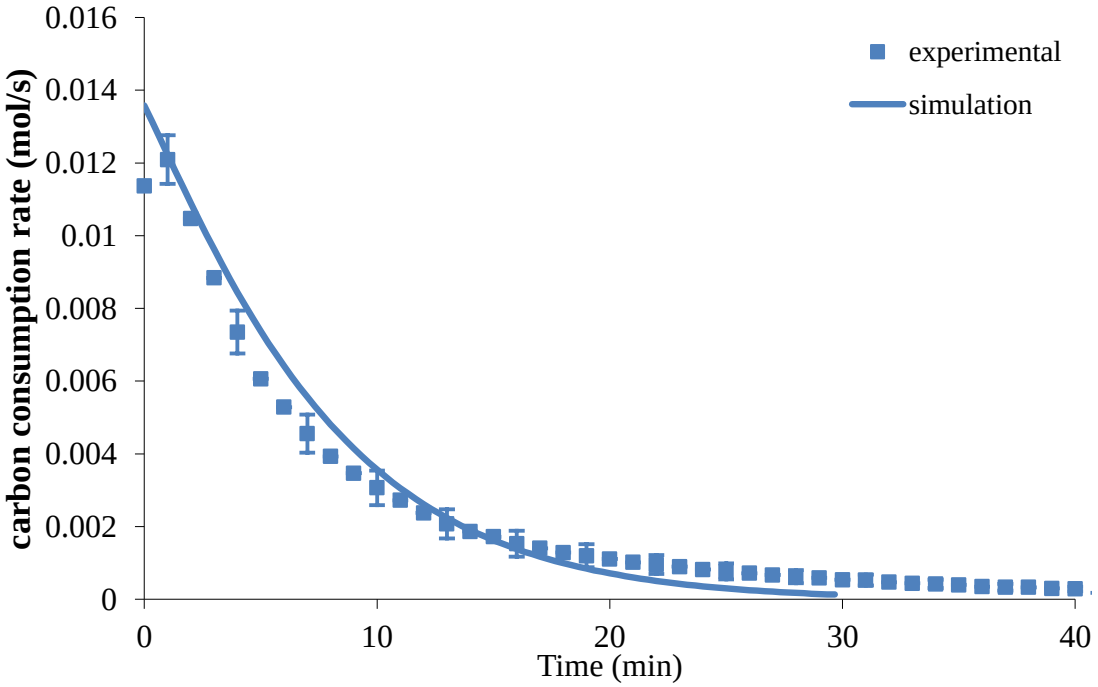

Figure 4.6: Simulated and experimental results of carbon consumption rate for steam gasification of pure coal char at 900°C.

Comparison between simulation results and experimental data was also made for blended biomass and coal chars, and for different gasification temperatures as used in the experiments. The model simulation results are all in close agreement within error range for the producer gas profile and overall carbon consumption rates, where the error values were calculated as standard error among three individual experimental data sets of char gasification at operating point. From the above figures, the initial data points differ from the model prediction during the initial stage, which can be attributed to the slight non-spherical shape of char particle at this stage, so that the consumption rate of protruding parts of char could be faster; as the gasification proceeded, the entire char particle became more spherical, therefore the experimental data points are closer to the simulation curves during the later stage. From the above comparison, confidence in the developed model has been gained and thus the model has further been applied to examine the effects of gasification temperature, char structure and blending ratio of biomass and coal. The results are presented as follows. Where possible, experimental data are also included.

4.3.2 Effect of gasification temperature

Figures 4.7 and 4.8 show the simulation results and experimental data for carbon conversion in steam gasification of pure biomass char (Figure 4.7) and pure coal char (Figure 4.8) at three temperatures 850°C, 900°C and 950°C. The carbon conversion is the relative carbon consumed which is defined as the ratio of initial carbon mass in the char minus the carbon consumed in the gasification process to the initial carbon mass. At the start of the gasification, the carbon conversion is zero as no carbon is consumed yet, but the carbon conversion approaches unity when the gasification is near completion when the majority of the carbon has been consumed.

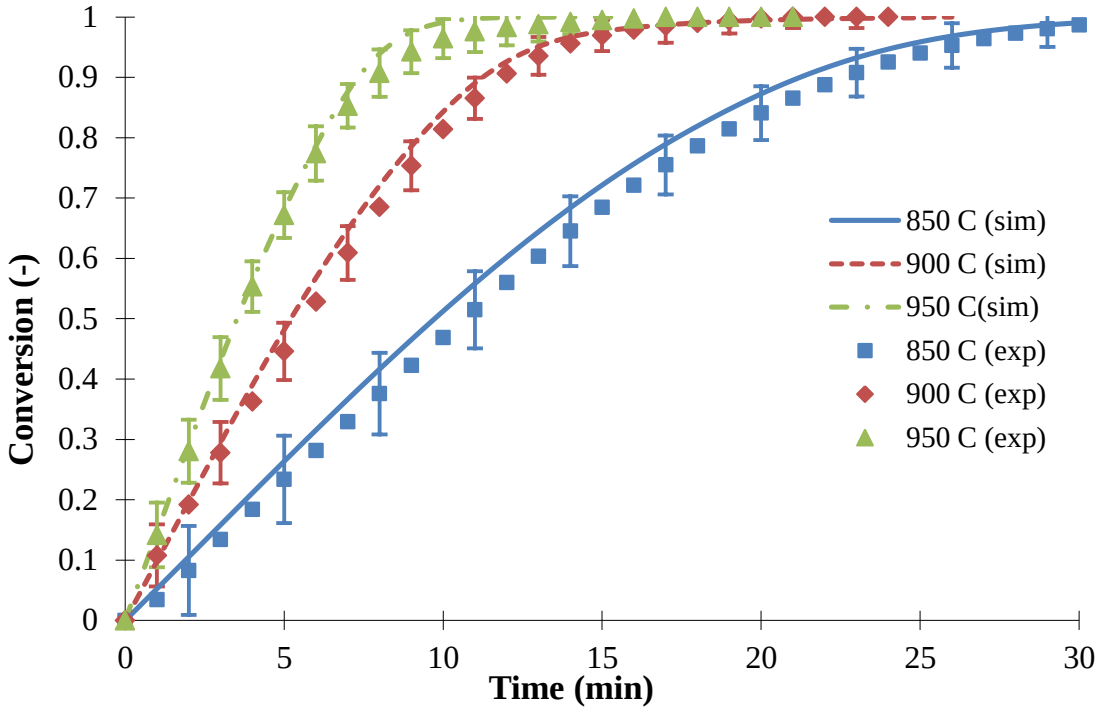

Figure 4.7: Effect of gasification temperature on conversion dynamics of pure woody biomass chars.

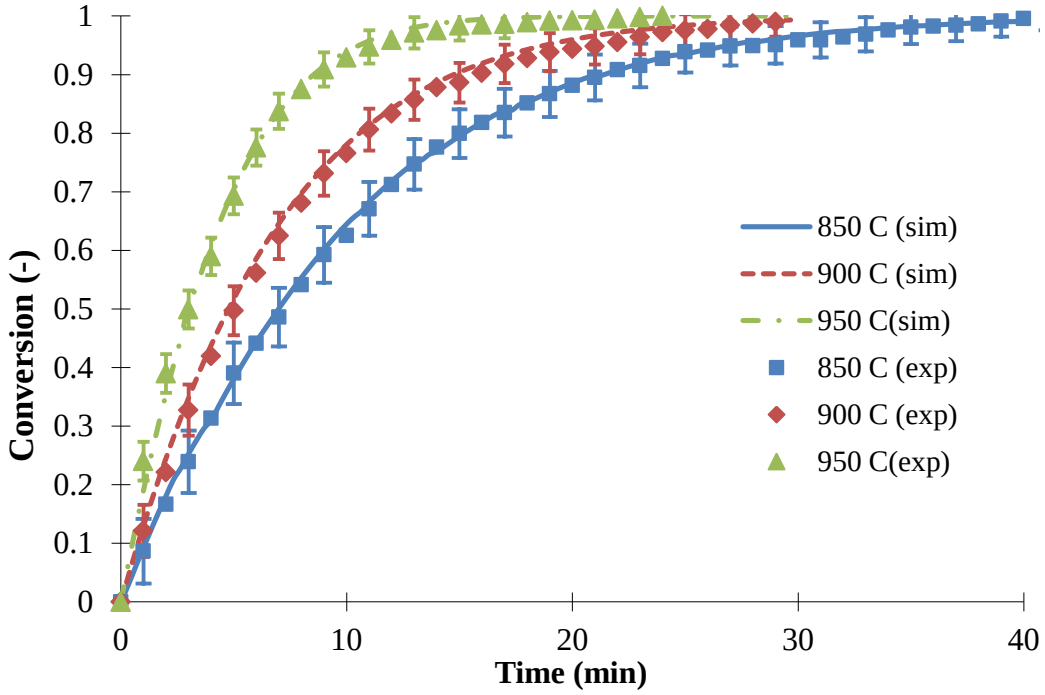

Figure 4.8: Effect of gasification temperature on conversion dynamics of pure coal chars.

From the conversion dynamic curves of biomass and coal, it is clearly seen that the gasification temperature enhanced the reaction rates for both types of chars. Furthermore, different reaction characteristics can be observed between the biomass char and the coal char. For the biomass char, the reaction rate remained approximately constant at the initial stage, indicated by the linear increase of the conversion dynamic curve. For the coal char, the exponential shape of the conversion dynamic curve indicates that the gasification reaction order is a first order reaction.

The close agreement between the model simulation and the experimental results further confirms the analysis of the gasification mechanism presented in the previous chapter. In gasification of the biomass char, the reactions mainly occur on and near the char particle surface thus constant reaction kinetics can be observed in the early stage of the gasification. However, in the later stage of the gasification, the surface becomes progressively reduced with char diameter shrinking, and the reaction rates relative to the original char mass are reduced, resulting in a curved conversion curve. For the gasification of coal char, the reaction can occur in the micro-pores within the char particle due to the lower transfer resistance, therefore the intrinsic reaction rates follow traditional first order kinetics.

Another interesting phenomenon observed is that increasing the temperature from 850°C to 900°C has a more significant impact on the gasification of biomass char than in the gasification of coal char. Further increase in the gasification temperature from 900°C to 950°C has more impact in the coal char gasification than in the biomass char gasification. Such a phenomenon could be explained as the results of the competing effect of heterogeneous reactions and gaseous species diffusion within the char matrix. Since biomass char has a larger internal reactive surface area and smaller pore size compared with the coal char, the mass transportation within the char particle is the dominant factor for the biomass char gasification whereas for the coal char gasification, the intrinsic reaction is more important. As the temperature increases, the rate of mass transportation of gases is enhanced more significantly at the lower temperature range (850 to 900^{o}C). On the other hand, the intrinsic reaction rate can be increased more significantly at the higher temperature range (900 to 950^{o}C). Therefore, the overall rate of biomass char conversion is more sensitive to the temperature increase at a relatively lower temperature range but the gasification rate for the coal char is more sensitive to the higher temperature range.

4.3.3 Effect of microstructure of the solid chars

The overall specific reaction surface area (S) of the micro-pores in the char particle is the key parameter in the model which influences the char gasification process. This can be understood from its impacts on the gasification reaction rate and on the intra-particle transportation of the reaction species, referring to Equations (4.26) and (4.33). From Equation (4.26), the reaction rate of heterogeneous reaction (R_j) is proportional to the specific reaction surface area, while Equation (4.33) shows that the mean pore diameter (d_p) is inversely proportional to the effective reaction surface area. For biomass char, which is more porous than coal char, the specific reaction surface area is greater thus the intrinsic reaction rate is higher when compared to the coal char. However, the transportation of the gaseous species is also affected by the Knudsen Diffusivity effect which is the rate controlling factor of the overall diffusion due to the restriction of small pore diameter. Conversely, for coal char with smaller specific reaction surface area, reaction rates are lower but the pore diameter is higher compared to the biomass char. Therefore, in the gasification of coal char, the reaction rate becomes the rate controlling factor.

Considering both the effect of the intrinsic reaction rate and the overall transportation of gaseous species during the gasification process, in biomass char gasification the reactions on the char particle surface proceed faster than those in the micro-pores due to the greater resistance to gas transportation through the micro-pores. Therefore, the solid matter (carbon) on the surface layer of the biomass char will be consumed faster than that within the char particle. This can be clearly illustrated from the simulation results for biomass char gasification at 900°C as shown in Figure 4.9 in which the carbon conversion rate for three locations at the outer surface, at the middle location along the radius and in the centre of the char particle, is plotted as a function of elapsed time. The Figure 4.9 clearly shows the difference in the reaction rates along the radius resulting in a significant conversion gradient along the particle radius. It is also found that the surface shrinks in the gasification, which is indicated by the shorter time of carbon conversion completion at the surface compared to the other parts within the biomass char particle.

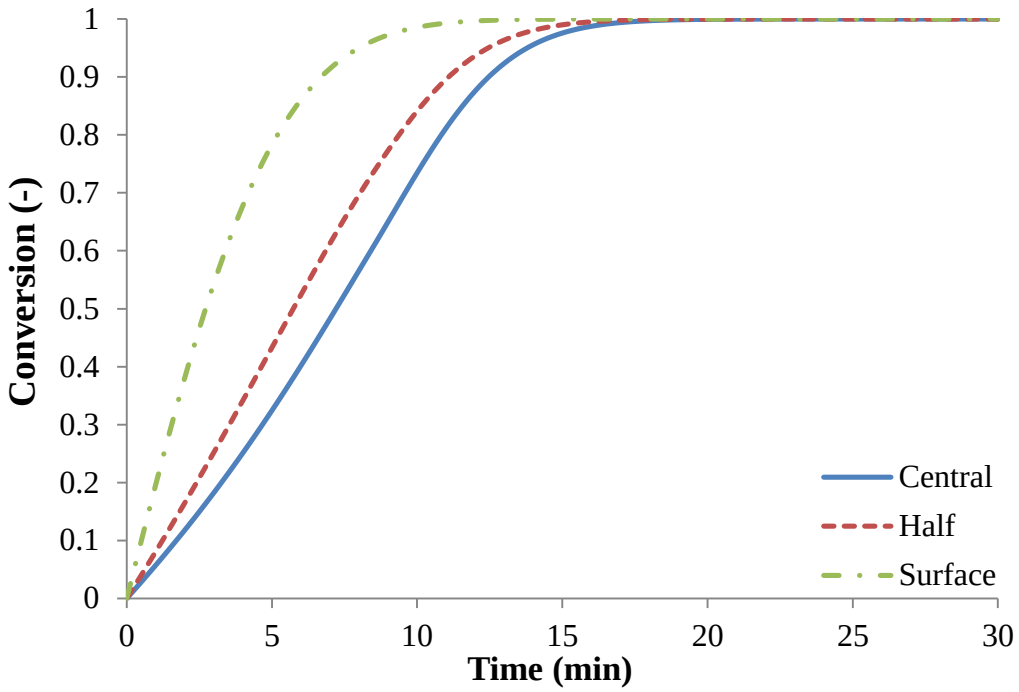

Figure 4.9: Predicted local conversion dynamics of biomass char at the char surface, mid-radius and in the char center, at 900^{o}C.

On the other hand, the simulation results for the coal char gasification (Figure 4.10) show that the conversion of the coal char is more uniform compared with the biomass char. Based on this finding, all the local conversion dynamics at different radial positions are very close to each other, indicating much less resistance for the reactant gas species to transfer within the char particles. Further analysis of the coal gasification process can reveal that the surface shrinkage is much slower than the biomass char gasification thus the overall reaction rate is slower than the biomass char gasification. This can be confirmed by the longer gasification completion time at the same temperature compared to the biomass char gasification.

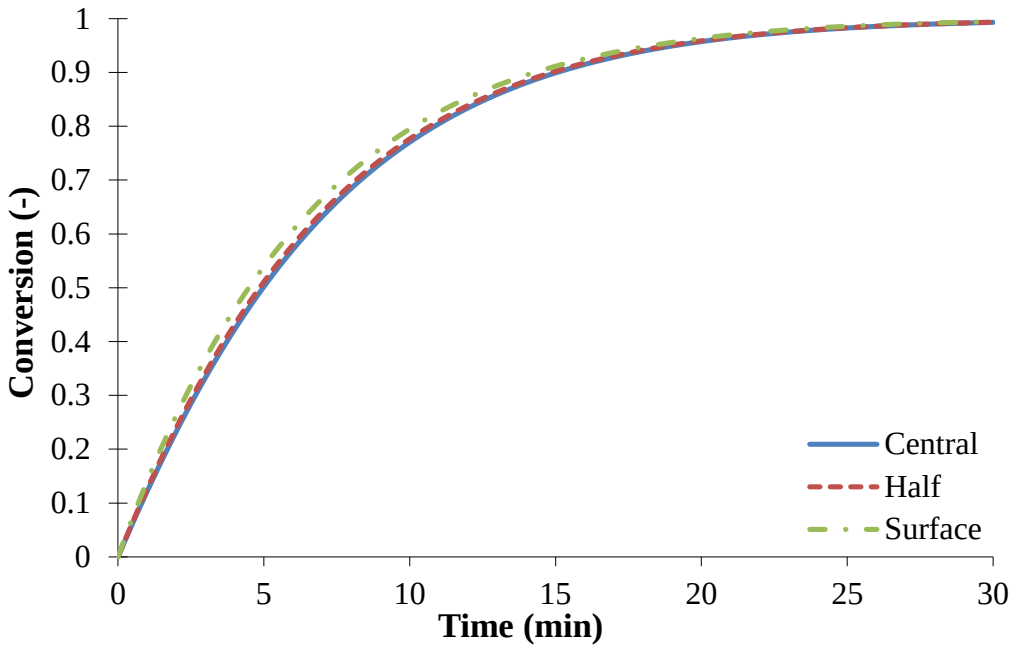

Figure 4.10: Predicted local conversion dynamics of coal char at the char surface, mid-radius and in the char center, at 900^{o}C.

4.3.4 Effect of biomass and coal blending

The gasification process of blended biomass and coal chars has also been simulated using the developed model with the physical and chemical properties being determined, based on the actual fractions of each solid in the blend char rather than on the blending ratio of the original materials. This is because the char yield of the coal is significantly higher than the biomass. In this work, the initial parameters such as surface area, porosity and density were also calculated based the actual fraction of each fuel in the blended char. The simulation results for gasification of blended chars with coal-to-biomass blending ratios of 20:80, 50:50, 80:20 are presented in Figures 4.11, 4.13 and 4.15 for the gas production profile and gas composition, and in Figures 4.12, 4.14 and 4.16 for the carbon consumption rate. In the figures, experimental data are also included for comparison with the simulation results and close agreements between the model simulation results and experimental data are observed.

The simulation results for the blended chars show that the gasification of blend chars is more likely to follow first order reaction kinetics without an apparent constant reaction rate appearing in the early stage as observed in the gasification of pure biomass char (Figures 4.3 and 4.4). This further confirms the findings from the experiments in Chapter three, in which the characteristics of blend char gasification are closer to those of pure coal chars (Figures 4.5 and 4.6). This behaviour may be attributed to a number of factors. Firstly, in the char generation, the biomass lost more volatile components than coal thus the actual char mass formed from the biomass was less than that from the coal. In addition, the microstructures between the pure biomass and coal are different, and the coal becomes more influential than the biomass when blended together.

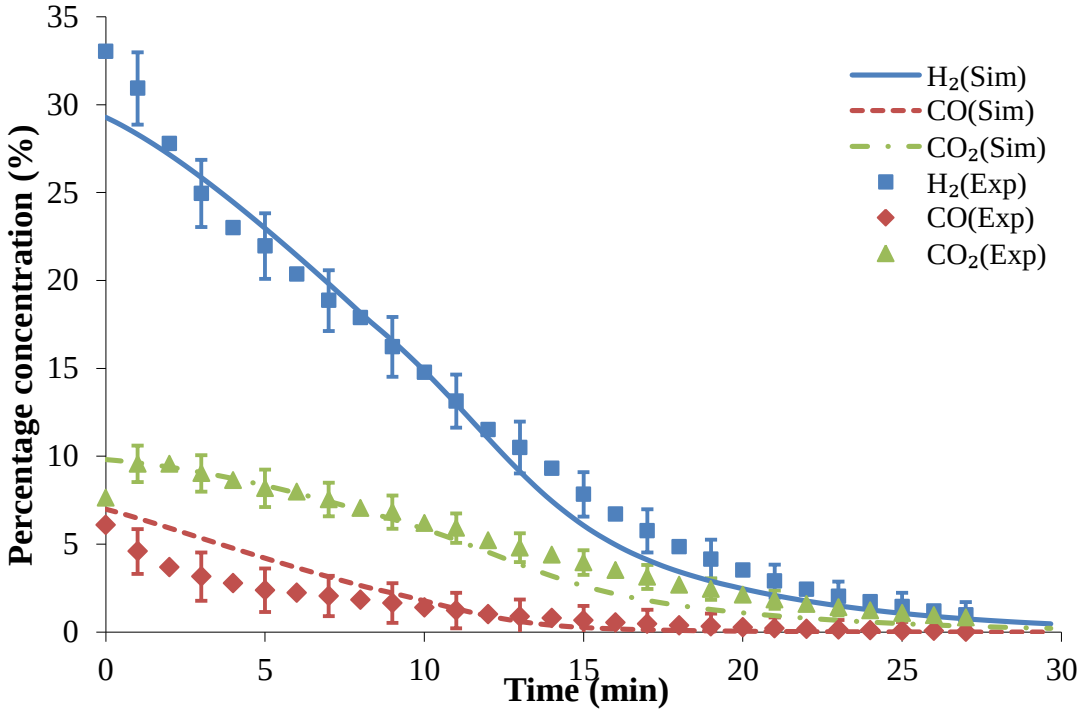

Figure 4.11: Comparison of model simulated and measured results of gas production rate and gas composition in gasification of blend char with coal-to-biomass ratio of 20:80.

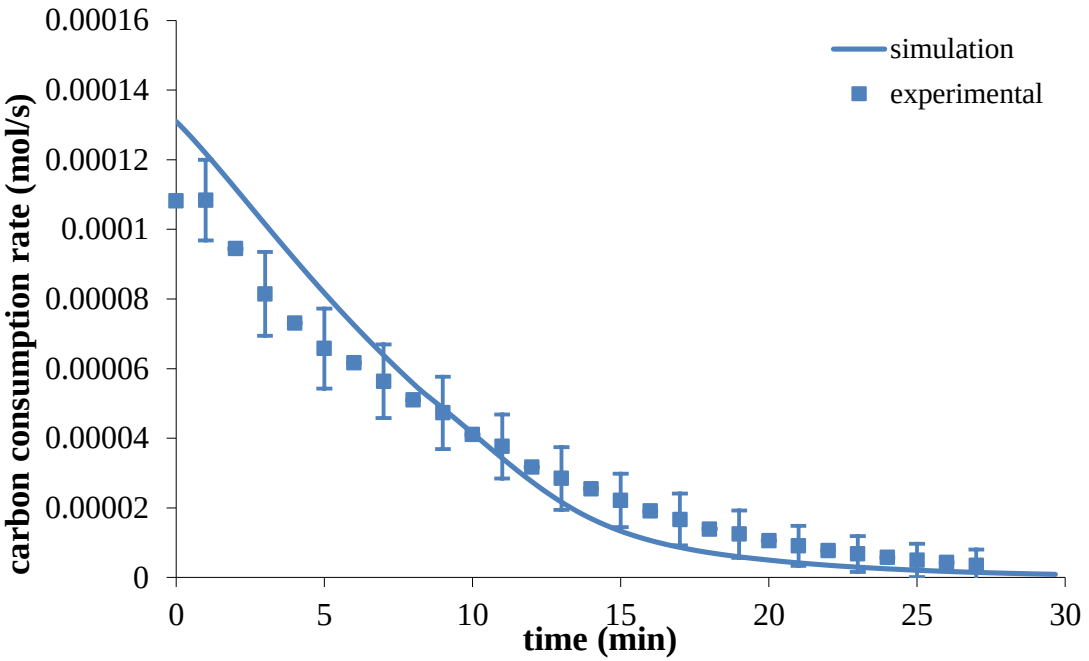

Figure 4.12: Comparison of model simulated and measured result of carbon consumption rate in gasification of blend char with coal-to-biomass ratio of 20:80.

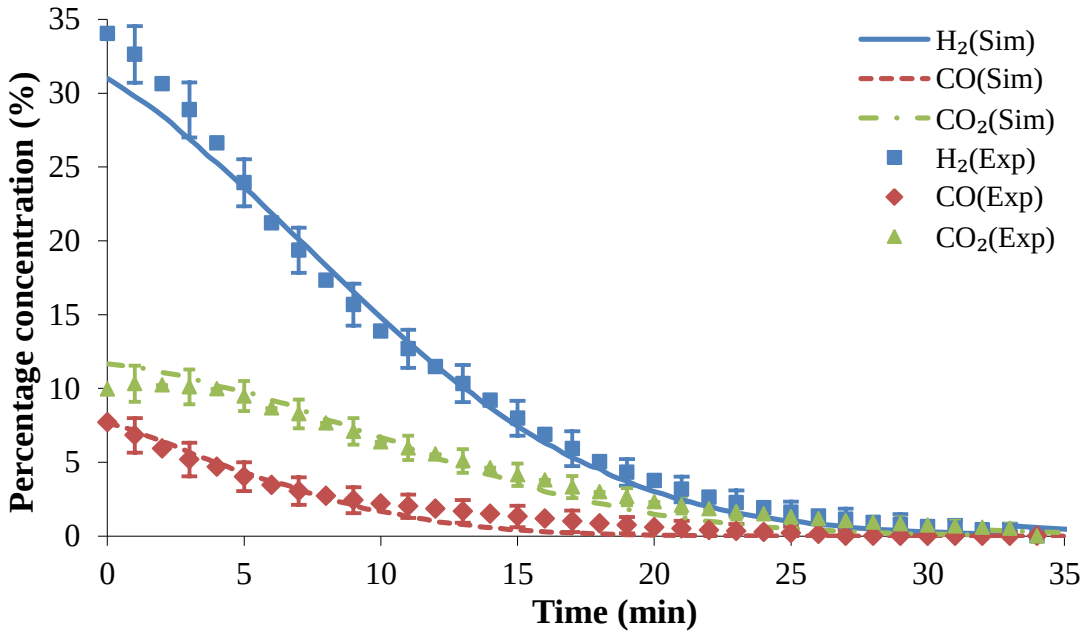

Figure 4.13: Comparison of model simulated and measured results of gas production rate and gas composition in gasification of blend char with coal-to-biomass ratio of 50:50.

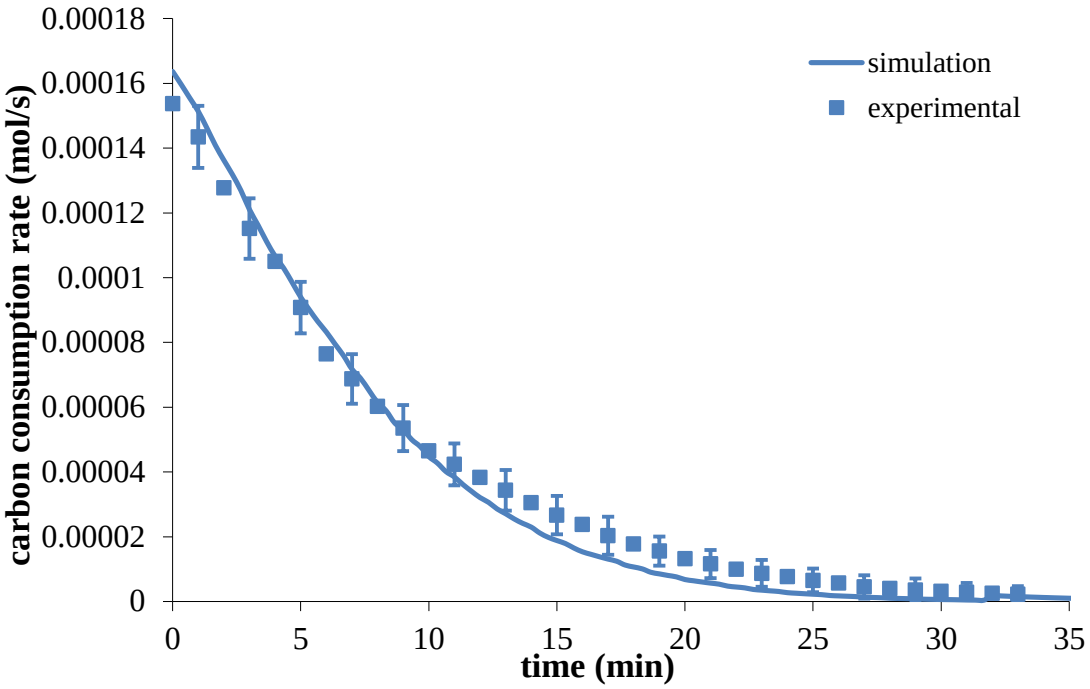

Figure 4.14: Comparison of model simulated and measured results of carbon consumption rate in gasification of blend char with coal-to-biomass ratio of 50:50.

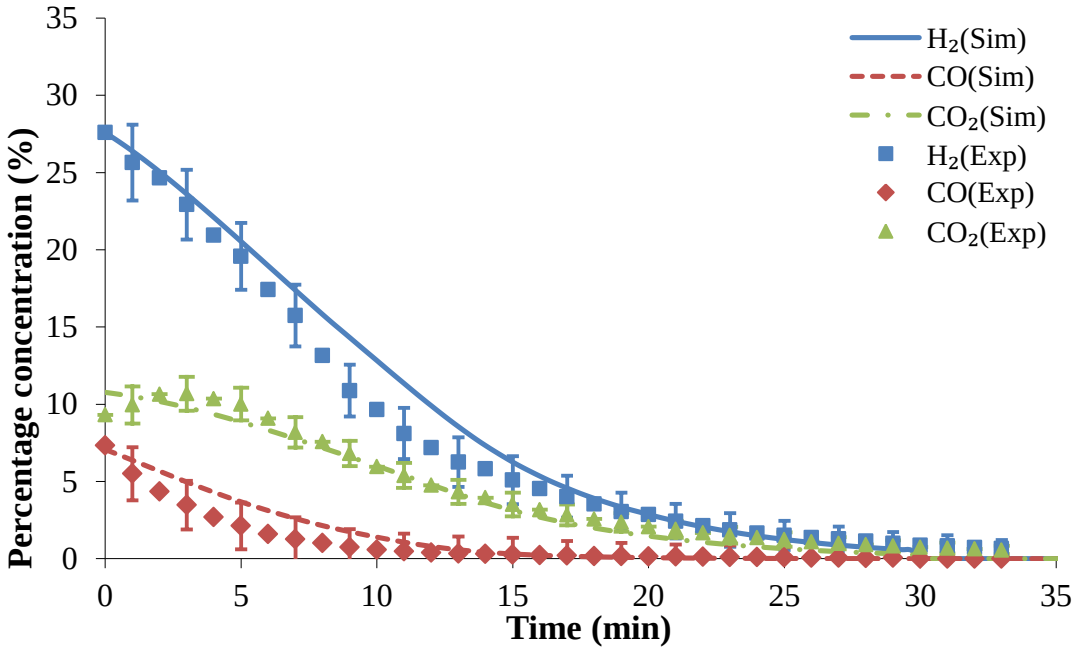

Figure 4.15: Comparison of model simulated and measured results of gas production rate and gas composition in gasification of blend char with coal-to-biomass ratio of 80:20.

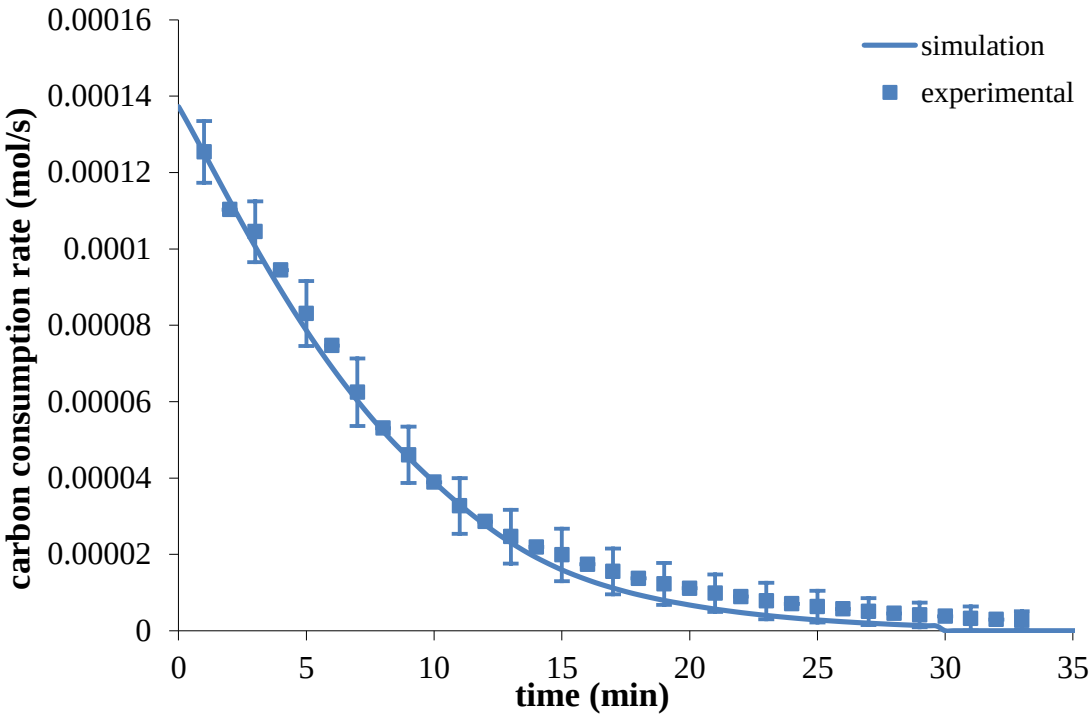

Figure 4.16: Comparison of model simulated and measured result of carbon consumption rate in gasification of blend char with coal-to-biomass ratio of 80:20.

4.4 Conclusion

In this work, a dynamic mathematical model has been developed for simulation of the steam gasification of biomass char, coal char and blended biomass-coal char. This model is based on the reaction mechanism in the gasification, mass conservation and mass transfer as well as char structure characteristics. The reactions considered include: steam-gasification reaction, water-gas shift reaction and Bouduard reaction. The mass transfer process takes into account both diffusion and convective bulk flow of the reactant gas (steam), resultant gas species (H_2, CO, CO_2) and the carrier gas (N_2). The heat transfer is not included in the model since the particle size of the chars is very small thus the intra-particle temperature gradient is insignificant. The model has been solved using a numerical method to predict the gas production rate, gas composition and carbon consumption rate. In addition, the model can also predict the concentration distribution of gas species and carbon conversion rate along the char radial direction, from the centre to the outer surface of the particle.

The developed model is validated using experimental data and close agreement has been found between the model simulation results and the experimental data. The model simulation results show that the char structure (specific reaction surface area and micro-pore size) has significant impacts on both intrinsic reaction rate and the intra particle mass transportation while the magnitude of these two competing processes determines the overall gasification process. The difference in the char structure is the key factor contributing to different gasification characteristics between biomass char and coal char.

The developed model is also applied to investigate the gasification of blend chars in which the solid material properties are interpolated based on the actual fraction of two fuels in the char. The close agreement between the modelled and experimental results suggests that the simple method to determine the blend properties is adequate for the simulation of gasification of the blend chars. The developed model presented in this paper will be employed in further studies on co-gasification of blended coal and biomass in large scale bubbling fluidized bed gasifiers.

References

Arnold, J. H. (1933). "Vapor Viscosities and the Sutherland Equation." *Journal of chemical physics*, 1, 170-176.

Ballal, G., Li, C.-H., Glowinski, R., and Amundson, N. R. (1989). "Single particle char combustion and gasification." *Computer Methods in Applied Mechanics and Engineering*, 75(1–3), 467-479.

Baxter, L. L., and Robinson, A. L. (2004). "Effects of intraparticle heat and mass transfer on biomass devolatilization: Experimental results and model predictions." *Energy and Fuels*, 18, 1021-1031.

Bhatia, S. K. (1987). "Modeling the pore structure of coal." *AIChE Journal*, 33(10), 1707-1718.

Bhatia, S. K., and Perlmutter, D. D. (1980). "A random pore model for fluid-solid reactions: I. Isothermal, kinetic control." *A.I.Ch.E Journal*, 26, 379-386.

Biggs, M. J., and Agarwal, P. K. (1997). "The CO/CO2 product ratio for a porous char particle within an incipiently fluidized bed: a numerical study." *Chemical Engineering Science*, 52(6), 941-952.

de Souza-Santos, M. L. (2004). *Solid Fuels Combustion and Gasification*, Marcel Dekker, New York.

Ebahimi, A. A., Ebrahim, H. A., Hatam, M., and Jamshidi, E. (2008). "Finite element solution for gas-solid reactions: Application to the moving boundary problems." *Chemical Engineering Journal*, 144, 110-118.

Everson, R. C., Neomagus, H. W. J. P., Kasaini, H., and Njapha, D. (2006). "Reaction kinetics of pulverized coal-chars derived from inertinite-rich coal discards: Gasification with carbon dioxide and steam." *Fuel*, 85(7-8), 1076-1082.

Fei, H., Hu, S., Xiang, J., Sun, L., Fu, P., and Chen, G. (2011). "Study on coal chars combustion under O2/CO2 atmosphere with fractal random pore model." *Fuel*, 90(2), 441-448.

Fermoso, J., Arias, B., Pevida, C., Plaza, M. G., and Pis, J. J. (2008). "Kinetic models comparison for steam gasification of different nature fuel chars." *Journal of Thermal Analysis and Calorimetry*, 91(3), 779-786.

Higman, C., and Burgt, M. v. d. (2003). *Gasification*, Elsevier.

Jackson, R. (1977). *Transport in porous catalysts, Elservier, Amsterdam*.

Klose, W., and Wölki, M. (2005). "On the intrinsic reaction rate of biomass char gasification with carbon dioxide and steam." *Fuel*, 84(7–8), 885-892.

Krishna, R., and Wesselingh, J. A. (1997). "The Maxwell-Stefan approach to mass transfer." *Chemical Engineering Science*, 52, 861-911.

Matsumoto, K., Takeno, K., Ichinose, T., Ogi, T., and Nakanishi, M. (2009). "Gasification reaction kinetics on biomass char obtained as a by-product of gasification in an entrained-flow gasifier with steam and oxygen at 900–1000 °C." *Fuel*, 88(3), 519-527.

Molina, A., and Mondragon, F. (1998). "Reactivity of coal gasification with steam and CO_2." *Fuel*, 77, 1831–1839.

Ollero, P., Serrera, A., Arjona, R., and Alcantarilla, S. (2002). "Diffusional effects in TGA gasification experiments for kinetic determination." *Fuel*, 81(15), 1989-2000.

Paviet, F., Bals, O., and Antonini, G. (2008). "The effects of diffusional resistance on wood char gasification." *Process Safety and Environmental Protection*, 86(2), 131-140.

Perry, R. H., Green, D. W., and Maloney, J. O. (1997). *Perey's Chemical Engineerings' Handbook.*, McGraw-Hill, New York.

Sadhukhan, A. K., Gupta, P., and Saha, R. K. (2009). "Characterization of porous structure of coal char from a single devolatilized coal particle: Coal combustion in a fluidized bed." *Fuel Processing Technology*, 90(5), 692-700.

Wang, F. Y., and Bhatia, S. K. (2001a). "A generalised dynamic model for char particle gasification with structure evolution and peripheral fragmentation." *Chemical Engineering Science*, 56(12), 3683-3697.

Wang, F. Y., and Bhatia, S. K. (2001b). "A generalized dynamic model for char particle gasification with structure evolution and peripheral fragmentation." *Chemical Engineering Science*, 56, 3683-3697.

Welty, J. R., Wicks, C. E., Wilson, R. E., and Rorrer, G. (1969). *Fundamentals of Momentum, Heat and Mass Transfer*, Wiley, New York.

Zhu, W., Song, W., and Lin, W. (2008). "Catalytic gasification of char from co-pyrolysis of coal and biomass." *Fuel Processing Technology*, 89(9), 890-896.

Chapter 5 Mathematical Modelling and Model Validation for Co-gasification of Blended Coal-Biomass in A Bubbling Fluidized Bed Gasifier

In this chapter, a one-dimensional mathematical model of co-gasification of blended biomass and coal pellets in a bubbling fluidized bed (BFB) gasifier have been developed. In the co-gasification, a mixture of steam and air is fed from the bottom of the fluidized bed while the feedstock is fed from above the bed. The feed solid fuel undergoes firstly drying and then devolatilization followed by char gasification. The fed steam reacts at the bed bottom layer with the char, which also reacts with feeding air (combustion) for providing heat to the system for gasification, solid fuel devolatilization and drying. At the same time, gaseous species of steam and resultant gases from solid fuel devolatilization flow upward through the bed and react to form the producer gas. The results from the previous two chapters, which quantified the gasification reactivities of chars from different feedstocks, are integrated into the model as the input parameters. A series of co-gasification experiments was performed in a 50 kW bubbling fluidized bed gasifier at CRL Energy Ltd., Lower Hutt, New Zealand, and the experimental results have been used to validate the developed mathematical model. Finally the model has been employed to examine the sensitivities of operation conditions on the yield and composition of the producer gas.

5.1 Introduction

In the previous two chapters, the steam gasification reactivity of biomass and coal blend pellets was studied. The objective in this part of the study was to develop a mathematical model that can reliably simulate the gasification process of coal and biomass in a bubbling fluidized bed gasifier by considering the practical gasification process and incorporating the char gasification reactivity obtained from the previous two chapters into the new developed gasifier scale model. The desired gasifier scale model is expected to be able to predict the producer gas composition, gas

yield and other key system parameters such as product composition and temperature profile at different operating conditions.

Mathematical modelling of fluidized bed gasification is complicated since understanding and quantification of reaction kinetics and bed hydrodynamics, which are important phenomena in the gasification process, are required. Once the mathematical formulae have been established, selection of a numerical technique to solve the model is needed and requires careful consideration because the gasification model normally contains a set of highly non-linear differential equations, and in this case, the possibility of numerical instability could generate an un-converged solution. The level of complexity of a reaction kinetic model increases with the dimensions to be considered and the accuracy of the reaction rates being mathematically described. Therefore a trade-off between the model accuracy and the levels of details in determination of bed hydrodynamics and reaction kinetics needs to be carefully balanced. Since the focus of this project was to investigate the co-gasification of coal and biomass on producer gas composition and gas yield, the model to be developed in this chapter will emphasise reaction aspects whereas the hydrodynamics are described using simplified correlations and equations published in the literature.

Figure 5.1 shows the flow diagram of a bubbling fluidized bed gasifier with air and steam as the gasification agent. Solid fuel is fed into the gasifier above the bed and reacts with the gasification agent which is injected from the gasifier bottom. Gases of both the gasification agent and resultant gases flow through the bed in two pathways: (1) part of the gases passes between the bed materials particles that maintain the bed fluidisation, and (2) the excess gas flows through the large void space of the bed in the form of gas bubbles. The gases from those two pathways mix above the bed and flow upward through the freeboard region before leaving the reactor top as the producer gas.

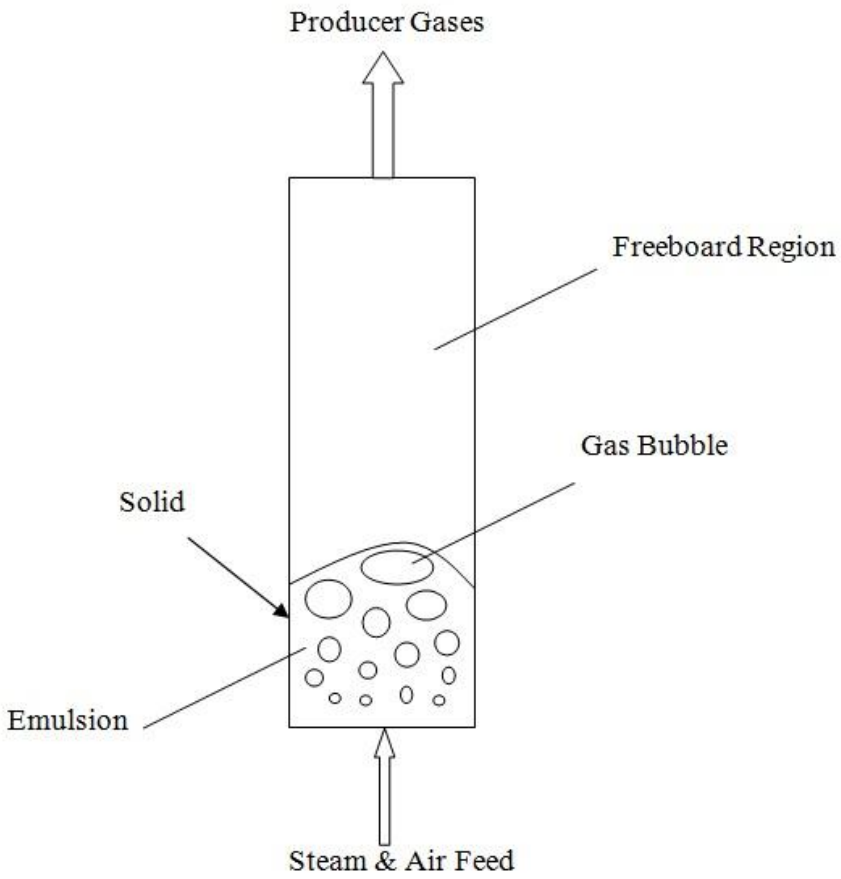

Figure 5.1: Schematic diagram of bubbling fluidized bed gasifier.

5.2 Model Development

5.2.1 Two phases theory of bubbling fluidized bed

The above-described bubbling fluidisation of the bed can be modelled by a two phases flow model (Sadaka et al. 2002) as illustrated in Figure 5.2. In this model, it is proposed that part of the bed is occupied by solid particles and gases at the minimum fluidisation velocity which makes the bed fluidized. This part of the bed is also called the emulsion phase with a volume fraction of $(1-\varepsilon_b)$. The remaining part of the bed is occupied with the excessive gases as gas bubbles and this part of the bed is called the bubble phase with a volume fraction of ε_b. In the emulsion phase, the volume fraction of the gases is ε_{mf} while that of the solid particles is $(1-\varepsilon_{mf})$. In the gasification model, the heat and mass transfer both between the emulsion phase and the

bubble phase and between solid and gases in the emulsion phase will be considered. Furthermore, the net gas being generated in the emulsion phase reactions is assumed to flow to the bubble phase.

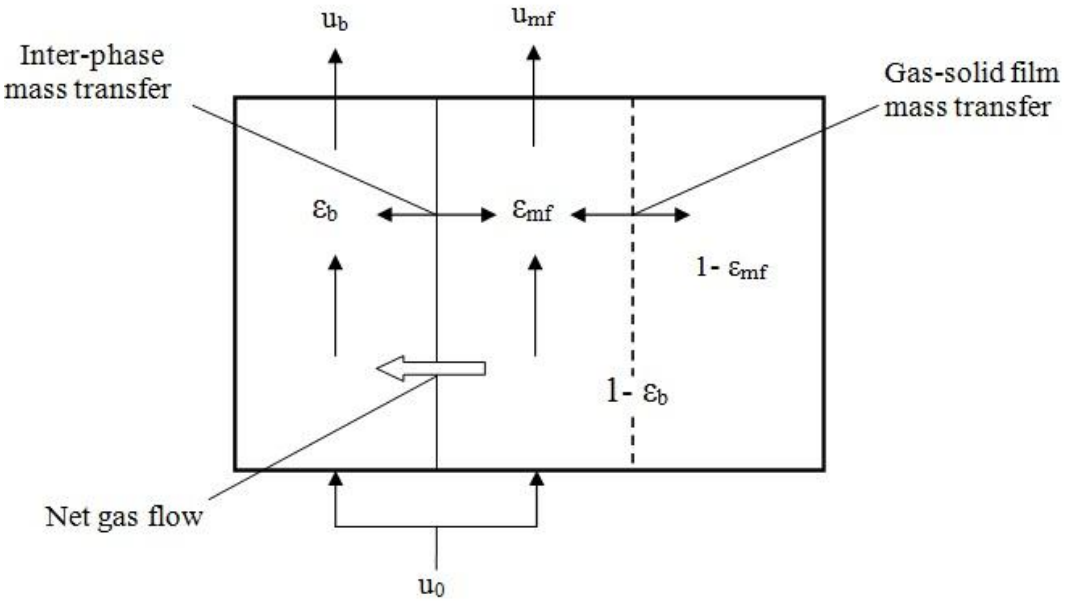

Figure 5.2: Schematic diagram of two phases flow model.

The reactions taking place in the gasifier can be summarized in three categories:

I. Devolitalization or Initial Pyrolysis

R_1: Coal/Biomass → C (solid) + H_2O, H_2, CO, CO_2, CH_4 (gas) (5.1)

II. Heterogeneous Reactions between Solid Char and Gases

R_2: $C + \varphi O_2 \rightarrow 2(1-\varphi)CO + (2\varphi - 1)CO_2$ (char combustion) (5.2)

R_3: $C + H_2O \rightarrow H_2 + CO$ (steam gasification of char) (5.3)

R_4: $C + CO_2 \rightarrow 2CO$ (Boudouard reaction of char) (5.4)

In the above char combustion reaction (5.2), the adjustable parameter, φ, is a function of temperature(de Souza-Santos 2004):

$$\varphi = \frac{2 + 2500e^{-6240/T}}{2 + 5000e^{-6240/T}} \tag{5.5}$$

III. Homogeneous among Gases

R_5: $CO + H_2O \leftrightarrow H_2 + CO_2$ (water gas shift) (5.6)

R_6: $H_2 + 1/2O_2 \rightarrow H_2O$ (5.7)

R_7: $CO + 1/2O_2 \rightarrow CO_2$ (5.8)

R_8: $CH_4 + 2O_2 \rightarrow CO_2 + 2H_2O$ (5.9)

The i^{th} component of gaseous species being considered in the gasification model is:

N_2 (i=1);

O_2 (i=2);

H_2O (i=3);

H_2 (i=4);

CO (i=5);

CO_2 (i=6); and

CH_4 (i=7)

Therefore the concentration of the gaseous species can be written as a column vector in the following form:

$$\mathbf{C} = \begin{bmatrix} C_{N2} \\ C_{O2} \\ C_{H2O} \\ C_{H2} \\ C_{CO} \\ C_{CO2} \\ C_{CH4} \end{bmatrix} = \begin{bmatrix} C_1 \\ C_2 \\ C_3 \\ C_4 \\ C_5 \\ C_6 \\ C_7 \end{bmatrix} \quad (5.10)$$

In order to incorporate the two phase model into the gasification model, the concentrations of gaseous species in each phase (emulsion and bubble) need to be calculated separately and two vectors (**C**) are used. $\mathbf{C_E}$ represents the concentration vector of gas species in the emulsion phase and $\mathbf{C_B}$ represents concentration vector of gas species in the bubble phase. Therefore, the concentration of the ith gas component of these two phases is written, respectively, as $C_{B,i}$ and $C_{E,i}$.

5.2.2 Assumptions in developing the gasification model

1) The char generated from the initial pyrolysis (devolatilization) is assumed to be pure carbon, and the shape of the particle is assumed to be a sphere;

2) Gas pressure in the bed *P* is assumed to be a linear function of the bed height measured from the bed bottom;

3) The Ideal Gas Law applies, which is reasonable as only small molecular weight gaseous species are involved in the model and the operating temperatures and pressure are within the valid range of Ideal Gas Law;

4) The mass transfer phenomena being considered in this model are: mass transfer across emulsion and bubble interface, mass transfer between gas and solid char in the emulsion phase, axial diffusion of gases between the emulsion phase and the freeboard space which is the space above the bed in the gasifier, and internal mass transfer of gas species within the solid char;

5) Heat transfer being considered in this model includes: heat transfer between solids and gases in the emulsion phase; heat conduction between emulsion phases gas in the bed; and the gases in the free board region. Heat transfer between the emulsion and bubble phases is ignored as the gas exchange between the two phases is sufficient to maintain the gases as isothermal. In addition, the temperature of the char is assumed to be the same as that of the inert bed material (for example sand). The radiation heat transfer in the bed and freeboard is negligible (De Souza-Santos 1989); there is no heat accumulation in the interface as the convective and conductive heat transfers are not applied between the bed and freeboard; the enthalpy flow from fluidized bed top to freeboard region will be due to the upward gas flow only;

6) The entire fluidized bed solids include raw fuel, char and sand, which are assumed to be perfectly mixed.

7) In the bed, the emulsion phase remains at the minimum fluidisation state, and the gas velocity in this phase equals the minimum fluidisation velocity at all times, while excessive gas flows through the bubble phase; the emulsion phase gas and freeboard gas are assumed to be plug flow with axial dispersion. Bubble phase gas is assumed to be pure plug flow;

8) Total bed height (h) is assumed to be constant; bubble fraction (ε_b) through the bed is assumed to be constant and uniform along z direction.

Fluidisation bed hydrodynamics are fatal to the accuracy of simulation results and implicit calculation that couples sophisticated hydrodynamics evaluation with the reaction kinetics cannot be achieved in a 1D model, therefore external verification of certain key assumptions in the simplified hydrodynamics is essential. A cold model test was performed in a transparent column that has the same inner diameter as the actual BFB column. The perfect mixing of bed solids in assumption (6) were observed at the operational superficial gas velocity. Assumption (2) and (8) were verified in actual gasification operations, where a linear pressure profile and approximately 10% constant bed height expansion due to reaction were detected throughout the whole run. Additionally, the uniform bubble fraction assumption was further verified by an individual simulation study. The results of this illustrated that bubble fraction variation along z direction due to net gas generation was insignificant at the current level of bed height (up to 0.5 m). The sphericity of char particles in assumption (1) is a precondition of implementing the finite reaction volume method (equation 5.36 & 5.37). This was verified by visualizing the char particles from the bed after the run, and it was found that the remaining char particles were highly spherical since irregular shaped char could be chopped by the bed material collision. Assumptions (4), (5)&(7) were obtained from other researchers ((Yan et al. 1998)).

5.2.3 Conservative equations

The mass balance equations of the gaseous species in both phases are established, respectively, for the emulsion phase and bubble phase as follows:

For the emulsion phase,

$$\begin{aligned}&(1-\varepsilon_b)\varepsilon_{mf}\frac{\partial \mathbf{C_E}}{\partial t}+\nabla\cdot\left((1-\varepsilon_b)u_{mf}\mathbf{C_E}\right)=\\&=a_B K_{BE}\left(\mathbf{C_B}-\mathbf{C_E}\right)+\nabla\cdot\left((1-\varepsilon_b)\varepsilon_{mf}\mathbf{D_m}\cdot\nabla\mathbf{C_E}\right)+(1-\varepsilon_b)\mathbf{vR_E}-\mathbf{\Delta F}\end{aligned} \tag{5.11}$$

For the bubble phase,

$$\varepsilon_b \frac{\partial \mathbf{C_B}}{\partial t} + \nabla \cdot \left(\varepsilon_b u_b \mathbf{C_B}\right) = a_B K_{BE} \left(\mathbf{C_E} - \mathbf{C_B}\right) + \varepsilon_b \mathbf{v}\mathbf{R_B} + \Delta \mathbf{F} \tag{5.12}$$

Where a_B is the average interphase area between the two phases and K_{BE} is the interphase mass transfer coefficient. $\mathbf{D_m}$ is a 7×7 matrix in which the i^{th} diagonal element equals the diffusivity of the i^{th} component in the gas mixture, while off-diagonal elements are zero. **v** is the stoichiometric coefficient matrix and **R** is the column vector of intrinsic reaction rates per unit phase volume.

$$\mathbf{v} = \begin{bmatrix} 0 & 0 & 0 & 0 & 0 & 0 & 0 & 0 \\ 0 & -\varphi & 0 & 0 & 0 & -0.5 & -0.5 & -2 \\ v_{31} & 0 & -1 & 0 & -1 & 1 & 0 & 2 \\ v_{41} & 0 & 1 & 0 & 1 & -1 & 0 & 0 \\ v_{51} & 2-2\varphi & 1 & 2 & -1 & 0 & -1 & 0 \\ v_{61} & 2\varphi-1 & 0 & -1 & 1 & 0 & 1 & 1 \\ v_{71} & 0 & 0 & 0 & 0 & 0 & 0 & -1 \end{bmatrix} \tag{5.13}$$

In the above **v** matrix, the unknown coefficients v_{31} to v_{71} represent the yield of the producer gas species. As the char is assumed to consist of pure carbon, these five unknown coefficients can be determined from the linear correlation of co-pyrolysis yields of coal and biomass with the proportion of each fuel (biomass or coal) in the blend.

Energy balance of the gases in the bubbling fluidized bed is established with the gas being assumed to be a homogenous continuum since the temperature of the gases in the emulsion phase and the bubble phase is assumed to be the same. In this case, only axial heat conduction and solid-gas heat transfer are considered in the energy balance equation.

$$\frac{\partial H}{\partial t} + \nabla \cdot \left(u_{mf} \left(1-\varepsilon_b\right) \sum_{i=1}^{7} C_{E,i} C_{P,i} + u_b \varepsilon_b \sum_{i=1}^{7} C_{B,i} C_{P,i} \right) =$$
$$= \nabla \cdot \left(k_m \nabla \left(T_{bg}\right)\right) + hA\left(T_{sand} - T_{bg}\right) + \sum_{j=1}^{7} \Delta H_{Rj} R_j \tag{5.14}$$

H is the specific enthalpy of the gas mixture in the bed which is determined by:

$$H = \sum_{i=1}^{7} \left[\varepsilon_{mf} (1 - \varepsilon_b) C_{E,i} + \varepsilon_b C_{B,i} \right] C_{P,i} T_{bg} \tag{5.15}$$

in which,

T_{bg} is the bed gas temperature (K);

$C_{p,i}$ is the molar heat capacity of the i^{th} gas species (J/mol·K) (Perry et al. 1997);

k_m is the heat conductivity of the gas mixture (J/m·K);

H_{Rj} is the reaction heat of the j^{th} reaction (J/mol).

The fed solid fuel conversion rate is calculated by:

$$\frac{dM_S}{dt} = F_S - \int_{z=0}^{h_b} R_1 \frac{Mw_C}{y_C} (1 - \varepsilon_b) A_{bed} dz \tag{5.16}$$

The average conversion rate of solid char is determined by:

$$\frac{dM_C}{dt} = \int_{z=0}^{h_b} (R_1 - R_2 - R_3 - R_4) Mw_C (1 - \varepsilon_b) A_{bed} dz \tag{5.17}$$

By integrating the above equations, the solid char conversion rate is calculated by:

$$\frac{dX_C}{dt} = \frac{X_C M_C}{M_C + \int_{z=0}^{h_b} R_1 Mw_C (1 - \varepsilon_b) A_{bed} dz} - X_C + \frac{(1 - X_C) \int_{z=0}^{h_b} (R_2 + R_3 + R_4) Mw_C (1 - \varepsilon_b) A_{bed} dz}{M_C} \tag{5.18}$$

The above equation gives an approximated value of the average conversion rate of solid char in the entire fluidized bed. In the above equations (Equation 5.18), the first two terms on the right hand side represent the rate of change in mean char conversion due to generation of char from pyrolysis of raw solid fuel, and the third term represents the rate of change in char conversion due to consumption by combustion and gasification reactions.

The change rate in the solid temperature of the bubbling fluidized bed (inert bed material and solid char):

$$\frac{dT_S}{dt} = \frac{\int_{z=0}^{h_b} hA\left(T_{bg} - T_{sand}\right)dz}{M_{Sand}C_{p\,Sand} + M_C C_{p\,Char}} \tag{5.19}$$

5.2.4 Solid fuel properties

Solid fuel properties are important parameters that influence the gasification characteristics. These properties include: 1) pyrolysis char yield y_C, which is calculated by summation of the char yield of individual solid fuel times the blend ratio; 2) devolatilization stoichiometric coefficients v_{31} to $v_{7,}$ defined as the molar ratio of pyrolysis gaseous products to carbon in the char; 3) the initial specific exposed area S_0 of char; and 4) the initial char void fraction ε_{char0}.

For different types of solid feedstocks, the devolatilization stoichiometric coefficients in the first column of stoichiometric matrix are different. These coefficients are calculated as the sum of molar numbers of gaseous product divided by the total molar numbers of carbon in the char, since the reaction rate calculations were based on per unit molar amount of carbon for calculation convenience. For blended biomass and coal pellets, since the devolatilization product distribution and char yield are linearly related to the blend ratio, the total amount of pyrolysis gaseous species and char yield can be estimated by the summation rule, and the devolatilization coefficient for each gas component is calculated by the sum of these gas species generated from two solid fuels divided by the sum of the char yield. In a similar way, the values of S_0 and ε_{char0} for the blended coal biomass pellets are estimated as the summation of the individual parameters times the fractions in the blended char.

The initial devolatilization, also called initial fast pyrolysis, is the first stage in the gasification process, and the product yield and distribution from this stage plays a dominant role in the subsequent gasification process. The char yield, volatile gas yield and gas composition from the initial fast pyrolysis are used as input parameters in the modelling of the subsequent gasification process. Therefore, modelling of the initial fast pyrolysis is also needed to provide these input parameters into the whole gasification process model.

5.2.5 Modelling of initial fast pyrolysis process (devolatilization)

In modelling the initial fast pyrolysis, the Broido-Shafizadeh kinetic scheme has been selected to describe the decomposition routine of solid fuel, which is illustrated in Figure 5.3 (Chan et al. 1985; Font et al. 1990; Shafizadeh and Chin 1977; Thurner and Mann 1981).

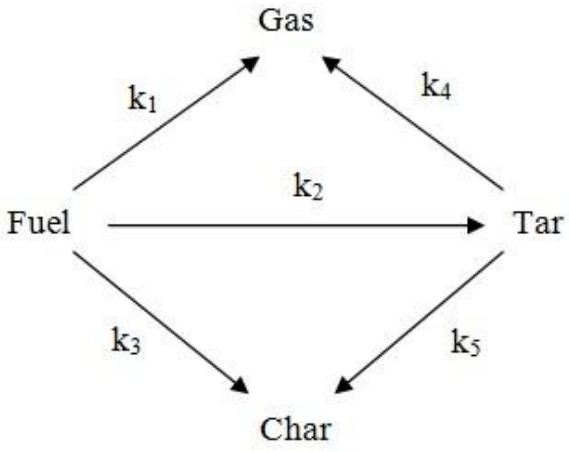

Figure 5.3: Broido-Shafizadeh thermal decomposition mechanism.

The reason for selection of the Broido-Shafizadeh scheme was that the pyrolysis product distribution can be evaluated as a function of temperature, therefore the effect of different gasification temperatures on devolatilization yields can be taken to account. Moreover such a mechanism is simple enough as the pyrolysis stage was very fast compared to the subsequent gasification processes; therefore it was not necessary to employ sophisticated pyrolysis calculation at such a high operating temperature. The pyrolysis of a single particle may take about 0.5 s at 800^{o}C and less than 0.1 s at 900 ^{o}C. Therefore, the dynamics of the intermediate stages such as primary and secondary pyrolysis can be simplified and the fed solid fuel particles can be assumed to form their final products (volatile gases, char and tar) in a single step. When tar is ignored, the yields of char (y_C) and the volatile gases (y_V) can be calculated as follows (Arenillas et al. 2001; Chan et al. 1985):

$$y_V = \frac{1}{k_1 + k_2 + k_3}\left(k_1 + \frac{k_2 k_4}{k_4 + k_5}\right) \tag{5.20}$$

$$y_C = \frac{1}{k_1 + k_2 + k_3}\left(k_3 + \frac{k_2 k_5}{k_4 + k_5}\right) \tag{5.21}$$

The rate constants, k_1 to k_5, are expressed in the Arrhenius form:

$$k_j = k_{0,j} \exp(-E_{A,j} / \boldsymbol{R}T) \tag{5.22}$$

In the biomass fast pyrolysis, the volatile gases consist mainly of H_2, CO, CO_2 and CH_4, and the composition of each species varies with temperature which can be estimated by a power function of temperature as proposed by Meesri and Moghtaderi (Meesri and Moghtaderi 2002) thus:

$$y_i = y_{0,i} T^{Ci} \tag{5.23}$$

For the coal fast pyrolysis, the relationship of the volatile composition of each volatile gas species as a function of temperature is fitted, based on the reported data from the literature (Meesri and Moghtaderi 2002; Seo et al. 2010). This relationship has a linear form as follows:

$$y_i = y_{0,i} + c_i T \tag{5.24}$$

5.2.6 Intrinsic reaction rates

The reactions involved in the gasification process are different between the emulsion phase and the bubble phase as described in Section 5.2.1. For the bubble phase, only homogeneous reactions take place, that is, the first four elements of the vector $\mathbf{R_B}$ are equal to zero in the bubble phase, therefore the bubble phase reactions will be: water gas shift reaction ($R_{B,5}$), combustion of H_2, CO and CH_4($R_{B,6}$, $R_{B,7}$, $R_{B,8}$), which rates can be determined by correlations published in the literature.

Reaction rate for water gas shift reaction (Karim and Mohindra 1974):

$$R_{B,5} = k_{0,5} e^{-E_{A,5}/RT} \left(C_{B,3} C_{B,5} - \frac{C_{B,4} C_{B,6}}{K_{5,0} e^{-\Delta G_5 / RT}} \right) \tag{5.25}$$

Reactions rates for combustion reactions of hydrogen, carbon monoxide and methane (de Souza-Santos 2004); (Yan et al. 1998):

$$R_{B,6} = k_{0,6} e^{-E_{A,6}/RT} C_{B,2} {C_{B,4}}^2 \tag{5.26}$$

$$R_{B,7} = k_{0,7} e^{-E_{A,}7/RT} C_{B,2} C_{B,5}{}^{2} \tag{5.27}$$

$$R_{B,8} = k_{0,8} e^{-E_{A,}7/RT} C_{B,2} C_{B,7} \tag{5.28}$$

Therefore the reaction rates of all of the reactions in the bubble phase are expressed in kinetic terms as follows:

$$\mathbf{R_B} = \begin{bmatrix} R_{B,1} \\ R_{B,2} \\ R_{B,3} \\ R_{B,4} \\ R_{B,5} \\ R_{B,6} \\ R_{B,7} \\ R_{B,8} \end{bmatrix} = \begin{bmatrix} 0 \\ 0 \\ 0 \\ 0 \\ k_{0,4} e^{-E_{A,4}/RT} \left(C_{B,3} C_{B,5} - \dfrac{C_{B,4} C_{B,6}}{K_{4,0} e^{-\Delta G_4/RT}} \right) \\ k_{0,5} e^{-E_{A,5}/RT} \left(C_{B,2} C_{B,4}{}^{2} \right) \\ k_{0,6} e^{-E_{A,6}/RT} \left(C_{B,2} C_{B,5}{}^{2} \right) \\ k_{0,7} e^{-E_{A,7}/RT} \left(C_{B,2} C_{B,7} \right) \end{bmatrix} \tag{5.29}$$

For the emulsion phase, all reactions R_1 to R_8 (Equations 5.1-4, 5.6-9) take place although reactions R_1 to R_4 are for solid char and gases while reactions R_5 to R_8 are among the gases only.

For reaction R_1 (Reaction 5.1), the rate of devolatilization of fed solid fuel is counted as char generation (Babu and Chaurasia 2004) and the reaction rate is determined by:

$$R_{E,1} = k_{1,0} e^{D/Ts + L/Ts^2} \frac{M_S y_C}{Mw_C (1 - \varepsilon_b)} \tag{5.30}$$

where M_S is the total mass of the fed solid fuel in the gasifier, y_C is the mass fraction of the pyrolysis char yield, and Mw_C is the molecular weight of carbon.

For heterogeneous reactions R_2, R_3 and R_4, the reaction rates are influenced by the following five stages: 1) external mass transfer of reactant gas species from bulk emulsion gas to char surface; 2) internal diffusion of the reactant gas species in the char particles; 3) adsorption of gas molecules to the reactive sites of char matrix; 4) reactions between gas molecules and carbon atoms on the reactive sites; and 5) resultant gas diffusion to the char surface and then to the external gas stream.

The overall reaction rate of the j^{th} heterogeneous reaction for j = 2, 3, 4 is determined as:

$$R_{E,j} = R_{j,\max}\eta_j f_{mt,j}\frac{V_{char0}}{A_{bed}h_b(1-\varepsilon_b)} \tag{5.31}$$

Where $R_{j,max}$ is the maximum reaction rate per unit volume of char:

$$R_{E,j,\max} = \frac{C_{TS}\theta_i}{t_{mean,j}} \tag{5.32}$$

in which C_{TS} is the total number of moles of reaction sites per unit volume of char:

$$C_{TS} = \frac{S_0}{D_{AC}{}^2\,\mathrm{NA}}(1-X_C)\sqrt{1-\psi(1-X_C)}\left(\frac{D_p}{D_{p,0}}\right)^3 \tag{5.33}$$

where

D_{AC} is the average diameter of carbon atom $D_{AC} = 0.3\times10^{-9}$ m;

NA is the Avogadro number;

S_0 is the initial specific exposed area per unit volume of char;

θ_i is the coverage fraction of i^{th} gas component on the exposed surface of char matrix; and

ψ is the evolution parameter of the random pore model (Fermoso et al. 2010).

In the developed gasification model, the dynamics of char particle surface adsorption of reactant gases and desorption of product gases are negligible in comparison with the internal resistances for the gas diffusion. Therefore, the char particle surface is assumed to be at equilibrium state and the surface coverage by the i^{th} gas species is expressed in the Langmuir form (Hong 2000; Roberts and Harris 2006):

$$\theta_i = \frac{K_{eq,i}P_{A,i}}{1+\sum_{i=1}^{n}K_{eq,i}P_{A,i}} \tag{5.34}$$

The average time taken for gas molecules to react with a single carbon atom on the char in the j^{th} reaction may be determined by the Arrhenius function (Murphy and Shaddix 2006):

$$t_{mean,j} = t_{mean,0}e^{E_A j/RT_S} \tag{5.35}$$

The numerical values in the above expression were obtained from the justified char gasification kinetics in chapter 3 and 4, as the intrinsic volumetric reaction kinetics is the product of the total

number of occupied carbon sites per unit char volume and the average time taken for completion of the reaction taking place in an individual carbon site.

The effect of internal diffusion of gaseous species within a char particle is approximated by the effective reaction volume method by introducing an effective factor, η. The effective factor is defined as the ratio of the volume-averaged reaction rate to the maximum reaction rate that could be achieved if the internal diffusion rate was infinity. η is an unique function of Thiele modulus ϕ, and is approximated by the correlation for spherical geometry in the developed model (Veldsink et al. 1995):

$$\eta = \frac{1}{V_s R(C_{i,\max})} \int_{V_s} R(C_i)\, dV = \frac{1}{3\phi^2}\left(\frac{3\phi}{\tanh(3\phi)} - 1\right) \tag{5.36}$$

The Thiele modulus of the n^{th} order j^{th} reaction for the i^{th} gas component is determined as:

$$\phi = \frac{D_p}{6}\left(\frac{(n+1) k_{ap,j} C_i^{\,n-1}}{2 D_i^{eff}}\right)^{1/2} \tag{5.37}$$

in which $k_{ap,j}$ is the apparent reaction kinetic constant of the heterogeneous reaction:

$$k_{ap,j} = \frac{R_{\max,j}}{C_i^n} \tag{5.38}$$

In Equation (5.37), D_i^{eff} is the effective diffusivity of i^{th} gas component in the solid char matrix and is estimated by using the Bosanquet formula in this developed model (Krishna and Wesselingh 1997):

$$D_i^{eff} = \left(\frac{1}{D_{i,m}} + \frac{1}{D_{i,K}}\right)^{-1} \tag{5.39}$$

Where $D_{i,m}$ and $D_{i,K}$ are, respectively, the free diffusivity in the gas mixture and Knudsen diffusivity of i^{th} component in the char structure (Welty et al. 2001):

$$D_{i,m} = \frac{1}{1-y_i} \sum_{\substack{j=1 \\ j \neq i}}^{n} \frac{\varepsilon}{\tau} D_{ij}^{b} y_j \tag{5.40}$$

$$D_{i,K} = \frac{d_{pore}}{3} \sqrt{\frac{8RT}{\pi MW_i}} \tag{5.41}$$

In Equation (5.40), $D_{i,j}$ is the binary diffusivity of i^{th} gas component in the j^{th} reaction. In Equation (5.41), d_{pore} is the mean pore diameter, which is calculated by:

$$d_{pore} = \frac{4\varepsilon_{char}}{S} \tag{5.42}$$

In the emulsion phase, external mass transfer resistance of gases to and from the char particle surface can be significant, especially for the char combustion reaction. In order to reflect this mass transfer resistance, an external mass transfer factor ($f_{mt,j}$) is introduced, defined as the ratio of the actual volumetric reaction rate to the maximum theoretical reaction rate if the mass transfer resistance was equal to zero. If one assumes that there is no accumulation of gaseous species on the apparent surface of char particle, the total mass transfer rate of the i^{th} gas species from the bulk fluid to the apparent surface is equal to the consumption of this component over the whole volume of char particle. The external mass transfer factor is calculated by:

$$f_{mt,j} = \left(1 + \frac{D_p k_{ap,j} C_i^{\,n-1} \eta_j}{6k_j} \right)^{-1} \tag{5.43}$$

In which k_j is the film mass transfer coefficient of the gas component between the gas stream and the char particle surface in the emulsion phase (Perry et al. 1997):

$$k_j = \frac{D_{i,m}}{D_p} \left(2 + 0.6 Re^{0.5} Sc^{1/3} \right) \tag{5.44}$$

The gas reactions are the same for both the emulsion phase and the bubble phase, thus the following reaction rates used in the bubble phase (Equations 5.25-28) can be applied to the emulsion phase for $R_{E,j}$, j = 5, 6, 7, 8.

Rate for water gas shift reaction (Karim and Mohindra 1974):

$$R_{E,5} = k_{0,5} e^{-E_{A,5}/RT} \left(C_{E,3} C_{E,5} - \frac{C_{E,4} C_{E,6}}{K_{5,0} e^{-\Delta G_5/RT}} \right) \tag{5.45}$$

Reaction rates for hydrogen, carbon monoxide and methane combustion in the emulsion phase have the same expression as in the bubble phase (Equations 5.26-28):

$$R_{E,6} = k_{0,6} e^{-E_{A,6}/RT} C_{E,2} C_{E,4}^{\ 2} \tag{5.46}$$

$$R_{E,7} = k_{0,7} e^{-E_{A,}7/RT} C_{E,2} C_{E,5}^{\ 2} \tag{5.47}$$

$$R_{E,8} = k_{0,8} e^{-E_{A,}7/RT} C_{E,2} C_{E,7} \tag{5.48}$$

In the mass balance equations (Equations 5.11 and 5.12), the net gas flow rate from emulsion gas to bubble (**ΔF**) is needed, which is related to the devolatilization and the heterogeneous reactions. This term has been determined by (Yan et al. 1998) thus:

$$\mathbf{\Delta F} = \frac{\mathbf{C}}{\sum_{i=1}^{n} C_i} (1-\varepsilon_b) \left(\varepsilon_{mf} \sum_{i=1}^{n} \sum_{j=5}^{n} \nu_{ij} R_{E\,j} + \sum_{i=1}^{n} \sum_{j=1}^{4} \nu_{ij} R_{E\,j} \right) \tag{5.49}$$

Also in Equations (5.11) and (5.12), the inter-phase mass transfer coefficient for i^{th} gas component is used and calculated by (Sit and Grace 1981):

$$K_{BE,i} = \frac{u_{mf}}{3} + \sqrt{\frac{4 D_{i,m} e_{mf} u_b}{\pi d_b}} \tag{5.50}$$

In which a_B is the specific inter-phase area: $a_B = 6/d_B$.

5.2.7 Calculations of fluidized bed hydrodynamics

Hydrodynamics of the fluidized bed are useful to determine the gas flow velocity, pressure drop in the bed and gas fractions both in the emulsion and bubble phases. The gas velocity is also used to calculate the inter-phase mass transfer coefficient as presented in Equation (5.50). The

superficial velocity profile of the gas along bed height direction is approximated by using Newton's method, and the change rate in the superficial velocity is determined from the net gas volume generation:

$$u_{0,z+\Delta z} = u_{0,z}\frac{T_{bg,z+\Delta z}}{T_{bg,z}} + \left.\frac{du}{dz}\right|_z \Delta z \tag{5.51}$$

$$\frac{du_0}{dz} = \frac{\boldsymbol{R}T_{bg}}{P}\left(\varepsilon_b \sum_{i=1}^{n}\sum_{j=4}^{n} v_{ij}R_{B\,j} + (1-\varepsilon_b)\varepsilon_{mf}\sum_{i=1}^{n}\sum_{j=4}^{n} v_{ij}R_{E\,j} + (1-\varepsilon_b)\sum_{i=1}^{n}\sum_{j=1}^{3} v_{ij}R_{E\,j}\right) \tag{5.52}$$

As described in Sections (5.2.1) and (5.2.2), the gas velocity in the emulsion phase is equal to the minimum fluidisation velocity u_{mf}, and thus the gas velocity in the bubble phase can be determined based on the excessive gas and the bubble phase volume fraction (Kunni and Levenspiel 1991):

$$u_b = \frac{u_0 - (1-\varepsilon_b)u_{mf}}{\varepsilon_b} \tag{5.53}$$

In calculating the inter-phase mass transfer coefficient (Equation 5.50), the mean bubble size, d_b, is needed and can be determined by (S. Mori 1975):

$$d_b = D_{BM} - (D_{BM} - D_{B0})e^{-0.3z/D_{\text{bed}}} \tag{5.54}$$

In which D_{BM} and D_{BO} are determined from the superficial gas velocity (u_o) and the minimum fluidisation velocity (u_{mf}):

$$D_{BM} = 0.652\left(A_{\text{bed}}(u_0 - u_{mf})\right)^{0.4} \tag{5.55}$$

$$D_{B0} = 0.347\left(\frac{A_{\text{bed}}}{n_d}(u_0 - u_{mf})\right)^{0.4} \tag{5.56}$$

The volume fraction of the bubble phase (ε_b) and that of the emulsion phase (1-ε_b) of the fluidized bed are important factors which can be determined from both theoretical analysis and hydrodynamics experiments. Theoretically the volume fraction of the emulsion phase is equal to the ratio of the bed height at the minimum fluidisation state (h_{mf}) to the bed height during the

actual fluidisation (h). The former, in turn, is related to the bed height at static state (h_{static}) and the gas volume fraction at bed minimum fluidisation (ε_{mf}):

$$1-\varepsilon_b = \frac{h_{mf}}{h} = \frac{h_{static}}{h\left(1-\varepsilon_{mf}\right)} \tag{5.57}$$

Therefore, the volume fraction of the bubble phase is:

$$\varepsilon_b = 1-\frac{h_{static}}{h\left(1-\varepsilon_{mf}\right)} \tag{5.58}$$

From the verification of the bed hydrodynamics, the change in volume fractions of both bubble phase and emulsion phase along the bed height are insignificant because the bubble rising velocity increases as thesuperficial gas velocity increases. In addition, the total bed height is not large enough to amplify the effect of gas velocity change, therefore, the volume fractions of the bubble phase and the emulsion phase are assumed to be constant along the bed height. It is also assumed that the fluctuation of the bed height during the gasification is negligible under the bubbling fluidisation condition thus the bed height, h, is also assumed to be constant in the model.

5.2.8 Calculations for the freeboard space

The freeboard space refers the space above the bed up to the gas exit location. The calculations for the freeboard region are less complicated compared to those for the bubbling fluidized bed. In the freeboard, because there is no solid char involved, the reactions being considered are the same as those in the bubble phase in the fluidized bed. The mass and energy balance calculations for the freeboard are also similar to those in the bubble phase, however, the volume fraction of the gases in the freeboard space is unity thus the freeboard space can be regarded as a bubble phase with unity volume fraction (ε_b =1) in the conservative equations. At the bottom of the freeboard, the boundary condition can be determined based on the gaseous species flowing out of the top of the fluidized bed both from the emulsion phase and from the bubble phase. According to assumption 5, the freeboard bottom temperature equals the gas temperature at the top of the bed. The upper boundary condition of the freeboard space is an open boundary; that is the divergence of both mass and energy flows is equal to zero.

5.3 Solving of the Developed Model for Co-gasification of Blended Coal and Biomass in a Bubbling Fluidized Bed Gasifier

5.3.1 Initial and boundary conditions in the modelling of bubbling fluidized bed gasification

The value of initial gas composition for all three regions (emulsion phase, bubble phase and freeboard space) are set to be the same as the air composition, i.e., 80% N_2 and 20 % O_2. All initial temperatures are set to be the same as the nominal operating temperature. Initial solid fuel mass, char mass and mean char conversion in the bed are set to be zero.

Inlet boundary condition at the bottom of the bubbling fluidized bed (z = 0; t > 0) is of the Dirichlet Type:

$$\mathbf{C_E} = \mathbf{C_B} = \text{concentrations of gas species of the fed gas of air-steam mixture.} \quad (5.59)$$

$$T_{bg} = T_{in} \quad (5.60)$$

Where T_{in} is the fed gas temperature of air and steam mixture, equal to 250^{o}C after preheating. The boundary condition at exit of the gasifier (z = 4 m, t > 0) is of the Neumann type:

$$\frac{\partial \mathbf{C_{FB}}}{\partial z} = 0 \quad (5.61)$$

$$\frac{\partial T_{FB}}{\partial z} = 0 \quad (5.62)$$

5.3.2 Numerical method for solving the PDEs

From the discussion, the mathematical model developed for gasification in a bubbling fluidized bed gasifier consisting of a set of non-linear partial-differential equations (PDEs) that describe the fundamental mass and energy balance, chemical reactions and hydrodynamics. In the model, 15 PDEs have been proposed to describe concentrations of seven gaseous species in both the emulsion phase and the bubble phase in the fluidized bed, and gas enthalpy profile along the bed height. In addition, eight PDEs have been established in the freeboard space for concentrations of the seven gas species and gas enthalpy profiles. The model also consists of four ordinary differential equations (ODEs) that describe the total mass of fed solid fuel, char, mean char

conversion and bed solid temperature, which are coupled with the previously mentioned 23 PDEs.

For solving the developed model, the spatial-derivatives of the deviation variables are firstly calculated by employing the finite difference method. Deviation variables in the PDEs of concentration profile of the gaseous species, temperature profile along the bed height, the fed raw solid fuel mass change, char mass change, mean char conversion rate and inert bed material temperature need to be solved simultaneously. In order to solve the model, the bed height is divided into n cells and the freeboard space is divided into m cells. The first order Euler method is used to manually discretize the spatial derivatives in the PDEs into algebraic forms. Therefore, the set of partial differential equations are converted into $15n+8m+4$ differential algebraic equations (DAEs). All deviation variables are lumped into a solution vector **Y**, and the time derivatives of **Y** are solved by employing the Matlab ode15s function which has good performance in solving DAE system with high non-linearity.

The numerical routine of solving the mathematical model is illustrated in Figure 5.4, in which the types of coal and biomass and the blending ratio are firstly selected. The initial bed hydrodynamic parameters are defined corresponding to the inlet flow of mixed air and steam at the bed bottom. The heat capacity values of the gas species are pre-defined from the nominated operating temperature prior to the start of model solving and these values are maintained constant while the other gas properties such as binary diffusivity and viscosity are implicitly evaluated as a function of instantaneous temperature. It has been found that the evaluation of values of heat capacity, C_p, outside the operation conditions is important since the implicit calculation could cause numerical instability. The mean bed temperature from the solution is finally compared with the nominated temperature, and the operating conditions must be reset if the temperature difference is larger than the pre-set tolerable value until an acceptable temperature result is obtained.

As the discrete DAEs are highly non-linear, it is possible that un-converged solutions can be encountered and the terms with the square root of variables could generate intermediate results with imaginary numbers during the solving process. In this case, the time to obtain acceptable solutions would be infinite, so relative numerical modification on the equations needs to be

performed. Local linearization on some terms has been done in order to avoid the numerical instability.

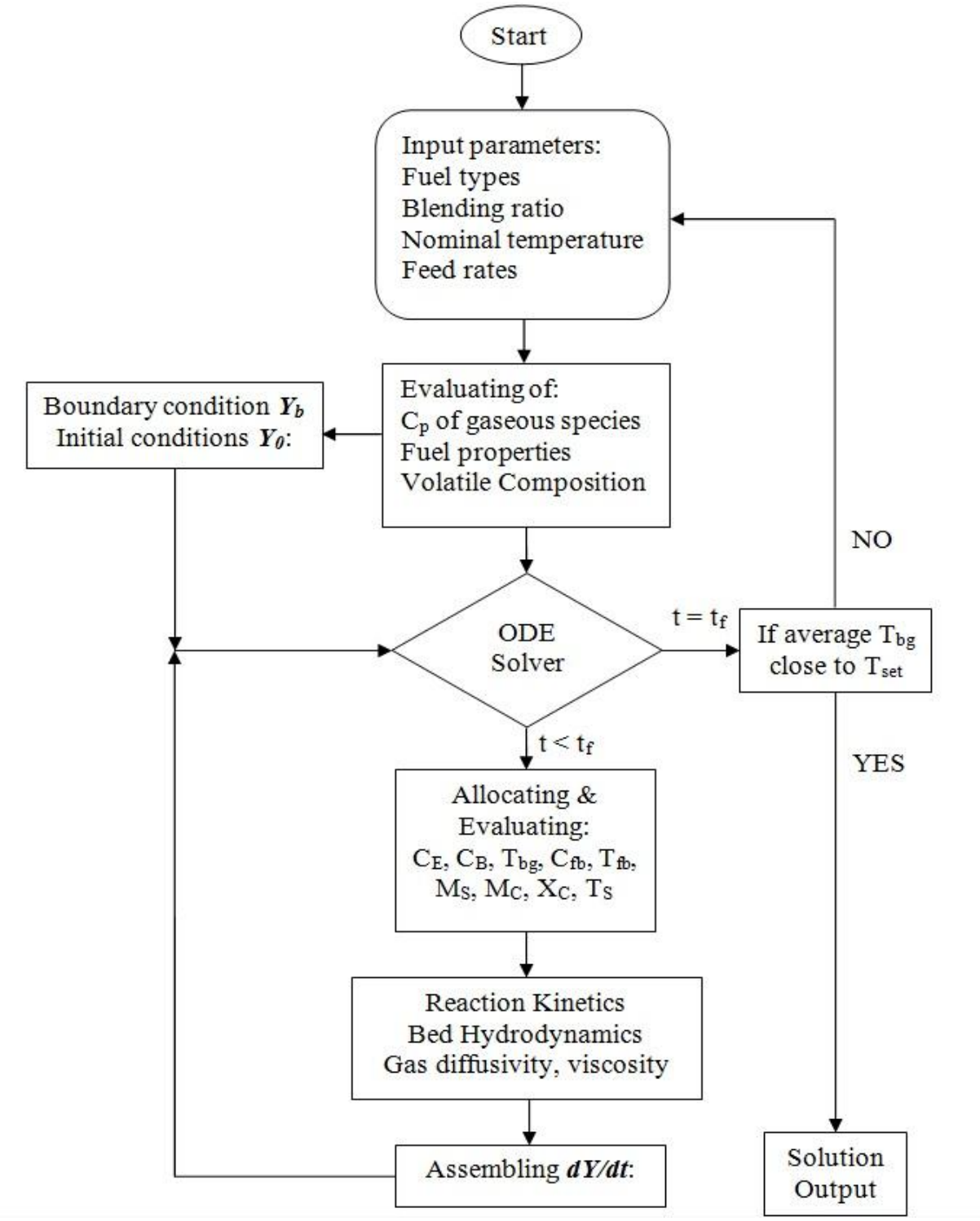

Figure 5.4: Numerical scheme of solving the gasifer model.

In the initial trials of solving the model, the problem of imaginary numbers in the intermediate results occurred for certain terms which were supposed to have very small positive values, but in reality they were calculated to be negative because of the accumulation of errors in each step. Therefore, the square root of these terms generated an imaginary number. With a thorough check on the results from each step of evaluating the time derivative of **Y**, the sources that generated the imaginary numbers were tracked. Subsequently these variables were set to zero if a negative value was obtained from the calculations.

The optimum number of calculation cells for this particular model for *n* and *m* was found to be 16, at which both convergence of the numerical results and a timesaving computing process could be guaranteed. Convergence of the producer gas component of gasification of 80% lignite and 20% eucalypt pellets at 900^{o}C was selected as an example to illustrate the numerical convergency, and presented in Figure 5.5, it can be seen that the absolute values of error in all gas components reduced rapidly as the number of cells increased from 2 and approached zero where the cell number equals 20.

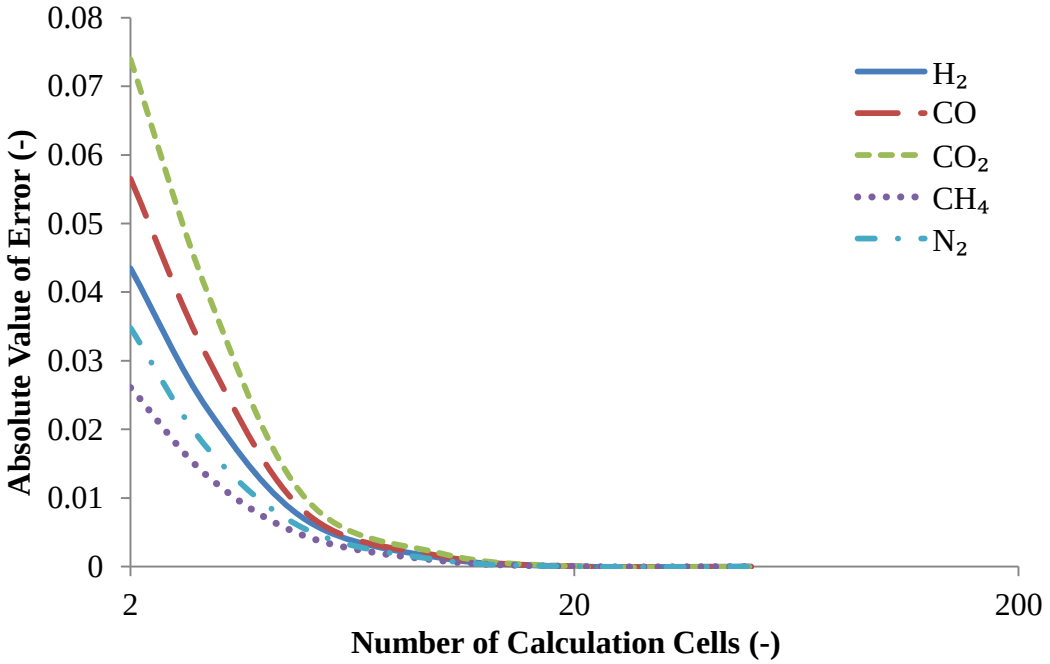

Figure 5.5: Absolute value of errors in producer gas components versus number of calculation cells for gasification of 80% lignite and 20% eucalypt pellets at 900^{o}C.

The calculations involved in the developed system were numerous, thus checking and correcting for possible mistakes contained in the programme was necessary and this was performed after the program could generate a solution. Apart from the elimination of the majority of typing errors by reading through the entire code, remaining typos, syntax and logical errors were tracked and corrected by preliminary sensitivity analysis in which the trends of model output variation were examined by changing the numerical values of input parameters. The model results were ensured to be qualitatively coincident with common physical and chemical principles before performing the subsequent experimental validation, which will be introduced in the following two sections of this chapter.

5.4 Experiments of Co-gasification of Blended Coal and Biomass in a Bubbling Fluidized Bed Gasifier

In this part of the study, a set of experiments was performed for gasification of coal, biomass and blended coal and biomass on a 50 kW bubbling fluidisation gasifier in CRL Energy Ltd., Lower Hutt, Wellington, New Zealand. The results obtained from the experiments have been used to validate the developed mathematical model by comparing the experimental data with the model simulation results for producer gas composition and temperature profile along the gasifier height.

5.4.1 Test materials and feedstock preparation

Two types of coals (lignite and sub-bituminous) were received from Hunterley mine in the Waikato region of New Zealand, and two types of biomass in the form of wood chips (radiata pine and Eucalyptus nitens) were supplied from a local sawmill, near Lower Hutt, Wellington, New Zealand. The received coals were firstly ground separately by a knife mill to reduce the size from roughly 1 cm to approximately 3 mm. Then the smaller coal particles were further ground by a ball mill into particles of about 500 μm in diameter. At the same time, the received fresh wood chips were oven dried to a moisture content of less than 8%. Then the dried chips were ground by the ball mill to powder form with particle size of less than 500 μm. Finally the coal and biomass particles were blended at the designated coal-to-biomass mass ratios of 70:30, 80:20

and 100:0. After this, the blends were thoroughly mixed by the ball mill before the mixture was pelletized in a pelletizer to form pellets of 7 mm (diameter) by 20 mm (length). The above process is illustrated in Figure 5.6. The proximate and ultimate analysis results for each type of the raw solid fuel are given in Tables 5.1 and 5.2.

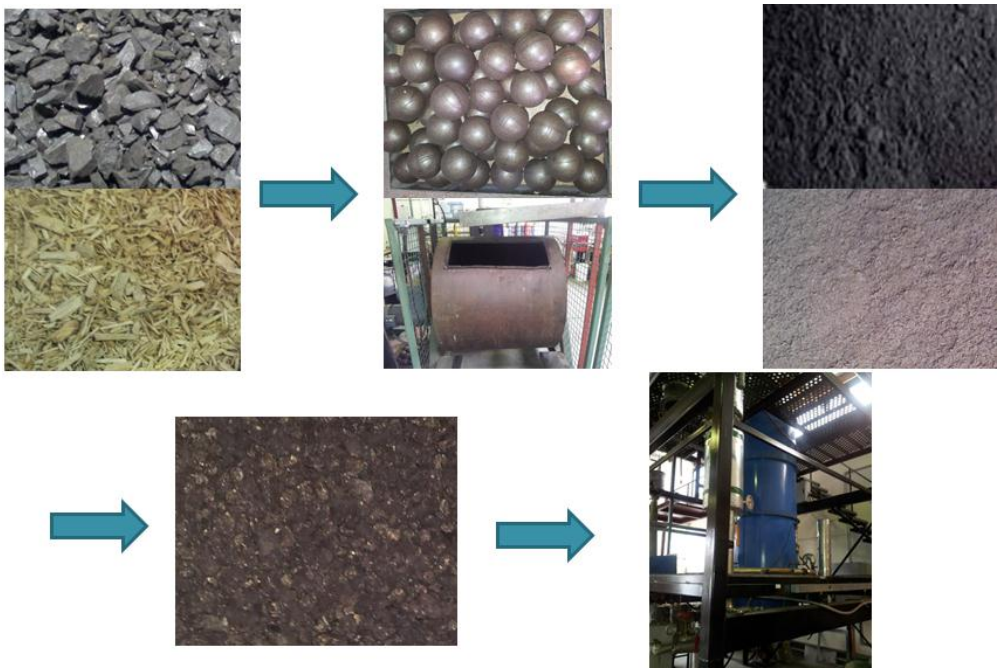

Figure 5.6: Preparation of feedstock of coal and biomass for co-gasification experiments.

Table 5.1: Proximate Analysis result of raw solid fuels(wet base)

Fuel type	Moisture (wt %)	Volatile matter (wt %)	Fixed carbon (wt %)	Ash (wt %)
Pine (dried)	7.8	77.9	13.8	0.34
E-niten (dried)	5.4	81.5	12.7	0.38
Lignite	19.1	41.9	34.1	4.9
Sub-bituminous	13.6	38.6	42.4	5.4

Table 5.2: Ultimate Analysis result of feedstock materials (dry and ash free base)

Fuel type	C (wt%)	H(wt%)	O(wt%)	N(wt%)	S(wt%)	H/C	O/C

Pine	51.4	5.9	42.4	0.27	0.01	0.11	0.83
E-niten	50.4	5.9	43.5	0.15	0.01	0.12	0.86
Lignite	66.6	4.8	27.1	0.72	0.81	0.07	0.41
Sub-bituminous	73.3	5.1	17.9	1.27	2.4	0.07	0.25

5.4.2 Experimental procedure and operation conditions

The experiments were performed at a 50 kW bubbling fluidized bed (BFB) gasifier at CRL Energy Ltd. The BFB gasifer is in the autothermal category in which the necessary heat for the endothermal gasification process is provided by partial combustion of char and combustible gas generated from the solid fuel devolatilization (fast pyrolysis). 40 kg of silicon sand was used as inert bed material which was loaded into the gasifier column before each run. In the experiment, the mixture of air and steam at fixed flow rate of 3 kg/hr was injected at the gasifier bottom through a gas distributor as gasification agent and fluidisation agent. The air feeding rate was adjusted depending on the set operation temperature. The solid fuel was fed at constant rate of 19 kg/hr into the bed by a feeding system which consisted of two stacking hoppers. The upper one was the primary hopper used to store the solid fuel during operation. The valve underneath it could be manually activated to control the amount of solid fuel being released to the secondary hopper located underneath. The bottom of the secondary hopper was connected to a feeding auger which continuously fed the solid fuel into the fluidized bed, with the feeding rate being automatically controlled at the set point. Before each run, the second hopper was filled with pure coal for heat-up use; thus the fuel initially stored in the second hopper was also start-up fuel.

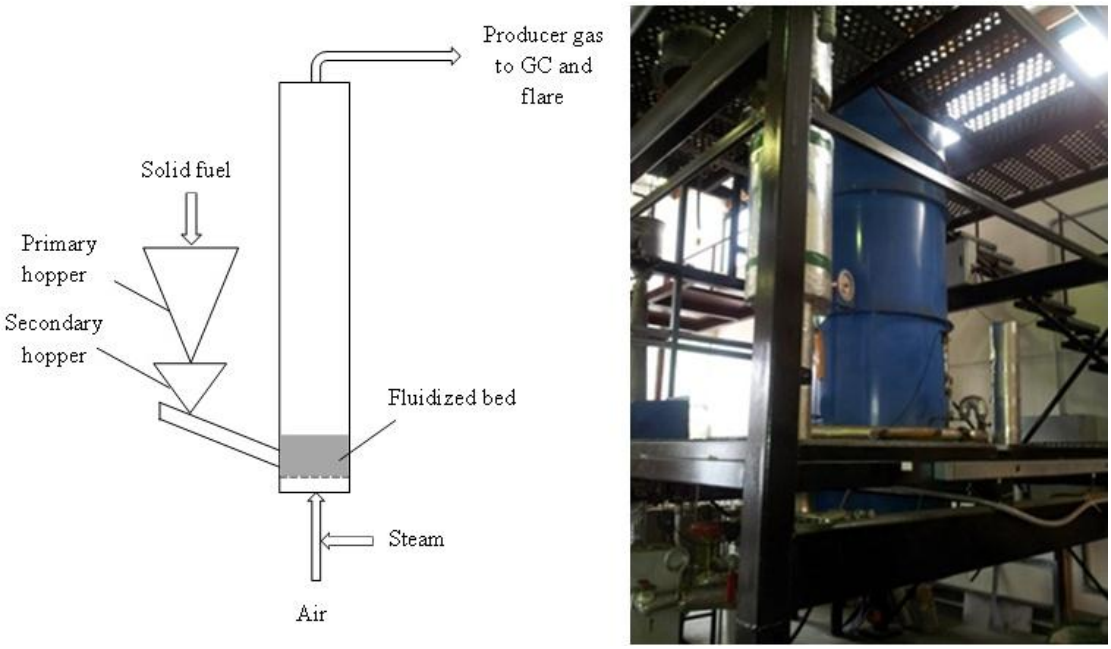

Figure 5.7: Flow diagram and side view of bubbling fluidized bed system for co-gasification runs.

Before the experiment, the gasifier was pre-heated to the required temperature of around 500°C using built-in electrical elements on the gasifier walls. Once the required temperature was reached, pure air was firstly fed into the column to attain bed fluidisation and then the start-up fuel, normally pure coal, was fed into the gasifier which was ignited and combusted by the air. At this stage, the gasifier was operated on the combustion mode while the bed temperature as well as the gasifier was further heated up to the set-point temperature. Once the required operation temperature for the gasification operation was reached, feeding rates of air and solid fuel were fine-tuned until the bed temperature became stabilized around the set point. When the remaining start-up solid fuel in the secondary hopper was nearly running out, the valve underneath the first hopper was activated and the test fuel was fed into the second hopper. At this time the system was switched from the start-up mode to the gasification mode by adding the steam into the gasification agent. The test fuel (pellets) was now added to the feeding system and fed into the bed. The ratio of air feeding rate and solid fuel feeding rate was then fine-tuned until the bed temperature returned to the set-point value.

During the BFB operation, temperature control was only achieved by manipulating the ratio between the air feed and solid feedstock rate; in general the elevation of the operating temperature was attained by increase the air to solid ratio and vice versa. Also, the oxygen level

of the producer gas was monitored by an oxygen sensor at the top of the column during the whole gasification run; zero oxygen content had to be ensured throughout the entire gasification run as an indication that the bed was maintained at normal fluidisation condition, with no shortcut of gasification agent through the bed.

A series of co-gasification runs was performed to validate the developed model. In these experiments, the set gasification temperatures were: 870, 900, 925 and 950°C. The mass proportions of raw biomass in the blending pellets were: 0%, 20%, and 30%. A higher biomass blending ratio was also tried but the set point temperature could not be achieved for gasification of feedstock pellets with biomass blending ratio above 30%. In the co-gasification of blended biomass and coal in the BFB gasifier, the heat of the bed was provided by combustion reactions of char and producer gases generated from the initial pyrolysis. Due to the low calorific value of biomass char and the low char generation, insufficient heat could be released to maintain bed temperature at the set point with co-gasification of biomass-coal blend at a high biomass ratio.

Table 5.3: Summary of co-gasification experiments been performed

Run number	Test Fuel	Temperature range (^{o}C)
1	100L	880-980
2	80L20E	850-950
3	70L30E	850-950
4	80L20P	850-950
5	70L30P	850-950
6	100S	880-1050
7	80S20E	850-950
8	80S20P	850-950
9	70S30P	850-950

The producer gas sampled from the top of the BFB gasifier was firstly cooled down through an ice bath to remove vapour and then analysed by an online micro-GC system the same as used in chapter 3 to determine the gas composition. The results from the experiments were then compared with the model simulation results under the same operating conditions and feedstock parameters.

5.5 Model Validation and Sensitivity Analysis

5.5.1 Model simulation and validation of steady state operation

The primary goal of developing a mathematical model is to predict the steady state producer gas composition of the gasifer at given operating conditions. The model can also be used to predict parameters which cannot be easily measured in an experiment such as gas composition changes along the gasifier height. In addition, the model can be used for sensitivity analysis with varying operation conditions or with changing feedstock. In order to gain confidence in the model application, the model developed should be validated by comparing the model simulation results with experimental data under the same operation conditions and with the same feedstock. Therefore, the model validation is also included in the following discussion.

In this section, the simulation results of gasification of pure lignite at 900^{o}C are selected as an example to illustrate the gasification characteristics based on the mathematical model. The producer gas concentration profile, the char conversion and the temperature profile along the gasifier height as well as the producer gas composition at the gasifer exit location are presented. The operating conditions of this particular gasification run are listed in Table 5.4.

Table 5.4: Operating conditions of lignite gasification run.

Air feed rate	60	(m^3 at 25^{o}C, 1 bar)
Steam feed rate	3	(kg/hr)
Coal feed rate	19	(kg/hr)
BFB inventory	40	(kg sand)
Bed operating pressure	5~10	(kPa, gauge)
Operation temperature	900	(°C)

Figure 5.8 shows the model-predicted water-free producer gas composition at the gasifier exit location as a function of elapsed time (solid lines) and comparison with experimental results at 120 min from the start of the experiment (dots) under the operation conditions given in Table 5.4. From the model prediction, the compositions of CO, H_2 and CH_4 increased with the elapsed time

from zero at the start of the experiment. The nitrogen concentration firstly increased from an initial 0.8 mol/mol to 0.9 mol/mol in the first two minutes and then decreased with the elapsed time until about 20 minutes, when concentrations of all gas species reached a steady state. The CO_2 concentration increased sharply from zero to about 0.1 mol/mol at the start of the experiment and then remained constant throughout the remainder of the experiment. This can be explained by the fact that oxygen was excessive during the initial period so almost all combustible substances were combusted, thus the producer gas consisted of only CO_2, N_2 and H_2O. Please note that in Figure 5.8, the water is not included.

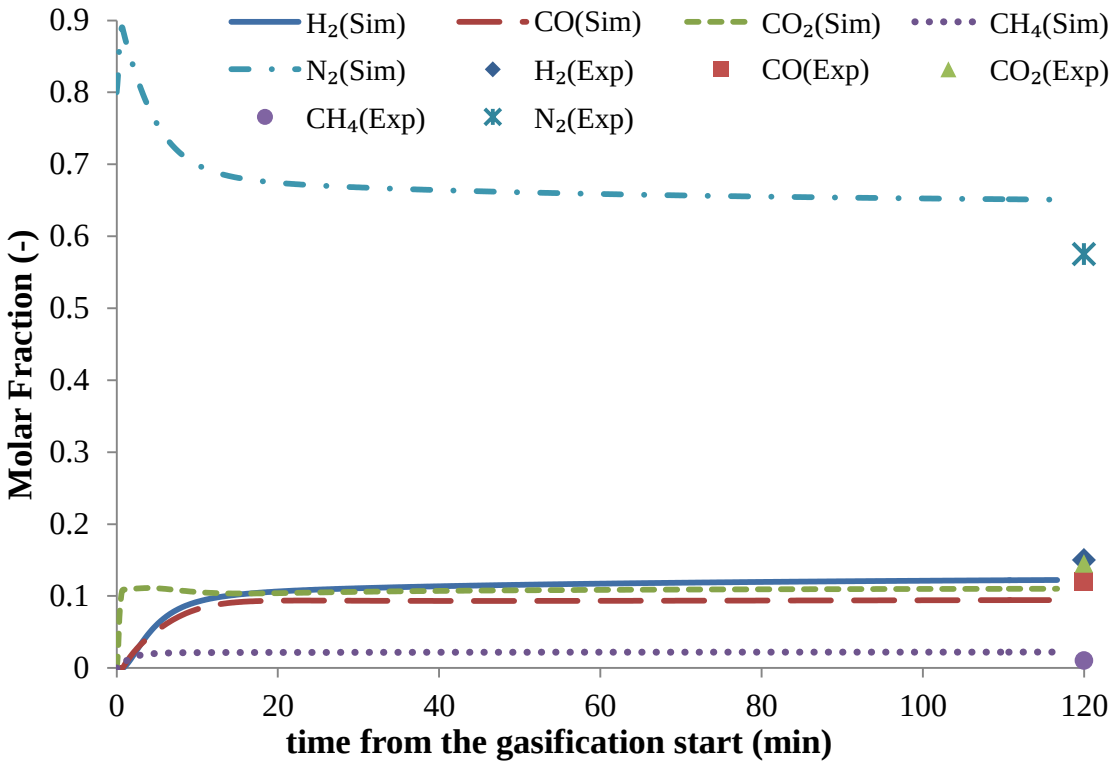

Figure 5.8: Model predicted water-free producer gas composition along the gasifier height (lines) and comparison with experimental results for producer gas composition at the gasifier exit (dots).

As the gasification proceeded, the excess oxygen was consumed by char at the lower region of the bed (Figure 5.9). Due to the char accumulation in the bed more solid fuel was fed (Figure 5.10), and therefore the combustible gas species in the producer gas in the upper layer of the bed could be conserved. In Figure 5.10, it can be seen that at the steady state of the operation, the model predicted gas composition is in close agreement with the measured results.

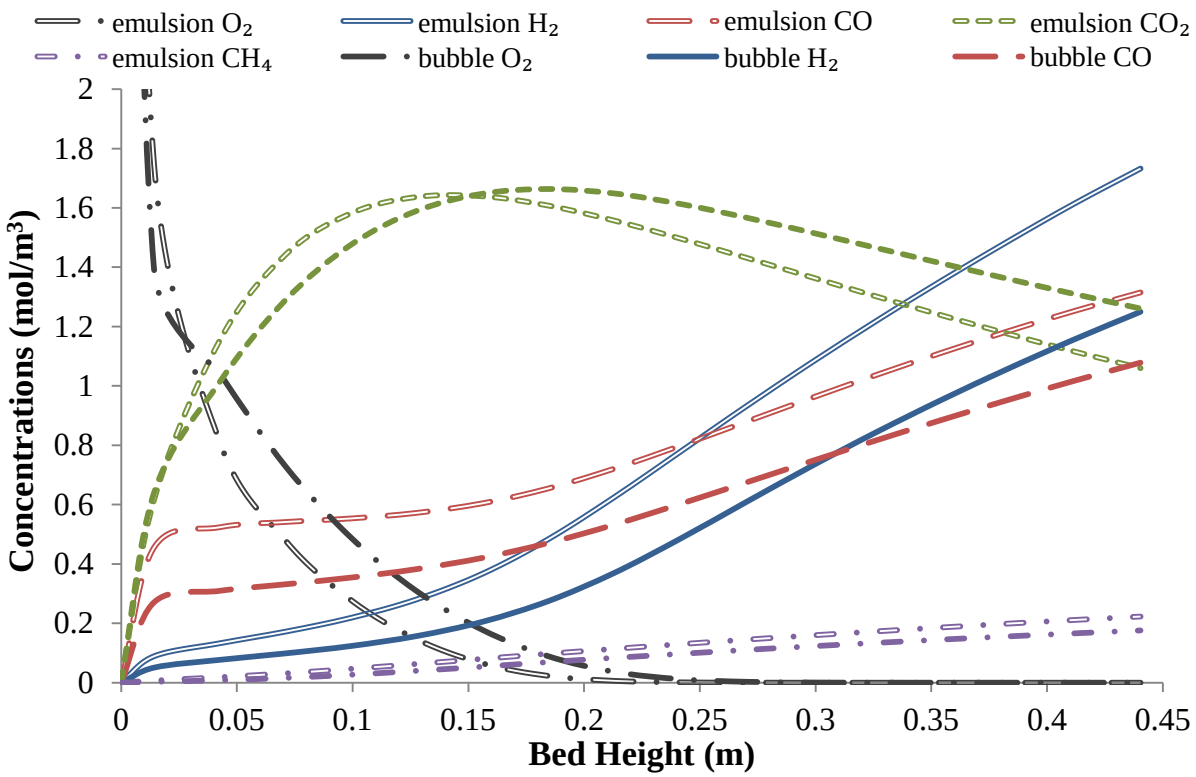

Figure 5.11: Steady state concentrations of various gas species through the bed height, respectively, in the emulsion phase (hollow lines) and in the bubble phase (solid lines).

Figure 5.9 shows the steady state concentrations of various gas species through the bed height. In the figure, the hollow lines represent the concentrations in the emulsion gas and the solid lines represent the bubble gas concentrations. It can be seen that oxygen concentration decreased along the bed height due to the oxygen consumption for combustion reactions. On the other hand, the concentrations of CO, H_2 and CH_4 increased with the bed height. Furthermore, the concentrations of these combustible gaseous species were higher in the emulsion phase than in the bubble phase because these gas species were generated in this phase. By contrast, the concentration of oxygen in the bubble phase was higher as there was less combustion occurring than in the emulsion phase where more combustible gas species and char were available for combustion.

Figure 5.10 shows the char accumulation in the bubbling fluidized bed as a function of elapsed time during the gasification experiment while the mean char conversion in the bed is illustrated

in Figure 5.11. It can be seen that the total char mass and mean char conversion increased from zero at the start, then the char generation rate increased with the elapsed time from the solid fuel (lignite) pyrolysis as the char generation was faster than the char consumption in the heterogeneous reactions. As time progressed, the conversion rate of char in the bed increased due to consumption by heterogeneous reactions. From the previous char reactivity study presented in Chapters 3 and 4, the specific reactivity increased with the conversion rate, therefore, the total consumption rate of char in the bed increased. On the other hand, the generation of char remained at the same rate because of the fixed solid fuel feeding rate. Finally the equilibrium was reached when the total consumption of char was equal to the generating rate from the pyrolysis of fed solid feed. From Figure 5.11, the mean char conversion at the equilibrium state was around 0.5 for this particular gasification run.

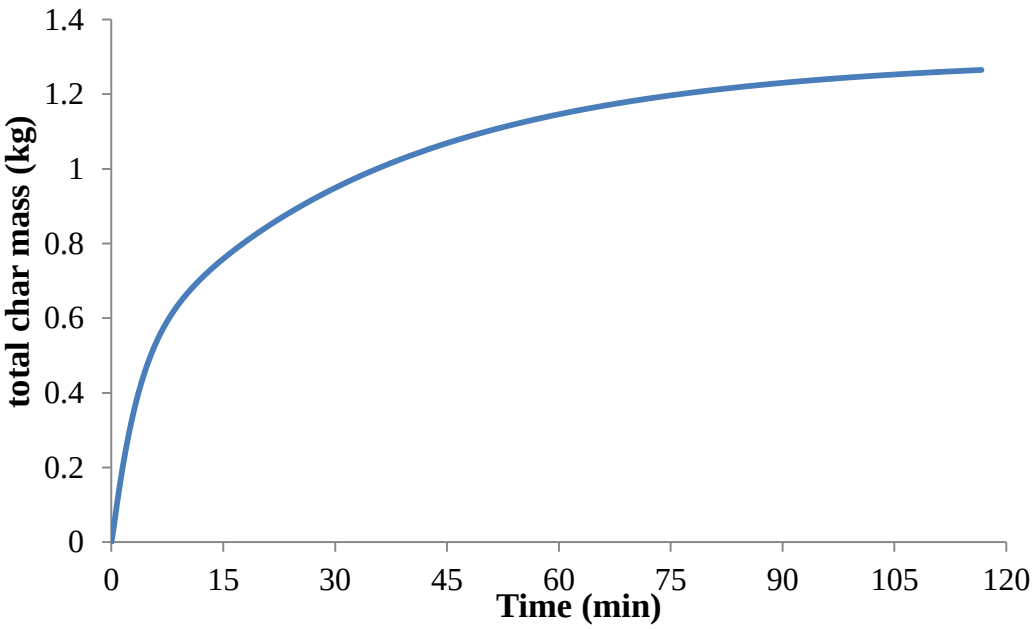

Figure 5.12: Accumulation of char in the bubbling fluidized bed as a function of elapsed time during the experiment.

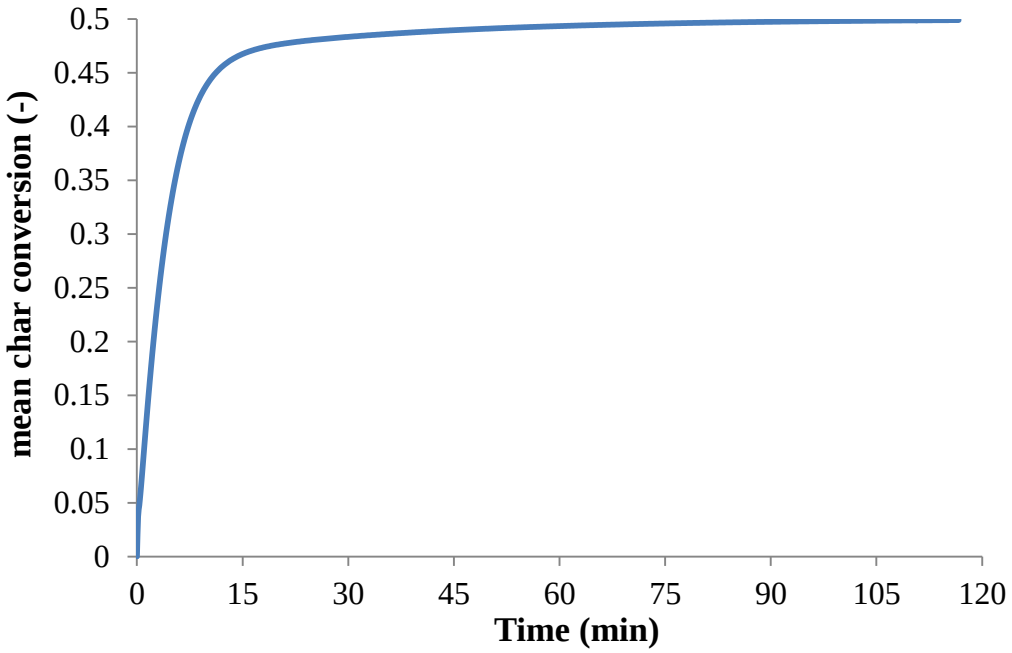

Figure 5.13: Mean char conversion through the bubbling fluidized bed as a function of elapsed time during the experiment.

Figure 5.12 shows the model predicted average gas temperature in the bubbling fluidized bed as a function of elapsed time during the experiment, while the gas temperature profile through the bed at the steady state of operation is shown in Figure 5.13. From Figure 5.12, the bed temperature increased above 900^{o}C for a short period from the start of the experiment because of the excessive oxygen available at this stage. In this short period of time, a complete combustion reaction was dominant, and hence more heat was released inducing elevation of the temperature in the bed. As the gasification proceeded, the amount of char in the bed increased and combustible substance became excessive, therefore, incomplete combustion reactions were dominant and the temperature dropped. Finally a steady state was reached when the total heat released from combustion was equal to the total heat consumed plus the net heat loss and heat carried out by the producer gas.

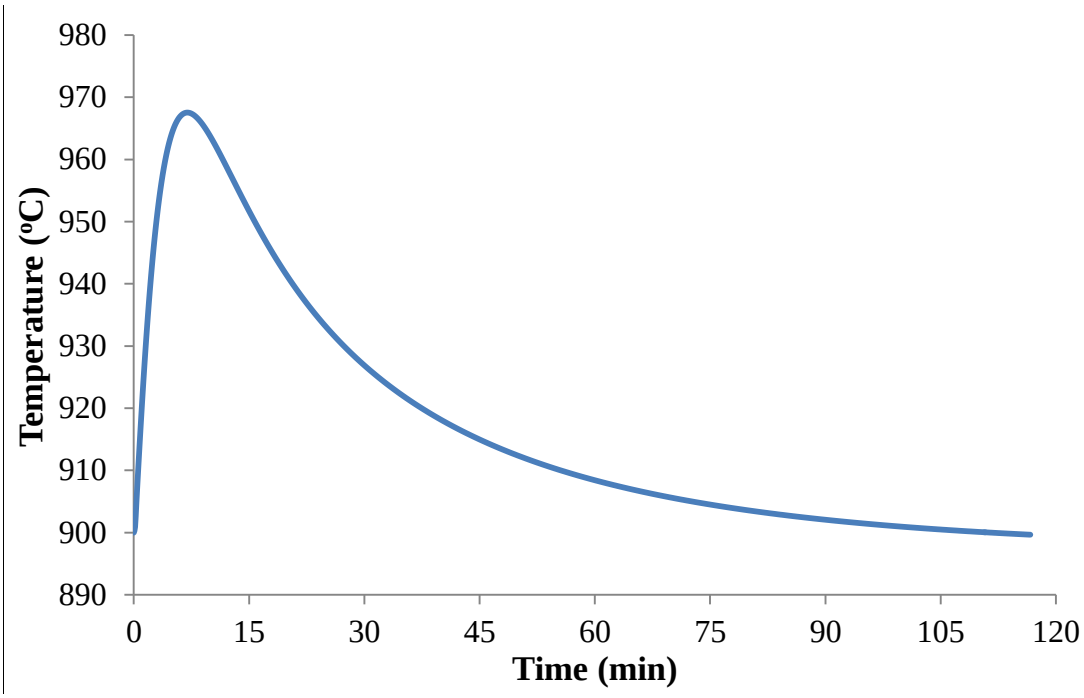

Figure 5.14: Model predicted average gas temperature in the bubbling fluidized bed as a function of elapsed time during the experiment.

From Figure 5.13, it can be seen at the steady state, the gas temperature rose after entering the gasifier, and reached a peak value of around 915 ^{o}C due to the combustion reactions in the lower part of the bed. The temperature profile corresponds to the oxygen concentration profile in Figure 5.9 in which the oxygen concentration dropped with the bed height and finally became depleted at the top of the bed.

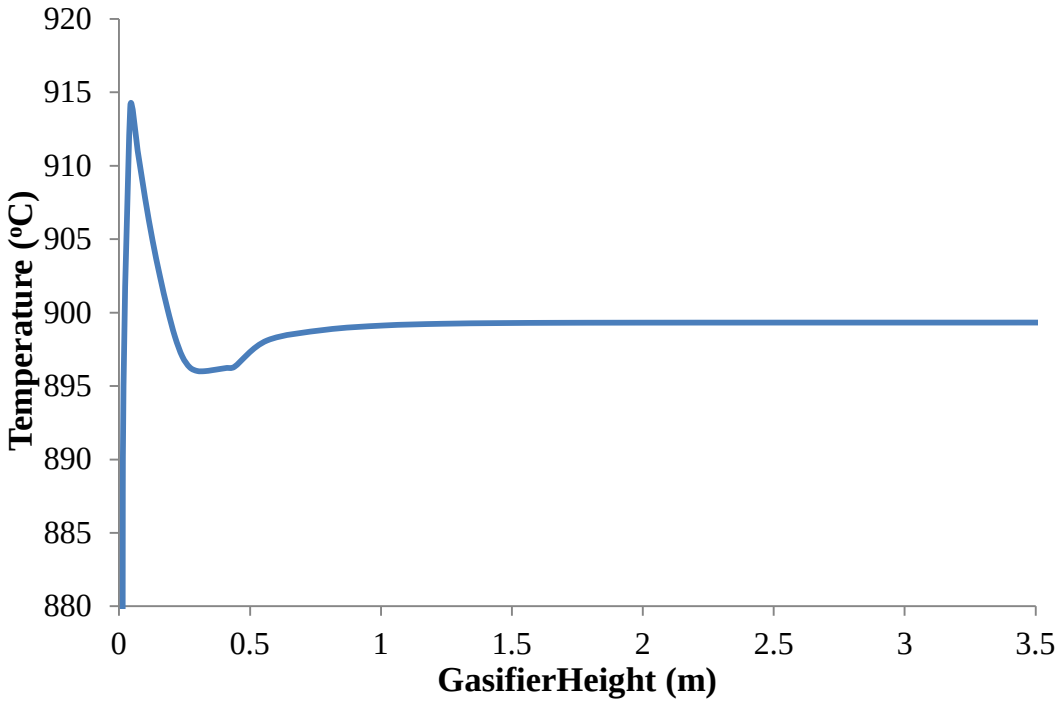

Figure 5.15: Model predicted gas temperature profile through the bubbling fluidized bed at the steady state of operation.

5.5.2 Model validation for gas composition change with time

Gas composition change with elapsed time is an important feature to validate the developed mathematical model. The dynamic change of simulation results reflects the characteristic time of the transient results to final steady state values, which is significant for predicting transient operation and future process control. In this section, the experimental data for co-gasification of blended coal and biomass at the coal (sub-bituminous) to biomass (*Pinus* radiata) ratio of 70S:30P at 950°C were compared to the model simulation results as shown in Figure 5.14.

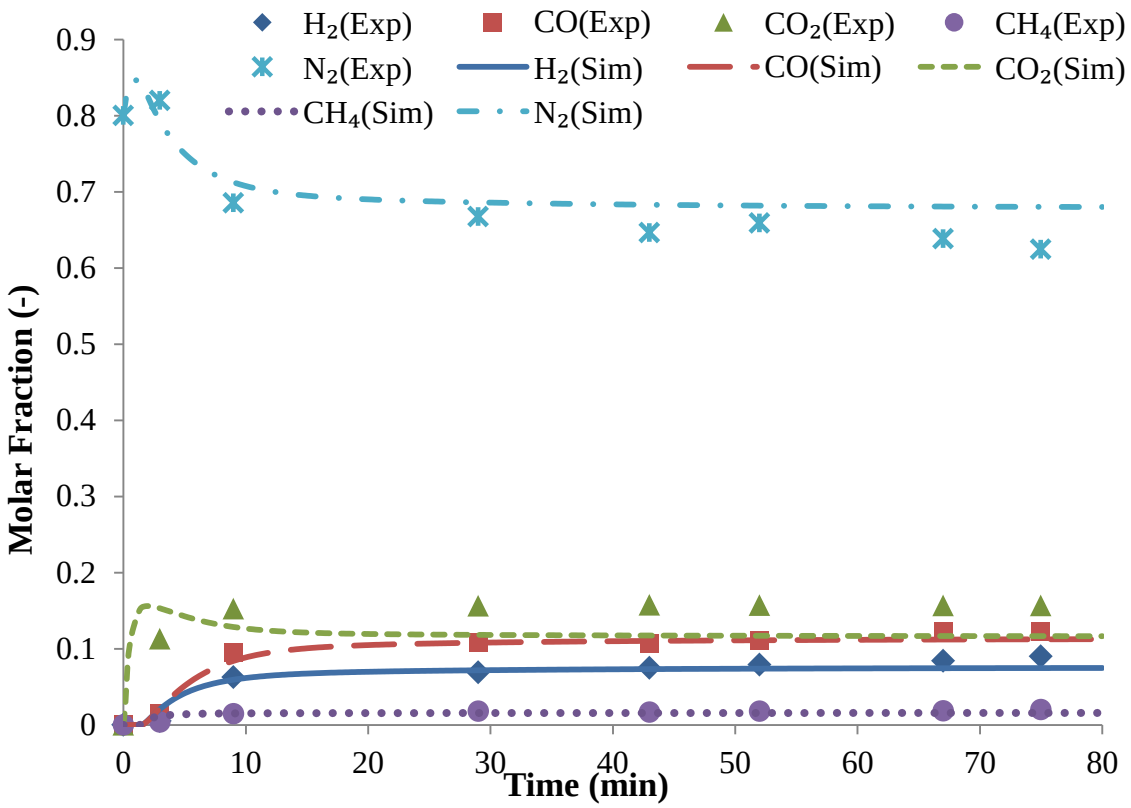

Figure 5.16: Comparison between experimentally measured (dots) and model predicted (lines) producer gas composition changes with time for co-gasification of blended coal (sub-bituminous) and biomass (Pine) at a ratio of 70S30P at 950^{o}C.

From Figure 5.14, it can be seen the experimentally measured gas composition at different times is close to the model predictions. From the model prediction, the CO_2 concentration initially increased sharply from zero to 0.16 mol/mol in about two minutes due to the initial total combustion, and then decreased to the value of 0.12 mol/mol after 20 minutes, then approached a steady value of 0.11 mol/mol. However, the sharp increase of the CO_2 concentrations was not detected from the experiment due to the delayed response and time taken for gas sampling. For the gas species of H_2 CO and CH_4, their concentrations increased gradually in the form of first order dynamic response to a step change. This phenomenon has been observed both from experimental measurements and model predictions as shown in Figure 5.14.

5.5.3 Effect of coal biomass blending ratio

Investigating the effect of biomass blending ratio on producer gas composition was the key objective in this study. The developed model has been run to simulate the four sets of experiments for co-gasification of blended coal and biomass at coal blending ratios from 0% (pure biomass) to 100% (pure coal) at an operating temperature range from 950 to 950 ^{o}C. The model simulation results for gas composition at steady state are compared with the experimental data at coal-to-biomass ratios of 70:30, 80:20 and 100:0. The results are shown in Figures 5.15 to 5.18, respectively, for blended lignite and eucalypt (Figure 5.15), blended lignite and pine (Figure 5.16), blended sub-bituminous coal and eucalypt (Figure 5.17) and blended sub-bituminous coal and pine (Figure 5.18).

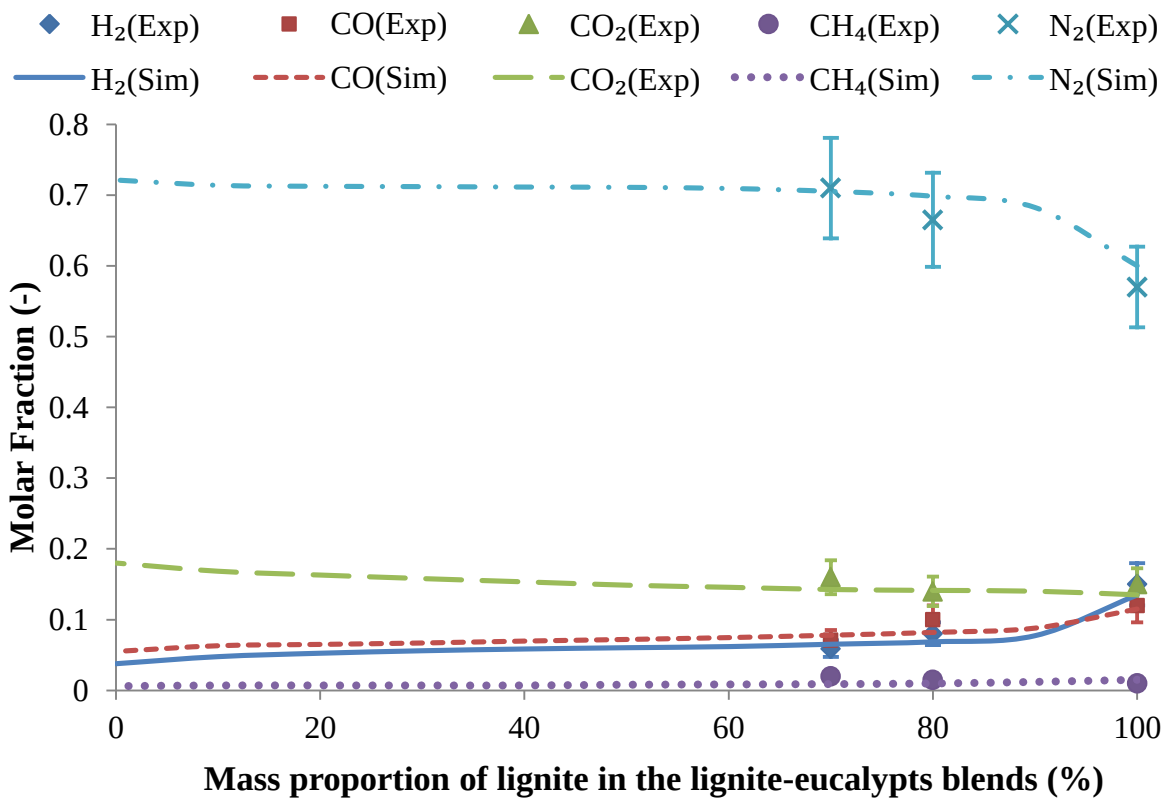

Figure 5.17: Model predicted and experimentally measured gas composition at steady state for co-gasification of blended lignite-eucalypt pellets at 900°C.

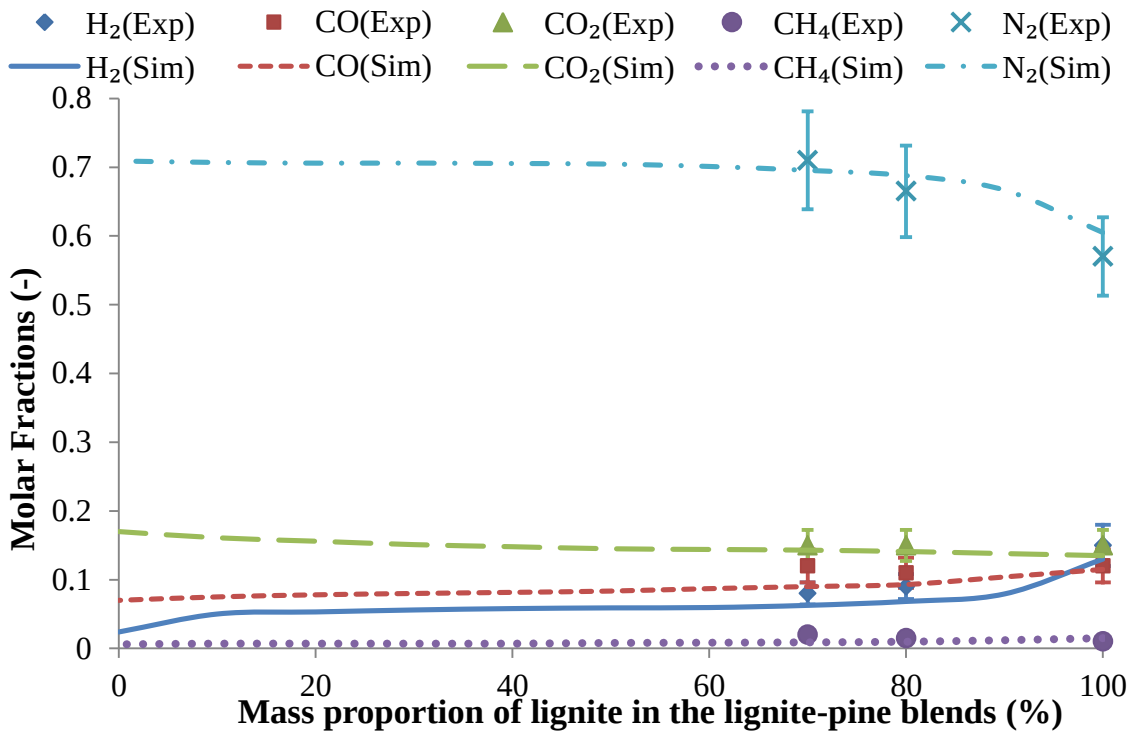

Figure 5.18: Model predicted and experimentally measured gas composition at steady state for co-gasification of lignite-pine pellets at 900 ^{o}C.

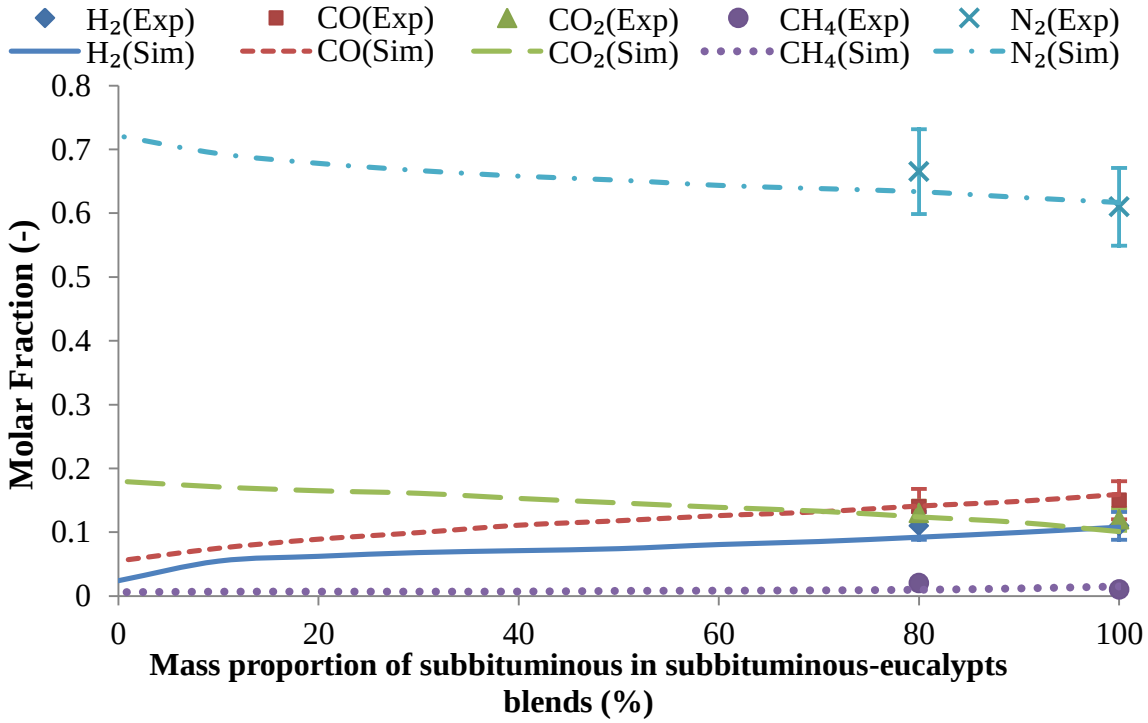

Figure 5.19: Model predicted and experimentally measured gas composition at steady state for co-gasification of subbituminous coal-eucalypt pellets at 900 ^{o}C.

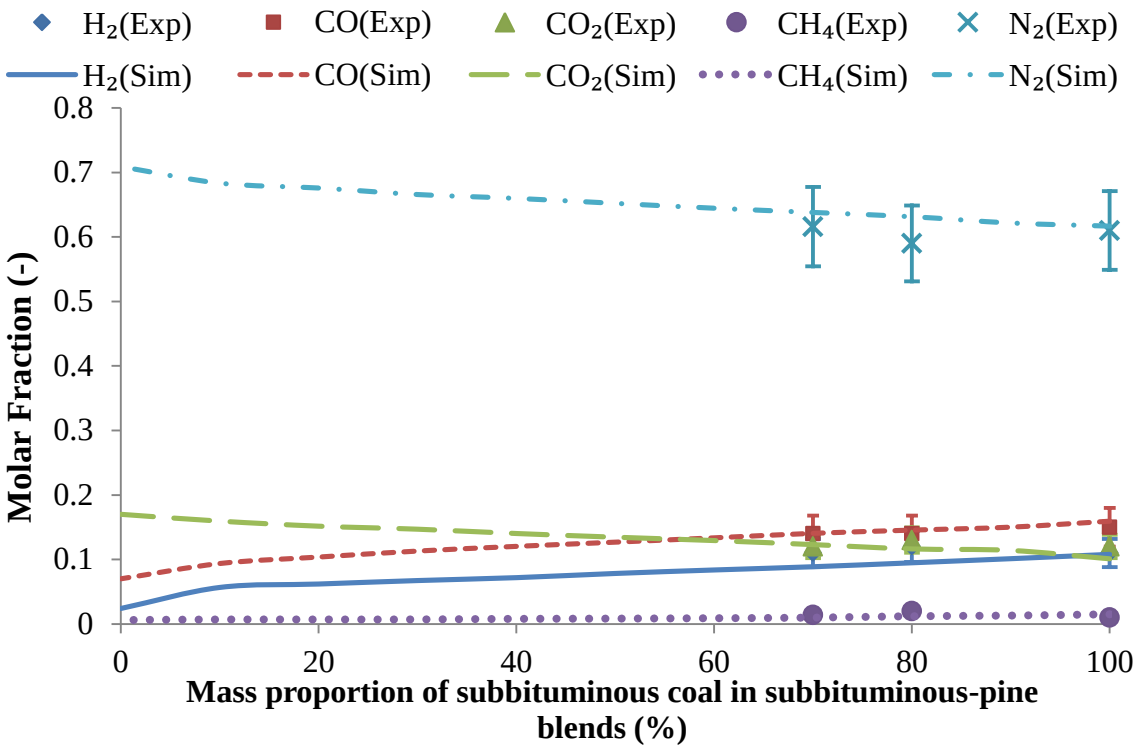

Figure 5.20: Model predicted and experimentally measured gas composition for co-gasification of sub-bituminous-pine pellets at 900 ^{o}C.

Figures 5.15 to 5.18 show the effect of solid fuel type and blending ratios on the producer gas composition. In a general trend, the concentrations of H_2 and CO decreased with increasing biomass blending ratio (or decreasing coal blending ratio), while for CO_2 concentration, the opposite trend was observed. This was because the biomass had a lower calorific value than coal, hence maintaining the same gasification temperature for co-gasification of feedstock with higher biomass ratio. In this case, a higher air feeding rate was needed and thus more H_2 and CO were consumed, resulting in reduced H_2 and CO concentrations. Furthermore, the impact of adding biomass to lignite was more significant than when adding biomass to sub-bituminous coal. Figures 5.15 and 5.16, show a sudden increase in H_2 and CO concentrations in the producer gas when the lignite blending ratio increased from 90% to 100% (pure lignite). The lower H_2 and CO concentrations at 90% lignite blending were because of the decrease in calorific value of the blended pellets when adding 10% biomass to lignite. In contrast, for the biomass-sub-bituminous coal blends, such sharp changes in H_2 and CO concentrations were not found, and this may be explained by the fact that the sub-bituminous coal has a higher char yield and calorific value than lignite, thus the required increase in air feeding rate was not changed significantly to achieve the

same set temperature and adding 10% biomass to sub-bituminous had less impact on the producer gas composition.

The coal type also affected the producer gas composition. From the ultimate analysis (Table 5.2), the sub-bituminous coal contains much more carbon than the lignite while both coals have similar hydrogen content. From Figures 5.15 to 5.18 it can be seen that, for co-gasification of sub-bituminous biomass pellets at high coal blending fractions, the CO concentration in the producer gas was higher than the CO_2 concentration while for co-gasification of lignite biomass pellets, the CO concentration was always lower than the CO_2 concentration in the producer gas. For gasification of the pure coals, the CO concentration for sub-bituminous coal was 0.16 mol/mol, which was about 0.04 mol/mol higher than the lignite coal, while the H_2 concentration for sub-bituminous coal (0.11 mol/mol) was about 0.03 mol/mol lower than that of pure lignite. This was because the calorific value of the sub-bituminous coal was higher and thus for the same gasification temperature, the required air feeding rate for sub-bituminous coal was lower than that for the lignite, hence overall consumption of combustible substance in the gas was less.

Comparing the producer gas composition for co-gasification of blended coal biomass with the two types of biomass, it was found that when blended with the coals, the biomass type (pine and eucalypts) had insignificant impacts on the producer gas composition, since pine and eucalypt had very similar element composition from the ultimate analysis (Table 5.2). The producer gas compositions from co-gasification of these two types of biomass blended with coal were similar except for the CO concentration, which was slightly higher from co-gasification of the pine coal pellets. The reason for this difference is believed to be the slightly higher char yield of pine wood. The other solid fuel properties value inputted to the model were similar, thus the simulation results for co-gasification of blended coal and eucalypt were similar to those of blended coal and pine.

Comparison between simulation results and experimental data was also made for co-gasification of the four raw materials. From the above figures 5.15 to 5.18, it can be seen that the model-predicted producer gas compositions are all in close agreement within 10% error range of the experimental data points. Discrepancy between the model prediction and experimental data can be raised from (1) inaccuracy in instrumental reading of air feed rate and (2) mismatches between producer gas samples and operating conditions. For the first reason, the instrumental

readings of air feed rates were used as the model input parameter; the difference between the model prediction and experimental data could be caused by the deviation between actual air being fed to the gasifier and the instrumental reading correlated from the revolution of the blower motor. For the second reason, the recorded operating condition of the taken sample could not truly reflect the real instantaneous operating conditions because of the continuous system creeping and response time of GC.

5.5.4 Effect of gasification temperature

The developed mathematical model has been used to investigate the effect of operation temperature on the producer gas composition. In the model the gas temperature in the bed, either the average temperature or the gas temperature profile through the bubbling fluidized bed, is an output parameter, with the term temperature being defined as the mean average gas temperature through the bed at steady state. It was found that the temperature was strongly related to the ratio of feeding air mass flow rate to the solid fuel feeding rate. In order to obtain different average gas temperatures in the bed, the input values of solid fuel feeding and feeding air mass flow rate were manipulated until the average gas temperature in the bed fell into the tolerated range at steady state (normally within $\pm 5^{o}$C from the set point). It should be noted that a similar approach was applied in the experiments in which the operation temperature was taken as a set point and the feeding air flow rate was adjusted while the solid fuel feeding rate was fixed. The model simulation results and the experimental data are shown in Figure 5.19 for co-gasification of blended lignite and eucalypt at a blending ratio of 70:30. The average gas temperature in the bed was varied from 850 to 950°C in the model simulation while the temperature was varied from 880 to 950°C in the experiments.

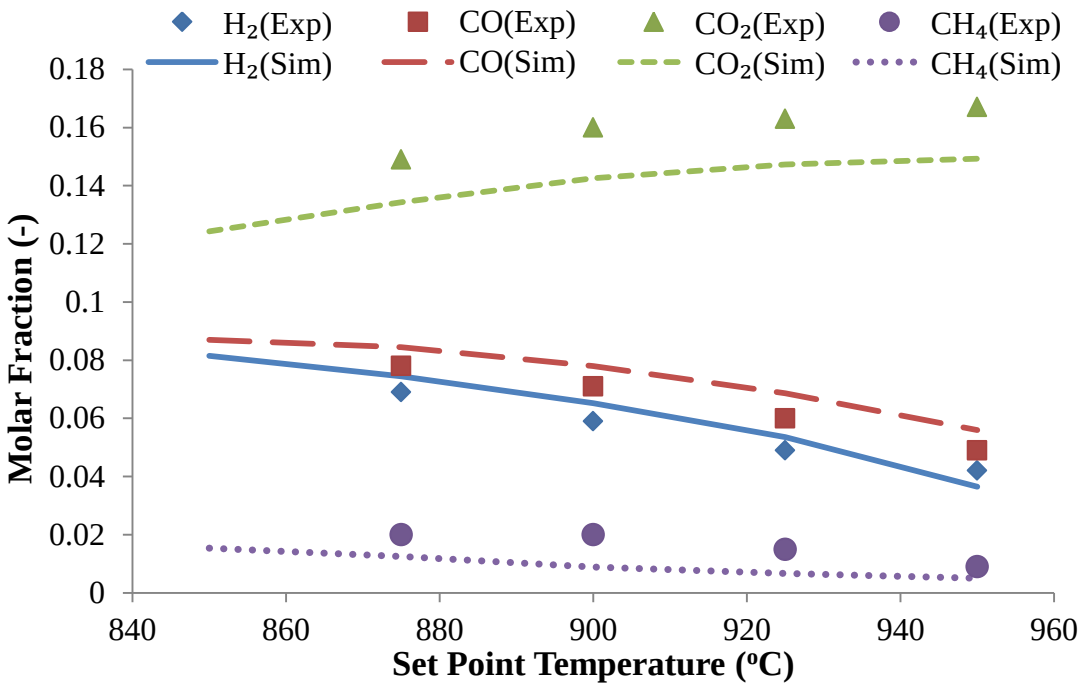

Figure 5.21: Effect of average gas temperature in the bed on steady state producer gas composition of blended lignite and eucalypt at a ratio of 70L-30E: Model simulation results and experimental data.

From Figure 5.19, it has been found that in general, the concentrations of combustible species (H_2, CO, CH_4) in the producer gas decreased as the temperature increased. In the opposite trend, the CO_2 concentration increased with the temperature, despite CO formation in carbon combustion reaction R_2 beingfavoured at elevated temperature, and becoming the dominant product at high temperature (for instance, CO/CO_2 ratio is about 12 at 900 ^oC) (TOMECZEK. 1994). This can be explained by the fact that in order to achieve higher gasifier temperature, a higher air to solid fuel ratio was required, therefore more combustible substances were converted into CO_2 and water. For gasification of pellets with other blending ratios and other feedstock, the gas compositions had similar temperature trends.

5.5.5 Effect of solid fuel properties

Solid fuel properties examined from the developed model included: devolatilzation performance of a solid fuel (gas yield and gas composition), and char yield and char reactivity. From the results of the model simulation, it was found that the producer gas quality in terms of H_2 and CO

contents increased with the total fraction of all combustible gas species and char yield in the solid fuel devolatilzation. As the yield of combustible gas species increased, more oxygen would be consumed at the lower part of the bed hence less combustible reactions occurred in the bed above the combustion zone and the producer gas would contain more combustible gases at the gasifier exit. The effect of char yield was more significant than the combustible gaseous species as higher char yield could shift the position of oxygen depletion to an even lower location within the bed, therefore the gasification zone was extended and H_2 and CO contents in the producer gas were further increased.

From the model simulations, it was also found that the overall char reactivity had an insignificant effect on the producer gas composition at the steady state, but had a significant effect on the gas composition change with elapsed time in the initial period of the gasification process. At steady state, the system outcomes only depended on the operation conditions and feeding rates of solid fuel and gasification agent. The gas composition at the steady state was influenced by the rate of char entering the system, but less dependent on the consumption rate of chars that stayed in the system.

Dynamic behaviour of producer gas composition was highly dependent on the char overall reactivity as the char reactions were the slowest steps among all processes involved in the gasification process. Therefore the char accumulated in the bed took a relatively longer time to reach equilibrium state at which the rate of char being generated was equal to total char consumption rate. At this point, the system reached steady state and the producer gas composition did not change with time. Therefore the time for the gasification system to reach steady state should be comparable with the characteristic complete conversion time of a single char as examined in Chapters 3 and 4. This is verified by the observation of the experimental runs in which it took 20-30 minutes for the BFB gasifier to reach steady state operation, which was similar to the single char complete conversion. From Figure 5.8, it has been seen that the pure lignite gasification reached steady state after about 35 minutes after the start of the gasification while for co-gasification of blended sub-bituminous coal and pine at a blending ratio of 70: 30%, the steady state was reached after around 25 minutes from the start of gasification.

Although overall char reactivity had an insignificant impact on the producer gas composition, the intrinsic reaction ratio between heterogeneous reactions of char with different gaseous species

had a significant influence on producer gas composition, especially for the ratio of combustion to water-gas reaction (R_2/R_3). The H_2 and CO contents increased with the increase in the intrinsic rates ratio of char combustion to gasification because more oxygen was consumed by char combustion at the lower region of bed, hence the height of the combustion zone (from bed bottom to oxygen depletion point) would be reduced and consequently more H_2 and CO could be generated in the elongated gasification zone.

5.5.6 Effect of air to solid fuel ratio

Air to solid fuel ratio (A/F) is an important variable in the gasification process, since it has direct influence on the gasifier bed temperature and, in turn, the producer gas composition. The temperature control during the gasification operation was achieved by manually adjusting the feeding ratio of solid fuels to air. To increase bed temperature, higher air or less solid feed rate was required and vice versa. At a high air feeding rate, the combustion reactions were promoted as more oxygen was supplied to the system. Consequently, more combustion heat was released from the burning of combustible substances: char, H_2, CO and CH_4. From both model simulation and experimental results, it was found that the concentrations of these combustible substances decreased while the CO_2 concentration increased with an increase in the A/F ratio.

The BFB gasifier was originally designed to gasify lignite, and in order to operate the gasifier at 900°C for gasification of lignite, the solid fuel and air feeding rates were found to be 19 kg/hr and 60 Nm^3/hr respectively. Figure 5.20 shows that in recorded gasification operating data of a certain time period with 19 kg/hr fixed pure lignite feed, the mean fluidized bed temperature increases as the air feed rate increases. For sub-bituminous coal, the required air to solid feed was less than that in gasification of lignite for maintaining the same bed temperature, due to the higher calorific value of sub-bituminous char. In this case, an air feeding rate of 55 Nm^3/hr was needed for a gasification temperature of 900°C while the coal feeding rate was kept at the same value as for lignite (19 kg/hr). This phenomenon has been both simulated from the developed model and from experimental observations.

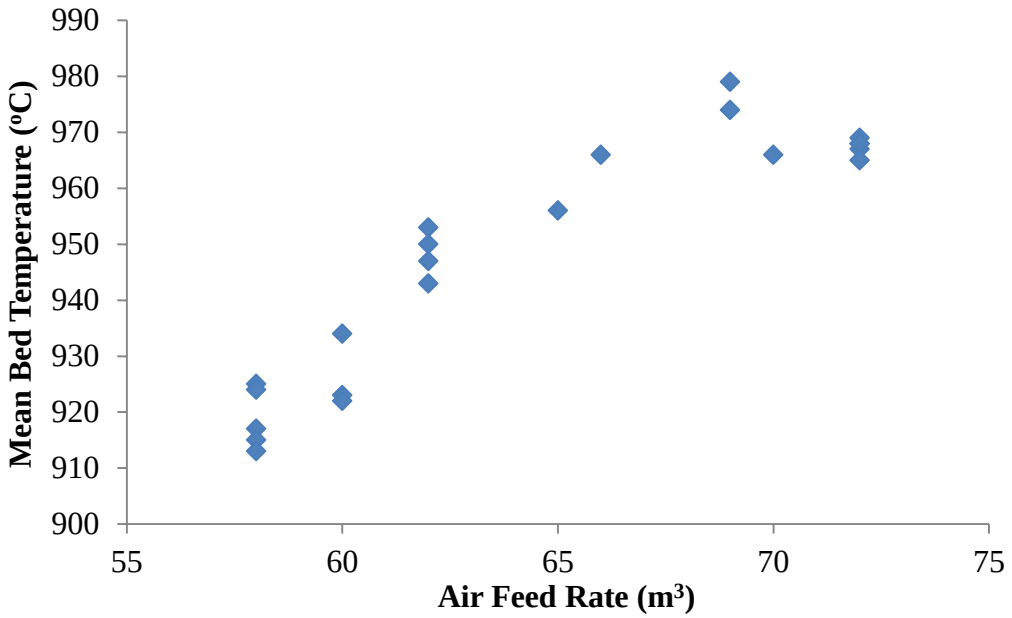

Figure 5.22: Recorded mean bed temperature with increased air and fixed solid fuel feed

5.6 Conclusion

In this part of the study, a one dimensional mathematical model was developed to simulate bubbling fluidized bed gasification of blended coal and biomass pellets. The model was based on a two phase theory in which the bubbling fluidized bed was divided into an emulsion phase and a bubbling phase. In the emulsion phase, gas flows within the bed at minimum fluidisation velocity while the solid particles are fluidized. The excessive gas flows only in the bubble phases in the form of plug flow in which only homogeneous reactions are considered. In the emulsion phase, both the heterogeneous and homogeneous reactions are included. The emulsion phase gas was treated as a plug flow reactor with axial mass and heat diffusion, while the bubbling gas was considered as PFR without dispersion, and all solids were considered as well mixed with gases in the emulsion phase. The internal diffusion within the emulsion phase, inter-phase mass transfer, solid-gas heat and mass transfer phenomena were taken into account. The internal diffusion of gaseous species was mathematically described by effectiveness factor.

A set of experiments was performed to validate the developed model, and it was found the model can predict the gas composition both at steady state and at the transition period from the start of

the gasification process. The numerical values between simulation and experimental results were very close.

From the parameter study, it was found that the gasification characteristics can be influenced by several factors. For the fuel properties, the steady state gas composition was strongly dependent on the char yield as well as devolatilization gas yield and distribution. The char reactivity had least influence on producer gas composition, however it had significant impact on the dynamic behaviour of the process. The operating conditions also had a significant influence on producer gas composition; generally for gasification at a particular temperature, the air to solid ratio was mainly determined by the calorific value of solid feedstock, hence the producer gas composition was subsequently determined.

The effects of blending of biomass with coal were studied, and it was found that adding biomass to coal had a negative influence on the producer gas. Such effect was more significant for lignite than for sub-bituminous coal. The biomass type had an insignificant impact on the gas composition.

References

Arenillas, A., Rubiera, F., Pevida, C., and Pis, J. J. (2001). "A comparison of different methods for predicting coal devolatilisation kinetics." *Journal of Analytical and Applied Pyrolysis*, 58-59, 685-701.

Babu, B. V., and Chaurasia, A. S. (2004). "Heat transfer and kinetics in the pyrolysis of shrinking biomass particle." *Chemical Engineering Science*, 59, 1999 – 2012.

Chan, W. R., Kelbon, M., and Krieger, B. B. (1985). "Modeling and experimental verification of physical and chemical processes during pyrolysis of large biomass particle." *Fuel*, 64, 1505–1513.

De Souza-Santos, M. L. (1989). "Comprehensive modelling and simulation of fluidized bed boilers and gasifiers." *Fuel*, 68(12), 1507-1521.

de Souza-Santos, M. L. (2004). *Solid Fuels Combustion and Gasification*, Marcel Dekker, New York.

Fermoso, J., Gil, M. V., Pevida, C., Pis, J. J., and Rubiera, F. (2010). "Kinetic models comparison for non-isothermal steam gasification of coal–biomass blend chars." *Chemical Engineering Journal*, 161(1–2), 276-284.

Font, R., Marcilla, A., Verdu, E., and Devesa, J. (1990). "Kinetics of the pyrolysis of almond shells and almond shells impregnated with $CoCl_2$ in a fluidized bed reactor and in a Pyroprobe 100." *Industrial and Engineering Chemistry Research*, 29, 1846–1855.

Hong, J. (2000). "Modeling char oxidation as a function of pressure using an intrinsic Langmuir rate equation," Brigham Young Univeristy.

Karim, G. A., and Mohindra, D. (1974). "A Kinetic Investigation of the Water Gas Shift Reaction in Homogeneous Systems." *Journal of the Institute of Fuel*, 219-223.

Krishna, R., and Wesselingh, J. A. (1997). "The Maxwell-Stefan approach to mass transfer." *Chemical Engineering Science*, 52(6), 861-911.

Kunni, D., and Levenspiel, O. (1991). *Fluidization Engineering*, Second Edition Ed., Butterworth_Heinemann.

Meesri, C., and Moghtaderi, B. (2002). "Lack of synergetic effects in the pyrolytic characteristics of woody biomass/coal blends under low and high heating rate regimes." *Biomass and Bioenergy*, 23(1), 55-66.

Murphy, J. J., and Shaddix, C. R. (2006). "Combustion kinetics of coal chars in oxygen-enriched environments." *Combustion and Flame*, 144, 710–729.

Perry, R. H., Green, D. W., and Maloney, J. O. (1997). *Perey's Chemical Engineerings' Handbook.*, McGraw-Hill, New York.

Roberts, D. G., and Harris, D. J. (2006). "A Kinetic Analysis of Coal Char Gasification Reactions at High Pressures." *Energy & Fuels*, 20, 2314-2320.

S. Mori, C. Y. W. (1975). "Estimation of bubble diameter in gaseous fluidized beds." *AIChE Journal*, 21(1), 109-115.

Sadaka, S. S., Ghaly, A. E., and Sabbah, M. A. (2002). "Two phase biomass air-steam gasification model for fluidized bed reactors: Part I—model development." *Biomass and Bioenergy*, 22(6), 439-462.

Seo, M. W., Goo, J. H., Kim, S. D., Lee, S. H., and Choi, Y. C. (2010). "Gasification Characteristics of Coal/Biomass Blend in a Dual Circulating Fluidized Bed Reactor." *Energy & Fuels*, 24(5), 3108-3118.

Shafizadeh, F., and Chin, P. P. S. (1977). "Thermal deterioration of wood." In: *ACS Symposium Series 43*, 57–81.

Sit, S. P., and Grace, J. R. (1981). "Effect of bubble interaction on interphase mass transfer in gas fluidized beds." *Chemical Engineering Science*, 36, 327-335.

Thurner, F., and Mann, U. (1981). "Kinetic investigation of wood pyrolysis." In: *Industrial and Engineering Chemical Process Design and Development 20*, 482–488.

J.Tomeczek. (1994). *Coal Combustion*, Krieger.

Veldsink, J. W., van Damme, R. M. J., Versteeg, G. F., and van Swaaij, W. P. M. (1995). "The use of dusty-gas model for the description of mass transport with chemical reaction in porous media." *The Chemical Engineering Journal*, 57, 115-125.

Welty, J. R., Wicks, C. E., Wilson, R. E., and Rorrer, G. L. (2001). *Fundamental of Mommentum, Heat, and Mass Transfer*, Wiley, New York.

Yan, H.-m., Heidenreich, C., and Zhang, D.-k. (1998). "Mathematical modelling of a bubbling fluidized-bed coal gasifier and the significance of 'net flow'." *Fuel*, 77(9–10), 1067-1079.

Chapter 6 Mathematical Modelling and Model Validation for Co-gasification of Blended Coal and Biomass in a Dual-Fluidized Bed Gasifier

This chapter presents a revised model developed in Chapter 5 for simulation of steam gasification of blended coal and biomass pellets in a dual fluidized bed (DFB) gasifier. Experiments were conducted using a 100 kW DFB gasifier at an operation temperature of 800℃ with a biomass blend ratio varying from 0 to 100% for investigation of the blending ratio effect on producer gas composition. The experimental results were also used to validate the revised mathematical model and close agreement was found when comparing the measured and simulation producer gas compositions.

6.1 Introduction

In Chapter 5, a mathematical model was developed for simulation of co-gasification of blended biomass and coal on a bubbling fluidized bed gasifier using air and steam as the gasification agent. When the mixture of air and steam is used as gasification agent, the gasification process involves combustion reactions which provide heat to the overall endothermic gasification reactions whereas when using pure steam as the gasification agent, an external heat supply is needed for the overall endothermic gasification reactions. Therefore the gasification characteristics in terms of producer gas composition are very different between these two gasification processes. Furthermore, as discussed in Chapter 5, there are some limitations in the air/steam gasification on the biomass blending ratio in order to achieve the target operation temperature, therefore, the co-gasification experiments were performed only for blended coal and biomass feedstock at high coal blending ratios (70–100%). However, the blending ratio is no longer a limitation for the co-gasification of blended coal and biomass pellets in the dual fluidized bed gasifier with steam as the gasification agent, as the heat needed is supplied by the circulating bed material.

In this part of the study, the characteristics of pure steam gasification of blended biomass and coal were investigated both theoretically and experimentally, in order to understand the effect of blending ratio on producer gas composition. The mathematical model developed in Chapter 5 has been revised to consider the differences in the gasification reactions in the steam gasification and the partial char flow to the combustion reactor in the dual fluidized bed (DFB) gasifier. In order to validate the revised mathematical model, gasification experiments were conducted on the DFB gasifier in the Department of Chemical and Process Engineering (CAPE), University of Canterbury. In the experiments, pellets of blended biomass and coal were used as feedstock with biomass proportion ranging from 0% to 100%, in order to cover the full blending ratio spectrum. The experimental results have been used to validate the revised mathematical model, which after the validation has been employed for parameter sensitivity analysis.

6.2 Dual Fluidized Bed Gasifier System

The 100 kW DFB gasification system used in this study consists of two main compartments, a bubbling fluidized bed (BFB) gasification reactor and a circulating fluidized bed (CFB) as shown in Figures 6.1 and 6.2. The solid fuel is fed into the bed of the BFB gasification reactor while the steam is injected from the reactor bottom through the steam distributor. The gasification reactions occur in the BFB reactor with external heat being supplied by the hot bed materials falling from the reactor top. At the BFB reactor bottom, the mixture of bed material, some unconverted solid fuel and some char flows through a chute into the bottom of CFB combustion reactor in which the char is combusted with air to heat up the bed material. The flue gas carries the hot bed material to the CFB reactor top and out the reactor into a cyclone where the hot bed material is separated from the flue gas. The flue gas flows out of the cyclone from the top while the hot bed material flows out from the bottom into the siphon then falls into the BFB gasification reactor for heat supply. Sand is commonly used as bed material and is circulated as a heat carrier to transfer heat.

Both the chute and the siphon are fluidized with controlled steam to prevent cross-flows of gases between the FFB and the BFB, and to maintain a high solid circulation rate. The producer gas generated in the BFB gasification reactor flows out of the reactor and the entrained fine particles

of char, ash and bed materials are separated from the producer gas in the BFB cyclone. The fine particles are then collected in the trap collector, which could be emptied during the gasifier operation if needed. At the same time, an equal amount of fresh bed material is introduced into the gasifier system through the sand charger located at the FFB to compensate for the lost bed material during the experiment. Samplings of the producer gas are conducted at the sampling port located after the BFB cyclone. In the current stage, the producer gas is incinerated in an afterburner and the flue gas is emitted to the air.

In the above description, the DFB gasification system uncouples the gasification and combustion reactions into two separate reactors, thereby increasing the degree of freedom of operation and enabling control of the gasification temperature from the combustion of char and, if needed, the supplementary LPG in the CFB reactor.

Figure 6.1: Image of the 100 kW DFB gasifier in CAPE.

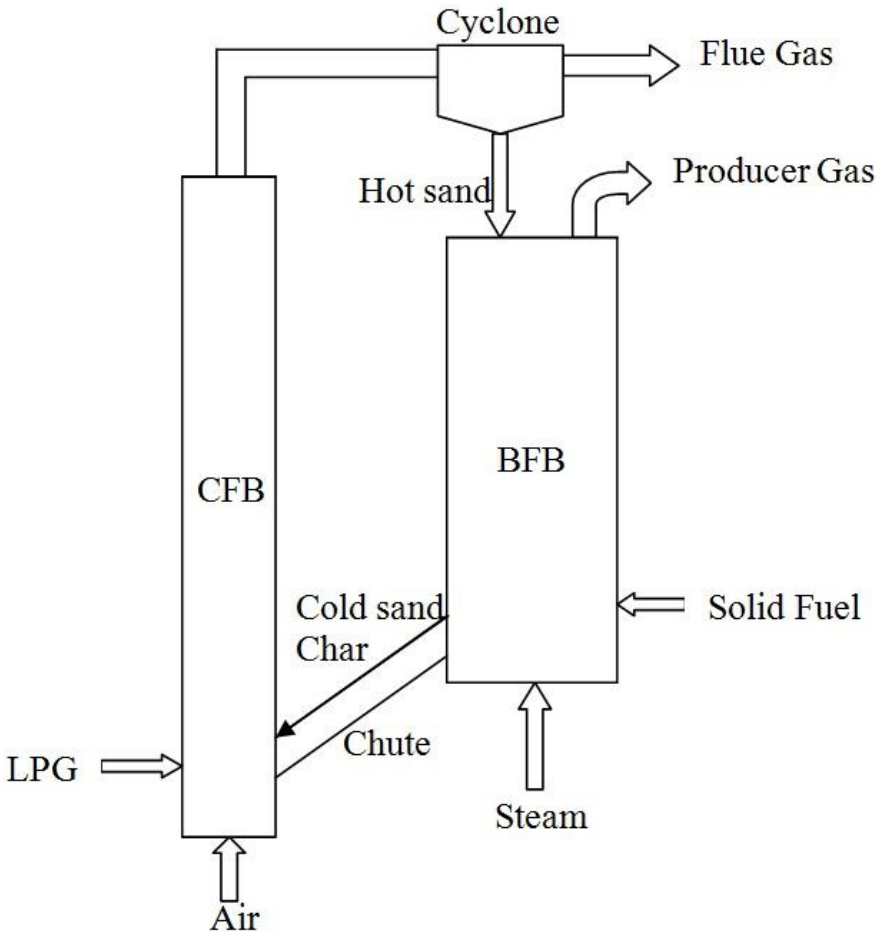

Figure 6.2: Flow diagram of the DFB gasification system.

6.3 Model Revision for Co-Gasification of Blended Biomass and Coal in the BFB Reactor

In this study, the focus of the mathematical modelling is on co-gasification of blended biomass and coal in the BFB reactor in which the steam gasification of solid fuels takes place. Most of the basic principles presented in Chapter 5 for the model developed are still valid, including: (1) the two phase theory applied to describe the bubbling fluidized bed; (2) the effective reaction volume method used to estimate the significance of internal mass transfer of reactive gaseous component in the solid char particle. However, in the steam gasification, combustion reactions are not considered as no oxygen is present but steam reactions are more pronounced.

6.3.1 Species and reactions contained in the model

The gas species being considered in this model are as follows in the order of i = 1, 2, …5 (Dupont et al. 2007):

(1) H_2O; (2) H_2; (3) CO; (4) CO_2; and (5) CH_4

The reactions taking place in the gasifier can be summarized as three main categories in the order of j = 1, 2, 3, 4.

i). Initial pyrolysis or devolatilization:

R_1: Coal/Biomass → C + H_2O, H_2, CO, CO_2, CH_4 (6.1)

ii). Heterogeneous reactions:

R_2: C + H_2O → H_2 + CO steam gasification of char (6.2)

R_3: C + CO_2 → 2CO Bouduard reaction of char (6.3)

ii). Homogeneous reactions:

R_4: CO + H_2O ↔ H_2 + CO_2 water gas shift reaction (6.4)

6.2.2 Conservative equations

The mathematical model consisted of 17 sets of partial differential equations plus four ordinary differential equations that describe mass and energy conservations for gases, solid fuel and char, char conversion rate and enthalpy change rate of inert bed material. Among those equations, the mass and energy balances for gases and rate of char conversion are similar to those presented in Chapter five and thus detailed description of these equations will not be included in this chapter. However, the other three equations, which describe the total mass of solid feedstock, char and bed material temperature, are different from those presented in Chapter five and will be described as follows.

For the emulsion phase:

$$\begin{aligned}&\left(1-\varepsilon_b\right)\varepsilon_{mf}\frac{\partial \mathbf{C_E}}{\partial t}+\nabla\cdot\left(\left(1-\varepsilon_b\right)u_{mf}\mathbf{C_E}\right)=\\&=a_B K_{BE}\left(\mathbf{C_B}-\mathbf{C_E}\right)+\nabla\cdot\left(\left(1-\varepsilon_b\right)\varepsilon_{mf}\mathbf{D_m}\cdot\nabla\mathbf{C_E}\right)+\left(1-\varepsilon_b\right)\mathbf{vR_E}-\mathbf{\Delta F}\end{aligned} \quad (6.5)$$

For the bubble phase:

$$\varepsilon_b \frac{\partial \mathbf{C_B}}{\partial t} + \nabla \cdot \left(\varepsilon_b u_b \mathbf{C_B}\right) = a_B K_{BE} \left(\mathbf{C_E} - \mathbf{C_B}\right) + \varepsilon_b \mathbf{vR_B} + \mathbf{\Delta F} \tag{6.6}$$

For bed gas energy balance (Yan et al. 1998):

$$\frac{\partial H}{\partial t} + \nabla \cdot \left(u_{mf} \left(1-\varepsilon_b\right) \sum_{i=1}^{7} C_{E,i} C_{P,i} + u_b \varepsilon_b \sum_{i=1}^{7} C_{B,i} C_{P,i} \right) =$$
$$= \nabla \cdot \left(k_m \nabla \left(T_{bg}\right)\right) + hA\left(T_{sand} - T_{bg}\right) + \sum_{j=1}^{7} \Delta H_{Rj} R_j \tag{6.7}$$

The conservation of total mass of fed solid fuel:

$$\frac{dM_S}{dt} = F_S - \frac{\alpha_S}{\tau} M_S - \int_{z=0}^{h_b} R_1 \frac{Mw_C}{y_C} \left(1-\varepsilon_b\right) A_{bed} dz \tag{6.8}$$

The conservation of total mass char:

$$\frac{dM_C}{dt} = \int_{z=0}^{h_b} \left(R_1 - R_2 - R_3 - R_4\right) Mw_C \left(1-\varepsilon_b\right) A_{bed} dz - \frac{\alpha_C}{\tau} M_C \tag{6.9}$$

The rate of change in mean average conversion of char is estimated as:

$$\frac{dX_C}{dt} = \frac{X_C M_C}{M_C + \int_{z=0}^{h_b} R_1 Mw_C \left(1-\varepsilon_b\right) A_{bed} dz} - X_C +$$
$$+ \frac{\left(1-X_C\right) \int_{z=0}^{h_b} \left(R_2 + R_3 + R_4\right) Mw_C \left(1-\varepsilon_b\right) A_{bed} dz}{M_C} \tag{6.10}$$

The change rate of bed material temperature:

$$\frac{dT_S}{dt} = \frac{\int_{z=0}^{h_b} hA\left(T_{bg} - T_{sand}\right) dz}{M_{Sand} C_{p_{Sand}} + M_C C_{p_{Char}}} + \frac{1}{\tau}\left(T_{sand.in} - T_{sand}\right) \tag{6.11}$$

Since the bed material (for example, sand) is circulated between the BFB and CFB reactors, the transportation of the fed solid fuel and the generated chars have to be taken into account. In

equations (6.8), (6.9) and (6.11), the term τ is the time constant of the bed material in the BFB reactor, which is the mean average retention time of the bed inventory:

$$\tau = \frac{M_{sand}}{\dot{M}_{sand}} \tag{6.12}$$

Where M_{sand} is the mean average holdup of the bed material in the BFB during steady state operation and $\dot{M}_{sand}$ is the mass circulation rate of the bed material between the BFB and the CFB reactors.

In Equations (6.8) and (6.9), the term α is the transportation selectivity factor of the specified material which is defined as is the ratio of actual mass flow rate of a specific solid particle through the chute over the theoretical mass flow corresponding to the bed circulation rate, and the subscripts *S* and *C* indicate the solid fuels and char respectively. The value of α varies with the biomass-coal blending ratio of the feedstock because the mass flow rate of solid fuel or char from BFB to CFB can be significantly different for different feedstock materials, due to the density difference between coal and woody biomass. This phenomenon is described in Section 6.2. The value of α reflects the particle distribution within the bubbling fluidized bed. Light particles, such as biomass char, tend to float on the top of the bed and their concentration near the chute inlet is thus very low. In this case, the α value is set as 0.05. On the other hand, the α value for coal char is set to be around 0.5, considering that the density of the coal char is much higher than the biomass char. Therefore, more coal chars are evenly distributed through the bed and more char particles are carried away from the bed bottom by the sand flow to the CFB. For the blended char particles, the α value is linearly related to the ratio of the density of the biomass and coal chars co-generated from the initial pyrolysis process over the bed material bulk density.

For the fed solid fuel, the α value is set to be 0.9 for pellets of biomass, coal and blended biomass and coal, as the solid fuel particle density for these three solid fuels is similar. The value of α has been checked by performing heat balance over the CFB by assuming complete combustion of all combustible inlet substances. In this way, the mass flow rate of raw solid and char passing through the chute can be determined.

6.4 Experiments and Materials

6.4.1 Experimental procedure and operation conditions

Before each gasification run, sand as bed material was fed into the CFB reactor and the BFB reactor evenly with a total mass of around 30 kg. Based on the measurement of bed material hold up after a sudden shutting down of the process, the average bed inventory in the BFB was around 17 kg for each run and the corresponding steady state bed height was about 0.45 m. During the start-up stage, air was fed into both the CFB and BFB bed by a 50 HP Roots blower at a nominal feed rate 700-800 L/min and 80-100 L/min respectively, to reach the required fluidisation state of bed material in the system. The sand circulation rate which is an important operating parameter was estimated from the CFB air flow rate by the extrapolation method (Kaiser et al. 2003), and the char transfer rate from BFB and CFB reactors also increased with the sand circulating rate (Kaushal et al. 2008). Once the desired fluidization state was achieved, the two reactors and the bed materials were heated up by combustion of LPG until the designated temperature was reached, which took approximately five hours. Then the operating conditions were fine-tuned to maintain the BFB set temperature until the system reached steady state. After that, the LPG supply to the BFB column was turned off and the air feed was switched to steam which was fed from the bottom of BFB reactor. The change-over of the feeding streams would cause a slight fluctuation of temperature in the BFB reactor; therefore, the system was further fine-tuned by altering the LPG flow to the CFB to maintain the BFB set-point temperature. In experiments, the temperature in the BFB reactor is a target control parameter, and in order to maintain the set BFB temperature, the CFB must be heated to a temperature of about 60 to 100^{o}C higher than the set BFB temperature. In the experiments conducted in this study, the BFB was operated at a temperature range from 750 to 800^{o}C and thus the CFB temperature was controlled at 810 to 900^{o}C.

Once the target temperatures for the CFB reactor were achieved and steady state reached, the solid fuel was fed into the BFB at point 0.2 m above the base of the column and the system entered the gasification mode. The steam to biomass (S/B) mass feed ratio was initially set as 0.95, but this ratio was varied depending on the type of solid fuel. As discussed in Chapter 5, gaseous species and char were generated from the initial pyrolysis reaction of the solid fuel. At steady state, part of the generated char particles were consumed by gasification reactions and the

remaining char particles were carried away from the BFB to the CFB reactor by the circulating bed material (sand) through the chute and finally were burnt in the CFB reactor.

During the experiments, the LPG feeding rate to the CFB reactor was adjusted in order to maintain the BFB set point temperature. From the observations during the runs, it was found that the LPG feeding rate was related to the blending ratio of the solid fuel and increased with the biomass blending ratio. The average LPG feeding rate for 100% pine biomass fuel was around 20 L/min. However, for pure lignite, the LPG supply was turned off. This indicates that sufficient heat was provided by combustion of lignite chars in the CFB reactor. This observation confirms the hypothesis for the transportation selectivity factor of char, α_C, increasing from 0.05 for biomass char to 0.5 for coal char. For biomass char, which is less dense than coal char, the majority of char particles tended to float on the upper part of the bed and the char particle concentration near the chute entrance was less. However, for the coal char particles, which have a high density, the char particles were evenly distributed through the bed, therefore the char transfer rate from the BFB reactor to the CFB reactor was much higher than the biomass char. The numerical values of α for different combustible solid particles in the BFB were validated based on experimental observation of LPG consumptions in the CFB.

In most of the experimental runs, the system reached a new steady state in around 30 minutes after the solid fuel was fed into the BFB reactor. After the steady state was reached, the producer gas was sampled from the BFB cyclone top and the flue gas was sampled from the CFB cyclone top with the time interval between each sampling as 20 minutes. The gas samples were collected manually using a double-syringe device and analysed by a 3000A Micro GC. Dry producer gas composition in terms of molar fractions of four main producer gas components (H_2, CO, CO_2 and CH_4) was determined as for the experimental results. For each operating condition, at least three samples were taken and analysed, and experimental results were taken as the average of the three recorded data. In the experiments, the steady state gasification operation lasted for three to four hours for collection and checking of the gas analysis results.

6.4.2 Test material

Pellets of blended lignite and pine wood were used as the solid fuel in the co-gasification experiments. The pellets were sourced and processed in the same way as described in Chapter 5. However, the lignite and the pine wood were sourced at different times and thus the properties may have changed to a certain extent. The proximate and ultimate analysis results of the feedstock material are given in Tables 6.1 and 6.2 below.

Table 6.1: Proximate Analysis result of feedstock materials (wet base)

Fuel type	Moisture (wt%)	Volatile matter (wt%)	Fixed carbon (wt%)	Ash (wt%)
Pine (dried)	8	77.4	14.2	0.4
Lignite	34.6	32.9	28.3	4.2

Table 6.2: Ultimate Analysis result of feedstock materials (dry and ash free base)

Fuel type	C (wt%)	H (wt%)	O (wt%)	N (wt%)	S (wt%)	H/C	O/C
Pine	51.6	5.9	42.3	0.22	0.01	0.11	0.82
Lignite	68.4	4.9	25.2	0.72	0.8	0.07	0.37

The lignite and pine pellets were made by the same method as described in Chapter 5. The major difference between the feedstock used in this part of the study and that used in Chapter 5 was the moisture content of lignite: 34.6% for this chapter and 19.1% for Chapter 5. Therefore in the gasification operation, the corresponding amount of steam was reduced from the nominal steam feed to offset the effect of in situ gasification caused by the extra water vapour brought by the lignite. The co-gasification runs are summarized in Table 6.3.

Table 6.3: Summary of co-gasification experiments performed on the DFB system

Run number	Test Fuel	Temperature(^{o}C)	S/F ratio
1	100L	780-790	0.99-1.3
2	80L20P	770-780	0.95-1.4
3	70L30P	770-780	0.95-1.3
4	40L60P	800	0.93-1.4
5	100P	800	0.77-1.45

6.5 Model Validation and Sensitivity Analysis

The revised mathematical model has been solved using the same numerical technique as described in Chapter 5, for predicting gas composition and temperature profiles in the BFB gasification reactor in the co-gasification of blended biomass and coal with steam as the gasification agent. The simulation results are firstly assessed for two scenarios of pure lignite and pure pine wood. After this the model simulation results are compared with the experimental results. Following this the model is employed for parameter sensitivity analysis.

6.5.1 Assessment of simulation results in two scenarios

The two extreme scenarios of steam gasification of pure lignite coal and pine at 800^{o}C with steam to biomass ratio (S/F) 0.9 are presented in the next section. The dynamic gasification characteristics of these two types of fuels in terms of producer gas releasing profile, molar concentrations profile along the bed height of gaseous species, dynamic change of char mass and mean conversion and temperature profile are illustrated. From the foundation of these two basic scenarios, more numerical gasification results were generated for intermediate biomass mass blending ratios and deviated operating conditions, and compared with experimental data in the later section, in order to indicate the effect of blending ratio and operating conditions such as S/F and gasification temperature.

6.5.1.1 Steam gasification of pure lignite

From the mathematical model, the producer gas composition of the steam gasification of solid fuel and temperature profile along the gasifier height could be predicted at given operating conditions. The simulation results of gasification of the pure lignite and pure wood pellets will be displayed in this section in order to illustrate the difference of the gasification of these two types of substances. The following operating conditions listed in Table 6.4 below were used as input values in the model simulations.

Table 6.4: Operating conditions of BFB steam gasification.

Steam feed rate	6~18	(kg/hr)
Solid feed rate	12	(kg/hr)
BFB operating pressure	5	(kPa)
Bed inventory in the BFB	~17	(kg sand)
Nominal bed temperature	800	(°C)

The simulation results for steam gasification of pure lignite at 800°C are shown in Figure 6.3 for producer gas composition change with elapsed time counted from the start of solid fuel feeding. From the figure, it was found that the gas species of H_2, CO_2 and CH_4 in the producer gas composition increased rapidly from zero at the start and then reached steady state at about 20 minutes after gasification started. During this period, the concentration of CO increased gradually towards the steady value. The initial rapid change in the gas composition was the result of initial fast pyrolysis and the subsequent gradual changes were due to the transition of char accumulation and gasification reactions in the bed. It can be seen that after the initial rapid increase, the CO_2 concentration decreased gradually while the CO concentration increased. During the initial stage, CO was largely consumed by a water gas shift reaction when the steam concentration was high. With the char accumulation, less CO was consumed due to the following reasons: (1) steam was consumed by the char-steam reaction thus the water gas shift reaction rate was slowed; and (2) more CO was produced from the water gas reaction.

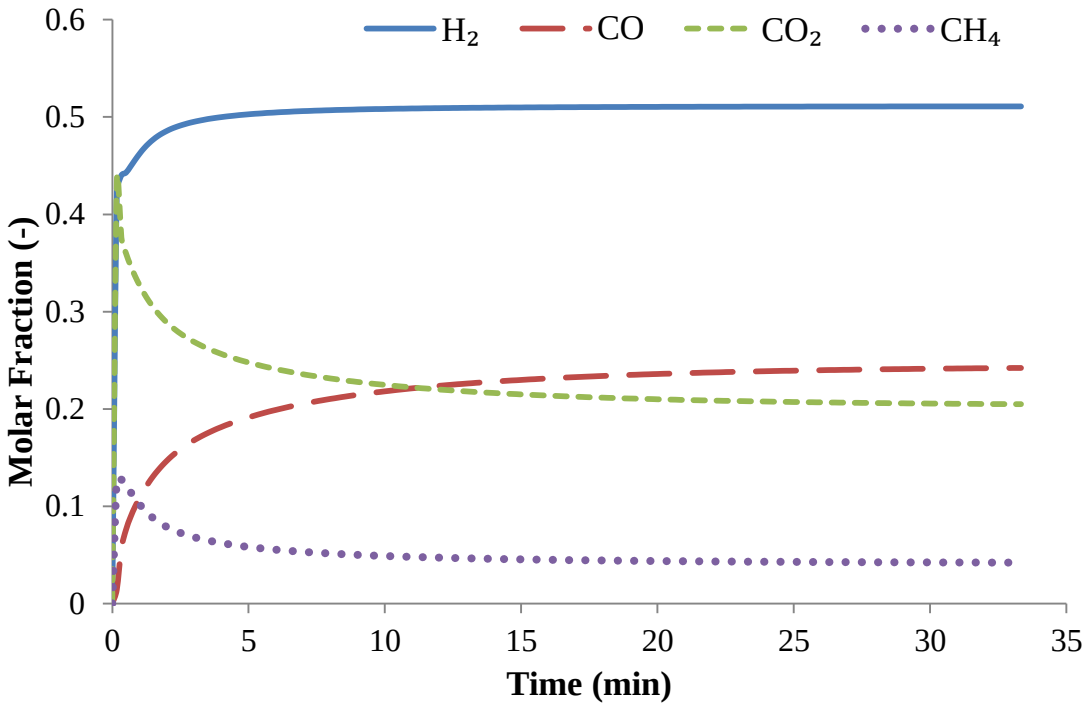

Figure 6.3: Model predicted producer gas composition for steam gasification of pure lignite at 800^{o}C.

Figure 6.4 shows the model simulation results of vapour-free gas concentration profile along the bed height at steady state in which the dash lines represent the concentrations of gas species in the emulsion phase and the solid lines represent the gas species concentrations in the bubble phase. It can be seen that the vapour-free producer gas concentrations increased along the bed height as the char and steam were converted to gas species. From the simulation results, it is interesting to note that there were some differences in the gas species concentrations between the emulsion phase and the bubble phase. The concentrations of H_2 and CO species in the emulsion phase were higher than those in the bubble phase because these substances were generated from the water gas reaction in this phase. However, the concentration of CO_2 in the bubble phase was higher as the forward water gas shift reaction rate in the bubble phase was higher, due to the higher concentration of steam in the bubble phase. Similar trends of gas composition profile in the two phases have been reported in the literature (Fiaschi and Michelini 2001) (Yan et al. 1998).

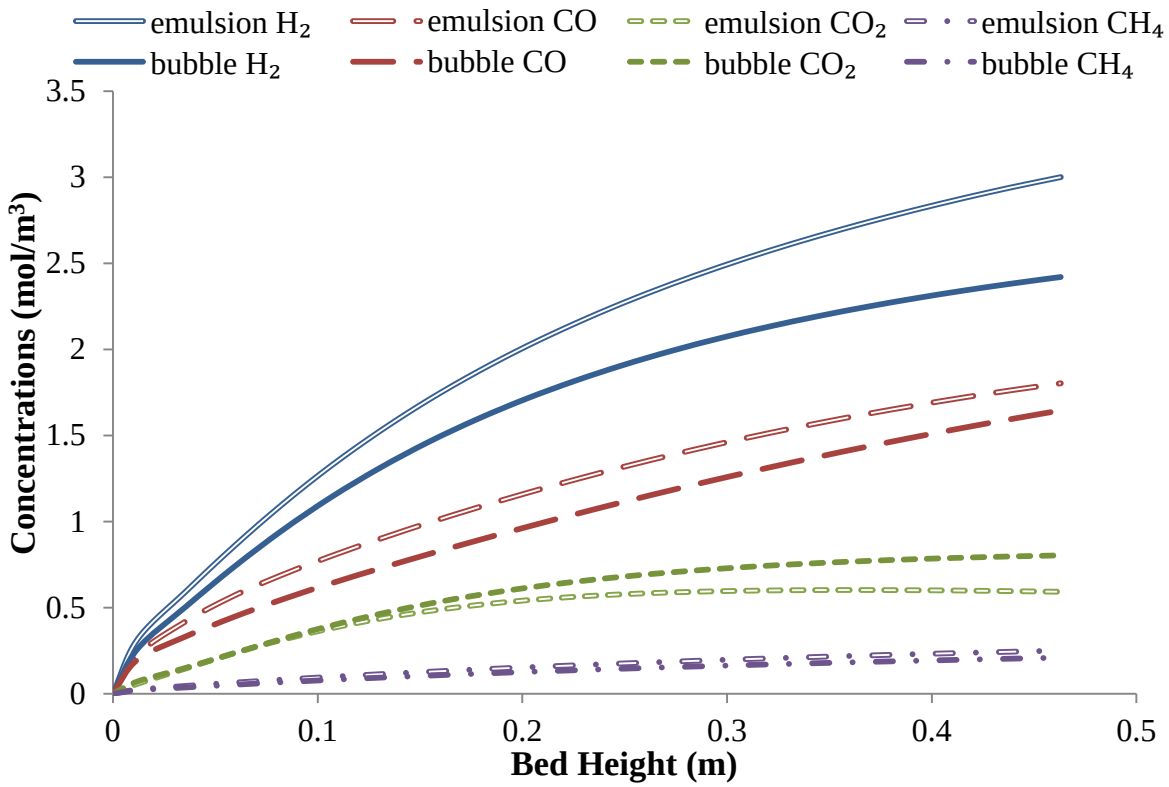

Figure 6.4: Model simulation results of steady state gas concentrations along the bed height. The hollow lines are for the emulsion phase and the solid line for the bubble phase.

Figures 6.5 and 6.6 show the model predicted total char mass in the bed and mean char conversion as a function of elapsed time from the start of steam gasification. It can be seen that the total char mass and mean char conversion increased from zero at the start of the gasification approaching equilibrium values after 35 minutes. In the initial stage of the gasification, the char generation rate from the pyrolysis reaction was faster than the overall char consumption rate, however, as the gasification proceeded, the conversion rate of char in the bed increased due to char consumption in the heterogeneous gasification reactions. From the char reactivity study presented in Chapters 3 and 4, the specific reactivity increased with the conversion and thus the total consumption rate of char in the bed increased. On the other hand, the generating rate of char remained the same at constant feeding rates of solid fuel and steam. After about 35 minutes, the equilibrium was reached when the total consumption of char was equal to the net char generating rate that is initial pyrolysis of the fed solid fuel minus transfer rate to CFB. From Figure 6.6, the mean char conversion at the equilibrium state was around 0.3 for the steam gasification of pure lignite at 800°C.

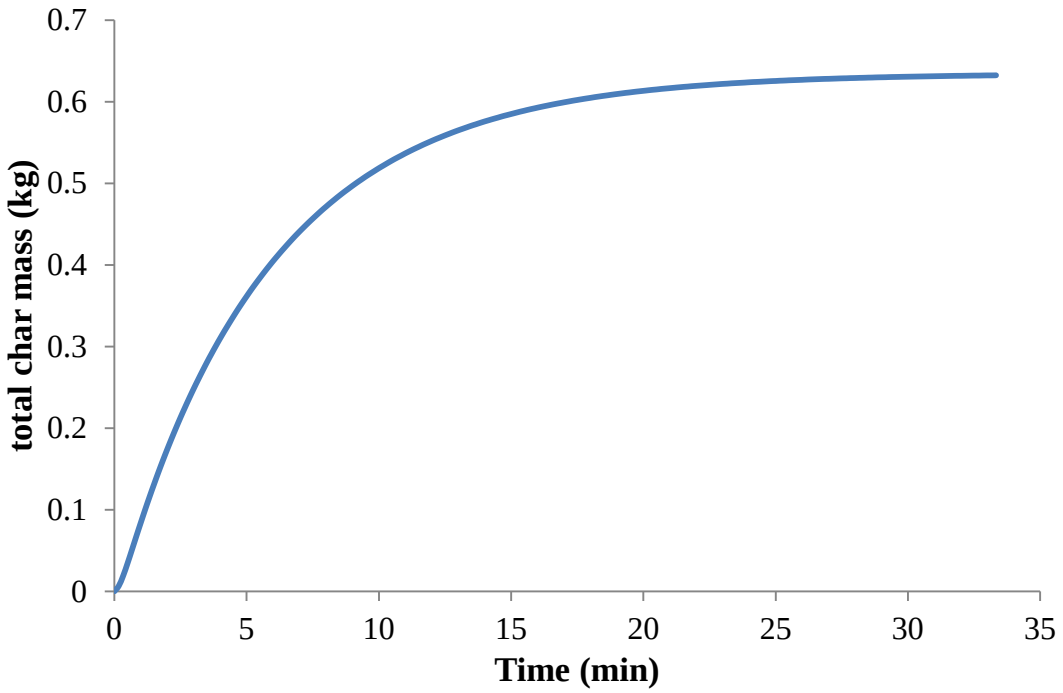

Figure 6.5: Model predicted total char mass in the bed in steam gasification of pure lignite.

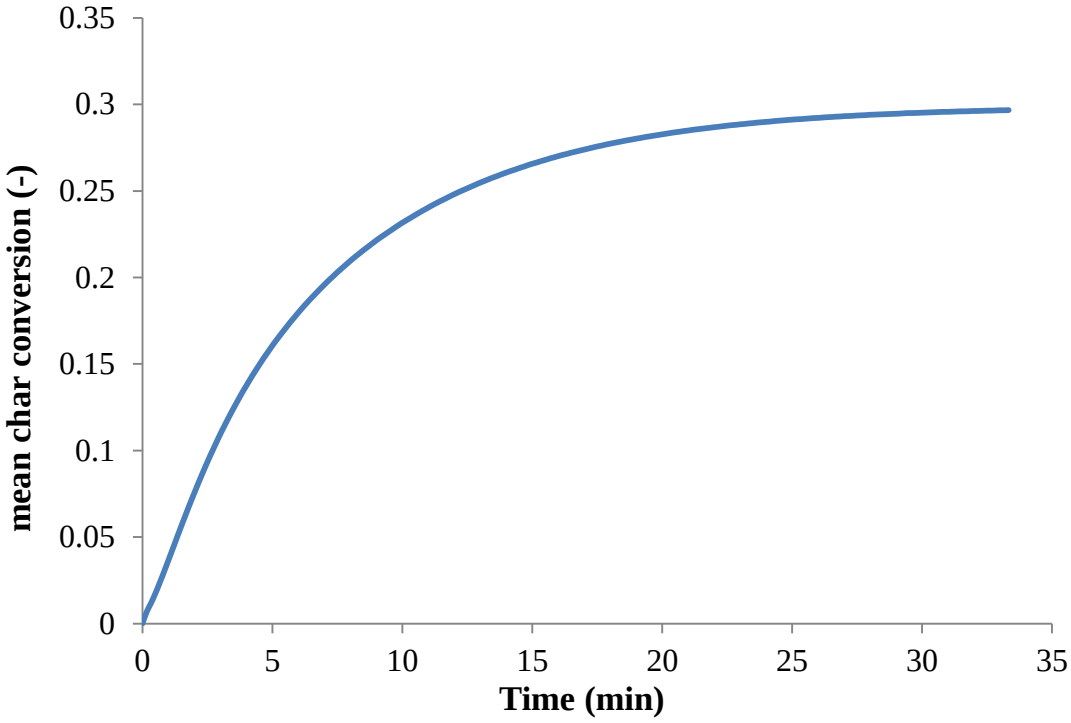

Figure 6.6: Model predicted mean char conversion as a function of elapsed time counted from the start of lignite gasification.

Figure 6.7 shows the model predicted changes in mean gas temperature through the bubbling fluidized bed as a function of elapsed time from the start of gasification. From this figure, the bed temperature increased from 800^{o}C after the solid fuel was fed into the bed, which is the net result of the exothermic water gas shift reaction (Equation 6.4) and the endothermic steam gasification reaction (Equation 6.2). Initially, the volumetric rate of the water gas shift reaction was high because of rapid releasing of CO from the fast pyrolysis of the solid fuel while the steam gasification reaction was slow with limited char available in the bed. As the amount of char in the bed increased, the volumetric rate of endothermic steam gasification reaction increased, and thus the heat released from the water gas shift reaction was consumed by the steam gasification reaction, and the gas temperature in the bed dropped reaching the steady state of the target temperature after about 35 minutes.

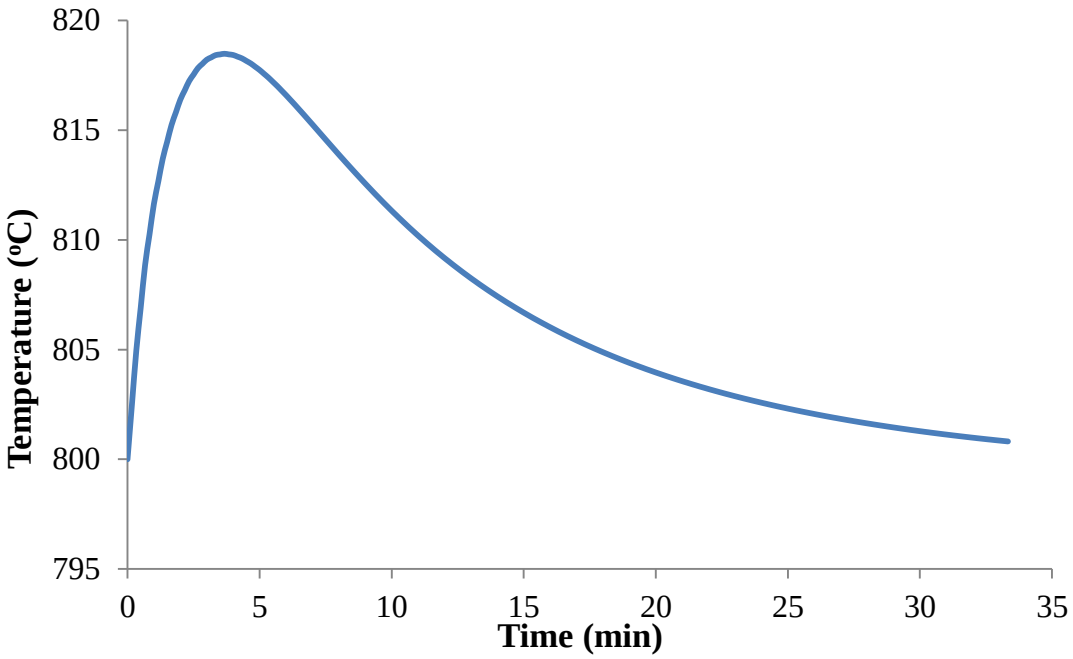

Figure 6.7: Model predicted changes of mean bed gas temperature in steam gasification of pure lignite.

At steady state, the model predicted gas temperature profile through the gasifier is shown in Figure 6.8, from which the gas temperature rose with the fluidized bed height (0~0.46 m) with the lowest temperature occurring at the bed bottom. The low temperature at the bed bottom was due to the low steam temperature being injected from the gasifier bottom while the rising temperature at the bed top (at around 800^{o}C) was caused by the heat transfer from the incoming

hot bed material (sand). Further increase in temperature through the freeboard region (above 0.45 m) was caused by the water gas shift reaction pushing forwards (exothermic). The steeper temperature gradient just above the bottom of the freeboard was due to the higher local rate of water gas shift reaction, caused by non-equilibrium composition of species after sudden mixing of emulsion and bubble gas. The subsequent temperature levelling out indicated the gas composition reached a new equilibrium.

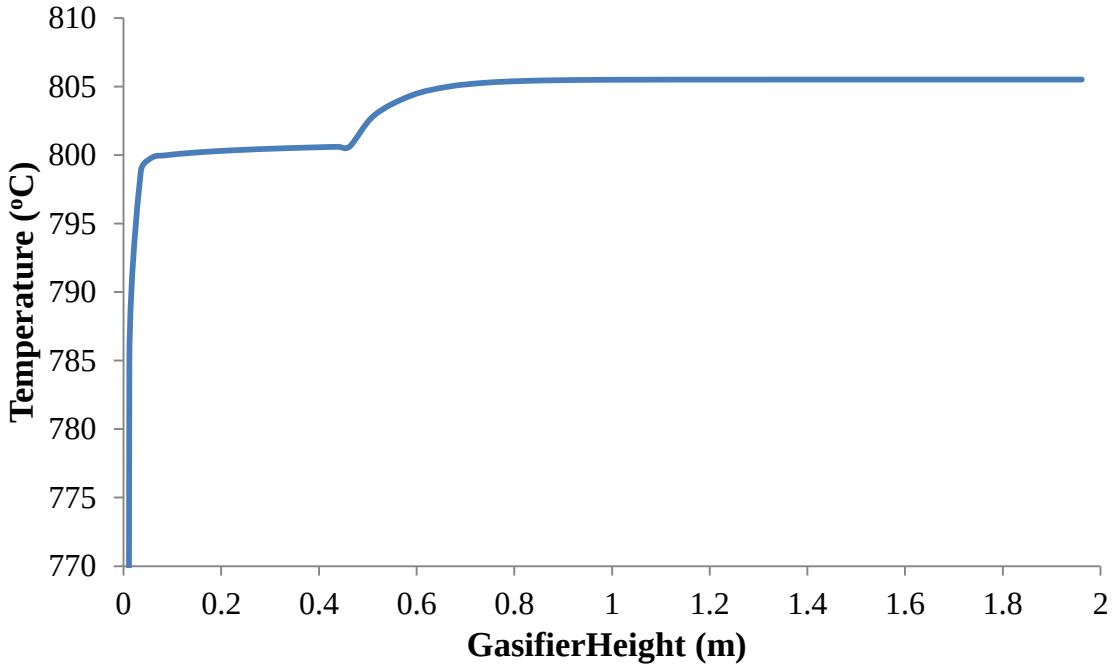

Figure 6.8: Model predicted gas temperature profile along the gasifier height at steady state in steam gasification of pure lignite.

6.5.1.2 Steam gasification of pure biomass

The revised gasification model has also been run to simulate the steam gasification of pure wood pellets (pine) under the same operation conditions as given in Table 6.3. The simulation results are shown in Figures 6.9 to 6.13 in the same order as those shown in the previous section on gasification of pure lignite. The changes of gas species concentrations for steam gasification of pure biomass were also a result of the char generation, char conversion and gasification reactions in a similar manner as described in lignite gasification. In Figure 6.9, the concentrations of vapour-free producer gas species as a function of time are illustrated. From the figure, it is found

that the molar fractions of the producer gases of H_2, CO_2 and CH_4 increased rapidly in the initial two minutes from zero at gasification start, and such rapid increase was due to the fast pyrolysis of the solid fuel fed into the system. After the initial stage, the concentrations of CO_2 and CH_4 dropped gradually while the H_2 concentration increased, all approaching a steady state level after about 10 minutes from the start of gasification. In this period, CO concentration increased gradually towards a constant value of 0.36 (mol/mol). The corresponding steady state concentration values for H_2, CO_2 and CH_4 were 0.35, 0.2 and 0.08 mol/mol.

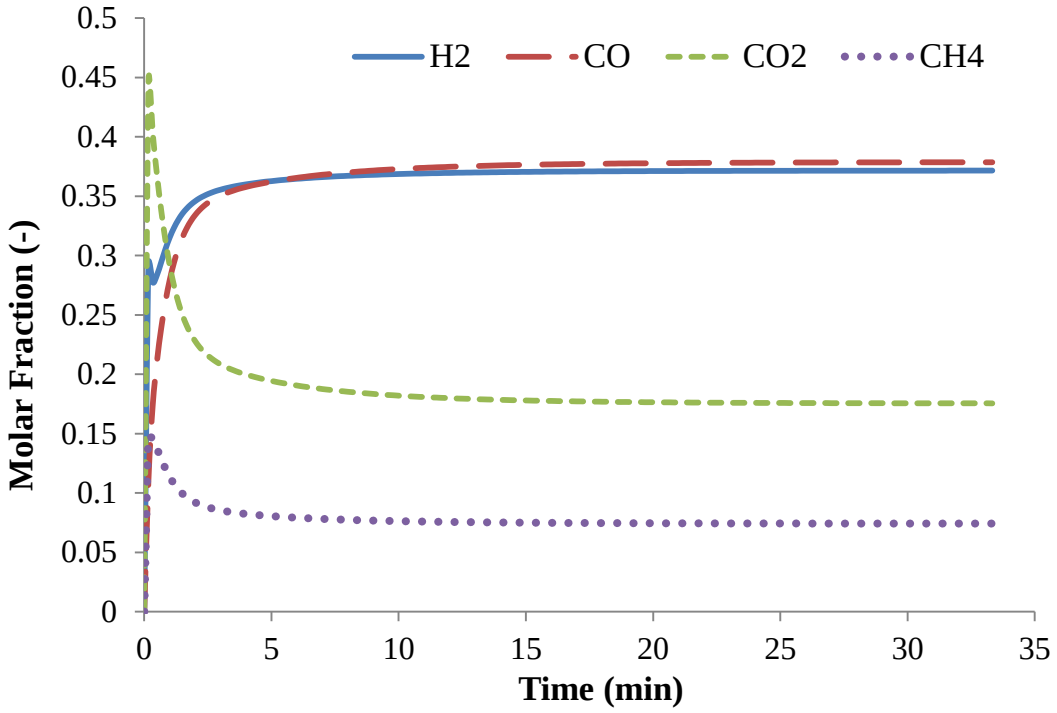

Figure 6.9: Model predicted producer gas composition for steam gasification of pure biomass (pine) at 800^{o}C.

Figure 6.10 illustrates the total char mass in the bubbling fluidized bed and Figure 6.11 shows the mean char conversion in the bed as a function of elapsed time from the start of gasification. From these figures, it can be seen that at the steady state, the total char mass in the steam gasification of pure wood pellet (0.09 kg) was much lower than that in the lignite gasification (0.62 kg) which is consistent with previous observations that the char generation of biomass was much lower than lignite. However, the mean char conversion in the biomass gasification was 0.5 which is higher than that of the lignite gasification (0.29). Again, this confirms that the biomass char reactivity is higher than the coal char.

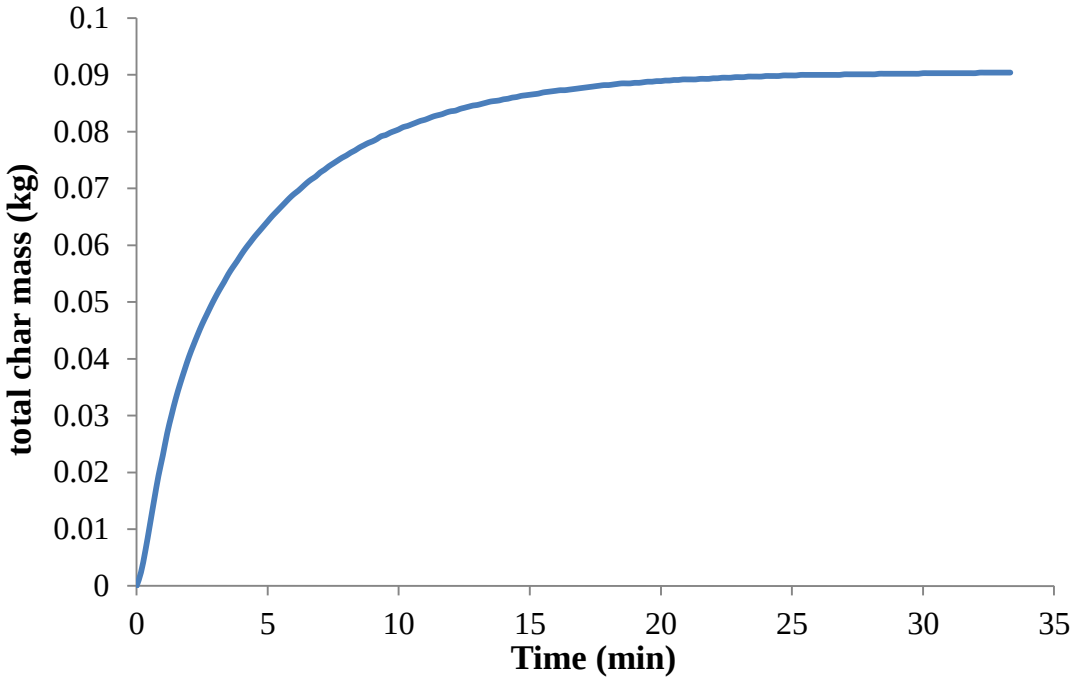

Figure 6.10: Model predicted total char mass in the bed in steam gasification of pure biomass at 800^{o}C.

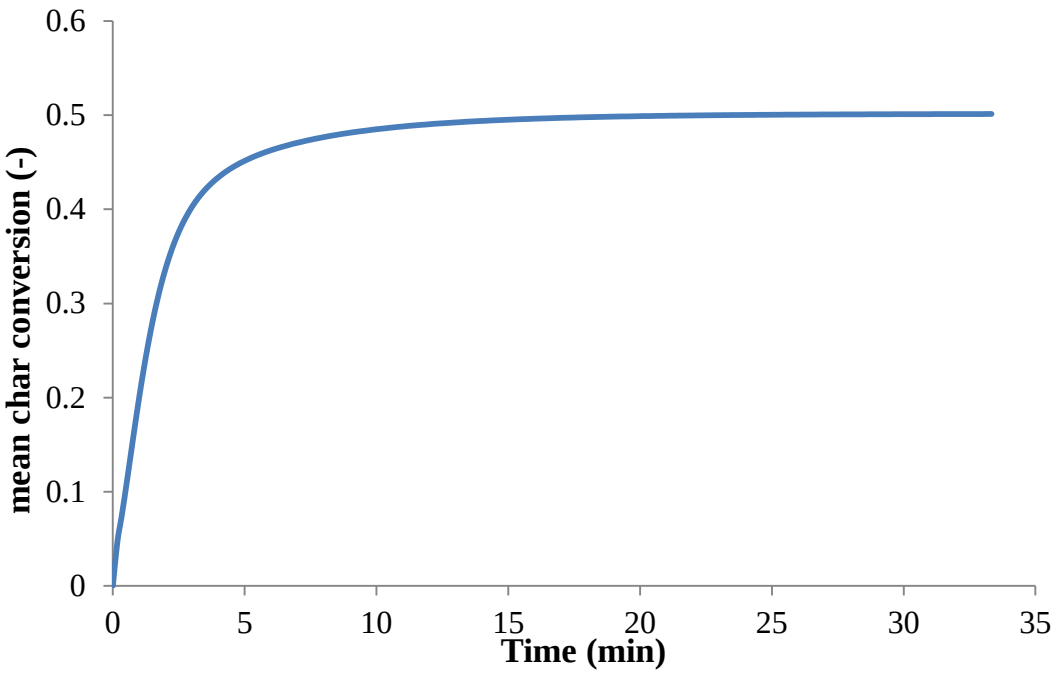

Figure 6.11: Model predicted mean char conversion as a function of elapsed time from the start of biomass gasification at 800^{o}C.

Figure 6.12 shows the mean gas temperature in the bubbling fluidized bed as a function of time and Figure 6.13 gives the gas temperature profile through the bed height at steady state of operation. From Figure 6.12, it can be seen that the general trend of the changes in mean bed temperature was similar to that in lignite gasification but the time for approaching steady state was shorter due to the higher char reactivity of pine wood. However, the gas temperature profile in the freeboard region for biomass gasification had a different pattern from that in the lignite gasification. The gas temperature increased rapidly from the bed bottom to above 802°C at about 0.45 m, then decreased and gradually approached 796°C in the freeboard region above the bed. The drop of temperature in the lower part of the freeboard was induced by an endothermic reverse water gas shift reaction. Compared with lignite gasification, a lower char transfer rate from BFB to CFB caused more steam to be consumed by reacting with biomass chars in the fluidized bed, thus the steam concentration at the freeboard bottom where emulsion and bubble gases mixed was lower than the equilibrium value, hence a backwards water gas shift reaction had taken place.

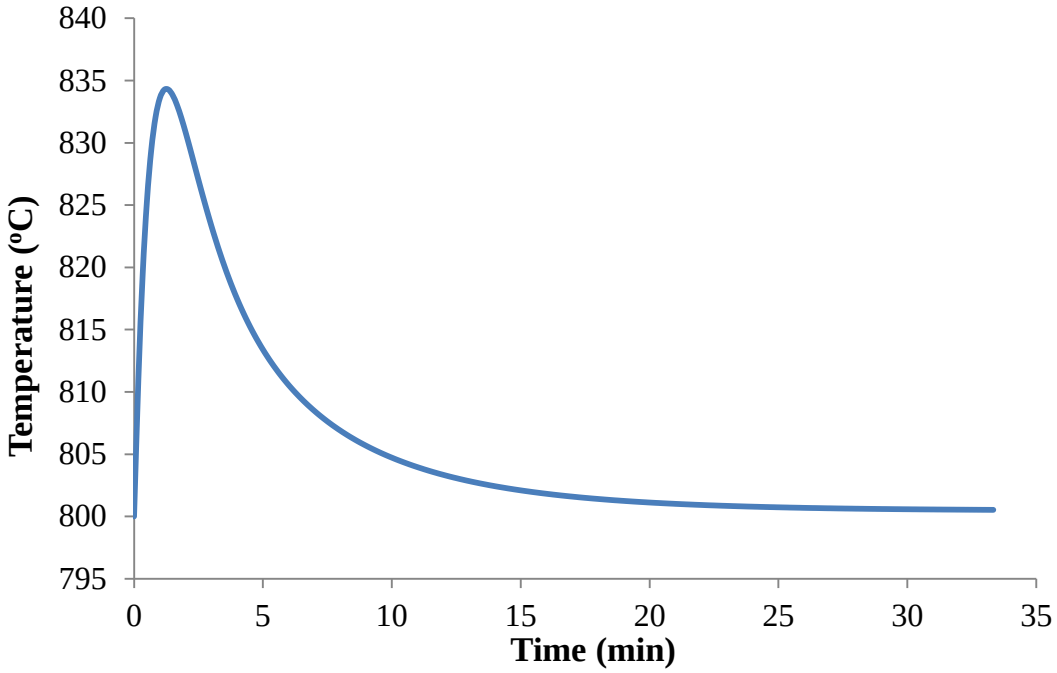

Figure 6.12: Model predicted changes of mean bed gas temperature in steam gasification of pure biomass (pine).

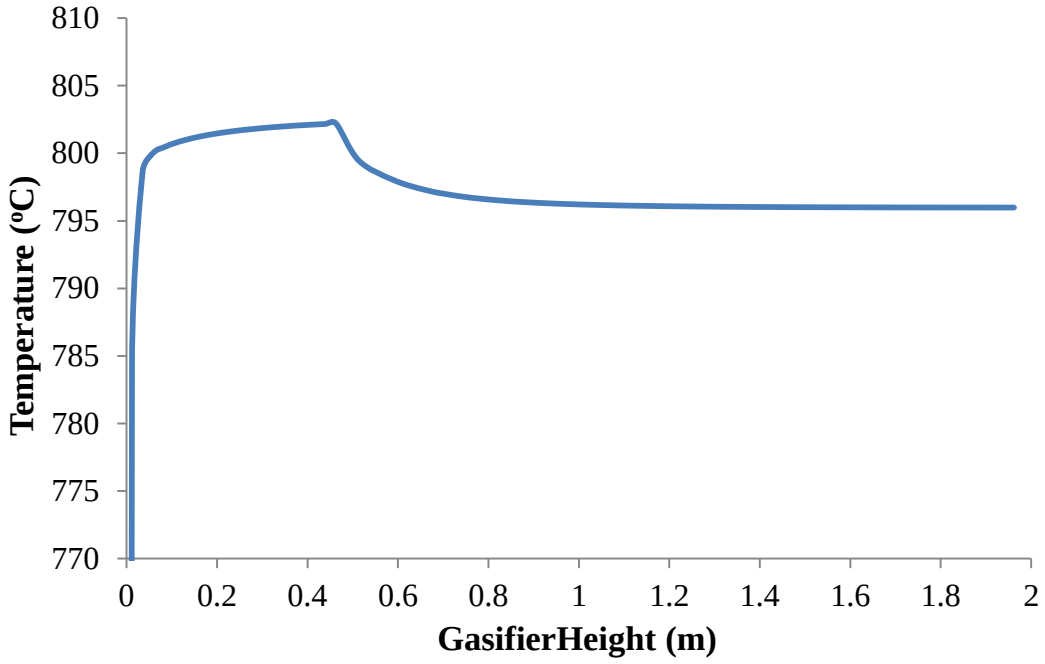

Figure 6.13: Model predicted gas temperature profile along the gasifier height at steady state in steam gasification of pure biomass (pine).

6.5.1.3 Comparison of producer gas composition in steam gasification of pure lignite and pure biomass

From the discussion in previous sections, the two types of solid fuels had quite different gasification characteristics including the gas composition and temperature profiles. The gas composition refers to the steady state if no specific definition is given, and applied for all later sections of this chapter. As discussed in the previous chapters, the key solid feedstock properties which influence the gasification characteristics include gas yield and gas composition from the initial pyrolysis (devolatilzation), char yield and char reactivity.

Table 6.5 gives the experimental data in this study and model simulation results from steam gasification of pure lignite and pure biomass (pine) at 800^{o}C. In general, the experimentally measured producer gas compositions for steam gasification of both pure lignite and pure biomass are in close agreement with those predicted from the revised mathematical model. These results are also consistent with reported data from other researchers (Soukup et al. 2009; Vélez et al. 2009).

Table 6.5: Producer gas composition from steam gasification of pure lignite and pure biomass (pine) at 800^{o}C: Experimental data and simulations results.

	H_2	CO	CO_2	CH_4
Fuel Type	(mol/mol)	(mol/mol)	(mol/mol)	(mol/mol)
Lignite	0.526 (0.511)*	0.227 (0.242)	0.186 (0.205)	0.061 (0.042)
Pine	0.347 (0.372)	0.360 (0.379)	0.174 (0.176)	0.118 (0.075)

Note: * the values in the brackets are the model simulation results.

From the experimental data presented in Table 6.5, it is observed that the producer gas composition varied significantly between the gasification of pure lignite and gasification of pine wood pellets. In the gasification of pure lignite, the H_2 concentration was much higher and concentrations of CO and CH_4 much lower than those from pine gasification, while the CO_2 concentration in both cases were similar. These differences have also been quantified from the model simulations. The difference in the producer gas composition of the two solid fuels can be attributed to two main reasons: (1) the difference in the devolitalization gas yield and its distribution; (2) the difference in char yield and reactivity.

The first reason is straightforward. With a higher fraction of a given gas species in the initial devolatilization process, the fraction of this gas species in the producer gas would be higher if the operation conditions were maintained the same. This can be confirmed from the gas analysis results as given in Table 6.6 from devolatilization of solid fuels.

Table 6.6: Gas analysis results from solid fuel devolatilization test at 800^{o}C.

Gas composition	H_2 (mol/mol)	CO (mol/mol)	CO_2 (mol/mol)	CH_4 (mol/mol)
Lignite (TOMECZEK. 1994)	0.611	0.198	0.07	0.121
Pine*	0.301	0.388	0.197	0.131

Note: *the values for pine were obtained from equation 5.22 in chapter 5.

In the devolatilization of lignite, H_2 was the major gaseous species and its concentration was as high as 0.611 mol/mol while the other gas species of CO, CH_4 and CO_2 were much lower with corresponding values of 0.198, 0.121 and 0.07 mol/mol, respectively. For the devolatilization of pine wood, CO had the highest fraction in the gases (0.388 mol/mol), followed by H_2 (0.301 mol/mol). CO_2 and CH_4 had similar concentrations at 0.197 and 0.131 mol/mol respectively. Comparing the values in Tables 6.4 and 6.5, it can be seen that the gasification producer gas composition was strongly related to the product distribution of the devolatilization gas composition of each solid fuel although there were some changes in the concentrations of gas species due to the gasification reactions.

Char yield and reactivity were another factor that caused the difference in the producer gas composition between lignite and biomass steam gasification. The difference in the char yield would directly contribute to the char accumulation in the bed and the char reactivity affected the gasification reactions which would produce various gas species. The effect of char reactivity on producer gas composition will be further discussed in detail later in this chapter.

The dynamic behaviour of steam gasification of lignite and of pine wood pellets was also significantly different. In other words, the mean response time for the system to reach the steady state was different between steam gasification of the two types of feedstocks. Figures 6.6 and

6.12 illustrate the dynamic change in the mean gas temperatures in the bubbling fluidized bed in the gasifier. From these figures, the time for temperature to reach the steady state for the lignite gasification was over 30 minutes, whereas for pine gasification the steady state of temperature was reached after 17 minutes from the start of gasification. This time difference was the result of different char reactivity. As discussed in previous chapters, the dynamics of the gasification process are highly dependent on the char's overall reactivity, which is the slowest step among all processes also referred to as the rate determining stage. It has been known that the biomass char was more reactive than the coal char, especially at low temperatures. In Chapter three it was found that the typical time of total conversion of a single pine char particle was approximately 20 minutes in the steam gasification at 800^{o}C, however for the lignite char gasification under the same conditions, the time was one hour.

6.5.2 Effect of steam to solid fuel (S/F) ratio

Steam to solid fuel (S/F) ratio was an important operating parameter in the gasification process since it influenced the producer gas composition. The effect of the S/F ratio on producer gas composition was investigated by using the revised mathematical model for the S/F ratio ranging from 0.4 to 1.5 by varying the steam feeding rate with the solid fuel feeding rate being fixed. The simulation results as well as experimental data for in-steam gasification of various solid fuels at 800°C are shown in Figures 6.14 to 6.17.

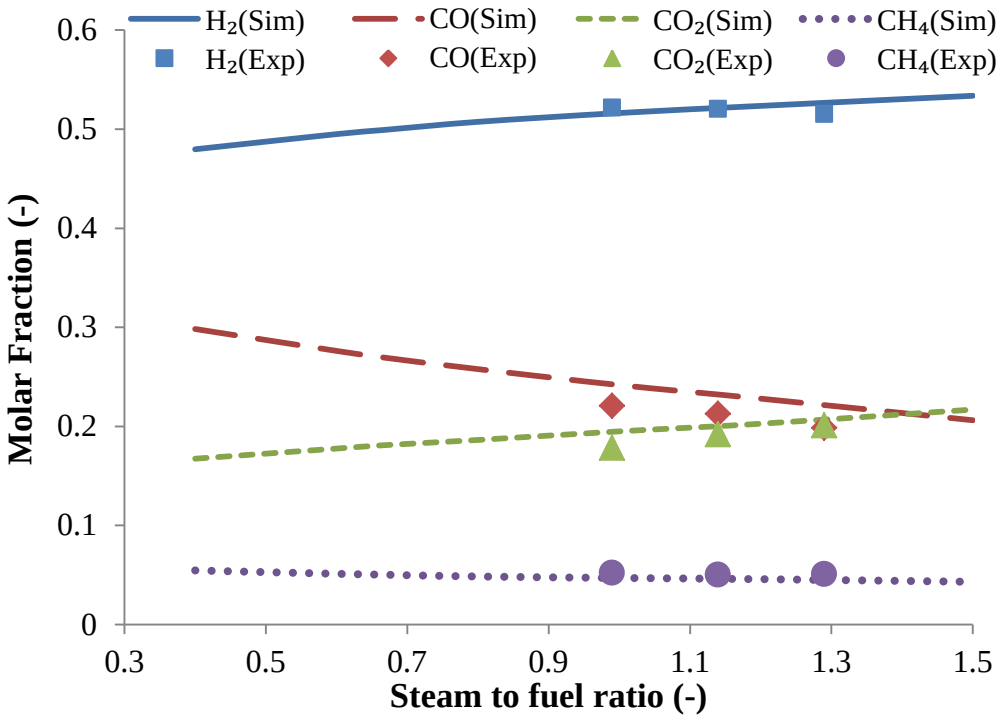

Figure 6.14: Simulation results and experimental data on effect of S/F ratio on producer gas composition in steam gasification of pure lignite at 800^{o}C.

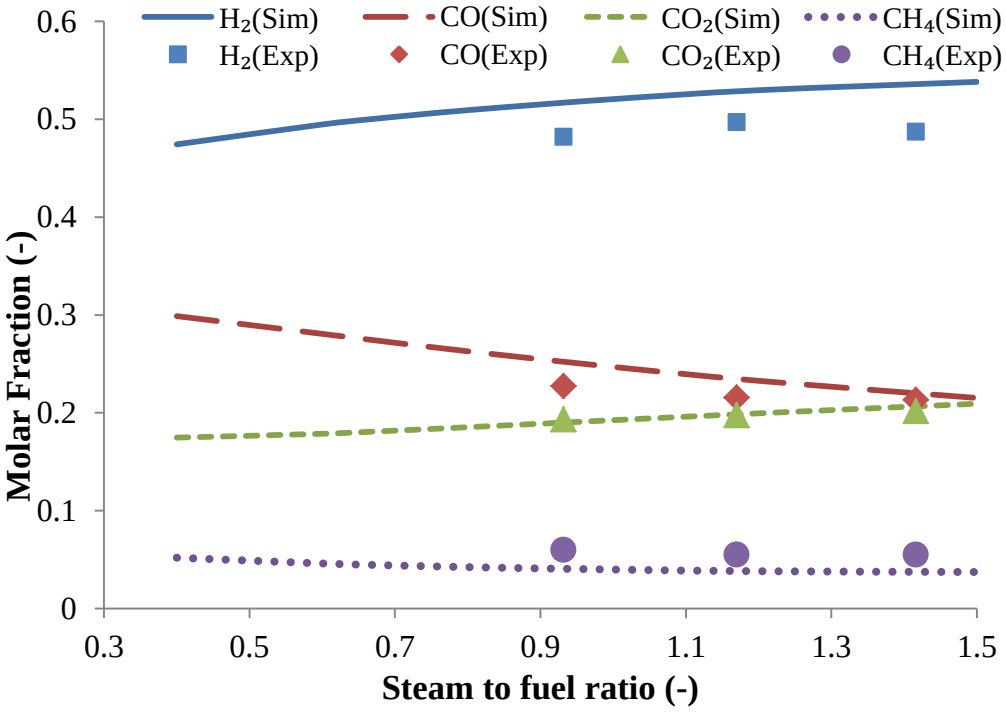

Figure 6.15: Simulation results and experimental data on effect of S/F ratio on producer gas composition in steam gasification of 80L:20P pellets at 800^{o}C.

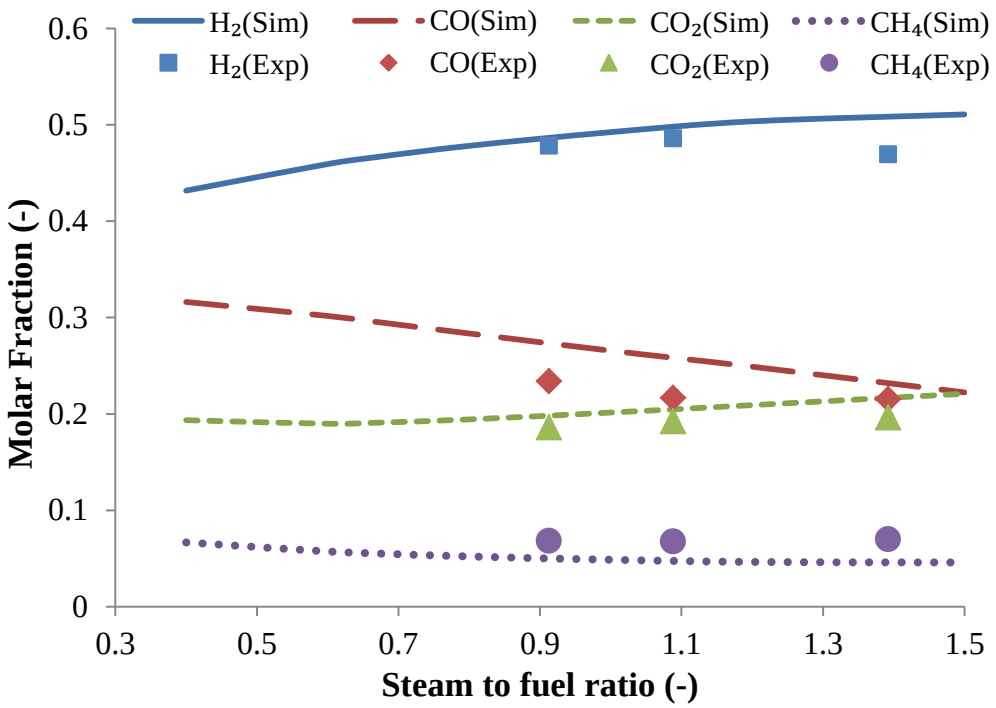

Figure 6.16: Simulation results and experimental data on effect of S/F ratio on producer gas composition in steam gasification of 40L:60P pellets at 800^{o}C.

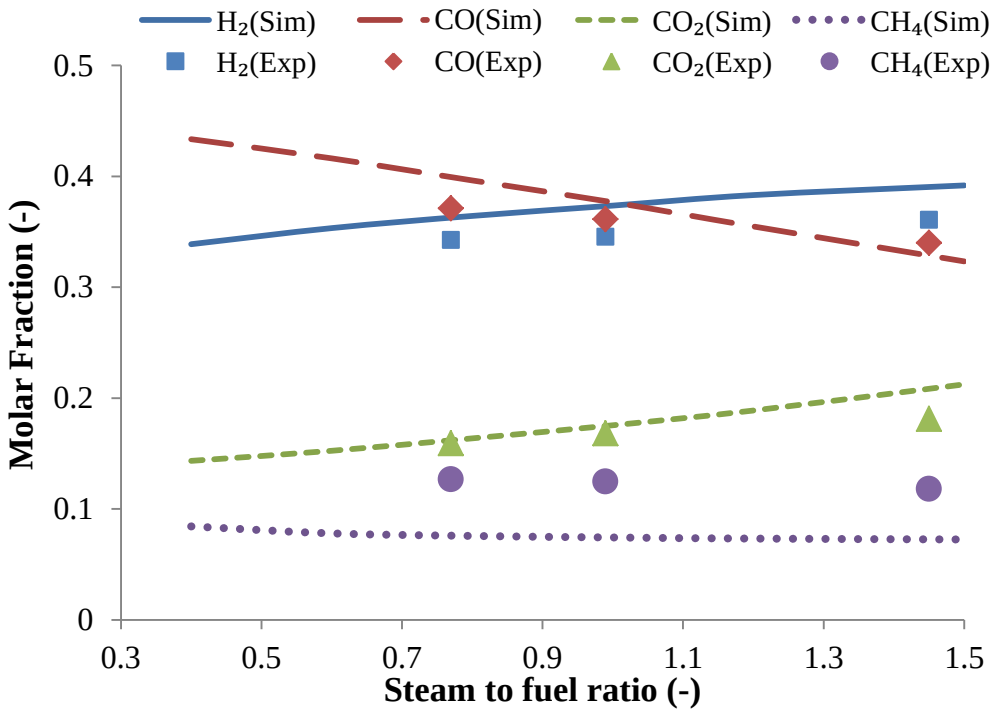

Figure 6.17: Simulation results and experimental data on effect of S/F ratio on producer gas composition in steam gasification of pine pellets at 800^{o}C.

Figure 6.14 shows the results for steam gasification of pure lignite from which it can be seen that with the S/F ratio increasing from 0.4 to 1.5, the CO concentration in the producer gas dropped from 0.30 to 0.216 mol/mol while the H_2 concentration increased from 0.48 to 0.534 mol/mol and the CO_2 concentration increased from 0.167 to 0.217 mol/mol. Similar trends for the changes in gaseous species concentrations with varying S/F ratios can be found in Figures 6.15, 6.16 and 6.17 respectively, for steam gasification of solid fuel with blending ratios of 80L(lignite):20P(pine), 40L:60P and 100P. These trends are also found consistent with published data from other studies (Franco et al. 2003); (Rapagnà et al. 2000); (Miccio et al. 2012); (Gordillo and Belghit 2011; Z'Graggen and Steinfeld 2008); (Shen et al. 2008).

The producer gas composition is related to three reactions in the gasification process which have been considered in this study: (1) water gas shift reaction (Equation 6.4), (2) steam gasification gas reaction (Equation 6.2) and (3) Bouduard reaction (Equation 6.3). As the S/F ratio increased, the water vapour concentration was increased hence the forward reaction of water gas shift reaction was promoted, and thus more H_2 and CO_2 were produced by consuming CO and H_2O (Gil et al. 1999). The steam gasification reaction was also enhanced which consumed steam and char generating H_2 and CO. This was the other attributor to the increased H_2 content at a higher S/F ratio. This trend was closely predicted by the revised model for gasification of pure lignite and blended lignite and biomass.

As the water gas shift reaction is faster than the steam gasification reaction, the CO consumption in the water gas shift reaction was more than the CO consumption in the steam gasification reaction. Furthermore, although the Bouduard reaction in forward direction was favoured by the increasing content in CO_2 due to the water gas shift reaction, it was much slower than the water gas shift reaction, thus the contribution of the Bounduard reaction was insignificant. Therefore, the net CO content decreased with the increase in the S/F ratio.

Figures 6.14 to 6.17 show that the CH_4 content in the producer gas slightly decreased with the S/F ratio for all of the solid fuels examined. The CH_4 generated from solid fuel pyrolysis was considered as the inert gas species. Although a methanation reaction (equation 2.6) and steam methane reforming reaction (equation 2.11) were involved in the gasification process, their reaction rates were very slow thus their effects on the CH_4 concentration were insignificant. The decrease in CH_4 content in the producer gas was largely caused by the generation of other gas

species (H_2 and CO_2) with an increasing steam feeding rate (Kalinci et al. 2009). In this way, the concentration of CH_4 in the producer gas was diluted as a result of increased generation of other gaseous species.

6.5.3 Effect of blending ratio in the solid fuel feedstock

The revised model has been used to simulate the steam gasification of blended biomass coal solid fuel with biomass blending ratio from 0 to 100%. The simulation results are shown in Figure 6.18 for comparison with experimental data obtained from this study, and in Figure 6.19 for comparison with experimental data of co-gasification of non-pelletized biomass and coal reported in the literature (Aigner et al. 2011).

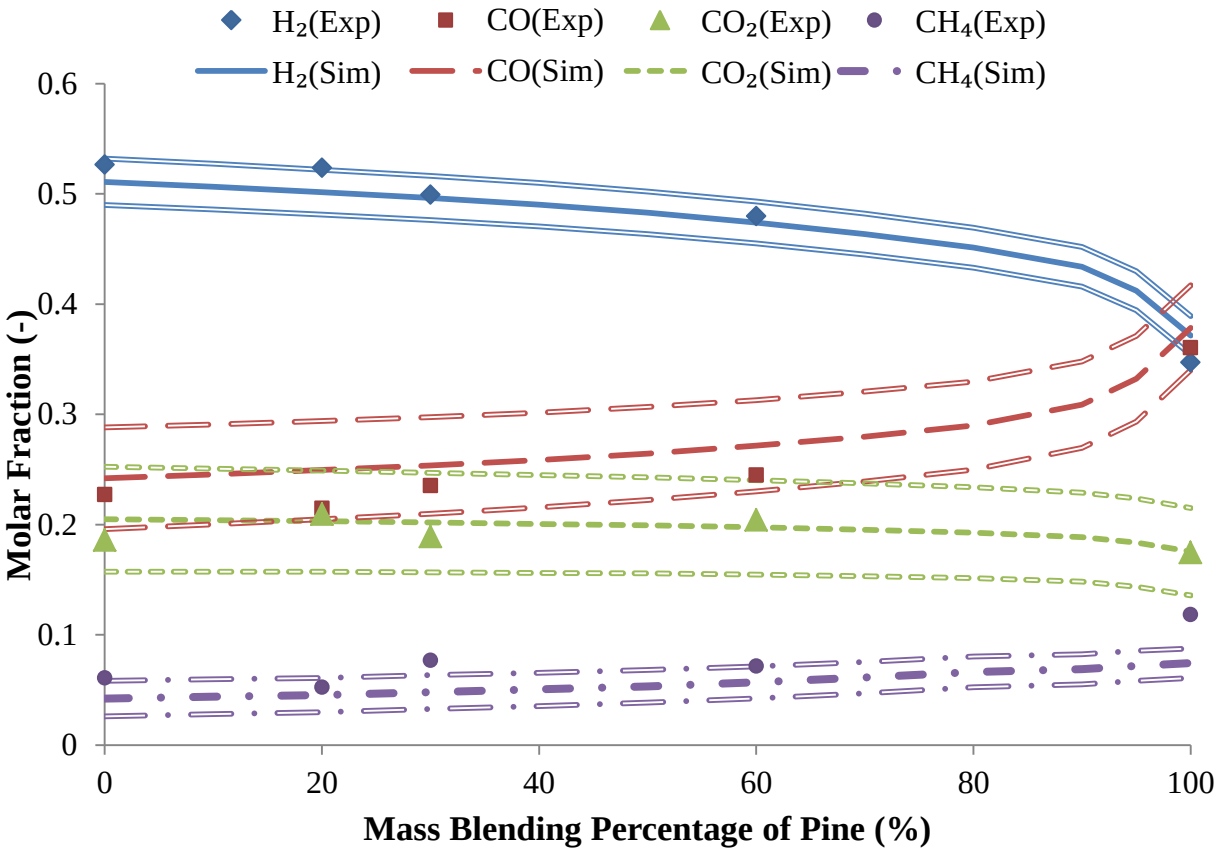

Figure 6.18: Model predicted (lines) and measured (dots) producer gas composition in steam gasification of blended lignite and pine pellets at various blending ratios at 800°C.

Figure 6.18 illustrates the model simulation results and experimental data of the producer gas composition in steam gasification of blended biomass and lignite pellets with various blending ratios at the gasification temperature of 800^{o}C. In general, as the mass blending percentage of pine increased from 0 to 100%, the model predicted H_2 content dropped while the CO content increased, and the CO_2 and CH_4 contents remained relatively unchanged. The experimental data points of the producer gas composition at varying pine blending ratios are in close agreement with the model predictions within the uncertainty 10% range; since deviation among the three samples taken at each operating point was trivial as the mean average standard deviation is less than 0.005. The discrepancy could be attributed to an unrealistic estimation of the sand circulation rate $\dot{M}_{sand}$, estimated at 720 kg/hr from the preliminary cold run test and used as a constant input parameter of mathematical model. The uncertainty in the actual rate can be significant in real gasification runs. The effect of deviation in the sand circulation rate on the predicted producer gas composition is presented in Figure 6.18., where hollow lines represent upper and lower bounds of the uncertainty range of gas composition caused by ±200 kg/hr sand circulation rate variation from nominal sand circulation rate.

With pure lignite feedstock, the model predicted an H_2 content of 0.51 and CO content of 0.24, while the corresponding values for pure biomass feedstock were 0.37 for H_2 and 0.38 for CO. A synergetic effect of the pine mass blending ratio could be clearly observed as can be seen from both experimental data points and prediction curves in Figure 6.18. With adding some pine into the lignite and the pine blending ratio increasing from 0%, no significant change in the gas composition could be observed until the biomass blending ratio was increased to 20%. With further increase in the pine blending ratio the changes in the producer gas composition became apparent. A reduction in H_2 content was observed when the pine blending ratio reached 30% while increases in CO and CH_4 concentrations could be clearly observed. As the pine blending ratio was high approaching 100%, the changes in the producer gas species were significant with the molar fractions of H_2 and CO_2 dropping to 0.34 and 0.18 while CO and CH_4 contents increasing to 0.35 and 0.11 respectively.

From previous discussion in this chapter, it has been shown that lignite and pine have distinctly different gasification behaviours and producer gas composition. In theory, the producer gas

composition from gasification of the blended biomass and coal could be linearly related to the blending ratio. However, a non-linear relationship between the producer gas composition and the blend ratio has been observed in Figure 6.18, particularly for H_2 concentration, which indicates a synergetic effect with blended solid fuel.

At given operating conditions (S/F ratio and mean bed temperature), the gasification behaviour and producer gas composition were mainly affected by solid fuel properties: pyrolysis gas yield, product distribution, char yield and char reactivity. The char yield, pyrolysis gas yield and its product distribution could be linearly related to the properties of each fuel (coal or biomass). Therefore, these properties were not the key factor for the non-linearity in the producer gas composition and the synergy effect must have played a role in this behaviour.

However, the reported studies showed inconclusive results on the synergy in co-gasification of blended coal and biomass, as reviewed in Chapter 2. This is believed to be due to the differences in the blending methods. Some studies fed coal and biomass separately and mixed them in the gasifier while others blended these two fuels more uniformly by pelletizing. The main difference between the pelletizing blending and non-pelletized mixture of the two fuels was that the char reactivity was different as the non-pelletizing mixture was easily separated in the gasifier. From discussion in Chapters 3 and 4 of this study, the char reactivity of the pelletized blends was shown to have a nonlinear relationship with the blending ratio, and the influence of the biomass char was shown to be only significant at high a biomass blending ratio. Lignite had a greater influence than the blending ratio spectrum; that is the producer gas composition was closer to pure lignite in the blended biomass and coal fuel, which was more apparent for a medium to high coal blending ratio.

In order to test this hypothesis, the co-gasification results from Vienna University of Technology (VUT) (Aigner et al. 2011) were compared with simulation results by using the revised model in the present study. The gasifier being used and operating conditions in their study were the same as this study; the only difference being that in the VUT gasification experiments, coal and pine were fed separately and mixed in the gasifier, and therefore tended to segregate once being fed in. Since the char yield, gas yield and its product distribution of pellets were the same as the non-pelletized materials, the synergetic effect could be tracked if the linear relationship of producer gas composition was observed with the blending ratio.

Figure 6.19 shows the model predicted producer gas composition in comparison with VUT experimental data for steam gasification of non-pelletized lignite and pine pellets at various blending ratios. From the experimental data, it was found that the gas species contents had a linear relationship with the biomass blending ratio. The predicted producer compositions using the revised model were close to the experimental data, and the linear trends were also observed in the simulation results. In this set of model simulations, the coal and biomass were treated as two independent substances, therefore three more variables were added into the model: (1) raw solid fuel mass (2) total char mass in the bed and (3) overall conversion of the char, while other parameters were maintained the same as those used in previous simulations for gasification of pelletized solid fuel. In addition, the solid fuel properties of biomass were modified for the 100% wood gasification in VUT, since the gasifier configuration and the bed material inventory in the VUT experiments were different from those in the present study. Therefore, the producer gas compositions from steam gasification of pure lignite and of pure wood on the VUT gasifier were different from those obtained from the gasifier in the present study.

From the comparison of producer gas compositions from gasification of non-pelletized blends with those from gasification of pelletized blends, it could be concluded that the synergetic effect was caused by the pelletizing of the biomass and coal. For coal and biomass pellets, a “new” material was created with different reactivity, thus its producer gas composition was deviated from the linear interpreted values.

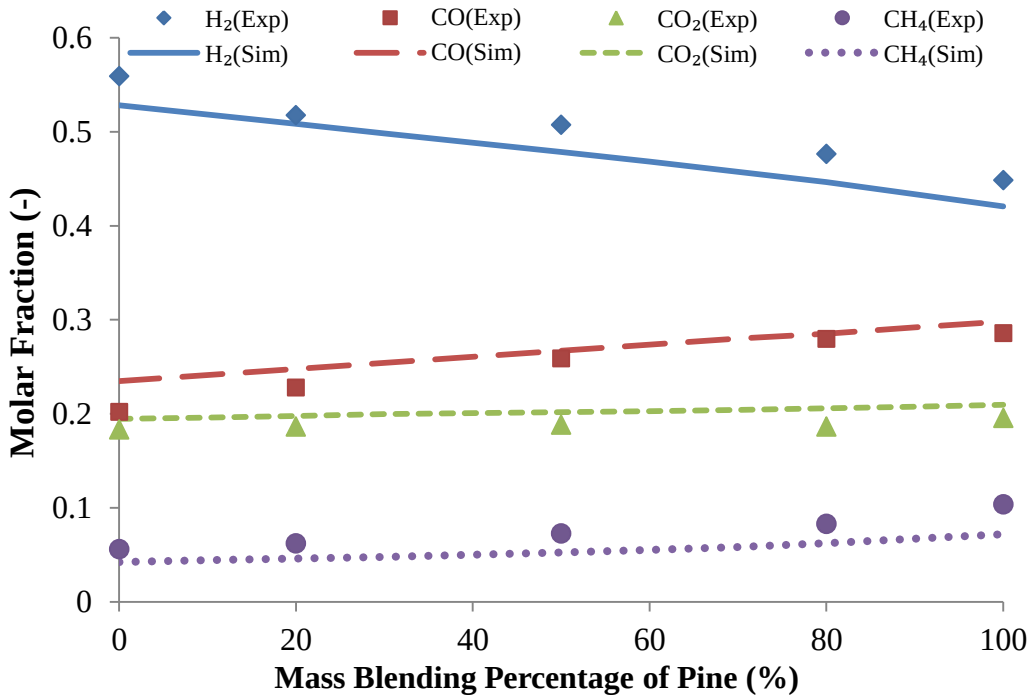

Figure 6.19: Model predicted (solid lines) producer gas composition and comparison with VUT experimental data for steam gasification of non-pelletized lignite and pine pellets at various blending ratios at 850^{o}C.

6.5.3 Effect of gasification temperature

The gasification temperature or the operation temperature is defined as the mean gas temperature through the bubbling fluidized bed. The effect of the gasification temperature on producer gas composition was studied by adjusting the other operation parameters including the feeding rates of steam and solid fuel to the BFB reactor, and the feeding rates of LPG and air to the CFB reactor. From the model simulation runs, it was found that the gasification temperature decreased with the steam and solid fuel feeding rates, and increased with the LPG and air feeding rates. However, the mean bed gas temperature of the dual fluidized bed gasifier system was not directly affected by the S/F ratio. The sand circulation rate was found to be the direct factor to control the gasification temperature, which was influenced by the LPG and air feeding rates. The normal bed material circulating rate in the model was 720 kg/hr, and the BFB temperature was 60-100^{o}C lower than the CFB temperature. It was found that the difference between the BFB temperature and the CFB temperature decreased with the bed material circulating rate. In the

analysis on gasification temperature effects, the steam and solid fuel feeding rates were maintained at a constant with the S/F ratio to be 0.9, while the bed temperature was adjusted by changing the bed material circulation rate. The model simulation results are shown in Figure 6.20 for the effect of the gasification temperature in the range of 750-860^{o}C on producer gas composition in gasification of pure lignite and in Figure 6.21 for gasification of pure biomass (pine).

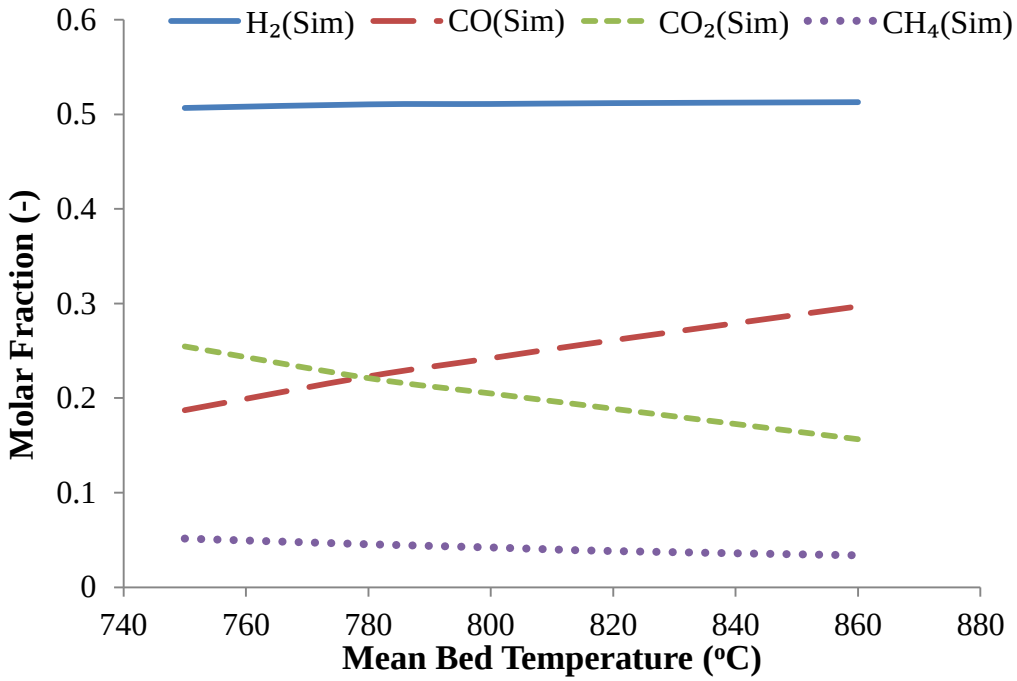

Figure 6.20: Model predicted gas composition in steam gasification of pure lignite as a function of gasification temperature.

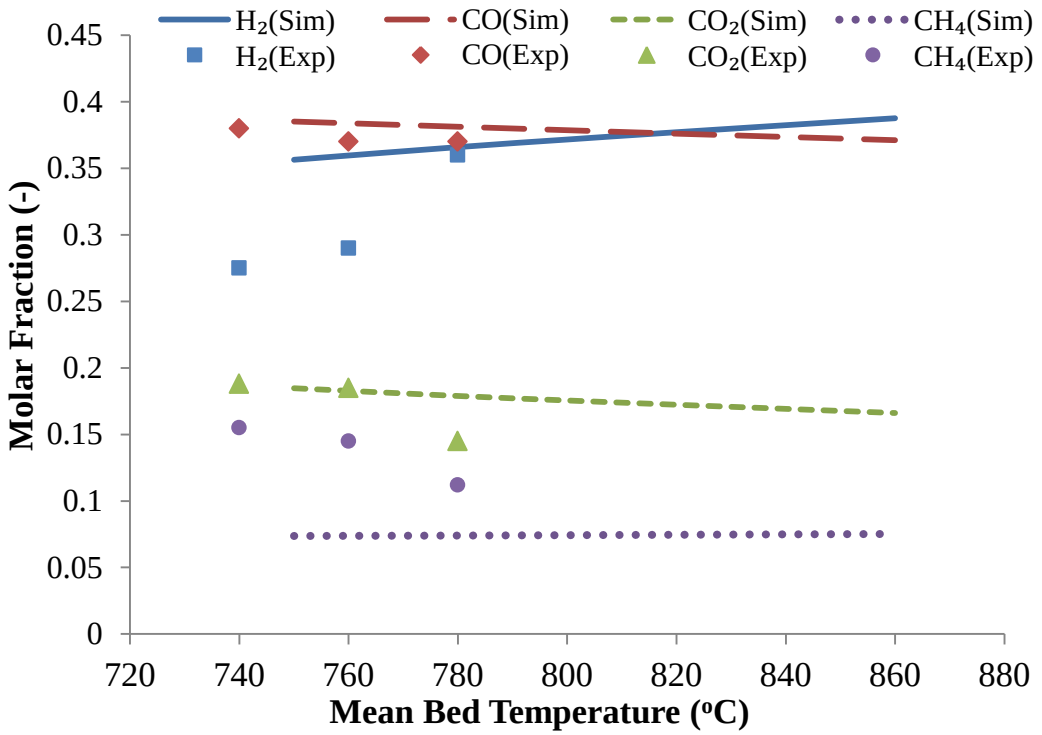

Figure 6.21: Model predicted gas composition in steam gasification of pure biomass (pine) as a function of gasification temperature (experimental data points from personal communication).

From Figure 6.20 for gasification of pure lignite, the H_2 content in the producer gas was relatively constant at values of 0.49-0.5 for the temperature range examined (750-860°C) while CO and CO_2 contents changed significantly from 0.22 to 0.33 for CO and from 0.23 to 0.14 for CO_2, respectively.

In Figure 6.21 for gasification of pine biomass, some available experimental data are also included for comparison. For the biomass gasification, experimental data and model simulation results show significant discrepancies on the effect of gasification temperature on the gas composition. The experimental data show much greater changes with gasification temperature than the model predictions in concentrations of H_2, CO_2 and CH_4. However, the CO concentrations from the model simulation and the experiments are similar although the trend for gasification of pure biomass (decreasing with temperature) was opposite to that in the gasification of pure lignite (increasing with temperature). The trend of concentrations of gaseous species from gasification of pure biomass as a function of gasification temperature was in

agreement with the results reported by other researchers (Rapagnà et al. 2000) (Vélez et al. 2009) (Kaushal et al. 2011).

Temperature influenced the producer gas composition in three steps of gasification: (1) pyrolysis product distribution, (2) the rates of heterogeneous reactions among gas species and char, and (3) water gas shift reaction equilibrium condition.

In gasification of pine wood, the gas product fractions from fast pyrolysis are affected by temperature in a different way. The overall gas production was relatively constant while H_2 content was increased; CO content was reduced while changes in CO_2 and CH_4 contents were insignificant as described in Chapter 5. For the heterogeneous reactions among gas species and char, higher temperature most favoured the Boudouard reaction which produced CO by consuming CO_2 and char whereas steam gasification reaction of char (generating CO and H_2) was less enhanced (de Souza-Santos 2004). To the least extent, the water gas shift reaction was favoured for forward direction (consuming CO for production of CO_2) at higher temperatures. Therefore, balancing all of the above factors, with increase in gasification temperature, the H_2 concentration was increased, and the CO and CO_2 concentrations were decreased while the CH_4 concentration remained relatively constant.

However, some differences between gasification of lignite and gasification of pine wood have been observed, particularly for the trend of CO and the CO_2 fractions changing with temperature, due to the differences in the three steps as described above. In gasification of lignite, the char yield was much higher and the volatile yield much lower than those of biomass in the fast pyrolysis. However, it is unclear how important these differences were in the final producer gas composition. In order to quantify the effect of the pyrolysis product distribution, a set of simulation runs was performed using a correlation of Loison and Chauvin (Loison and Chauvin 1964) to determine the volatile gas composition of coal in the fast pyrolysis as a function of temperature:

$$X_i = a_i + b_i X_v + c_i \left(X_v\right)^2 \tag{6.13}$$

In which X_i is the mass fraction of gas species i, X_v is the total volatile mass fraction in the pyrolysis product and a_i, b_i and c_i, are coefficients.

In this set of simulation runs, the fractions of volatile gas species were assumed to be the functions of the total volatile yield and would not change with temperature, in order to evaluate the effect of temperature related devolatilization product distribution on the producer gas composition. In this way, the simulation results on this basis for lignite gasification (Figure 6.22) can be compared with the previous simulation results (Figure 6.20) in which the fractions of volatile gas species changed with temperature. From Figure 6.22, it can be seen that the simulation results of producer gas composition with fixed volatile product distribution had similar trends to those as shown in Figure 6.20. However, in Figure 6.22, the concentration of H_2 was about 0.01-0.02 lower, concentration of CO was 0.02-0.04 lower but the CO_2 concentration was about 0.01-0.02 higher than the corresponding values in Figure 6.20 while the CH_4 concentration in both figures was identical. Therefore it can be concluded that the effect of fast pyrolysis volatile gas distribution has limited effects but the water gas shift reaction equilibrium condition has the major impacts on the producer gas composition as a function of gasification temperature.

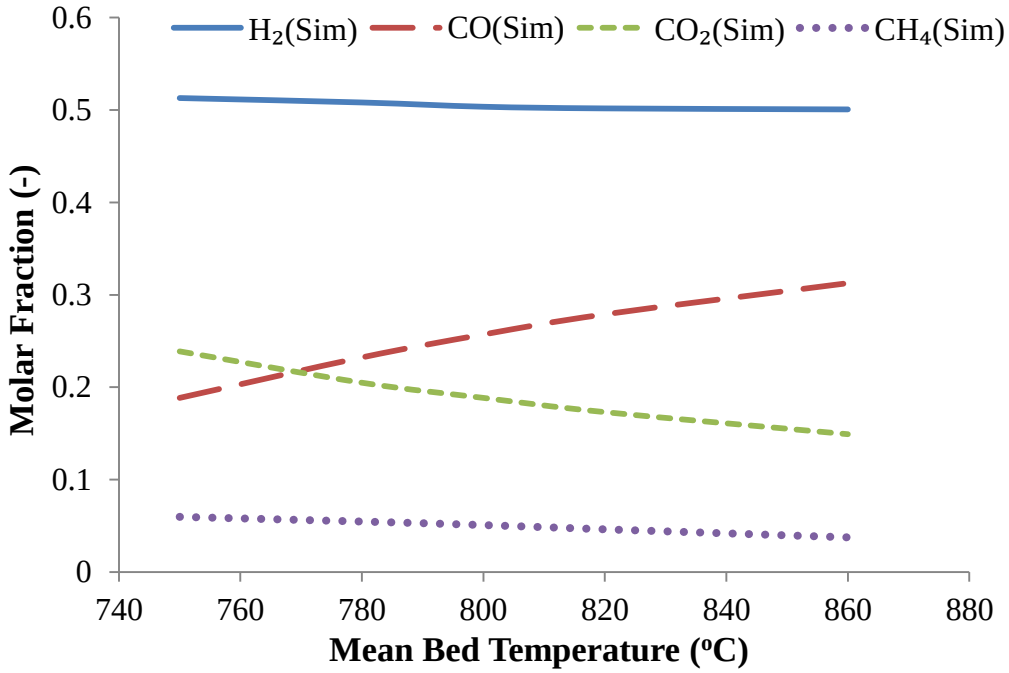

Figure 6.22: Model simulated producer gas composition for gasification of pure lignite as a function of gasification temperature with constant volatile gas fractions.

6.5.4 Effect of char reactivity on producer gas composition

Char reactivity is defined as the volumetric char reaction rates with gas species in the heterogeneous reactions, which are affected by char size, shape, microstructure and porosity. In Chapter 3, it was concluded that the internal diffusion rate within the char particles and intrinsic reaction rate kinetics had a direct influence on the char reactivity. In Chapter 5, the char reactivity was mathematically described by the effective volume method (Equation 5.29), and it was found that in an oxygen blown gasifier, char reactivity had an indirect influence on the producer gas composition, as the rate of char being consumed in the bed will not alter the relative ratios among feed streams into the system. Therefore, the effect of char reactivity on producer gas composition could not be regarded as an influential factor. This was confirmed by the model simulation results.

However, no combustion reactions occurred in the steam gasification as there was no oxygen present in the gasifier. In this part of the study, the effect of char reactivity on producer gas composition was investigated by the revised mathematical model for steam gasification of various solid fuels. The gasification temperature was also assumed to be 800°C. In doing so, the char reaction rate values in the previous simulations were regarded as reference values and these values were firstly reduced and then increased by a factor of 2. The simulation results for gasification of blended lignite and biomass (pine) at the blending ratio of 70L:30P are shown in Figure 6.23.

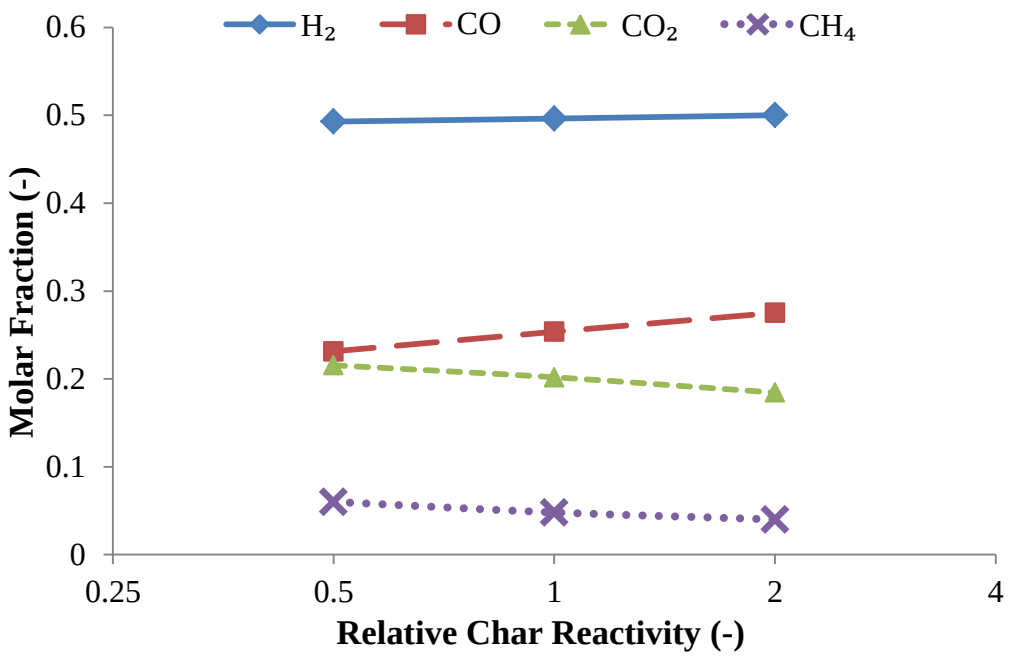

Figure 6.23: Effect of char reactivity on producer gas composition for steam gasification of blended 70L:30P pellets at 800°C.

From Figure 6.23, it has been found that with the char reactivity increasing by four times the CO content increased from 0.231 to 0.275, and CO_2 and CH_4 contents decreased from 0.216 to 0.185 and from 0.06 to 0.04, respectively. However, H_2 content change was less significant, increasing from 0.493 to 0.5.

As the overall char reactivity increased, the heterogeneous reactions between the char and the gaseous species were promoted. With the increase in char reactivity, more H_2 was generated from the steam gasification reaction and more CO was generated from both the steam gasification reaction and the Bouduard reaction which would increase the concentrations of H_2 and CO. However, from Figure 6.23, the increment in CO content was much more significant than for the H_2. This is because from both the Bouduard reaction and the steam gasification reaction, for consumption of two moles of C (one mole in each reaction), three moles of CO and one mole of H_2 were generated. Therefore, the char reactivity had most significance on CO in the producer gas. The CO_2 content decrease is also expected as it was consumed in the Bouduard reaction in which one mole of CO_2 consumption would generate two moles of CO. Of course with more CO available in the gas, some of the homogeneous reactions were also promoted thus the CO increase and CO_2 decrease could not be simply balanced in these two heterogeneous

reactions. However, the symmetric trend of CO increase and CO_2 decrease has been observed in Figure 6.23 and has also been reported in literature (Babu and Sheth 2006). The model simulations for steam gasification of other solid fuels revealed that the effects of char reactivity have a different impact for different types of chars and the results are summarised in Table 6.7.

Table 6.7: Relative changes in producer gas composition for char reactivity increase by four times from half to twice the reactivity value from that used as normal value in the simulation. The positive value means an increase while the negative values represent a decrease in concentration of the specific gas species.

Fuel Type	H_2	CO	CO_2	CH_4
Lignite	1.25%	11.66%	-10.59%	-13.37%
75L25P	1.17%	10.03%	-10.34%	-14.49%
50L50P	0.79%	7.78%	-9.79%	-15.62%
25L75P	0.81%	5.18%	-8.54%	-13.91%
Pine	1.04%	1.83%	-3.92%	-3.01%

From Table 6.7, it can be seen that the lignite char reactivity had most influence on the concentrations of almost all of the gas species except for CH_4, while the char reactivity of blended 50L:50P char had the greatest effect on the CH_4 concentration. The pine char reactivity had least impact on almost all of the gas species except for H_2 which was increased by an average value across all types of chars.

Such difference in the char reactivity effect for different chars is believed to be due to the difference in the char density which caused different circulating rates of the chars from the BFB reactor to the CFB reactor and thus the different residence time in the bed during the gasification. The residence time of different char particles in the bed is an important factor affecting the gasification reactions and producer gas composition (Wang and Kinoshita 1993). For pine char which was quite light and tended to float on the top of the bed, almost all of the char particles were consumed in the BFB and the rate of char reaction did not significantly influence the producer gas composition. For coal char which was denser and the circulating rate to the CFB was higher, the coal chars were partially gasified in the BFB. Therefore the increased char reactivity enhanced the heterogeneous reactions and significantly affected the producer gas

composition. As a result, the higher the coal ratio in the blended pellets, the more impact of the char reactivity on the producer gas composition.

6.5 Conclusion

The mathematical model developed in Chapter 5 has been revised for simulation of steam gasification of blended biomass and coal in a dual fluidized bed gasifier. The model has been solved to predict the gas composition both in the initial start-up transition period and at the steady state. The model provides a powerful tool for better understanding of the gasification process and for parameter sensitivity analysis.

In order to validate the revised model, a series of gasification runs was performed on a 100 kW dual fluidized bed gasifier for steam gasification of blended biomass (radiata pine) and coal (lignite) at biomass blending ratios ranging from 0% to 100%. For preparing the solid fuels, lignite and pine particles were pelletized as pre-set ratios for the tests. The experimental results of the producer gas compositions were compared with the model simulation results and close agreement has been observed. The effects of blending ratios of pine and lignite, steam to solid fuel ratio, gasification temperature and char reactivity have been investigated.

From the parameter study, it was found that the blending ratio in the blended pine and lignite had significant impact on the producer gas composition: the producer gas from gasification of pure lignite had much higher H_2 content and lower CO content than that from the gasification of pine pellets. This difference can be attributed to the differences in the initial pyrolysis gas product distribution and the char reactivity between these two solid fuels.

The investigation on the blending ratio effects for the blended pine and lignite revealed that a synergetic effect was significant in the steam gasification. With a biomass blending ratio of less than 50% (or lignite more than 50%), the producer gas composition was similar to that in the gasification of pure lignite. However, for a high pine blending ratio, the producer gas composition changed non-linearly with the blending ratio and changed rapidly at pine blending ratio above 90%, approaching the producer gas composition of pure pine gasification. From a literature review, inconsistent findings have been reported in terms of the synergic effect in

gasification of blended biomass and coal. The results from this study (using pelletized blend) have been compared with the reported results in the literature for steam gasification of non-pelletized lignite and wood. As the literature results showed a linear relationship between the producer gas composition and blending ratio, it is concluded that the synergetic effect was mainly caused by the pelletizing of the blends during which the char reactivity in the blend was changed.

From the examination on the effects of steam to the solid fuel ratio and gasification temperature, the steam to solid fuel ratio was found to have a positive impact on H_2 and CO_2 contents but negative influence on CO content, because the forward water gas shift reaction was enhanced at high steam concentrations. With elevated temperature, the H_2 content was increased while CO and CO_2 contents were decreased as combined results of changes in the pyrolysis gas products distribution and promoted backward water gas shift reaction.

The effect of char reactivity on the producer gas composition was found to be significant in the gasification of the solid fuels tested in this study. It was found that with an increase in the char reactivity, the CO content increased the most and the CO_2 content decreased for a relatively similar extent as the CO while CH_4 content decreased to a lesser extent and H_2 content change was the least. In general, the char reactivity effect was the most significant for pure lignite and the least for pine; for blended pellets this effect was decreasing with an increasing pine blending ratio. The char reactivity effect was attributed to the rate of char circulating from the BFB reactor to the CFB reactor as well as char consumption in the bed which was, in turn, due to the char density difference among various chars.

References

Aigner, I., Pfeifer, C., and Hofbauer, H. (2011). "Co-gasification of coal and wood in a dual fluidized bed gasifier." *Fuel*, 90(7), 2404-2412.

Babu, B. V., and Sheth, P. N. (2006). "Modeling and simulation of reduction zone of downdraft biomass gasifier: Effect of char reactivity factor." *Energy Conversion and Management*, 47(15–16), 2602-2611.

de Souza-Santos, M. L. (2004). *Solid Fuels Combustion and Gasification*, Marcel Dekker, New York.

Dupont, C., Boissonnet, G., Seiler, J.-M., Gauthier, P., and Schweich, D. (2007). "Study about the kinetic processes of biomass steam gasification." *Fuel*, 86(1–2), 32-40.

Fiaschi, D., and Michelini, M. (2001). "A two-phase one-dimensional biomass gasification kinetics model." *Biomass and Bioenergy*, 21(2), 121-132.

Franco, C., Pinto, F., Gulyurtlu, I., and Cabrita, I. (2003). "The study of reactions influencing the biomass steam gasification process." *Fuel*, 82(7), 835-842.

Gil, J., Corella, J., Aznar, M. a. P., and Caballero, M. A. (1999). "Biomass gasification in atmospheric and bubbling fluidized bed: Effect of the type of gasifying agent on the product distribution." *Biomass and Bioenergy*, 17(5), 389-403.

Gordillo, E. D., and Belghit, A. (2011). "A two phase model of high temperature steam-only gasification of biomass char in bubbling fluidized bed reactors using nuclear heat." *International Journal of Hydrogen Energy*, 36(1), 374-381.

Kaiser, S., Löffler, G., Bosch, K., and Hofbauer, H. (2003). "Hydrodynamics of a dual fluidized bed gasifier. Part II: simulation of solid circulation rate, pressure loop and stability." *Chemical Engineering Science*, 58(18), 4215-4223.

Kalinci, Y., Hepbasli, A., and Dincer, I. (2009). "Biomass-based hydrogen production: A review and analysis." *International Journal of Hydrogen Energy*, 34(21), 8799-8817.

Kaushal, P., Proell, T., and Hofbauer, H. (2011). "Application of a detailed mathematical model to the gasifier unit of the dual fluidized bed gasification plant." *Biomass and Bioenergy*, 35(7), 2491-2498.

Kaushal, P., Pröll, T., and Hofbauer, H. (2008). "Model for biomass char combustion in the riser of a dual fluidized bed gasification unit: Part II — Model validation and parameter variation." *Fuel Processing Technology*, 89(7), 660-666.

Loison, R., and Chauvin, R. (1964). "Pyrolyse rapide du charbon." *Chemie et Industrie*, 91(269).

Miccio, F., Ruoppolo, G., Kalisz, S., Andersen, L., Morgan, T. J., and Baxter, D. (2012). "Combined gasification of coal and biomass in internal circulating fluidized bed." *Fuel Processing Technology*, 95(0), 45-54.

Rapagnà, S., Jand, N., Kiennemann, A., and Foscolo, P. U. (2000). "Steam-gasification of biomass in a fluidized-bed of olivine particles." *Biomass and Bioenergy*, 19(3), 187-197.

Shen, L., Gao, Y., and Xiao, J. (2008). "Simulation of hydrogen production from biomass gasification in interconnected fluidized beds." *Biomass and Bioenergy*, 32(2), 120-127.

Soukup, G., Pfeifer, C., Kreuzeder, A., and Hofbauer, H. (2009). "In situ CO_2 capture in a dual fluidized bed biomass steam gasifier – Bed material and fuel variation." *Chemical Engineering & Technology*, 32(3), 348–354.

J.Tomeczek. (1994). *Coal Combustion*, Krieger.

Vélez, J. F., Chejne, F., Valdés, C. F., Emery, E. J., and Londoño, C. A. (2009). "Co-gasification of Colombian coal and biomass in fluidized bed: An experimental study." *Fuel*, 88(3), 424-430.

Wang, Y., and Kinoshita, C. M. (1993). "Kinetic model of biomass gasification." *Solar Energy*, 51(1), 19-25.

Yan, H.-m., Heidenreich, C., and Zhang, D.-k. (1998). "Mathematical modelling of a bubbling fluidized-bed coal gasifier and the significance of 'net flow'." *Fuel*, 77(9–10), 1067-1079.

Z'Graggen, A., and Steinfeld, A. (2008). "A two-phase reactor model for the steam-gasification of carbonaceous materials under concentrated thermal radiation." *Chemical Engineering and Processing: Process Intensification*, 47(4), 655-662.

Conclusions and recommendations

In this research, mathematical models have been developed and experimentally validated on gasification of coal, biomass and blended coal and biomass in two bubbling fluidized bed gasifiers, one with air steam and gasification agent and the other with pure steam as gasification agent. In order to quantify the char reactivity in steam gasification, experiments were conducted in a bench gasifier and a mathematical model was developed, and the results were employed in the gasifier models.

Firstly an extensive literature review was performed on properties of biomass and coal related to gasification, the gasification process, types of gasifiers and existing mathematical modelling work published in literature. From the literature review on the co-gasifiication process, inconsistent results were found on synergy effects; some studies showed a synergetic effect between the biomass and coal on producer gas composition and char reactivity, while others reported no noticeable energy being observed. After analysis of these reported studies, the difference appeared to lie in the blending method of the two fuels. When the biomass and coal were fed separately into the gasifier, these tended to segregate and gasify separately thus no synergy was observed. However, if the two fuels were pelletized before feeding to the gasifier, the synergy during gasification between these two fuels was apparent. Also from the literature research, no comprehensive mathematical models were reported on the co-gasification process in fluidized bed gasifiers. Therefore, the objectives of this research were to investigate the co-gasification characteristics and to develop comprehensive mathematical models to simulate the co-gasification process of biomass and coal.

In Chapter 3, the steam gasification reactivity of biomass char, coal char and chars of blended biomass and coal was experimentally investigated in a bench scale gasification system at three temperatures. Gas production rate, carbon (char) conversion rate and its reactivity were determined from continuous gas analysis using a Micro-GC. The sample char pellets were generated from lignite and Eucalyptus nitens at different mass blending ratios (biomass to coal) of 0:100 (pure coal), 20:80, 50:50, 80:20 and 100:0 (pure biomass).

From the experimental results, the gasification of biomass chars, coal chars and the chars of blended biomass and coal can be represented by three stages: i). initial heat-up and slow gasification stage, ii). fast gasification rate stage and iii). falling rate stage. The initial heat-up stage of char was very short in which the gasification rate increased to the maximum values. These maximum values were found to vary with the coal-to-biomass ratio; the highest for coal char and the lowest for biomass char. The overall gasification rate of biomass char maintained at a relatively constant level after the initial heat-up period, followed by a falling rate towards the end of the process. For gasification of the coal char, the reaction rate decreased continuously after the maximum value had been reached. The reaction rate of the blended coal and biomass chars fell between those of coal char and the biomass char but was closer to that of the coal char gasification. This can be explained by the fact that the biomass lost more mass during the initial pyrolysis when the char was produced.

The difference in char microstructure is also believed to contribute to the gasification characteristics and thus EMS scanning was performed on pure coal char, 50:50 blended char and pure biomass char. EMS image analysis indicated that the biomass char had a more amorphous structure; however, the effective pore size was smaller than coal char. The coal char had a more packed cluster structure but large cracks were present. The chars of blended biomass and coal were similar to the coal char.

From the analysis on char structure and the char gasification kinetics, the distinct gasification characteristics of the coal char and the biomass char were due to the differences in vapour diffusion rate within the char particles. The internal resistance to the vapour diffusion in the biomass char is significant and intrinsic reaction is fast due to its larger reactive surface area exposed to the gasification agent caused by its more amorphous structure. Therefore, a significant gradient in the steam concentration along the char radius results in a homogeneous overall reaction rate through the whole char volume. On the other hand, for the gasification of the coal char, the denser structure and larger effective pore size causes more homogeneous overall reaction rate through the whole char volume.

Based on the above observations and analysis results, a dynamic mathematical model was developed for simulation of the steam gasification process of biomass char, coal char and blended char. This model was based on the reaction mechanism in the gasification, mass

conservation and mass transfer as well as char structure characteristics. The reactions considered in the model include: steam-gasification reaction, water-gas shift reaction and Bouduard reaction. The mass transfer process took into account the convective bulk flow, the bulk gas and the Knudsen diffusion of the reactant gas (steam), the producer gas species (H_2, CO, CO_2) and the carrier gas (N_2). The heat transfer was not included in the model since the particle size of the chars was very small thus the intra-particle temperature gradient was insignificant. The mathematical model was solved using a numerical method to predict the gas production rate, gas composition and carbon consumption rate. In addition, the model could also predict the concentration distribution of gas species and carbon conversion rate along the char radial direction, from the centre to the outer surface of the particle.

The developed model was validated by the experimental data obtained in Chapter 3 and close agreement was found between the simulation results and the experimental data. The model simulation results showed that the char structure properties including specific reaction surface area and micro-pore size have significant impacts on both the intrinsic reaction rate and the intra particle mass transportation while the magnitude of these two competing processes determines the overall gasification process. The difference in the char structure properties is the key factor contributing to different gasification characteristics between biomass char and coal char. Gasification characteristics of the blended chars was predicted by blended char properties which were interpolated based on the actual fraction of the two fuels in the char. The developed model proposed in this study has been incorporated into a gasifier scale model on co-gasification of blended coal and biomass in bubbling fluidized bed gasifiers.

In Chapter 5, a one-dimensional mathematical model was developed to simulate bubbling fluidized bed gasification of coal and biomass blend pellets with air/steam as the gasification agent. The model was based on two phase theory which divided the bed into an emulsion phase and bubbling phase. The emulsion phase gas was treated as plug flow with axial mass and heat diffusion, while the bubbling phase was considered as plug flow without dispersion, and all solids were considered as well mixed through the whole bed. The internal diffusion, inter-phase mass transfer, solid-gas heat and mass transfer phenomena were taken into account. The internal diffusion of gaseous species in char particle was described by the effectiveness factor for spherical geometry. In order to validate the developed gasifier scale model, a series of co-

gasification experiments was performed on a 50 kW bubbling fluidized bed gasifier at CRL Energy Ltd., Lower Hutt, New Zealand. Two types of coal (lignite, sub-bituminous) and two types of biomass (pine and eucalypt) were selected as the feedstocks. A mixture of air and steam was used as the gasification agent and fed from the bottom of the column, and the required heat was provided by combustion reactions of char and combustible producer gas. The model simulation results have been compared with the experimental data obtained both at steady state and as a function of time. The parameters for comparison included producer gas composition and profile with time, temperature profile with time, total char mass and mean char conversion as the key characteristics of gasification. The discrepancy between simulation and experimental results was within a range of ± 10%.

After validation, the model was employed on sensitivity studies from which it was found that the gasification characteristics can be influenced by char yield, char reactivity and initial fast pyrolysis products. The steady state producer gas composition is strongly dependent on the char yield and is also affected by devolatilization gas distribution. The char reactivity has the least influence on producer gas composition; however it has significant impact on the dynamic behaviour of the gasification process.

The effect of the blending ratio of biomass to coal was studied, and it was found that adding biomass to coal reduced the gasification rates and reduced the concentrations of H_2 and CO. Such effect was more significant for lignite than subbituminous coal. The gas composition difference for different types of biomass of eucalypt and pine was not significant, since these two types of biomass had very similar properties.

The above gasifier scale model was then modified to simulate the steam gasification of biomass, coal and their blends, in a bubbling fluidized bed as part of a dual fluidized bed gasifier system. In this model, pure steam was used as the gasification agent and part of the solid char was transferred from the gasification reactor to a separate reactor for combustion to provide heat to the gasification process. The modified model was validated by a series of gasification experiments which were performed on a 100 kW dual fluidized bed gasifier in the Department of Chemical and Process Engineering, University of Canterbury. The operation temperature was controlled at 770-800°C. The solid fuels tested were blended coal and pine at coal-to-pine mass ratios of 100:0 (pure coal), 80:20, 70:30, 50:50, 40:60 and 0:100 (pure pine). Silica sand was

used as inert bed material which was circulated as a heat carrier. The model simulation results were compared with the experimental data for the same parameters as discussed earlier in the air/steam gasification and close agreement was also observed.

The modified steam gasification model has also been employed for sensitivity analysis for variables of char reactivity, mass blending ratio of the solid fuel, steam to solid fuel ratio and gasification temperature. From the parameter sensitivity studies, it was found that the lignite coal and pine pellets had significant impact on the producer gas composition. Producer gas from lignite gasification had a higher H_2 content and lower CO content than those from pine gasification since the two materials had distinctively different pyrolysis gas product distribution and char reactivity. The effect of char reactivity on producer gas composition was found to be significant in the gasification system being used in this study, since the deviation in rate of char comsumption could change the overall mass balance around the bubbling fluidized bed gasifier and the relative ratio between the feed streams was altered. It was found the increased char reactivity caused increase in CO content and decrease in CO_2 content in the producer gas.

From the analysis of the influence of blending ratio of pine and lignite in the solid fuel feedstocks on producer gas composition, a synergetic effect was clearly observed as the producer gas composition changed non-linearly with the blending ratio. For a pine blending ratio of less than 50%, the producer gas composition from gasification of blended pellets was close to that of gasification of pure lignite. However, with a pine blending ratio above 70%, the producer gas composition approached that of pure pine gasification. The results from this study are different from the reported results of non-pelletized lignite and wood gasification, from which a linear relationship of producer gas composition with blending ratio was observed. Therefore, it is concluded that the synergetic effect was mainly caused by the pelletising of the biomass and coal as the feedstock for gasification.

The steam to solid fuel ratio was found to have a positive impact on H_2 and CO_2 content and negative influence on CO content, because of promoted forward water gas shift reaction at a high steam feed rate. With elevated temperature, H_2 content was increased while CO and CO_2 contents were decreasing as combined results of changing in the pyrolysis gas products distribution and promoted backward water gas shift reaction at higher temperature.

In this thesis, the reaction kinetics of gasification was the main focus to be investigated and the behaviour of solid material in the gasifier was emphasized in the mathematical model. Hence calculation of the hydrodynamics of the fluidized bed was simplified in order to avoid the potentially numerous problems caused by coupling reaction kinetics with bed hydrodynamics. Since the bed hydrodynamics may play an important role in solid-gas systems and thus may have significant effect on the gasifier outcomes, further improvement on the modelling of the co-gasification process could be done by developing a more comprehensive model which couples reactions kinetics with a rigid bed hydrodynamic model. Although the developed 1-dimensional gasifier model, which uses simplified bed hydrodynamics, is suitable for sensitivity analysis of fuel type and operating conditions, a 2-dimensional model could be desirable from the CFD approach for better understanding of the process by predicting species distributions along the radius and height directions of the gasifier.